Characterization of Unbound Granular Materials for Pavements

A. A. Araya

Characterization of Unbound Granular Materials for Pavements

PROEFSCHRIFT

ter verkrijging van de graad van doctor
aan de Technische Universiteit Delft,
op gezag van de Rector Magnificus Prof.ir. K.C.A.M. Luyben
voorzitter van het College voor Promoties,
in het openbaar te verdedigen op
dinsdag 29 maart 2011 om 12:30 uur

door

Alemgena Alene ARAYA

Master of Science in Transport and Road Engineering,
IHE/TUDelft, the Netherlands

geboren te Mekelle, Ethiopia

Dit proefschrift is goedgekeurd door de promotor:
Prof. dr. ir. A.A.A. Molenaar

Copromotor:
Ir. L.J.M. Houben

Samenstelling promotiecommissie:

Rector Magnificus	voorzitter
Prof. dr. ir. A.A.A. Molenaar	Technische Universiteit Delft, promotor
Ir. L.J.M. Houben	Technische Universiteit Delft, copromotor
Prof. Dipl.-Ing. Dr. R. Blab	Vienna University of Technology
Prof. K.J. Jenkins, PhD.	University of Stellenbosch
Prof. E. Tutumluer, PhD.	University of Illinois at Urbana-Champaign
Prof. ir. A.F. van Tol	Technische Universiteit Delft
Dr. ir. A.A. van Niekerk	Provincie Gelderland
Prof. ir. A.Q.C. van der Horst	Technische Universiteit Delft, reserve lid

Published and distributed by:

Alemgena A. Araya
Email: a.a.araya@tudelft.nl, alemgena@yahoo.com

Road and Railway Engineering Section
Faculty of Civil Engineering and Geosciences
Delft University of Technology
P.O. Box 5048
2600 GA, Delft, the Netherlands

ISBN 978-90-8570-731-8

Key words: granular road base materials, mechanical behavior, triaxial test, repeated load CBR test

Printing: Wöhrmann Print Service, Zutphen, the Netherlands

I dedicate this dissertation to my parents,
who pave the foundation of my career,
my father the late Alene Araya and
my mother Truwerk Mesele.

AKNOWLEDGEMENT

The work presented in this dissertation started with a literature review carried out at the Institute of Road Construction and Maintenance of the Vienna University of Technology. The research was conducted at the Road and Railway Engineering Section of the Delft University of Technology. The author wishes to express his appreciation to his colleagues at the section for their assistance and cooperation to the research.

Special thanks and my sincere gratitude go to Prof.dr.ir. A.A.A. Molenaar and Assoc. Prof. ir. L.J.M. Houben. Their overall guidance and the diligent review of test results and reports were invaluable and greatly appreciated.

The research was funded by Delft University of Technology. In addition many thanks are due to the following institutes and persons that supported this project. Austrian Academic Exchange Service (ÖAD), Prof. Ronald Blab - Vienna University of Technology, Prof. Kim Jenkins - Stellenbosch University, Amdemichael Menkir and Efrem G/Egziabher - Core Consulting Engineers P.L.C Ethiopia and Mekelle University.

It is acknowledged with profound gratitude and sincerity the contribution of Assoc. Prof.dr.ir. M. Huurman and Ir. Milliyon F. Woldekidan for their invaluable assistance, advice and discussions on the finite element modeling and analysis. I am grateful for their guidance and support, without their contribution the numerical work would not have been possible.

The extensive experimental work could not have been successfully completed without the supportive contribution of my ex-officemate and most helpful person in the laboratory Jan-Willem Bienties, Marco Poot, Dirk Doedens, Paul Vermeulen, Jan Moraal and Radjan Khedoe. The assistance offered by Ally and Girum, who did their additional masters thesis in my PhD project, and the road engineering PhD candidates (Diederik, Dongxing, Gang, Jian, Milliyon, Minliang, Mo, Mohamad, Ning, Sadegh and Yue) in the laborious experimental work was also indispensable.

Words of thanks are also extended to Assoc. Prof. ir. M.F.C. van de Ven for sharing his South African pavement engineering and materials experience. The support and assistance offered from the laboratory of geotechnology and the recycling laboratory particularly from Ing. W. Verwaal and R.A. Penners are highly appreciated.

The assistance provided by the secretariat of our section Jacqueline Barnhoorn and Sonja van den Bos and the laboratory manager Abdol Miradi is gratefully appreciated. The brotherly support and concern from my friend Dr. Eyasu T. Hagos not only gave me encouragement for my work but also provided a comfort to my family especially during our first year in the Netherlands.

Last but not least, my special love goes to my wife, Senait, for her understanding, patience and support and my son, Abel, who spiced my writing with his inquisitive questions. My deepest gratitude goes to my parents, brothers and sisters for their love and encouragement. I also would like to take this opportunity to thank all friends and colleagues, who encouraged and supported me in some way but are not mentioned above by name, for their warm friendship and encouragement.

SUMMARY

This research is focused on the characterization of the mechanical behavior of unbound granular road base materials (UGMs). An extensive laboratory investigation is described, in which various methods for determination of the mechanical properties of granular materials are examined for their applicability, particularly in developing countries. Further, the mechanical behavior of unbound granular materials as a function of the moisture content and the degree of compaction is investigated. A study into the modeling of the stress dependent mechanical behavior of granular materials is presented. Finally, verification and validation of a relatively simple characterization technique, the repeated load CBR test (RL-CBR), by the results of cyclic load triaxial testing are provided and overall practical implications of the research are presented.

The laboratory investigation involves a large range of granular materials, mainly (sub-)tropical road base and subbase materials. The performed tests yield fundamental parameters that describe the strength, stiffness and resistance to permanent deformation of the materials tested. In addition to the (sub-)tropical road base and subbase materials, a recycled mix-granulate widely used in pavement construction in the Netherlands and a base course and frost protection material from Austria are incorporated to a limited extent in the laboratory testing program.

Most roads in developing countries are either unpaved or have a thin asphalt surfacing, and as a consequence the granular base and subbase layers provide the bulk of the bearing capacity. Although the important structural contribution of these unbound granular layers is understood, engineering practice still greatly relies on tests which mainly give index properties of these materials. Pavement structures are designed based on empirical design methods related to a single design chart, restricting the incorporation of marginal materials or new materials for which the empirical data sets are not available.

The reasons that pavement design and construction in developing countries rely on empirical design procedures that are basically developed for completely different conditions are:

- the affordability and complexity of the cyclic triaxial tests required to determine the stress dependent mechanical behavior of granular materials;
- the perceived complexity and unfamiliarity with the computational tools (non-linear multilayer or finite element analysis) required to model the performance of pavements using this mechanical behavior despite the availability of powerful digital computers and their penetration even to remote places.

In order to promote the introduction of Mechanistic-Empirical design methods in developing countries, this research was set up with two goals:

i. to make the characterization technique for the mechanical behavior of granular road base materials more accessible to practice through the development of a simple and effective characterization technique;
ii. to further develop the understanding of the stress dependent mechanical behavior of unbound (sub-)tropical base and subbase materials.

To achieve the first aim an innovative and relatively simple testing procedure, the RL-CBR test, is developed to characterize the mechanical behavior of the UGMs. RL-CBR testing is performed on the various granular materials in steel moulds without and with strain gauges. With the strain gauges the confining condition and hence the stress state of the specimen is estimated through mould deformation measurements. The finite element method (FEM) is used to model the RL-CBR testing and interpret the test results into mechanical behavior. Due to the non-uniform complex stress distribution in the RL-CBR compared to the triaxial test, fundamental material properties such as the stiffness modulus are less easy to determine.

Extensive triaxial testing on the various granular materials is performed to realize the second goal. The result of this investigation is also used to validate and verify the results of the RL-CBR tests. Moreover, the effect of influence factors such as moisture content, degree of compaction, material type etc. on the mechanical behavior is investigated. For the unbound granular road base materials, particularly the natural gravels, the effect of the moisture content on the mechanical behavior was found to be more significant than the effect of the degree of compaction. Relative to the failure and permanent deformation behavior the resilient deformation behavior is less affected by the moisture content and the degree of compaction.

The RL-CBR testing serves well its purpose to get a good estimate of the fundamental mechanical properties of granular road base materials from a rather simple characterization technique. The practical accessibility of characterizing the mechanical behavior of UGMs can therefore be enhanced through RL-CBR testing. This is proven by the fact that good correlations have been found between the stiffness results of the two characterization techniques, i.e. the complex triaxial test and the newly developed repeated load CBR test.

SAMENVATTING

Dit onderzoek betreft de karakterisering van het mechanisch gedrag van ongebonden granulaire funderingsmaterialen. Een uitgebreid laboratorium-onderzoek wordt beschreven, waarin verschillende methoden voor de bepaling van de mechanische eigenschappen van granulaire funderingsmaterialen worden onderzocht op hun toepasbaarheid, in het bijzonder in ontwikkelingslanden. Verder wordt het mechanisch gedrag van ongebonden materialen als functie van het vochtgehalte en de verdichtingsgraad onderzocht. Een onderzoek naar de modellering van het spannings-afhankelijke mechanisch gedrag van granulaire materialen wordt gepresenteerd. Ten slotte wordt een relatief eenvoudige karakteriserings-techniek, de CBR-proef met herhaalde belasting (RL-CBR), geverifieerd en gevalideerd aan de hand van de resultaten van de triaxiaalproef met cyclische belasting en worden algemene praktische implicaties van het onderzoek gepresenteerd.

Het laboratoriumonderzoek betreft een breed scala van granulaire materialen, voornamelijk (sub-)tropische funderingsmaterialen. De uitgevoerde proeven leveren fundamentele parameters die de sterkte, stijfheid en de weerstand tegen permanente vervorming van de geteste materialen beschrijven. In aanvulling op het onderzoek aan de (sub-) tropische funderingsmaterialen is een beperkt laboratoriumonderzoek uitgevoerd op menggranulaat (gerecycled bouw- en sloopafval), dat in Nederland op grote schaal wordt gebruikt in de wegenbouw, alsmede op twee ongebonden funderingsmaterialen uit Oostenrijk.

De meeste wegen in ontwikkelingslanden zijn ofwel onverhard of hebben een dunne asfaltlaag, en als gevolg daarvan leveren de ongebonden funderingslagen het grootste deel van de draagkracht. Hoewel de belangrijke structurele bijdrage van deze ongebonden lagen wordt begrepen, vertrouwt de wegenbouwpraktijk nog steeds sterk op proeven die in hoofdzaak index-eigenschappen van deze materialen geven. Wegverhardingen worden ontworpen op basis van empirische methoden met een enkele ontwerpgrafiek waardoor de toepassing wordt beperkt van marginale materialen of nieuwe materialen, waarvoor empirische gegevens niet beschikbaar zijn.

De redenen dat het ontwerp van wegverhardingen in ontwikkelingslanden steunt op empirische ontwerpprocedures, die in principe zijn ontwikkeld voor geheel andere condities, zijn:

- de betaalbaarheid en de complexiteit van cyclische triaxiaalproeven die nodig zijn om het spanningsafhankelijk mechanisch gedrag van granulaire materialen te bepalen;
- de vermeende complexiteit van en onbekendheid met rekenprogramma's (niet-lineaire meerlagen analyse of eindige elementen analyse) die nodig zijn om het gedrag van wegverhardingen inclusief het meer fundamenteel gedrag van ongebonden funderingsmaterialen te

modelleren, ondanks de beschikbaarheid van krachtige computers zelfs in afgelegen plaatsen.

Om de invoering van mechanistisch-empirische ontwerpmethoden voor wegverhardingen in ontwikkelingslanden te bevorderen, is dit onderzoek opgezet met twee doelstellingen:

i. de karakteriseringstechniek voor het mechanische gedrag van ongebonden funderingsmaterialen beter toegankelijk te maken voor de praktijk;
ii. het inzicht in het spanningsafhankelijke mechanisch gedrag van ongebonden (sub-)tropische funderingsmaterialen verder te vergroten.

Om het eerste doel te bereiken is een innovatieve en relatief eenvoudige proef, de RL-CBR, ontwikkeld om het mechanisch gedrag van de ongebonden funderingsmaterialen te karakteriseren. De RL-CBR proeven zijn uitgevoerd op de verschillende ongebonden funderingsmaterialen met en zonder rekstroken op de stalen mal. Met de rekstroken zijn de vervormingen van de mal tijdens de proef gemeten waardoor de steunspanning op het proefstuk, en daarmee de spanningstoestand in het proefstuk, beter afgeschat kan worden. De eindige elementen methode (FEM) is gebruikt om de RL-CBR proeven te modelleren en de proefresultaten te interpreteren in termen van mechanisch gedrag. Als gevolg van de complexe, niet-uniforme spanningsverdeling in het RL-CBR proefstuk zijn de fundamentele eigenschappen van het materiaal, zoals de stijfheidsmodulus, minder eenvoudig te bepalen dan bij de triaxiaalproef.

Uitgebreide series triaxiaalproeven zijn uitgevoerd op de diverse funderingsmaterialen om het tweede doel te realiseren. De triaxiaalproef resultaten zijn ook gebruikt om de resultaten van de RL-CBR proeven te valideren en verifiëren. Bovendien zijn de effecten van invloedsfactoren zoals vochtgehalte, verdichtingsgraad, materiaalsoort e.d. op het mechanisch gedrag onderzocht. Voor de ongebonden funderingsmaterialen, en dan vooral voor de natuurlijke materialen, bleek het effect van het vochtgehalte op het mechanisch gedrag groter te zijn dan het effect van de verdichtingsgraad. In vergelijking met de sterkte en de weerstand tegen blijvende vervorming wordt het elastisch vervormingsgedrag minder beïnvloed door het vochtgehalte en de verdichtingsgraad.

De RL-CBR proef beantwoordt goed aan haar doel om een goede schatting van de fundamentele mechanische eigenschappen van ongebonden funderingsmaterialen te verkrijgen met een vrij eenvoudige karakteriseringstechniek. De praktische toegankelijkheid van het bepalen van het mechanisch gedrag van ongebonden funderingsmaterialen kan daarom worden verbeterd door RL-CBR proeven. Dit is bevestigd door de goede correlaties tussen de stijfheden verkregen met de twee karakteriseringstechnieken, de complexe triaxiaalproef en de nieuw ontwikkelde CBR-proef met herhaalde belasting.

TABLE OF CONTENT

USED ACRONYMS /ABBREVIATIONS

AASHO	American Association of State Highway Officials
AASHTO	American Association of State Highway and Transportation Officials
AL	Average Limit: an average grading of the upper and the lower grading limits
ARD	Apparent Relative Density
AS	Australian Standard
ASTM	American Society for Testing and Materials
BS	British Standard
CBR	California Bearing Ratio
CCP	Constant Confining Pressure
CEC	Cation Exchange Capacity
CEN	European Committee for Standardization
DD	Dry Density
DEM	Discrete Element Methods
DOC	Degree of Compaction
EDXRF	Energy Dispersive X-Ray Fluorescence system
EN	European Norm
ERA	Ethiopian Roads Authority
ESA	Equivalent Standard Axle
FC	Ferricrete
FE	Finite Element
FEM	Finite Element Methods
FWD	Falling Weight Deflectometer
G1	Grade 1: for crushed rock South African grade 1 base materials
HCT	Hollow Cylinder Triaxial
LDPE	Low Density Polyethylene
LL	Liquid Limit
LVDT	Linear Variable Displacement Transducer
MAX	Maximum
MB	Methylene Blue
MBA	Methylene Blue Adsorption
MC	Moisture Content
MCBR	Modified CBR
M-E	Mechanistic-Empirical
MF(T)	Monotonic Failure (test)
MG	Mix Granulates
MIN	Minimum
MMPD	Maximum Modified Proctor Density
MPD	Maximum Proctor Density
MTS	Material Testing System
NAT	Nottingham Asphalt Tester
NCHRP	National Cooperative Highway Research Program
OMC	Optimum Moisture Content
ORN	Overseas Road Notes

PD(T)	Permanent Deformation (test)
PE	Poly Ethylene
PI	Plastic index
PL	Plastic Limit
PSI	Present Serviceability Index
PVC	Polyvinyl Chloride
RD(T)	Resilient Deformation (test)
RL-CBR	Repeated Load CBR
RREL	Road and Railway Engineering Laboratory
SAMDM	South African Mechanistic Design Method
SF	Safety Factor
SG	Strain Gauge
SMPD	Single-point Modified Proctor Density
SPD	Single-point Proctor Density
TRL	Transport Research Laboratory
TRRL	Transport and Road Research Laboratory
UGLs	Unbound Granular Layers
UGMs	Unbound Granular Materials
VCP	Variable Confining Pressure
WB	Weathered Basalt
WDXRF	Wavelength Dispersive X-Ray Fluorescence system
WOSG	Without Strain Gauge measurements
WSG	With Strain Gauges measurements
XRF	X-Ray Fluorescence
ZKK	Zusammensetzung Kornklassen (in German) - Grain composition classes: for the Austrian frost protection (ZKK32) and base course (ZKK63) granular materials

CHAPTER 1

INTRODUCTION

1.1 GENERAL INTRODUCTION

The economic and social development of nations all over the world relies to a large extent on the quality of its road transportation system. Vast amounts of money have been invested and are being invested in the construction of roads and large expenditures are required to ensure that these roads can continuously fulfill their function.

The economic role of the road infrastructure and the amount of money invested in its construction and maintenance indicate the importance of good pavement design and management procedures. Poorly designed road pavements will suffer from premature failure, which will lead to high reconstruction costs and to great economical losses. Over-designed pavements on the other hand will involve a waste of limited funds. Pavement design is a process intended to find the most economical combination of layer thicknesses and material types for the pavement, taking into account the properties of the subsoil, the traffic to be carried during the service life of the road and the climatic conditions. Generally pavement design methods can be subdivided into two main groups.

Empirical and mechanistic design methods

Design methods derived purely from empirical studies of pavement performance are named 'empirical methods'. Methods which make use of the calculated stresses and strains within the pavement, together with studies of the effect of these stresses and strains on the pavement materials (mechanistic behavior) are usually called 'mechanistic methods', 'theoretical methods' or 'analytical methods'.

Many of the pavement design procedures presently employed are still empirically based. They were developed from years of experience with existing roads, supplemented with the analysis of test sections or even major research projects like the AASHO Road Test [1]. These methods use empirical specifications i.e. material and recipe based, and material characteristics are appraised by simple index tests. Such material and recipe based specifications do not specify materials in terms of required fundamental engineering (mechanical) properties such as strength, stiffness and resistance to permanent deformation. They rather evaluate whether a material can be expected to behave in more or less the same way as similar materials with which experience exists under similar conditions.

The major drawback of empirical methods is that they indeed only operate within the limits of the experience on which they are based. Extrapolation from that to, for instance, higher axle loads, tire configurations such as super single tire, or marginal materials and different climatic conditions can lead to major problems. Because of this drawback, increasing effort is presently being spent almost throughout the world in the development of analytical or mechanistic design procedures. These methods are based on the analytical capability to calculate stresses, strains and deformations in a pavement subjected to an external load taking into consideration the climatic conditions. Based on the critical values of stresses and strains, the long term performance of the pavement and thus the service life can be estimated, which is a function of physical distress such as cracking and rutting.

The two methods are complimentary and should always be seen in this way [2]. Empirical methods require theoretical understanding to help extend them to different conditions, whilst mechanistic methods require empirical information for calibration. Neither method is ideal on its own, but the combination of the two provides a competent basis for design namely the 'Mechanistic-Empirical' (M-E) method.

In the analytical approach the road pavement is treated as a structure and its mechanical behavior evaluated in terms of parameters in a similar manner to that used for concrete and steelwork structures. A conditional prerequisite for the success of the mechanistic approach is that the behavior of the constituent materials is properly understood [3]. In flexible pavements, particularly when unsurfaced or thinly surfaced, granular layers play an important structural role in the overall performance of the pavement structure.

1.2 THE ROLE OF GRANULAR LAYERS IN PAVEMENTS

A road pavement in general is a layered structure of selected materials placed on top of a natural or filled subgrade. The pavement layers comprise of the top asphalt layer, base and/or subbase with/without an underlying capping layer, as shown in Figure 1.1. The granular base and subbase layers have to perform as both a short-term construction platform and also as a long term durable structure for the overlying pavement [4]. In most pavements in developing countries, the main structural element is formed by granular layers with thick base and subbase layers placed over the subgrade (Figure 1.1 (b)). For economical reasons the asphalt cover is very thin with a limited structural function. It mainly provides protection against water ingress and often the asphalt cover is omitted altogether.

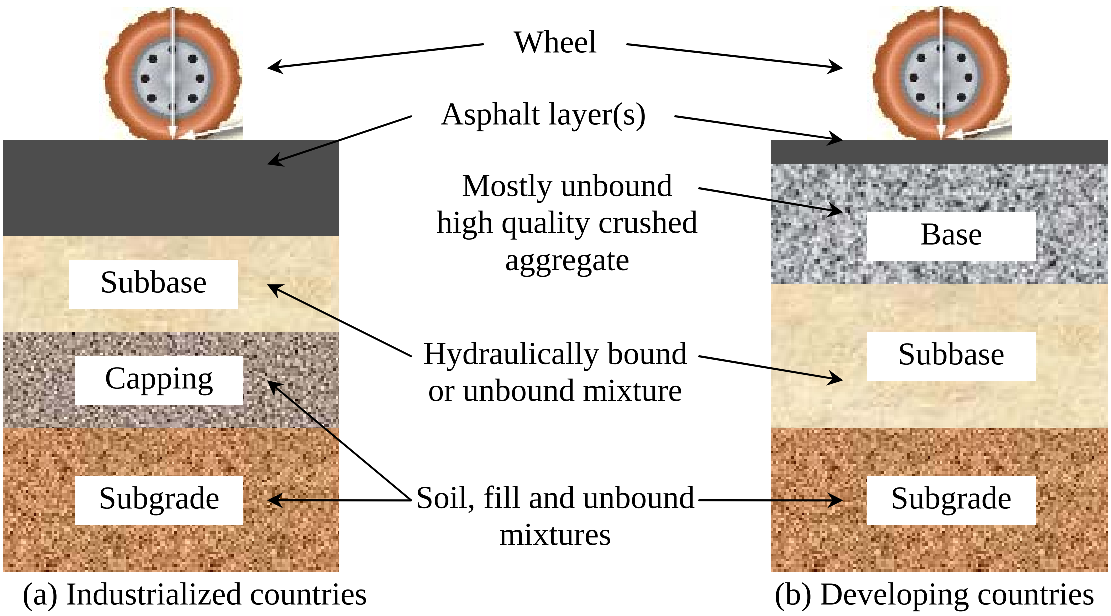

Figure 1.1 Schematic pavement structure typical sections and material options

In many of the mechanistic pavement design procedures used today, granular materials do not feature strongly. These design procedures focus on designing the asphalt layer, given the subgrade condition, the traffic loadings and the climatic conditions. This is due to the fact that in the industrialized countries, where these design procedures originate, the main structural element is the asphalt layer and the significance of the granular base and subbase are virtually reduced to that of a working platform. As Sweere [5] noted, the Shell Pavement Design Manual is a clear illustration of this: through the fixed ratio of the stiffness of the (sub-)base and the subgrade, see section 2.3.2, the structural contribution of the unbound granular (sub-)base is limited and granular materials hardly play a role in the design.

Pavements in developing countries do have only thin asphalt surfacing, and as a consequence the granular base and subbase layers provide the bulk of the bearing capacity. Despite the extensive use of granular materials, in the empirical pavement design procedures employed in those countries, granular base and subbase materials are often not used to their fullest extent. Moreover, though those light structured pavements are designed for relatively low traffic intensities, they are usually subjected to very heavy traffic due to excessive overloading and severe climatic conditions such as high temperatures, high moisture contents and wet and dry seasons.

In such pavements the granular layers have the following roles:

- ability to carry a significant portion of the load applied by a vehicle (during construction and service time) and spread to a magnitude that will not damage the underlying layers, particularly the subgrade;
- resistance to the built up of permanent deformation within each layer;
- provision of an adequately stiff layer on which the overlaying layers can be compacted;
- provision of an adequately durable and stiff layer to support any overlaying layers in the long term during in-service conditions.

To fulfill these requirements and establish more rational pavement design and construction criteria it is essential that the response of granular layers under traffic loading is taken into consideration and thoroughly understood. It becomes very important to properly characterize the behavior of unbound aggregate layers and subgrade soils of the layered pavement structure in order to predict pavement responses, which is essential in the framework of a mechanistic-empirical pavement design approach. The M-E design process relies on inputs such as the resilient (stress dependent elastic) modulus and Poisson's ratio of the material.

On the other hand, day-to-day engineering practice specifies and constructs roads based on a completely different set of parameters with very little correlation between the M-E design inputs and the common engineering parameters of the material. The factors impeding the more fundamental and mechanical approach of the behavior and performance of granular bases and subbases are basically related to the complexity of the characterization techniques, e.g. cyclic loading triaxial tests, required to determine the stress dependent mechanical behavior of granular materials.

The aim of this research is, therefore, to develop a characterization technique for the mechanical behavior of unbound granular base and subbase materials (mainly (sub-)tropical materials) that is more easily accessible to practice, in order to promote the introduction of M-E design methods in developing countries. In addition it also provides a thorough understanding of the stress dependent mechanical behavior of unbound base and subbase materials.

1.3 OBJECTIVE AND SCOPE OF THE STUDY

The general aim of this research, as mentioned in the previous section, is to establish an innovative and relatively simple material characterization technique to enable a more easy application of the mechanical behavior of unbound granular materials in day-to-day practice of pavement design.

To achieve this aim the following research objectives were derived:

- understanding existing pavement design procedures, defining performance parameters required for granular pavement materials, and assessing existing characterization techniques for unbound base and subbase materials; (Objective 1; O1)
- reduction of the complexity and elaborateness of the required tests by developing an innovative testing procedure, a repeated load CBR (RL-CBR) test, to characterize the mechanical behavior of these materials for analytical pavement design; (Objective 2; O2)
- furthering of the understanding of the stress dependent mechanical behavior of these materials, through triaxial and RL-CBR testing, and establish sound understanding of the influence of intrinsic material properties and conditions (origin, grading, compaction, moisture content etc) on their mechanical behavior. (Objective 3, O3)

The research was thus set up to test an extensive amount of (sub-)tropical granular base and subbase materials ranging from a very high quality crushed rock base material to rather marginal ferricrete and weathered basalt natural aggregates. A very large amount of base and subbase aggregates has been transported from Africa to the Netherlands and were sieved and recomposed for various characterization tests. Limited testing has also been carried out on temperate zone base and frost protection materials and recycled mix granulates.

Coarse grained granular base and subbase materials require large specimen sizes for testing the materials with their full gradation. Given this large specimen sizes requirement, the constant confining pressure (CCP) triaxial test was the only feasible and used type of triaxial test. For the other type of test playing a major role in this research, the Repeated Load CBR (RL-CBR) test, a larger mould, 250 mm diameter and bigger penetration plunger, 81.5 mm diameter, was manufactured instead of the standard CBR mould and plunger size.

In summary, the above three main objectives break down into the following key research activities and tasks performed. Firstly reviews of current pavement design methods, material specification and investigation of the use of new, marginal and recycled materials within the pavement industry. Secondly the development and assessment of new laboratory test equipment and methodologies to provide routine performance data for unbound granular materials (UGMs) for pavement design. Finally assessment of the practical implications, how the above mentioned testing techniques can be incorporated and routinely used with the introduction of M-E pavement design in the road industry. The detailed research tasks, methodology and research map of how these objectives have been completed is given in section 3.2 and 3.3.

1.4 STRUCTURE OF THE DISSERTATION

This dissertation is divided into seven chapters. Chapter 2 presents a summary of the present knowledge about the behavior and characterization of UGMs and their consideration in existing pavement design.

In chapter 3 details of the research strategy and methodology are described. Materials used in the extensive experimental program are elaborated along with their preliminary characterization testing.

The mechanical behavior of the materials from triaxial testing is presented in chapter 4, and modeling of those behaviors is discussed. The influence of moisture content and degree of compaction on strength and resilient deformation is illustrated.

Chapter 5 presents the characterization technique using RL-CBR tests. The detailed testing techniques, the finite element modeling of the test and the influence of the stress level, moisture content and degree of compaction on the resilient and permanent deformations are discussed.

In chapter 6 the outcome of the innovative characterization technique, the RL-CBR, in chapter 5 is validated with the result of the triaxial testing described in chapter 4.

Chapter 7 deals with the important features and practical aspects that can be considered in a similar future experimental research and their practical implications for the road industry.

Finally, chapter 8 gives the conclusions with general recommendations for both practicing engineers and academic researchers.

Figure 1.2 gives an overview of the structure of this dissertation.

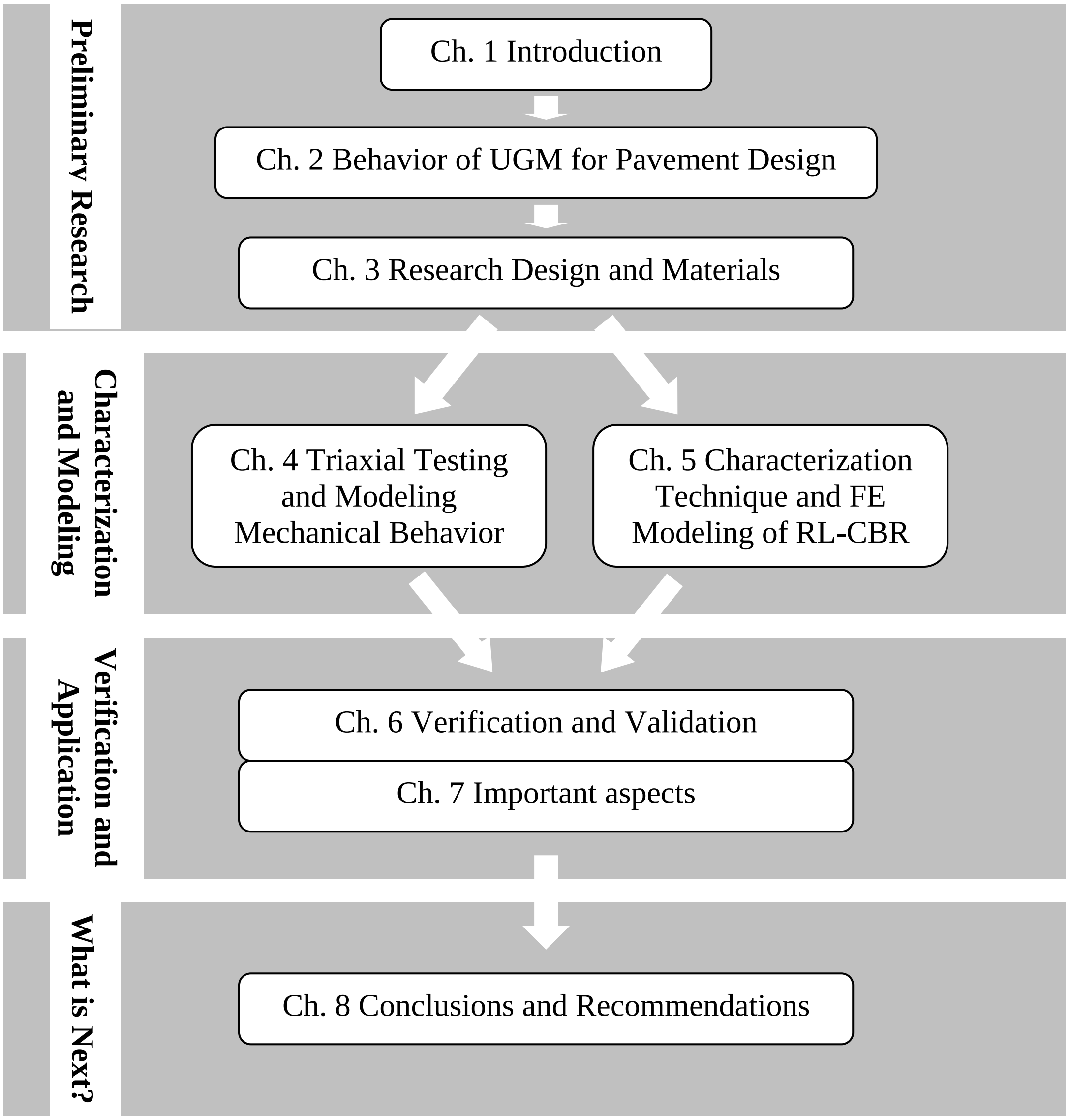

Figure 1.2 Structure of the dissertation

REFERENCES

1. AASHO, *The AASHO Road Test: Special Reports 61A - 61E*. 1961, Highway Research Board: Washington D.C.
2. Rolt, J., *Structural Design of Asphalt Pavements*, in *Road Engineering for Development*, R. Robinson and B. Thagesen, Editors. 2004, TJ International Ltd.: Padstow, Cornwall.
3. Lekarp, F., U. Isacsson, and A. Dawson, *State of the Art. I: Resilient Response of Unbound Aggregates*. Journal of Transportation Engineering, ASCE, 2000. **126**(1): p. 66-75.
4. Edwards, J.P., *Laboratory Characterization of Pavement Foundation Materials*, in *Centre for Innovative and Collaborative Engineering (CICE)*. 2007, Loughborough University: Loughborough.
5. Sweere, G.T.H., *Unbound Granular Base for Roads*, in *Faculty of Civil Engineering and Geosciences*. 1990, Delft University of Technology: Delft.

CHAPTER 2

THE BEHAVIOR OF UNBOUND GRANULAR MATERIALS FOR PAVEMENT DESIGN

2.1 INTRODUCTION

An examination of the history of pavement design reveals an evolutionary process that began with rule-of-thumb procedures and gradually evolved into empirical design equations based on experience and road test pavement performance studies. As Elliott and Thompson [1], Monismith [2], de Beer [3] stated, this evolution and transformation has been accompanied by the development of an understanding of material behavior, load-pavement distress relationships and environment interactions. Through the years, much of the development has been hampered by the complexity of the pavement structural system both in terms of its indeterminate nature and in terms of the changing and variable conditions to which it is subjected.

Major advancements in layered theory of pavements have been made since its introduction in the early 1940s. Recently very sophisticated analytical or mechanistic methods for the design of new pavements and reconstruction or strengthening of existing ones have been developed. Although these methods are theoretically sound, a gap still exists between actual pavement behavior (practice) and theory [3].

At the beginning of this research project a literature survey was conducted at the Vienna University of Technology which reviews existing pavement design procedures, the design criteria for unbound granular layers and behavior and characterization of unbound granular materials [4]. The purpose of this literature survey is to ensure that the research is based upon existing information and expertise that maximize the output value and minimize research iterations. The main areas relate to:

- developing an understanding of the role of unbound granular layers (UGLs) in pavements;
- outlining flexible pavement design procedures with emphasis to design criteria for UGLs;
- developing an understanding of the effect of material properties and material conditions on the mechanical behavior of unbound granular materials (UGMs);

- reviewing the laboratory characterization techniques for the determination of these pavement design input parameters with a brief summary of field assessment techniques.

Flexible pavement design procedures in general and pavement design systems for developing countries in particular are summarized in section 2.2 with an emphasis on the input parameters and design criteria employed for UGLs in pavements. The mechanical behavior of pavement UGMs and their characterization techniques are discussed in sections 2.3 and 2.4. Conclusions drawn and further research requirements are summarized in section 2.5.

2.2 SUMMARY OF FLEXIBLE PAVEMENT DESIGN PROCEDURES

Almost all standardized flexible pavement design procedures until some thirty years ago were empirical methods. Many countries today, particularly developing countries, still rely on such empirical methods, realizing that more sophisticated mechanistic design procedures often require too many assumptions regarding material behavior and too complicated material testing techniques to be of direct practical use.

The advent of the powerful digital computers and their penetration even to remote places [5] has created, these days, the possibility of the practical use of analytical solutions to determine stresses and strains in pavements. Computer programs such as BISAR, CHEVRON, CIRCLY and VESYS were developed that allow for computation of stresses and strains at any point in a multi-layered pavement structure. Such programs form the analytical backbone of today's mechanistic design procedures. Today, much effort is spent on further developing these procedures, both improving the existing analytical tools for determination of pavement responses and by performing extensive long-term pavement performance studies. The NCHRP 1-37A project Guide for Mechanistic-Empirical (M-E) Design [6] is an example outcome of such efforts.

In this section, a brief review of both the empirical and mechanistic design procedures will be limited to the design principles and parameters of the UGLs and their performance criteria. Furthermore pavement design procedures employed in developing countries will be described.

2.2.1 Empirical design methods

The CBR-method

The CBR-method is the most widely known empirical pavement design method. It was developed by the California Division of Highways in the late nineteen-thirties by examining the quality and thickness of base, subbase and subgrade materials under both failed and sound sections of flexible pavements throughout the Californian highway system. From these data, curves were formulated for determining the total depth of the pavement structure (base, subbase and imported fill) required to carry the anticipated traffic [7, 8]. It can be noted that the original CBR design curve, Figure 2.1, is only based on the wheel load and subgrade CBR-value. The number of load applications and the material quality overlaying the subgrade are not considered as an input when designing the total thickness.

The performance criteria for development of the design curves is based on limiting the shear stress at the top of the subgrade to a level below failure, which in turn limits the permanent deformation of the subgrade. There is no specific design parameter and performance criterion for the other unbound granular and asphalt layers.

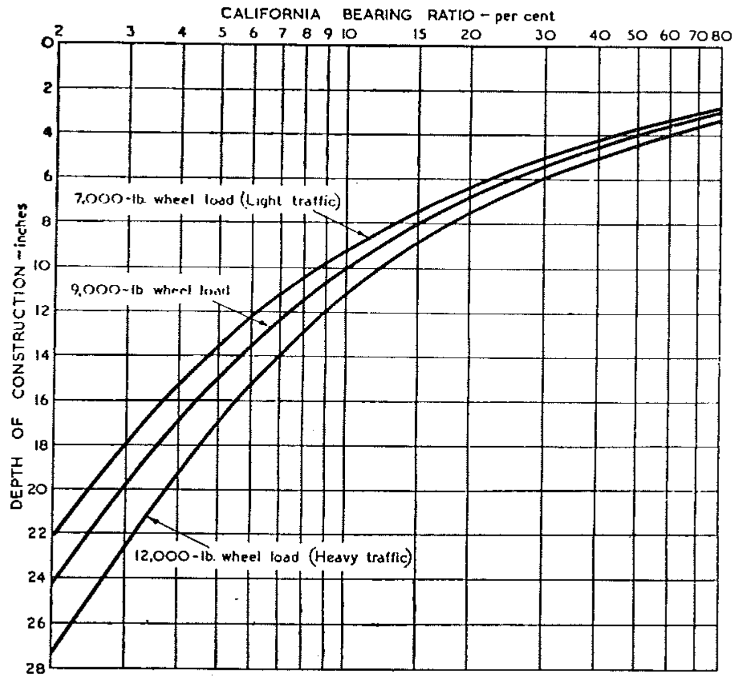

Figure 2.1 California State Highway Department 1940's CBR method thickness design curve [7, 9]

The 1993 AASHTO design method

The AASHTO Guide for the Design of Pavement Structures published in 1993 [10] is an updated version of the AASHTO Guide 1986 [11] which in turn is preceded by the AASHTO Interim Guide of 1972 which was developed based on the findings of the AASHO Road Test in the years 1959 – 1961. The updated guide is also based on those findings but adding new considerations such as the use of resilient modulus to characterize soil support and granular layers.

The performance criterion for the flexible pavements is generally in terms of present serviceability index (PSI). For aggregate surfaced roads the rut depth and aggregate loss of the surface layer are incorporated in the guide in addition to the serviceability. The serviceability of a pavement is its ability to serve the traffic (automobiles and trucks) that is using the facility. The basic design philosophy of this guide is the serviceability-performance concept, which provides a means of designing a pavement based on a specific total traffic volume and a minimum level of serviceability desired at the end of the performance period.

For a required reliability of the design, the soil support and the expected amount of traffic, a "structural number SN" is obtained from a nomograph in the guide. The required design structural number SN is then met by selecting a combination of surfacing, base and sub-base layers:

$$SN = \sum a_i D_i m_i \qquad \text{2-1}$$

Where SN = Structural Number
a_i = i^{th} layer coefficient
D_i = i^{th} layer thickness
m_i = i^{th} layer drainage coefficient

The structural capacity of the UGLs is basically characterized by their layer coefficient which is a function of the resilient modulus of the layer. The resilient modulus of the UGMs should be determined through cyclic load triaxial tests. The guide also provides charts that allow the resilient modulus of the base and subbase layers to be estimated from other laboratory data such as CBR in the absence of triaxial test facilities.

The 1993 AASHTO design procedure is a purely empirical one, although it allows for the use of a fundamental material parameter, the resilient modulus, from the repeated loading triaxial tests as input to the design. These fundamental parameters are not used as such in a structural analysis, but simply substitute empirical input parameters like CBR and R-values.

2.2.2 Mechanistic-Empirical design methods

The Shell pavement design method

The Shell pavement design manual [12] can be considered as a mechanistic design method because it is based on analytical principles. The strains and stresses in the pavement caused by a standard axle-load are calculated using the linear-elastic multilayer computer program BISAR and the calculated strain values are compared to allowable strains. The design procedure starts with an estimation of the asphalt and unbound layer thicknesses required to satisfy given strain criteria. The BISAR computer program allows for computation of stresses and strains at any given point in the pavement structure. The primary criteria for design in the manual are considered to be:

- the maximum vertical compressive strain at the top of the subgrade to prevent excessive permanent deformation;
- the maximum horizontal tensile strain in the asphalt layer, generally at the bottom to limit asphalt fatigue cracking.

Allowable values of strains are given in the manual as a function of the number of load applications. The manual contains a number of design charts for a number of combinations of subgrade modulus, temperature, asphalt stiffness and asphalt fatigue characteristics. Depending on the materials used and the prevailing conditions either the subgrade or the asphalt strain may be the deciding criterion. A particular design curve is generally made up of two differently shaped curves, associated with the two failure criteria, as shown in Figure 2.2.

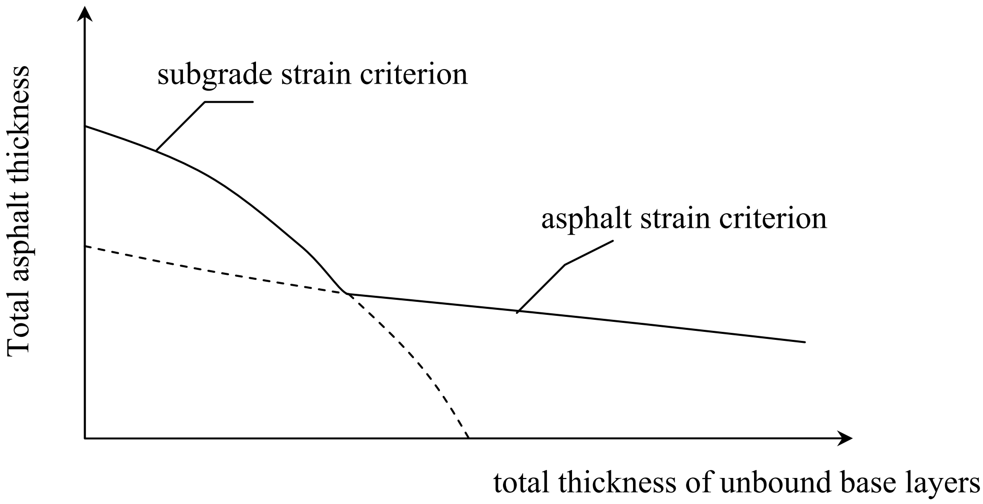

Figure 2.2 Simplified design principle of Shell pavement design method [12]

The vertical compressive strain at the top of the subgrade is a performance failure criterion for the design. However, the design method does not include a design criterion for the base course. This layer is only characterized by its stiffness, E. The stiffness of the granular base, E_2, is considered to be a function of the thickness of the base layer (h_2, in mm) and the stiffness of the subgrade, E_3, according to:

$$E_2 = k * E_3 \quad \text{with} \quad k = 0.2\, h_2^{0.45} \qquad \text{and} \qquad 2 < k < 4 \qquad 2\text{-}2$$

As Sweere [13] noted this approach of fixed E_2/E_3 ratio might be incorrect by today's state of art in pavement engineering. From a practical point of view it implies that a base of high quality of a basaltic crushed aggregate would have the same stiffness as a base of low quality river gravel when built with the same thickness on the same subgrade. Furthermore, using a chart based method rather than a computer based computational method, to have separate entries into the design for the stiffness of all layers, is another constraint of the design method.

AUSTROADS pavement design method

The Australian guide to the structural design of road pavements [14] was first published in 1987 by the National Association of Australian State Road Authorities [15] and was revised in 1992 and 2004 by AUSTROADS. The design procedure which is contained in the guide is mechanistic in nature. A set of example design charts for specific input parameters, which has been derived from the mechanistic procedure, is included.

In addition, a specific procedure is provided for the design of granular pavements with thin bituminous surfacing (a bituminous seal or an asphalt layer less than 25 mm thick). This is an empirical procedure which has been used extensively in the country. The origin of this unbound granular thickness chart, Figure 2.3, tracks back to the CBR pavement design method summarized in section 2.2.1. The original charts are adopted after thorough investigation and studies and several improvements have been made since then by many researchers such as Davis [8], MacLean [16], Leigh and Croney [17], NAASRA [15] and Potter et al. [18].

The AUSTROADS [14] design guide is based on the structural analysis of a multi-layered pavement subjected to traffic loading in terms of total number of equivalent standard axle loads (ESA). Pavement materials are assumed to be homogeneous, elastic and isotropic (except for unbound granular materials and subgrade). Response to loading is analyzed using linear-elastic multilayer theory and specifically the computer program CIRCLY.

The subgrade materials and unbound granular layers are assumed to be elastic and cross-anisotropic. This anisotropy is regarded as a device to compensate for the absence of a lateral stress dependent mechanism for the elastic modulus [19]. The elastic parameters required are the vertical and horizontal shear modulus and the vertical and horizontal Poisson's ratios. In the guide, the ratio of vertical to horizontal modulus is assumed to be 2 and both Poisson's ratios are equal. The guide suggests to determine the vertical modulus (E_V) of a subgrade through laboratory testing, if not to adopt an empirical relation such as E_V = 10*CBR.

Similar to the subgrade materials the guide characterizes the unbound granular materials by their anisotropic elastic characteristics using a modulus in horizontal direction which is half of the one in the vertical direction and the Poisson's ratios are assumed to be equal. In the design procedure it is necessary only to assign the modulus at the top of the granular layers, a value that should be obtained through cyclic load triaxial tests, other methods or from presumptive values given in the guide. With respect to other granular sub-layers, the guide recognizes that their modulus will be controlled by the stiffness of underlying layers rather than the intrinsic characteristics of the granular layer itself.

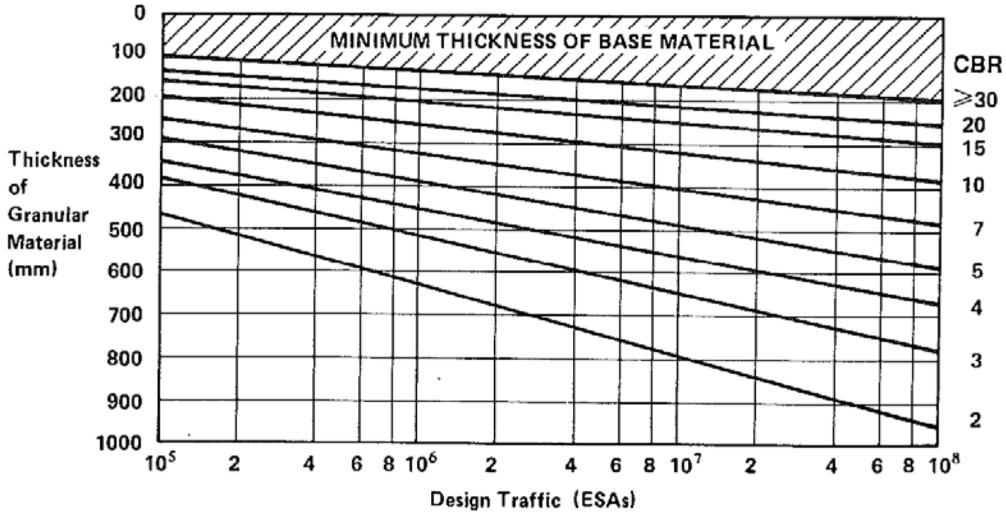

Figure 2.3 AUSTROADS design chart for granular pavements with thin bituminous surfacing [14]

For granular materials placed directly on the subgrade, sub-layering is required and is subjected to the constraints that the sub-layer thickness must be approximately in the range 50–150 mm and that the ratio R of moduli of overlaying sub-layers does not exceed 2 [20, 21]. After selecting the number of sub-layers, n, the modular ratio R may be calculated from the relationship:

$$R = \left[\frac{E_{topofbase}}{E_{subgrade}} \right]^{1/n} \qquad 2\text{-}3$$

The modulus of each layer may then be calculated from the modulus of the underlying layer, beginning with the subgrade whose modulus is known.

The performance criteria for the flexible pavements in this design guide are the critical responses of the pavement layers i.e. the maximum horizontal tensile strain at the bottom of the asphalt and cemented layers and the maximum vertical compressive strain at the top of the subgrade. No response criteria are considered for the unbound granular layers in the guide, the thickness and properties of unbound granular layers should be such that tensile stresses will not be generated in such materials.

2.2.3 Pavement design in developing countries

Overseas Road Note 31 design procedure

Overseas Road Note 31 [22] "A guide to the structural design of bitumen-surfaced roads in tropical and subtropical countries", first published by TRRL in 1962 and later revised in 1966, 1977 and 1993, is the most widely used design method in (sub)tropical developing countries like Ethiopia. This guide gives recommendations for the structural design of bituminous surfaced roads in tropical and subtropical climates. It is aimed for the design and construction of new road pavements and is prepared for roads which are required to carry up to 30 million cumulative equivalent 80 kN standard axles. The guide puts special emphasis on one aspect of pavement design which is of major importance in the design of roads for tropical areas. It gives a detailed procedure to estimate the moisture content at which the bearing capacity of the subgrade should be determined.

The bearing capacity of the subgrade is determined using the CBR test, to be carried out on the soil in the wettest condition likely to occur, and sub-grouped into six categories for design purposes. The material properties and their design requirements for the unbound granular base and subbase, which are the main load spreading layers of the pavement, are specified in terms of gradation and angularity in addition to strength requirements defined by the Ten Per Cent Fines Test [23] for crushed stones bases and CBR requirement for natural gravel bases and subbases.

The guide provides design charts from which a designer will select the one that is valid for the prevailing subgrade class and the traffic category. Charts are available for either a surface dressing or a premixed bituminous surface of limited thickness, range 50 – 150 mm, on different combinations and thicknesses of base and subbase materials. The Road Note 31 is a purely empirical design method based on a design principle of limiting the pavement distress to a level that experience has shown to be acceptable. This is primarily based on full-scale studies of the performance of as-built existing road networks [24-27].

For the unbound granular materials there are no specific design parameters related to fundamental material characteristics such as stiffness or strength. The quality of these materials is rather controlled through specifications qualifying their physical characteristics.

South African mechanistic design method (SAMDM)

The first simplified mechanistic design procedure in (sub)tropical developing countries was developed by Van Vuuren et al. in the early 1970's [28]. At the International Conference on the Structural Design of Asphalt Pavements in 1977 in Michigan, Walker et al. [29] published the first comprehensive statement on the state of the art of mechanistic pavement design in South Africa. The procedure was refined and improved since then, and in 1995 it was updated by Theyse [30] and Theyse et al. [31] for the purpose of revising the TRH4:1985 [32].

The method is a mechanistic design procedure based on calculations of stresses and strains in the pavement structure and limiting the calculated stresses and strains to allowable values. The basic material types considered in the design procedure are asphalt, granular, cemented and subgrade materials. The failure mode for each material type is linked to critical parameters calculated at specific positions in the pavement structure under loading. Transfer functions provide the relationship between the value of the critical parameter and the number of load applications that can be sustained at that value of the critical parameter, before the particular material type will fail in a specific mode of failure.

The pavement design life predictions are based on:

- maximum horizontal tensile strain at the bottom of the asphalt layer;
- maximum horizontal tensile strain at the bottom of the cemented layer;
- maximum vertical compressive stress at the top of the cemented layer;
- maximum shear stress in the granular layers;
- maximum vertical strain at the top of the subgrade layer.

The SAMDM is one of the few mechanistic-empirical (M-E) design methods that incorporate a methodology for evaluating the structural capacity of granular materials. For such materials, the structural capacity evaluation requires the calculation of a Safety Factor (SF) against shear failure, which was formulated by Maree [33]. The SF is based on Mohr-Coulomb theory for static loading and represents the ratio of the material shear strength divided by the occurring shear stress, in the form of equation 2-4:

$$SF = \frac{K\sigma_3\left[\tan^2\left(45+\frac{\phi}{2}\right)-1\right]+2Kc\tan\left(45+\frac{\phi}{2}\right)}{\sigma_1-\sigma_3} \qquad 2\text{-}4$$

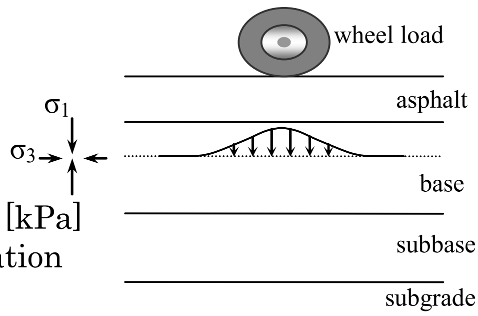

Where:

ϕ = angle of internal friction [°]
c = cohesion [kPa]
σ_1, σ_3 = major and minor principle stresses acting at a point in the granular layer [kPa]
K = constant relating to the level of saturation
= 0.65 for saturated conditions
= 0.8 for moderate moisture conditions
= 0.95 for normal moisture conditions

A safety factor smaller than 1 implies that the shear stress exceeds the shear strength and that rapid shear failure will occur for the static load case. Under real life dynamic wheel loading the shear stress will only exceed the shear strength for a very short time and shear failure will not occur under one load application, but shear deformation will rapidly accumulate under a number of load repetitions. If the safety factor is larger than 1, deformation will accumulate gradually with increasing number of load applications. In both cases the mode of failure will, however, be the deformation of the granular layer and the rate of deformation is controlled by the magnitude of the safety factor against shear failure [34]. One should note that this formulation is based on triaxial investigations conducted under a limited number (up to 20,000) of load repetitions.

In the current SAMDM a transfer function, a function that relates the Safety Factor and the allowable number of load applications, is included that was developed by Maree and Freeme [35] and Theyse et al. [34]. This transfer function is given in equation 2-5:

$$\text{Log}(N) = 2.605122(SF) + B \tag{2-5}$$

Where:
- N = allowable number of load applications
- SF = calculated safety factor
- B = constant depending on the road category
  - = 3.480098 for category A roads
  - = 3.707667 for category B roads
  - = 3.983324 for category C roads
  - = 4.510819 for category D roads

In the SAMDM design procedure the roads are classified in four categories, depending on their importance, traffic intensity and performance reliability. The required design reliability for the different required service levels is shown in Table 2-1.

Table 2-1 Road categories and approximate design reliabilities used in South Africa [32]

Road Category	Description	Approximate design reliability (%)
A	Interurban freeways and major interurban roads	95
B	Interurban collectors and major rural roads	90
C	Rural roads	80
D	Lightly trafficked rural roads	50

The particularity or uniqueness of the SAMDM design method is the incorporation of a performance criterion for the unbound granular layers in terms of a safety factor for shear failure. However, Jooste [36] illustrated that the design method is sensitive to material input parameters. Small changes in pavement layer properties such as stiffness of the base, subbase, Poisson's ratio etc. can lead to significant variations in predicted structural capacity. It is believed that this problem centers around two principal errors inherent in many published transfer functions [36]:

i) the implication of a predictive ability that often is not statistically sound;
ii) the assumption of a constant direct or indirect relationship between the design parameter and the number of load repetitions to failure.

To circumvent these problems further research is required to support the development of predictive transfer function equations with conclusive and statistically sound performance data.

2.2.4 Other base strain design considerations

Pavement performance in relation to base quality

For thinner pavements, small element pavements and surface dressed or even unsealed pavements it is evident that permanent deformation (PD) of unbound base and subbase layers should also be considered as a design criterion in addition to asphalt fatigue and subgrade rutting. Van Niekerk in his PhD research [37] has developed a number of design charts that are derived from a large number of finite element and subsequent rut depth calculations. These charts take account of both the "conventional" criteria (asphalt fatigue, ε_t, and subgrade rutting, ε_v) and permanent deformation of the granular base and subbase layers.

These charts present ε_t, ε_v and maximum failure ratio $\sigma_1/\sigma_{1,f}$-values and asphalt fatigue relations and rut depth lines in relation to the investigated variables, i.e. the top layer type and thickness, asphalt stiffness, subgrade modulus and wheel load magnitude. Van Niekerk has developed these charts based on permanent deformation tests up to 1 million load repetitions on mix granulates with various grading and degree of compaction (see Figure 2.4). i.e. a much higher number of load applications than used by Maree in developing the equations 2-4 and 2-5. For detailed information on the principles and interpretation of the charts reference is made to Van Niekerk's PhD dissertation [37].

It has been explained earlier that most analytical-mechanistic design methods are based on asphalt fatigue and subgrade permanent deformation as design criteria, in which the decisive of the two depends on the characteristics of the pavement structure. Van Niekerk [37] introduced additional design criterion in his charts by including an approach for rutting resulting from the base, subbase and the subgrade layers as design criterion.

The main strength of these charts is that the effect of pavement and loading variables and material quality can be quantitatively assessed. A major limitation of these charts is that the stress dependent permanent deformation (PD) behavior is described relative to the failure ratio ($\sigma_1/\sigma_{1,f}$). The PD was determined from triaxial tests performed at only one confining stress level (σ_3 = 12 kPa). In the same study, the PD triaxial tests performed on subbase sands demonstrate that the $\sigma_1/\sigma_{1,f}$-ratio doesn't uniquely describe the stress dependency of the PD behavior at significantly different σ_3-levels.

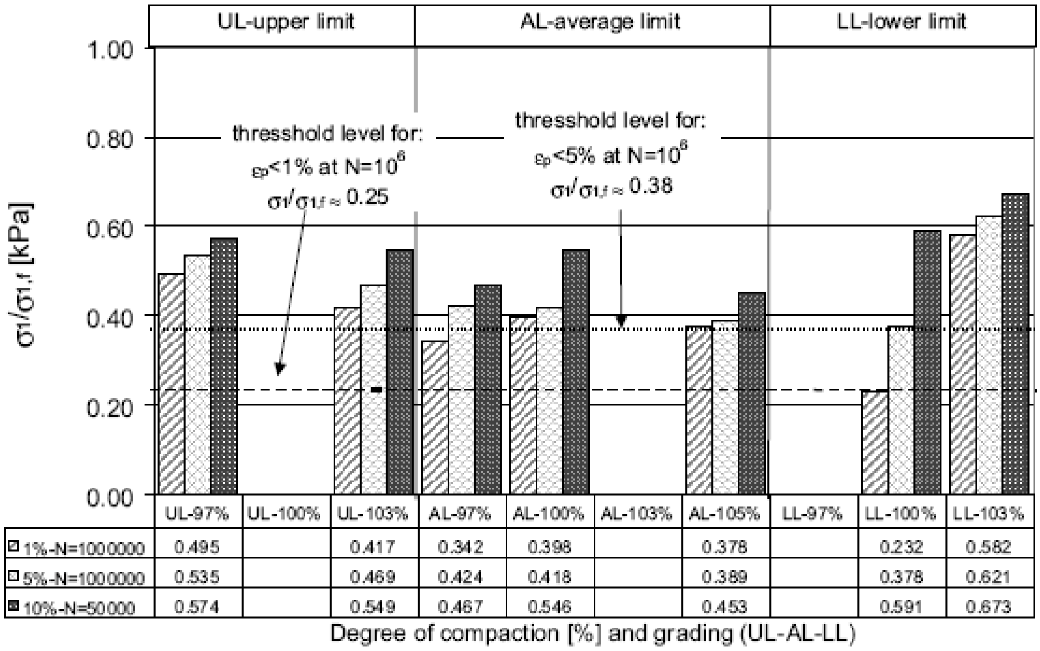

	UL-97%	UL-100%	UL-103%	AL-97%	AL-100%	AL-103%	AL-105%	LL-97%	LL-100%	LL-103%
1%-N=1000000	0.495		0.417	0.342	0.398		0.378		0.232	0.582
5%-N=1000000	0.535		0.469	0.424	0.418		0.389		0.378	0.621
10%-N=50000	0.574		0.549	0.467	0.546		0.453		0.591	0.673

Figure 2.4 $\sigma_1/\sigma_{1,f}$-ratios at which permanent deformation, ε_p =1%, 5% and 10% at number of load repetitions N =10^6, 10^6 and 5.10^4 [37]

Maximum strains in road bases and pavement performance prediction

Araya in his MSc thesis [38] has also attempted to develop a simple structural design criterion for unbound road bases through prediction of maximum vertical strain at top of the base under falling weight deflectometer (FWD) loading and relating it to the resilient and permanent deformations measured from triaxial tests on unbound road base materials. From a FWD database as used by Van Gurp [39] a relationship has been derived between deflection bowl parameters and the maximum vertical compressive strain at the top of the base layer. It should be noted that in the analysis it was not possible to derive a single equation covering a wide variety of pavement structures. It was however possible to derive a predictive equation, equation 2-6, for particular types of pavement structures where:

- unbound base layer stiffness is less than 1000 MPa;
- the upper unbound layer is stiffer than the lower unbound layer;
- the stiffness of the upper unbound layer should not exceed four times the stiffness of the underlying unbound layer.

$$\log \varepsilon_{VB} = 1.5615 + 0.3743 \log SCI_{300} + 1.0067 \log BDI_{600} + 0.8378 \log d_0 - 1.9949 \log d_{1800} + 0.6288 \log d_{300} \quad (2\text{-}6)$$

Where ε_{VB} = vertical compressive strain at the top of the base [μm/m]

d_r = deflection at a radial distance of r mm from the load center [μm]

SCI_{300} = surface curvature index, difference in center deflection and deflection at 300 mm [μm]
BDI_{600} = base damage index, difference in deflection at a radial distance of 300 mm and 600 mm [μm]
With goodness of fit $R^2 = 0.967$

As the main goal of the research was to develop a simple procedure to estimate whether or not failure in an unbound base is likely to occur, it was attempted to develop failure criteria for base materials similar as those available for subgrades. This means that the allowable number of load repetitions to failure is related to the vertical elastic strain at the top of the base, Figure 2-5 (a).

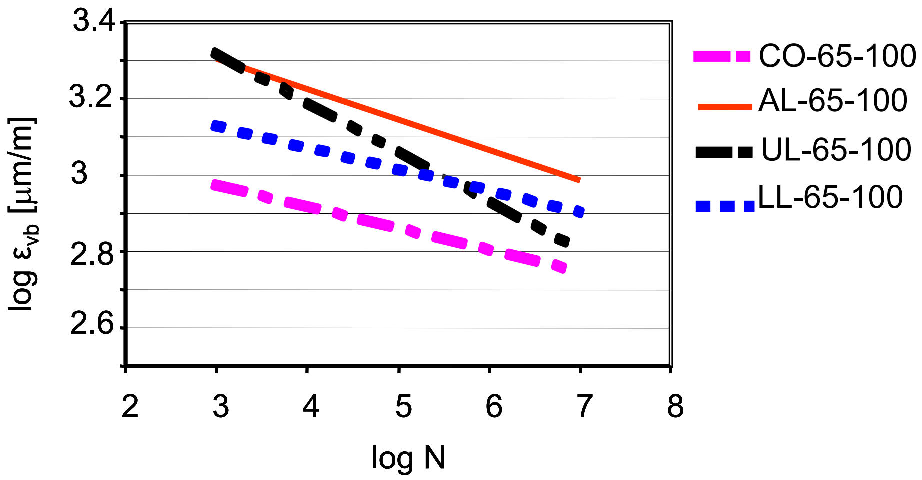

(a)

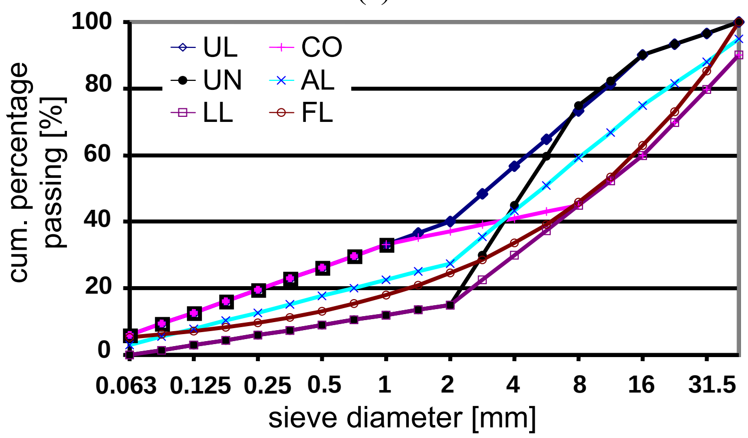

(b)

Figure 2.5 (a) Example of unbound base design criteria (relating vertical elastic base strain ε_{vb} and number of load repetitions N) [38] (b) gradation

In order to develop such failure criteria for unbound bases, use was made of the extensive research performed by van Niekerk [37] on the resilient and PD characteristics of such materials. In his research van Niekerk tested a large number of unbound base materials consisting of mixtures of crushed concrete and crushed masonry mix granulates (MG).

The failure criteria were developed by setting 4% permanent deformation in an unbound base as an acceptable amount. From the extensive resilient and PD triaxial tests on mix granulate base materials for various stress levels, mix compositions, degree of compaction (DOC) and gradings, failure lines such as in Figure 2-5 (a) were developed for four out of the different mix granulate gradations shown in Figure 2-5 (b). The four mix granulate materials differ in their gradation having the same mix composition i.e. 65% by mass crushed concrete and 35% crushed masonry and all compacted to 100% DOC.

2.3 REVIEW OF UNBOUND GRANULAR MATERIALS BEHAVIOR

Unbound granular materials (UGMs) are extensively used in bases and subbases of flexible pavements to provide load distribution. The bearing capacity of UGMs is a result of the shear resistance of the aggregate skeleton i.e. through aggregate interlock between particles. As loading and performance requirements of pavements continually increase, a better basic understanding of the mechanical behavior of UGMs and their response to loading is essential.

2.3.1 Mechanical behavior of unbound granular materials

As discussed in the section 2.2, the use of materials within pavement layers either requires a prior knowledge of satisfactory performance (empirical relationships used in combination with index testing) or a facility to be able to measure and predict performance.

Mechanical material properties can be measured using equipment developed at research establishments (section 2.4). The main requirement from the test is that the information generated is of a fundamental nature, such that a true understanding of material behavior can be obtained from it [40].

In this dissertation the term mechanical (fundamental) behavior refers to the failure behavior (strength), the resilient deformation behavior (stiffness) and the permanent deformation behavior.

An example of a stress – strain curve taken from a monotonic loading triaxial test is shown in Figure 2.6(A). The first part of the monotonic curve forms as the applied stress level increases, until it approaches the yield stress point, after which the strain continues, even with a reduction in stress. Under repeated loading conditions (well below the failure/yield stress level), materials undergo recoverable and irrecoverable components of deformation. The permanent and recoverable components for a single load cycle are shown in Figure 2.6(B). The recoverable component is referred to as a resilient modulus see section 2.3.1.2, while the irrecoverable component known as permanent deformation dictates the materials susceptibility to rutting [41].

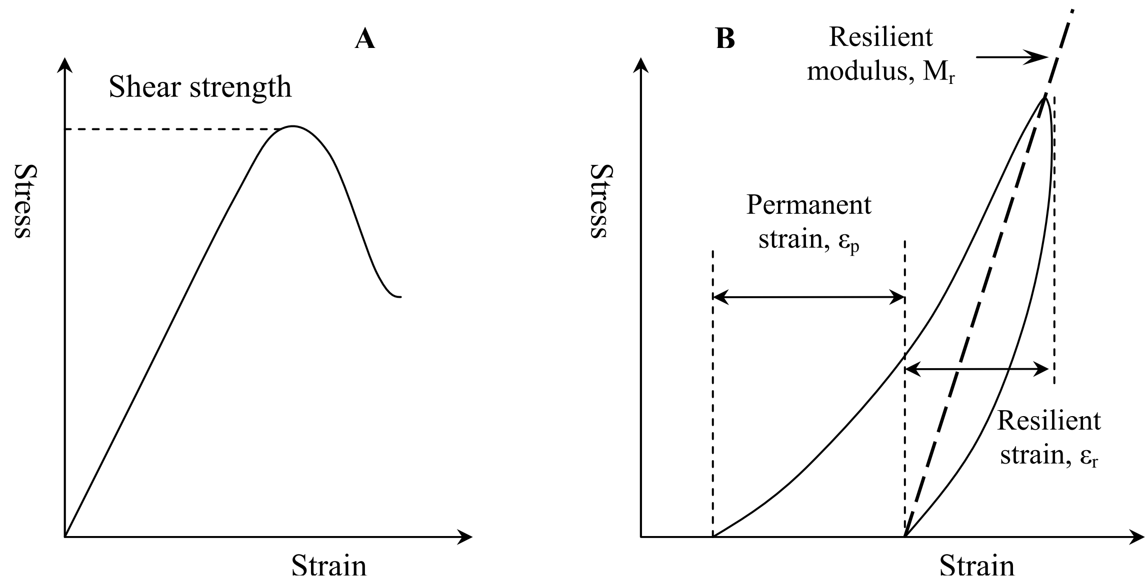

Figure 2.6 (A) Monotonic loading to failure (B) strains in UGM during one load cycle [41]

2.3.1.1 Resilient deformation behavior

The theory of elasticity traditionally defines the elastic properties of a material by the modulus of elasticity, E, and the Poisson's ratio, ν. Dealing with UGLs, the elastic modulus E is replaced by the resilient modulus to describe the stress-dependent elastic (recoverable) behavior of a material subjected to repeated loading.

The resilient properties of UGMs were first noted by Hveem in 1950's [13], who concluded that the deformation of such materials under transient loading is elastic in the sense that it is recoverable. The actual concept of resilient modulus was later introduced by Seed et al. [42] in characterizing the elastic response of subgrade soils and their relation to fatigue failures in asphalt pavements.

Granular materials are not truly elastic [41] but experience some non-recoverable deformation after each load application. In the case of transient loads and after the first few load applications, the increment of non-recoverable deformation is much smaller compared to the resilient/recoverable deformation, Figure 2.7.

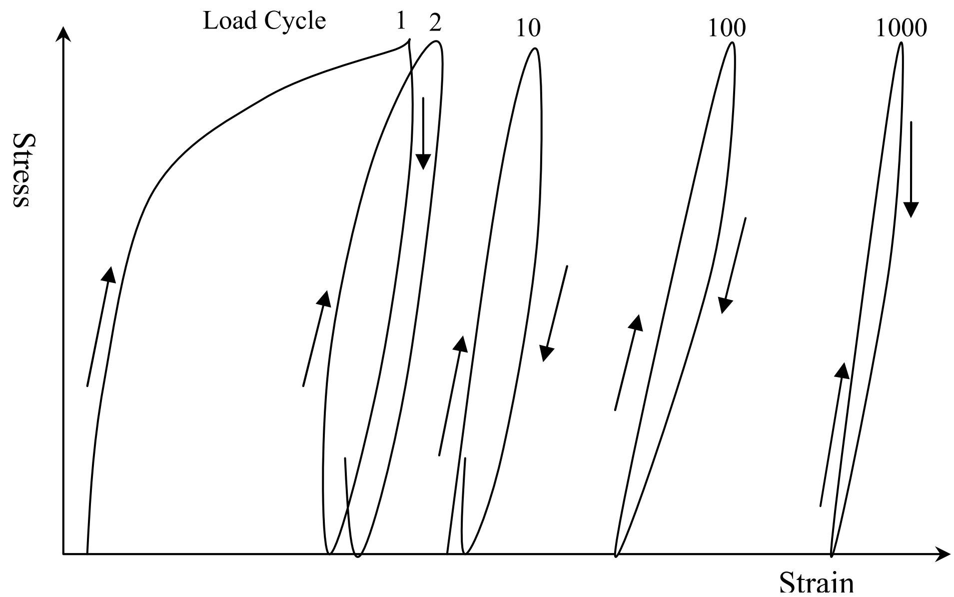

Figure 2.7 Granular material behavior under repeated loading [43]

The term “resilient” has a precise meaning. It refers to that portion of the energy that is put into a material while it is being loaded that is completely recovered when it is unloaded [44]. This resilient behavior of granular layers is the main justification for using elastic theory to analyze their response to traffic loads. The engineering parameter generally used to characterize this behavior is resilient modulus (M_r). The resilient modulus, equation 2-7, is defined as the ratio of the repeated axial deviator stress to the recoverable strain. Figure 2-8 shows a schematic sketch of cyclic load triaxial test principles.

$$M_r = \frac{\sigma_d}{\varepsilon_r} \qquad 2\text{-}7$$

Where: M_r = the resilient modulus
σ_d = the applied repeated deviator stress
ε_r = the axial recoverable strain

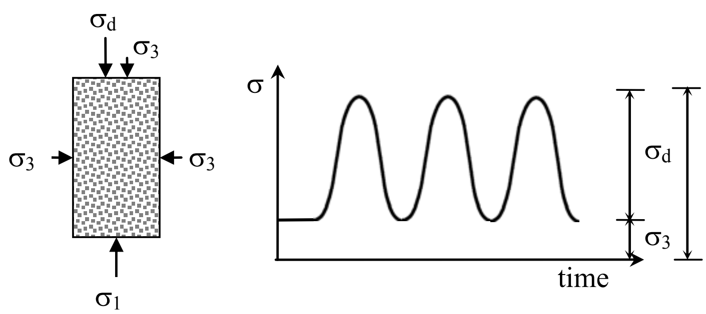

Figure 2.8 Schematic sketch of cyclic load triaxial test principles

By studying the literature on earlier research Lekarp et al. [45] presented a “state-of-the-art” on resilient behavior of unbound granular materials. Lekarp [46] found that the resilient behavior of unbound granular materials is affected by several factors like stress conditions, density, moisture content, fines content, grading, aggregate type, number of load applications, stress history, load duration, frequency and sequence. The influence of most of these factors will be further discussed in section 2.3.2.

A lot of effort has been made to develop models that can describe and predict the non-linear resilient behavior of unbound granular materials. Many researchers have developed models to describe the stress dependency of the resilient modulus. In this study four of the many available models that comprises from the oldest to the more advanced one that takes into account the anisotropic behavior of the resilient modulus, are discussed.

M_r–θ model

The M_r-θ model is a non-linear, stress-dependent power function model first described by Seed et al. [47]. Brown and Pell [13] obtained stiffness values of UGMs from pulse load tests on an instrumented pavement built in a test pit. By plotting the obtained M_r values on a double-logarithmic scale against the first stress invariant (bulk stress), a straight line was found. This method of representing the stiffness – stress relationship for UGMs has now become the standard method in pavement engineering. Figure 2.9 shows a schematic representation of this relationship, which is described by the well-known M_r-θ model:

$$M_r = k_1 \left(\frac{\theta}{\sigma_0} \right)^{k_2} \tag{2-8}$$

Where:	M_r	= resilient modulus	[MPa]
	θ	= bulk stress = $\sigma_1+\sigma_2+\sigma_3$	[kPa]
	σ_0	= reference stress = 1	[kPa]
	k_1	= material parameter	[MPa]
	k_2	= material parameter	[-]

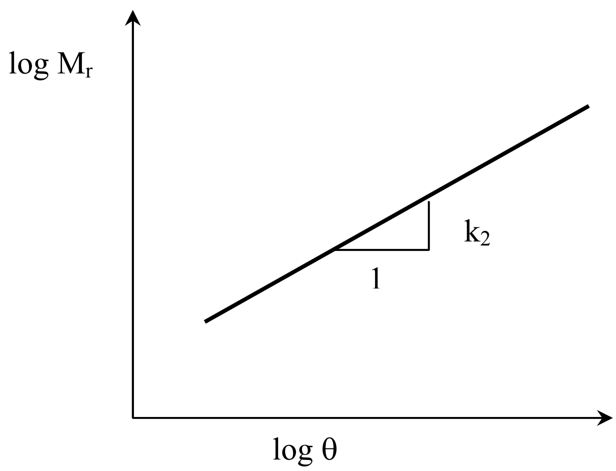

Figure 2.9 Schematic representation of M_r – θ plot

The M_r-θ model is a commonly used model to account for the stress dependency of the resilient modulus. Because of its simplicity the model is extremely useful and widely accepted for analysis of the stress dependence of material stiffness. However, this model has several drawbacks [48, 49]. Stress level is only considered by the bulk stress in this model. This means that all combinations of principal stresses giving the same sum will have the same effect on the resilient modulus, it does not account for the confining and deviator (or shear) stress separately. Furthermore, the model is often used with a constant Poisson's ratio to calculate the specimen's radial strain. Earlier research [37, 48, 50] shows that the Poisson's ratio does not stay constant, but varies with the applied stresses as well.

Uzan model

Further research by Uzan [49, 51] and others showed that the resilient modulus also depends upon the shear stress level as expressed in equation 2-9. The effect of deviator stress is taken into account in this model, which is one of the serious shortcomings of the M_r-θ model. This added condition can be used to explain why UGLs become less stiff in areas of high shear stresses such as at the edge of tire loading.

The model was first presented by Uzan [49] as follows;

$$M_r = k_1 \left(\frac{\theta}{\sigma_0} \right)^{k_2} \left(\frac{\sigma_d}{\sigma_0} \right)^{k_3} \qquad 2\text{-}9$$

Where: σ_d = deviatoric stress [kPa]
k_1 = model parameter [MPa]
k_2, k_3 = model parameters [-]

The model has also been further developed by Witczak and Uzan [51] for the three-dimensional case where the deviatoric stress is replaced with the octahedral shear stress, equation 2-10.

$$M_r = k_1 \left(\frac{\theta}{\sigma_0} \right)^{k_2} \left(\frac{\tau_{oct}}{\sigma_0} \right)^{k_3} \qquad 2\text{-}10$$

Where: τ_{oct} = octahedral shear stress [kPa]

TU Delft model

From an extensive laboratory characterization of the Netherlands subbase sands in Delft University of Technology, Road and Railway Engineering laboratory, Huurman [52] has derived a model, equation 2-11. The model is developed from the M_r-θ model by discriminating the role of the confining stress, σ_3, and the deviator stress, σ_d.

$$M_r = k_1\left(\frac{\sigma_3}{\sigma_0}\right)^{k_2}\left(1-k_3\left(\frac{\sigma_1}{\sigma_{1,f}}\right)^{k_4}\right) \qquad 2\text{-}11$$

Where:

Where:	σ_3	= minor principal stress	[kPa]
	σ_1	= major principal stress	[kPa]
	$\sigma_{1,f}$	= major principal stress at failure	[kPa]
	k_1	= model parameter	[MPa]
	k_2 - k_4	= model parameters	[-]

In the model the first absolute term, $k_1\sigma_3^{k2}$, describes the increase of M_r for increasing the confinement stress σ_3. The second term, $(1\text{-}k_3(\sigma_1/\sigma_{1,f})^{k4})$, which has been added to the model, describes the decrease of the M_r as loading approaches failure ($\sigma_1/\sigma_{1,f} \rightarrow 1$). The model describes well the resilient behavior of the subbase sands characterized at high stress level close to failure. The limitation of this model is, however, it can't describe an increment of the M_r for granular materials characterized with an increasing deviatoric stress but far from failure.

Furthermore, extensive work done by Huurman et al. [53] has shown that it is possible to relate the parameters k_1 and k_2 of the M_r-θ model to physical characteristics of the base and subbase materials, such as grading, angularity of particles and density.

Anisotropic Boyce model

Several studies [13, 54, 55] have shown that the resilient behavior of UGMs can be described using a non linear elastic model proposed by Boyce [56]. This model better describes the elastic behavior of UGMs by separating stresses and strains into volumetric and shear components. For the axisymmetric case of triaxial testing, where $\sigma_2 = \sigma_3$ and $\varepsilon_2 = \varepsilon_3$, the volumetric and shear components can be expressed as equation 2-12 through 2-15:

$$p = \tfrac{1}{3}\left(\sigma_1 + 2\sigma_3\right) \qquad 2\text{-}12$$

$$q = \sigma_1 - \sigma_3 \qquad 2\text{-}13$$

$$\varepsilon_v = \varepsilon_1 + 2\varepsilon_3 \qquad 2\text{-}14$$

$$\varepsilon_q = \tfrac{2}{3}\left(\varepsilon_1 - \varepsilon_3\right) \qquad 2\text{-}15$$

The original isotropic Boyce model was derived from an elastic potential which leads to the expressions of the volumetric and shear strains in equations 2-16 and 2-17:

$$\varepsilon_v = \frac{1}{K_a}\frac{p^n}{p_a^{n-1}}\left[1+\frac{(n-1)K_a}{6G_a}\left(\frac{q}{p}\right)^2\right] \tag{2-16}$$

$$\varepsilon_q = \frac{1}{3G_a}\frac{p^n}{p_a^{n-1}}\frac{q}{p} \tag{2-17}$$

Where:

	p	= mean normal stress (volumetric stress component)
	q	= deviatoric stress (shear stress component)
	ε_v	= volumetric strain
	ε_q	= shear strain component
	$\sigma_1, \sigma_2, \sigma_3$	= principal stresses
	$\varepsilon_1, \varepsilon_2, \varepsilon_3$	= principal strains
	K_a, G_a, n	= model parameters
	K_a	= Bulk modulus
	G_a	= Shear modulus
	p_a	= reference pressure = 100 kPa

The advantage of this model is that it simulates correctly the effect of the stress path q/p on the resilient behavior i.e. dilatancy for high values of q/p [57]. Sweere [13] recognized that this model can predict the results from both constant confining pressure and variable confining pressure triaxial tests. However, Sweere [13] noted that the model performs poor in predicting the volumetric strain due to the rigid condition set by Boyce for his model to be truly elastic. Therefore he modified the model by removing a requirement of reciprocity relation between volumetric and shear stresses and strains. He obtained a model containing independent relationships between ε_v and p and q on the one hand and ε_q and p and q on the other hand. However, this model contains five independent material parameters rather than three.

On the other hand, a special type of anisotropy known as cross-anisotropy is commonly observed in pavement UGMs due to stratification, compaction, and applied wheel loading in the vertical direction [58]. Resilient (elastic) pavement responses are primarily affected by this kind of directional dependency of stiffnesses.

Experimental results obtained by Desai et al. [59] substantiated the observed cross-anisotropic aggregate behavior. In a comprehensive laboratory study, Desai et al. [59] tested three uniform sized aggregates using a true triaxial testing device. In each test, the material was spooned into a cubical mold and then compacted by vibration in the vertical z-direction. An apparent deviation from isotropy was exhibited by the test specimens as obtained from the cyclic hydrostatic compression tests. This was attributed to both material anisotropy and specimen preparation with the lowest strains measured in the vertical direction of compaction. The strains measured in the horizontal plane, i.e. x- and y-directions, were typically similar in magnitude.

Moreover, experiments conducted in South Africa using an innovative K-mold test device (see section 2.4.2.2) on granular materials also showed lower horizontal aggregate stiffnesses and hence similar anisotropic behavior [60].

To account for this anisotropic nature of granular materials in pavements (anisotropy between the vertical direction and the horizontal ones) a generalized Boyce model for an anisotropic material was developed by Hornych [55, 57, 61]. The anisotropy is introduced by multiplying the principal stress σ_1 by a coefficient of anisotropy, γ, in the expression of the elastic potential which leads to the stress-strain relationships as in equation 2-18 and 2-19:

$$\varepsilon_v = \frac{p^{*n}}{p_a^{n-1}}\left[\frac{\gamma+2}{3K_a} + \frac{(n-1)}{18G_a}(\gamma+2)\left(\frac{q^*}{p^*}\right)^2 + \frac{\gamma-1}{3G_a}\left(\frac{q^*}{p^*}\right)\right] \qquad \text{2-18}$$

$$\varepsilon_q = \frac{2}{3}\frac{p^{*n}}{p_a^{n-1}}\left[\frac{\gamma-1}{3K_a} + \frac{(n-1)}{18G_a}(\gamma-1)\left(\frac{q^*}{p^*}\right)^2 + \frac{2\gamma+1}{6G_a}\left(\frac{q^*}{p^*}\right)\right] \qquad \text{2-19}$$

Where: γ = coefficient of anisotropy
p^* = modified mean normal stress = $(\gamma\sigma_1+2\sigma_3)/3$
q^* = modified shear stress = $(\gamma\sigma_1 - \sigma_3)$

Hornych et al. [57] reported that the generalized anisotropic Boyce model describes both the volumetric and shear strains quite well, see Figure 2.10, with good correlation index.

When modeling of resilient deformation behavior in section 4.5, the generalized four parameter cross-anisotropic Boyce model will be used along with the M_r-θ, Uzan and TU Delft models.

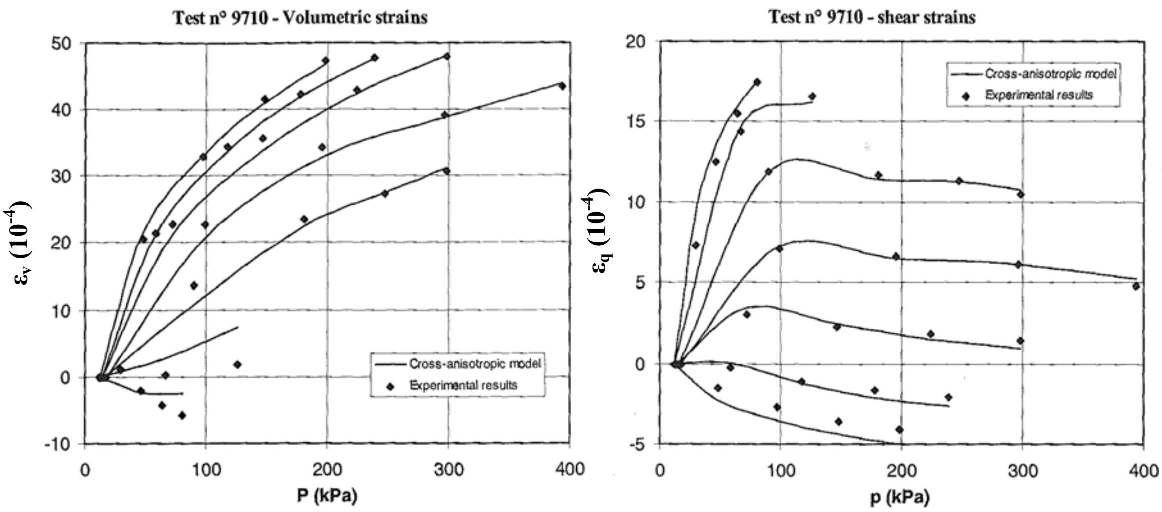

Figure 2.10 Example of fit obtained with Boyce anisotropic model [57]

2.3.1.2 Permanent deformation behavior

Permanent deformations represent the non-recoverable part of the deformations. Rutting is the most common damage caused by permanent deformations in UGLs.

Many researchers [13, 52, 62] have reported that the accumulation rate of permanent strain under repeated loading decreases with the number of load reputations. Barksdale [62] performed a comprehensive study of the behavior of different base course materials using cyclic load triaxial tests with 10^5 load applications. He established the first well known relationship using a lognormal method between the permanent strain, ε_p, and the number of load repetitions, N, equation 2-20. Sweere [13] has modified the lognormal approach and suggests a log – log relation of the permanent axial strain and the number of load applications, equation 2-21.

$$\varepsilon_p = a + b \log N \qquad \text{2-20}$$

$$\varepsilon_p = a \cdot N^b \quad \Rightarrow \quad \log \varepsilon_p = a + b \log N \qquad \text{2-21}$$

Other researchers [63-65] have followed another approach, trying to relate permanent deformation after a given number of cycles to the applied stresses and some tried to couple the effect of both stresses and number of load cycles. Lekarp [46] summarized the research on permanent deformations in a “state-of-the-art” report. He found that the development of permanent strain was affected by several factors like stress level, principal stress reorientation, number of load applications, moisture content, stress history, density, fines content, grading and aggregate type.

Another approach is to describe the plastic (permanent deformation) behavior of UGMs by means of the shakedown approach. The concept of shakedown in materials was originally developed to describe the deformation behavior of metal in pressure vessels under cyclic loading. Later this concept has been applied to describe the plastic behavior of UGMs under cyclic loading [47].

Werkmeister et al. [66] studied the permanent deformation behavior of UGMs using the shakedown approach and reported the cyclic load triaxial test results as either shakedown range A, B, or C, Figure 2-11. Range A refers to a plastic shakedown range, where the material after a post-compaction period becomes entirely resilient with no further permanent strain. Range B is defined as an intermediate response, or plastic creep, where the high plastic strain rate observed during the first load cycles decreases to a low, nearly constant level. Range C represents the incremental collapse where the permanent strain only increases with increasing number of load applications.

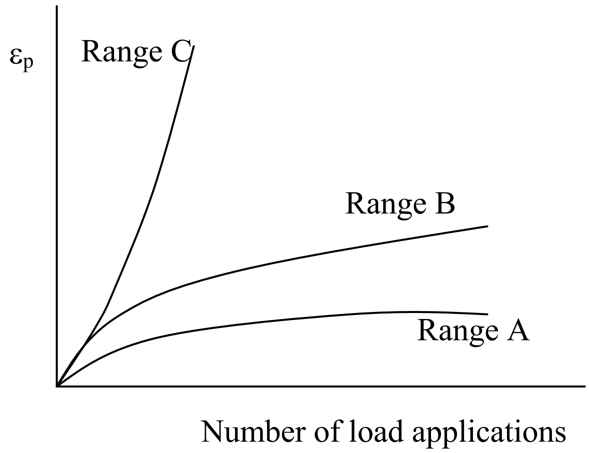

Figure 2.11 Different types of permanent deformation behavior, depending on stress level [67, 68]

2.3.2 Granular skeleton: factors affecting deformation behavior

In dealing with skeletons of granular materials the following two aspects need to be considered and need to be defined clearly. Granular material properties comprise the soil/stone grain properties and the soil/stone aggregate properties [69]. The soil/stone grain properties comprise aspects such as color, particle shape and texture, gradation, mineralogical composition, plasticity characteristics, etc. which can be considered as constant for any soil/stone over the typical service life in roads. The soil/stone aggregate properties comprise structure, density, void ratio, permeability, strength, etc., which vary with changing conditions (e.g. environmental, construction, remolding and loading etc).

2.3.2.1 Soil/stone grain properties

Gradation (Particle size distribution)

The gradation of UGMs as used in pavements is critical to the performance of the pavement structure. The earliest attempts at specifying materials for roads made use of simple breakdowns of the material in terms of a size-related classification [70]. Various performance-related studies and laboratory investigations have confirmed the importance of gradation in allowing compaction to be effected with the least effort and in ensuring interlock and a tight configuration of the soil particles in service [71].

Thom and Brown [43] studied the behavior of crushed limestone-material at different grading and arrived at the conclusion that the stiffness and resistance to permanent deformation decreased with increasing fines content. This could be explained by the presence of an amount of fines that is larger than the pore spaces between the large particles and thus hinders full particle to particle contact, Figure 2.12 (c). As a result the resistance against permanent deformation and stiffness decreases.

(a) no fines (b) enough fines (c) excess fines

Figure 2.12 Three physical states of aggregate mixtures [72]

By testing UGMs with gradations that follow the upper, middle and lower German Specification, Werkmeister [68] confidently concluded that the grading (within the limits tested) does not affect the deformation behavior of UGMs significantly. A grading closer to the lower limit should be ideally selected, to guarantee good water permeability and to avoid high moisture contents within the UGLs in a pavement construction.

However, Van Niekerk [37] recognized that UGMs with a more balanced grading perform better than the more uniformly graded materials. Araya [38] has also shown the significant influence of grading on the resistance to permanent deformation (see Figure 2.5).

Studies [73-75] have also shown that the performance of granular materials is significantly impacted by the aggregate's morphological properties, including particle shape, angularity, and surface texture. It is generally recognized that aggregates with equi-dimensional, angular shapes and rough surfaces increase the strength and durability of UGLs in pavements.

Grain shape and texture

Grain shape is established at three different scales: the global form, the scale of major surface features and the scale of surface roughness. Each scale reflects aspects of the formation history, and participates in determining the global behavior of the soil mass, from particle packing to mechanical response.

Two general groups can be identified with respect to grain shapes: natural aggregates that generally exhibit rounded shapes and crushed materials in which particle edges can be very sharp. The difference between the natural aggregate having rounded grains and crushed aggregate having sharp-edged grains is most significant on the permanent deformation behavior. Crushed materials are likely to have more grain abrasion, thus high resistance to permanent deformation, than the natural aggregates, especially at high stresses.

Hicks and Monismith [48] reported that the resilient modulus was higher for a crushed material than for a partially crushed material regardless of the aggregate gradation. Allen and Thompson [76] and Barksdale and Itani [73] found that the resilient modulus was higher for the crushed rock, than for gravel. These were all well-graded materials. Barksdale and Itani [73] also found that the gravel was more than two times more susceptible to rutting than the crushed aggregates.

In contrast Uthus et al. [77] reported that at high stress levels the resilient modulus curves for cubical crushed materials seem to level off, while rounded aggregates have much steeper curves and seem to give steadily increasing resilient moduli with increasing bulk stresses. This was also highlighted previously by Janoo and Bayer [52] who found that the angularity of aggregates had a considerable influence on the resilient modulus. Natural gravel gave higher resilient modulus properties than crushed materials prepared and tested at about the same density levels. This was explained by the ability of rounded gravel particles to better rearrange, in some cases to more stable structures.

On the other hand, Janoo [78] concluded from a laboratory study of unbound material that rounded particles caused significantly higher permanent deformations over time than angular aggregate particles when subjected to cyclic loading. In general it was found that rounded particles were able to slip easily, whereas angular materials had to overcome higher frictional forces at the contact interfaces. From this it was concluded that the angle of internal friction, and thereby the resistance against permanent deformation, increases with increasing angularity.

2.3.2.2 Soil/stone aggregate condition properties

Apart from the material's physical properties, the work of Proctor and others [71] showed that factors such as the moisture content, the magnitude and the manner in which the compactive effort was being applied, as well as the reactive support of the underlying material during the compaction process all had an important influence on the results that could be achieved.

Resilient behavior of UGMs has been found to be very sensitive to moisture content, density and stress level to which the material is exposed. Many studies have reported relationships between resilient behavior and other material properties. Thompson and Robnett [79] conducted an extensive study of resilient properties of Illinois soils. Rada and Witczak [80] presented a comprehensive evaluation of variables that influence the resilient modulus response of granular materials.

Moisture content

Water in a pavement structure has its origin from many sources; groundwater, surface water migrating through the shoulder, ditches or through cracks in the paved surface of the road. In many roads in developing countries the ditches are very shallow and in some cases the drainage system is not designed for large amounts of surface water, so due to the high intensity tropical rain the water level in the ditches may rise and penetrate into the pavement structure.

Water is a polar material, which means that the molecules have a definite positive and negative direction. This makes the molecules able to combine with the minerals in the aggregate surface. Water also tends to migrate into the layer's pore system by capillary attraction if the pores are small enough, which is related to the grain size distribution of the material and the amount of fines.

The water film on the surface of the grains influences the shear resistance. The occurrence of a moderate amount of moisture benefits the strength and the stress and strain behavior of UGMs. Having achieved total saturation, repeated load applications may lead to the development of positive pore water pressure. Excessive pore water pressure reduces the effective stress, resulting in diminishing deformation resistance of the material. Thus a high water content within an UGL causes a reduction in stiffness and hence deformation resistance of the layer.

Many researchers have studied the effect of water on the resilient modulus. Hicks and Monismith [48] reported an apparent reduction in resilient modulus with increasing water content. Barksdale and Itani [73] observed a significant decrease in resilient modulus for four materials tested upon soaking. All samples were run under drained conditions. Raad et al. [81]

concluded that the effect of water on the resilient properties seemed to be most significant in well-graded materials with a high amount of fines.

Through an extensive laboratory investigation into the influence of water on sand, granular base course material and tropical laterites, Sweere [13] has reached to the conclusion that moisture has a significant role in the stiffness behavior of granular materials. Laterites containing an excess of fines, having a structure of a matrix of fines with coarse particles floating in it similar to Figure 2.12 (c), were shown to have a moisture dependent stiffness. Other laterites, with a grading closer to the Fuller-curve and thus consisting of a skeleton of coarse particles, were shown to be far less moisture dependent with respect to their stiffness. The behavior of sands in this investigation upon change in moisture content was consistent with the skeleton-type of structure; the stiffness which is mainly derived from the skeleton itself was hardly dependent on the water content.

In the same study Sweere [13] found, surprisingly, for both a fine graded and a coarse graded crushed rock material a marked moisture dependent stiffness Figure 2.13. The stiffness of the fine graded material was more dependent on moisture than the stiffness of the coarse graded material, which is consistent with expectation. In general the effect of water on the behavior of granular materials is greatly related with the amount and nature of the fines.

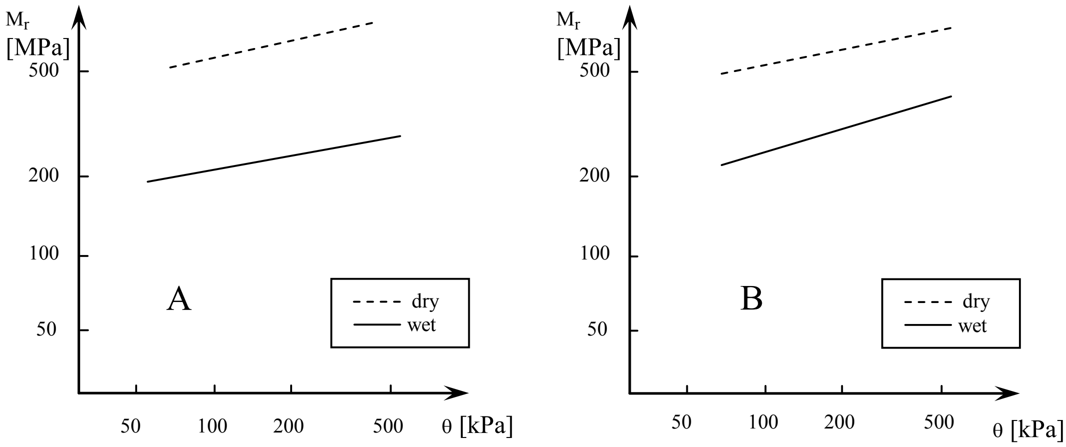

dry = degree of saturation ≈ 70%, wet = degree of saturation ≥ 90%

Figure 2.13 M_r-θ relation for crushed rock, A) fine grading and B) coarse grading, for wet and dry specimen condition [13]

Density

The density of the grain skeleton is one of the most important factors influencing the stiffness and resistance to permanent deformation. Barksdale [62] studied the effect of density on the deformation behavior of granular assemblies using cyclic load triaxial tests. He observed an increase in stiffness and resistance to permanent deformation with an increase in degree of compaction expressed as percent of maximum Proctor dry density. Similar results were obtained by Marek [82].

Hicks and Monismith [48] reported that the effect of density on the resilient modulus was greater for a partially crushed material than for a crushed material. They also found that the effect of density decreased with increasing fines content. An increasing dry density increases the shear strength of a material [43, 83]. A material having high shear strength may be more difficult to compact, as they also resist the shear stresses induced by the compaction.

Van Niekerk [37] has also investigated the influence of the degree of compaction (DOC) on the resilient modulus and resistance for permanent deformation for recycled mix granulates in 3 different gradings. He concluded that the resilient modulus in general increases significantly with increasing DOC. The rate of the increase was also found to be related to the grading. A 50%, 80% and 30% increase in modulus was observed for the upper, average and lower specification limits respectively for an increase from 97% to 105% DOC (expressed in percent maximum standard Proctor dry density). Figure 2.14 shows the increase of the resilient modulus (M_r-θ relation) with DOC for the average limit (AL) gradation after 4 days curing.

Uthus [47] showed that a well-graded material is mostly influenced by the dry density up to a certain level of fines content. The dry density of a material with a relatively high amount of fines seems to be important under dry conditions, but as the fines content increases the moisture content seems to override the effect of the dry density of the samples. For equal dry densities both the resilient and permanent deformation seems to increase as the fines content increases. Hence a high amount of fines gives a lower resilient modulus as well as lower shear strength depending on the moisture content.

The mechanical behavior of unbound granular layers in pavements is complex. A granular layer is a particulate, not a continuous medium. The response of an element of granular material in a pavement depends on its stress history and the current stress state in addition to the degree of saturation and density.

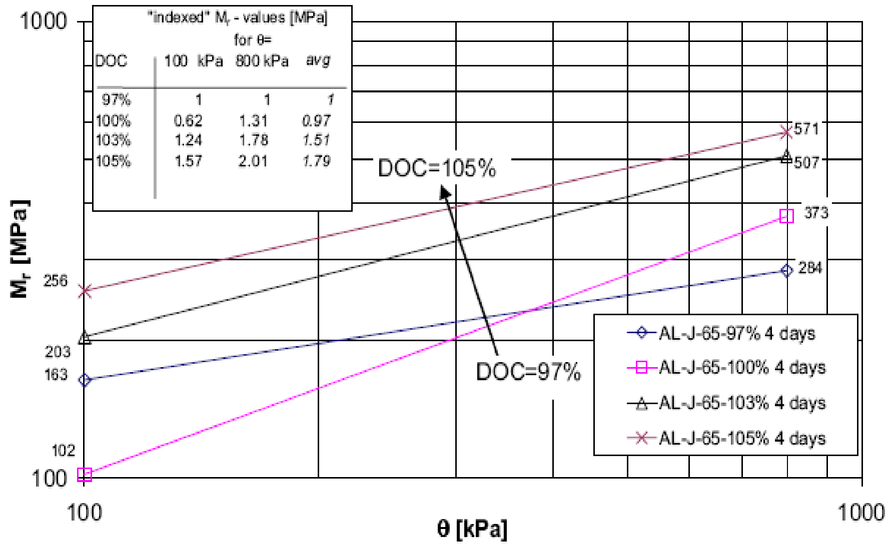

Figure 2.14 M_r –θ relation as a function of DOC for AL after 4 days curing [37]

Stress level

The response of a material to cyclic loading is very dependent on the stress level. Hicks and Monismith [48] reported that the stress level affects the resilient modulus most significantly. They found that in all cases the resilient modulus increased considerably with increasing confining stress, and slightly with increasing axial stress. Allen and Thompson [76] also found that the testing variable that affected the resilient modulus the most was the applied state of stress.

Uthus [47] also found that for all his tests the general trend is that the resilient modulus and the resistance to permanent deformation increase with an increasing mean stress and increasing confining stress. The stiffness and strength of the material tested is more dependent on the confining stress than on the deviatoric stress. The confining stress seems to be 3 to 5 times as powerful as the deviatoric one. He found it reasonable to interpret the resilient modulus as a function of mean stress or bulk stress, as the confining stress is the dominant parameter when using bulk or mean stress.

These trends mentioned above are true for relatively low load levels. However, Van Niekerk [37] has classified the loading regime into 'mild' and 'severe' loading and observed that the resilient deformation behavior is clearly influenced by the severity of loading. For his recycled crush concrete and masonry mix granulates developed granulate bonds are much more damaged under severe loading than under mild loading. For these materials the M_r-θ relations obtained under mild loading lay higher than those under severe loading.

2.4 CHARACTERIZATION OF UNBOUND GRANULAR MATERIALS

Characterization of pavement materials is a key requirement for the pavement design process. For the mechanistic-empirical pavement design process the characterization task involves obtaining material properties that identify the material response to external stimuli of pavement loading and environmental conditions.

2.4.1 Pavement loadings

The traffic loading that a pavement sustains can be divided into two key elements namely the stress applied and the number of repetitions of that stress. For design purposes these are often simplified into the number of passes of a standard axle load expressed in units of an equivalent standard axle [59]. However, from a fundamental point of view the actual pavement loadings are more complex, as the duration, frequency and magnitude of stress applied are not necessarily consistent throughout the pavement's life [41, 84]. The deeper within the pavement, the longer the stress pulse lasts for a given vehicle travelling at the same speed. In addition, the magnitude of stress varies depending on the magnitude of the traffic loads and the properties and thickness of the overlying pavement layers.

Considering the stress regimes typically induced by a moving wheel load, pavement elements experience various combinations of horizontal (σ_h), vertical (σ_v), and shear (τ) stresses as shown in Figure 2.15 [85].

Figure 2.15 shows the variations of stresses with time under a moving wheel load. The shear stress is reversed as the load passes and there is thus a rotation of the axes of principal stress. Chan [86] demonstrated that the rotation of principal stress doesn't have a significant influence on the stiffness modulus of granular pavement materials for a given applied stress. However, this phenomenon does have a major bearing on the permanent deformation of materials [84, 86].

The ability of test equipment to reproduce the fundamental stress state under a moving wheel is discussed further under section 2.4.2. However the reproduction of the rotation of principal stresses is not essential to being able to directly measure the material's stiffness modulus. The intention of this study is also not to develop or apply a fundamental laboratory testing technique but rather to simplify the advanced testing technique in order to approximate the fundamental properties in a more practical way.

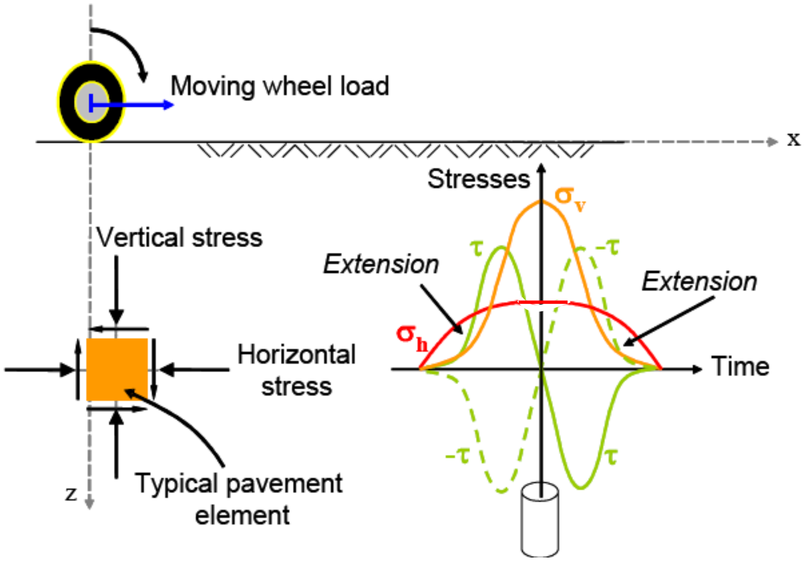

Figure 2.15 Stress regimes experienced by a pavement element under a moving wheel load [85]

2.4.2 Laboratory characterization techniques

A large number of laboratory testing techniques are presently being used to investigate compaction, bearing capacity and degradation of UGMs. Most of these tests are index tests, developed to provide input-data for empirical pavement design procedures or to provide a means of qualitative comparison of different materials. However, the fundamental material properties of UGMs cannot be derived from classification or index tests of the materials [41]. Direct measurement of those properties in-situ or within the laboratory is preferred. The main focus of this research study is on direct measurement under laboratory conditions.

A review of performance related tests of aggregates for use in unbound layers undertaken by the NCHRP [87] details the range of testing equipment available (from a US perspective) for determination of various material properties. In their assessment some of the techniques that can be used for determination of the stiffness modulus such as Hollow Cylinder Triaxial (HCT), K-mould etc appear only for shear strength measurement. On the other hand, they conclude that the shear strength of an aggregate skeleton has a much greater influence on the performance of an unbound aggregate pavement layer than any other aggregate property. Its stiffness is directly related to shear strength they agree that stiffness has a similarly large effect on performance.

In this section some of the main testing techniques that can be used to measure the stiffness modulus of UGMs will be reviewed. In addition these methods will be evaluated in terms of simplicity, affordability and availability of such techniques from developing countries perspective. Figure 2.16 shows the laboratory test methods and their stress states during testing.

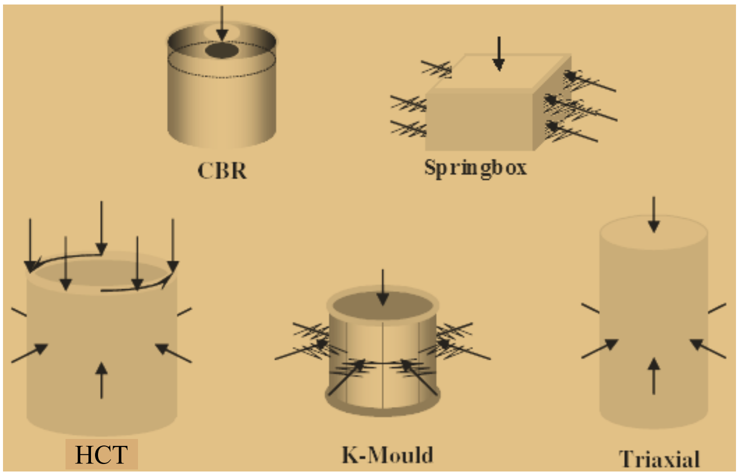

Figure 2.16 Laboratory tests showing stress states during testing [40, 84]

2.4.2.1 Hollow cylinder triaxial and cyclic load triaxial tests

Hollow cylinder triaxial

For an analytical design method, the most obvious way of measuring parameters from laboratory testing is to reproduce the loading conditions that will occur during the pavement service life. Hollow cylinder tests can replicate in a close match the complex pavement field loadings including the reversal of shear stresses. In a hollow cylinder triaxial (HCT) reversed shear stresses are simulated by applying torsion (cyclically) to a specimen shaped as a thin-walled hollow cylinder.

Tests on hollow cylinder specimens of soil were perhaps first reported by Cooling and Smith in nineteen thirties [88]. They applied torque on an unconfined specimen of soil. Since then, a number of researchers have conducted tests on hollow cylinder specimens to investigate various aspects of the mechanical behavior of soils and rocks. Saada and Baah [89] used the hollow cylinder specimen to study anisotropy in the deformation and strength of clays. Lade [90] put efforts towards the influence of stress reorientation on the stress–strain behavior of sands. Hight et al. [91] investigated the effects of principal stress rotation in soils. Seaad [92] discussed the advantages and limitations of hollow cylinder tests.

The testing apparatus usually includes an axial-torsional loading system, a confining pressure system, and a hollow cylinder triaxial cell. Three independent external stresses are applied: radial confining stress both inside and outside the specimen, axial and torsional stresses. The desired stress path is implemented through the changes in the confining pressure, axial stress, and torsional stress, Figure 2.17.

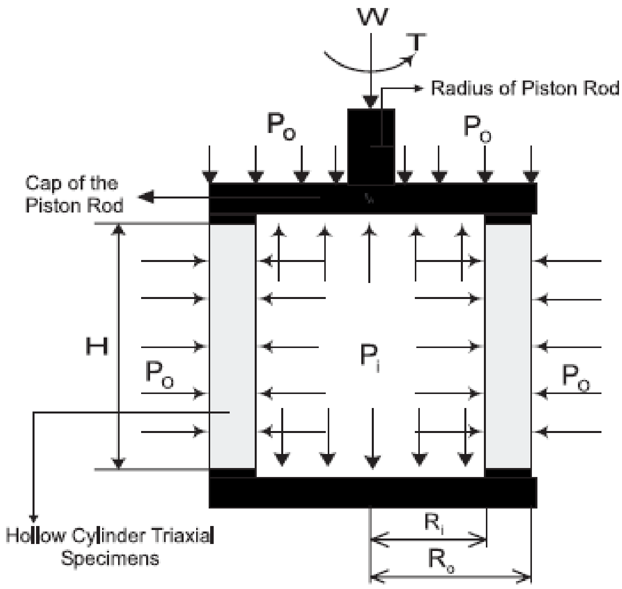

Figure 2.17 Schematic diagram of HCT and loading conditions [88]

The HCT is, however, a research tool with a number of practical limitations including complexity, availability and productivity. It is usually used for fine grained subgrade soils and sand particles; the maximum aggregate size is reported as being 12.5 mm [84]. HCT testing for fine grained materials for research application is already extremely complex, and such HCT testing for coarser grained base and subbase materials is even less feasible. The use of the relatively more accessible and simpler cyclic load triaxial test dominates most resilient modulus research.

Cyclic load triaxial

Triaxial testing was first developed for the determination of failure properties, namely the angle of internal friction and cohesion, for use in geotechnical engineering. Seed et al. [93] recognized that the monotonic slow stress increase used in such test does not necessarily give a satisfactory indication of the performance of soils under repeated loading condition. Moreover the in-service loading condition associated with granular pavement layers is likely to be well below that of failure [41]. Therefore, standard triaxial test equipment requires significant adaptations to simulate the large number of repeated loadings applied to pavement structures.

The ratio of specimen diameter to maximum particle size is another aspect that is still a topic of discussion in testing UGMs. Since most of the cyclic load triaxial equipment presently available have a specimen diameter of 150 mm or less, it only allows for testing of materials with a maximum particle size of say 25 mm as there is a general suggestion for the specimen diameter being at least 5 to 6 times the largest particle size [94-96]. Therefore triaxial tests on coarse base and subbase materials having nominal grading of, for instance, 0/50 mm or 0/63 mm are usually carried out on a so called scaled-down gradings, which means that particles larger than say 25 mm are replaced by finer particles.

The effect of scaling down the grading on the resilient behavior of UGMs has been studied at the Nottingham University and the Delft University of Technology [13, 97]. It is reported that a significant decrease in stiffness was found on reduction of the maximum grain size. Similarly, Thom [98] investigated the maximum particle size of granular materials to have a significant effect on stiffness. These results indicate that granular materials should be tested at their full grading to obtain the stiffness parameters needed for pavement design.

For that purpose a large scale triaxial testing facility is established at the Delft University of Technology in the Road and Railway Engineering Laboratory. Several researches [13, 37, 52] have been carried out with this large scale triaxial test set-up in testing coarse base and subbase materials. In this research, see chapter 4, this large scale triaxial testing (300 mm specimen diameter and 600 mm specimen height) is used to characterize the failure and resilient behavior of tropical and European coarse grained base and subbase materials.

The triaxial test is basically used for determination of a number of parameters. From the monotonic test e.g. one determines the internal angle of friction and cohesion and from the repeated load test the resilient strain and the permanent strain parameters. In the cyclic load triaxial test for establishment of the resilient and permanent deformation behavior, it is necessary to accurately measure the specimen deformations under the applied stress directions and magnitudes. This requires accurate displacement measuring devices such as linear variable displacement transducers (LVDTs) as shown in Figure 2.19.

As stated earlier, section 2.4.3, UGMs are highly stress dependent. For this reason resilient strain parameters like the resilient modulus M_r have to be determined at a number of stress levels for each material tested and these resilient characteristics of UGMs are not affected by loading history. Therefore a large number of tests for the determination of resilient parameters can be carried out on the same specimen, provided that the stresses applied are kept low enough to prevent substantial permanent volume-change of the specimen.

Permanent strains in UGMs are, on the contrary, affected significantly by the loading history [13, 37, 99]. Therefore, several triaxial specimens have to be tested to obtain the relationship between applied stress ratio and permanent deformation. Each test usually involves a large number of load applications (10^5 - 10^6) on each specimen, which renders the determination of permanent strain characteristics to be quite time-consuming.

1 specimen
2 membrane
3 specimen cap
4 specimen base
5 load cell
6 axial linear variable displacement transducers
7 radial linear variable displacement transducers
8 triaxial cell wall
9 pressure transducer
10 studs supporting the displacement transducers
11 drainage circuit

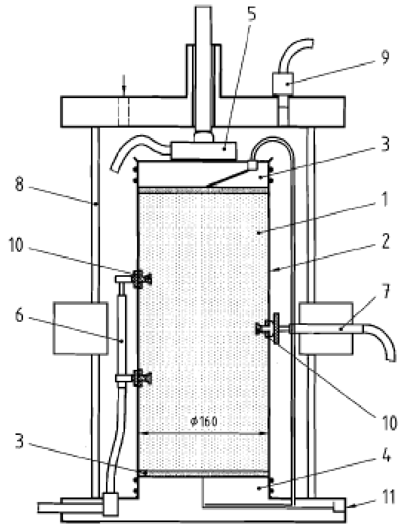

Figure 2.18 Schematic diagram of standard triaxial test measurements [95]

<u>Constant confining pressure (CCP) vs. Variable confining pressure (VCP)</u>
As shown in section 2.4.1 the lateral pressure applied to an element of material beneath the pavement gradually increases as a vehicle approaches and then decreases as the vehicle moves away. In CCP tests, it is only possible to apply one constant stress path. The VCP type test enables to apply a wide combination of stress paths by application of both a cyclic confining pressure and a cyclic vertical deviator stress. Such stress path loading tests better simulate actual field conditions, since in a pavement structure the confining stresses acting on the UGM are cyclic in nature.

In his investigation of aggregate skeletons of asphalt mixtures Muraya [100] has demonstrated the significant difference in permanent deformation resulting from the two confining methods. He has shown that for triaxial tests conducted at similar vertical to maximum (failure) stress ratios, tests conducted at cyclic confinement resulted in higher permanent deformation in comparison to the tests conducted at constant confinement.

The VCP triaxial test is considered to be a closer simulation of reality as both the constant overburden stress and the variable traffic induced increase of the horizontal stress can be simulated by applying horizontal stress by a constant component and a variable component in phase with the variable vertical stress. The major drawback of both the CCP and VCP confining stress triaxial tests is that only normal principal stresses can be applied. The shear stresses developing under a moving wheel load cannot be applied, unlike the hollow cylinder triaxial test.

<u>Advantages and limitations of cyclic triaxial testing UGMs</u>
The advantage of using cyclic triaxial systems to measure dynamic properties are widely discussed, and are primarily related to the relative capability of simulating the traffic loading actions in pavements. Compared to other methods for testing UGMs (e.g. CBR), the cyclic triaxial test is well suited. Some of the main advantages are:

- flexible load applications (amplitude, frequency, number of pulses);
- controlled confining pressure (variable or constant);
- accurate axial and radial strain measurements (permanent and resilient);
- results can be used directly in advanced material models to predict performance of UGMs in a pavement structure.

The method has also some drawbacks. The most important are:
- unable to simulate continuous rotation of principle stress directions;
- confinement is imposed by controlling externally applied confining pressure unlike the field confinement which develops as a result of resistance to material deformation and reorientation;
- unable to test undisturbed samples from the field;
- real size aggregates often require unpractical large samples for coarse materials;
- expensive and time consuming (much work required per sample);
- particularly for developing countries technically it is too complex, and too expensive to be used for routine road projects.

Many researches [84, 101, 102] have been carried out to look for an alternative characterization technique that can deliver a good estimation of the mechanical behaviors such as the resilient and shear properties of UGMs. Some of these techniques, the South African K-mould, the modified Hveem stabilometer and the Nottingham Springbox will be discussed in the next section as well as their pro's and con's.

2.4.2.2 The K-mould, modified Hveem stabilometer and springbox tests

K-mould

The K-mould was developed in South Africa by the Division of Roads and Transport Technology for rapid determination of elastic and shear properties of pavement construction materials [102]. The K-mould consists of an internal thick-walled cylinder (with an internal diameter of 152.4 mm) made up of eight equal case-hardened circular segments. Each segment is mounted on two horizontal shafts, which fit into two mounted linear ball bearings to allow each segment to move freely in a radial direction.

Semmelink [102] recognized that the main advantage of this test device is that the stiffness of the mould is infinitely variable and can therefore be adjusted to simulate the inherent lateral support of the material in its natural state. The K-mould spring plates can either be locked in place (preventing horizontal deformation of the specimen) or the specimen can be permitted to horizontally deform via the variable confinement provided by the spring plates.

The advantage of the K-mould compared to triaxial test is that it is more productive (in terms of ease of test set-up and instrumentation). The test only requires one specimen to determine a Mohr coulomb envelope and all the elastic and shear properties can be determined for each specimen. Moreover, the confining stress developed in such mechanism is close to the reality in the field. That is the confining stress in K-mould test is a result of material deformation and reorientation.

Disadvantages of the K-mould as recognized by Van Niekerk [37] are its present limited specimen height to diameter ratio and the fact that the rigid steel wall segments and springs result in a uniform deformation and thus most likely a non-uniform horizontal stress over the height of the specimen. Edward [84] has also noticed the complex construction of the segmented mould as main disadvantage.

Modified Hveem stabilometer

Ter Huerne [103] has also modified the Hveem stabilometer (HSM) in order to simulate hot mix asphalt mixtures compaction. In Hveem stabilometer the radial confining pressure on the sample occurs due to radial deformation, which is more or less identical to the way the radial stress develops during compaction under field conditions. The fundamental concept behind the Hveem stabilometer was that the characterization of a granular based material could be achieved by measuring its ability to carry a reasonable axial load without too much radial deformation [104]. However, in its standard form it does not have adequate control of the sample volume. To achieve accuracy on volume control over the sample and make the confining stress adjustable Ter Huerne [103] has modified the stabilometer.

The basic principles of the modified Hveem stabilometer (MHSM) are the same as the Hveem stabilometer; a vertical loading on the sample generates a radial displacement and this radial deformation generates a radial confining stress on the sample. Due to the modification, the confinement stress strain relationship on the sample is now approximately linear and the radial expansion volume can be measured accurately. The MHSM test provides the axial loading, axial deformation, radial stress and radial displacement. From these the axial and radial stresses and strains can be determined and the Voids in Mineral Aggregates (VMA) of the mixture can be derived to characterize the material behavior at any stage of the test.

A small uncertainty during the test is the way the sample deforms radially. For calculating the radial deformation from the piston displacement the assumption of homogeneous radial deformation of the sample was made i.e. no barreling. Laboratory measurements, however, indicated that little barreling did occur i.e. the diameter in the middle is 2 to 3% larger than the diameter at the top and the bottom of the sample which will have a small error on the calculated radial strains.

Springbox

A new laboratory test equipment known as 'Springbox' [84] was developed at Scott Wilson Pavement Engineering Limited for the characterization of unbound and weak hydraulically bound mixtures under repeated loading. It is basically based around the principle of a variable confinement test (self controlled), similar to the South African K-Mould.

The Springbox specimen is a cube with dimensions of 170 mm. The mould consists of a pair of horizontal faces, which are spring-supported and thus permit a horizontal strain, and the other pair fixed. The form of test is therefore to apply a vertical pulsed load to the full upper surface of the specimen, and recording both the vertical displacement and the displacement in the movable horizontal direction. A schematic representation along the longitudinal section of the Springbox mould is shown in Figure 2.19.

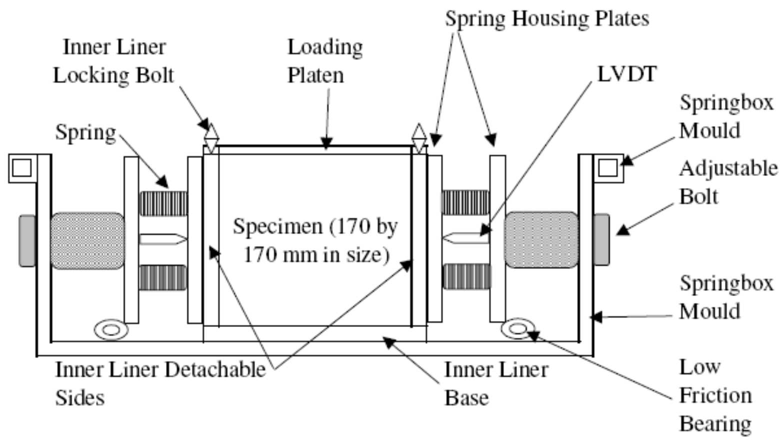

Figure 2.19 Longitudinal section through the Springbox apparatus [84]

The fact that the horizontal stress is not controlled but develops as a result of the vertical deformation is considered to be as an advantage in terms of simplicity of equipment and execution of testing. An important aspect of such apparatuses is however that the confinement is dependent on the spring stiffness characteristics of the apparatus. Another limitation for application of such testing apparatus, particularly in developing countries, is its complexity and the fact that it has been designed for use within the Nottingham Asphalt Tester (NAT) loading frame which is not available in these countries.

2.4.2.3 CBR and repeated load CBR tests

California Bearing Ratio

The California Bearing Ratio (CBR) test is a long established, very extensively applied test yielding an empirical measure of the quality of granular road materials. The CBR-test was developed initially for the evaluation of the laboratory and in-situ subgrade strength. Presently, the laboratory CBR-test is used throughout the world as a quick means of characterizing qualitatively the bearing capacity of soils and unbound base and subbase materials. The CBR-value still is an input value to many pavement design procedures, such as AASHTO [3] and TRRL [4] design methods.

The test is a penetration test in which a plunger with a cross sectional area of 1935 mm^2 (49.63 mm dia.) is pushed with a constant 1.27 mm/min displacement rate into a sample contained in a steel cylinder with a diameter of 152.4 mm (6 inch). Although vast experience is built up with this specific test it is actually at best a strength test which gives some information on the shear resistance of the material in relation to its degree of compaction and moisture content.

The CBR value is determined on the basis of the force F_a at 2.54 mm (0.1 inch) penetration, CBR_1, and the force F_b at 5.08 mm (0.2 inch) penetration, CBR_2, using equation 2-22.

$$\begin{aligned} CBR_1 &= \frac{F_a}{1935 * 6.9} * 100\% \\ CBR_2 &= \frac{F_b}{1935 * 10.3} * 100\% \end{aligned} \qquad 2\text{-}22$$

Where:

F_a, F_b = force at 2.54 and 5.08 mm penetration respectively [N]
1935 = surface of the load area [mm^2]
6.9 = contact stress on a standard sample of crushed rock at 2.54 mm penetration [MPa]
10.3 = contact stress on a standard sample of crushed rock at 5.08 mm penetration [MPa]

According to the European standard [60] the CBR value of the material is the higher percentage of the two, in most cases CBR_1 is larger than CBR_2.

In testing unbound granular materials problems arise regarding the ratio of mould and plunger dimensions to maximum particle size of the material to be tested. If for instance, the CBR-test is performed on a 0/45 mm graded material, the diameter of the CBR-plunger and the largest particles would be almost equal. The rigid CBR-mould of 152.4 mm internal diameter gives an unknown and uncontrollable confining stress to the material specimen. To avoid such problems, test specifications often prescribe removal of coarse particles from the test material. In case of coarse graded materials, this removal leads to testing of a material having a grading which differs substantially from the original material which influences the parameters to be measured.

Because of its longtime worldwide use, the CBR-test is also being used to obtain material stiffness parameters for input to analytical design procedures. Since these procedures require fundamental material properties like elastic modulus, E, for input, several empirical correlations between E and CBR have been developed. Sweere [13] noted, however, that deformation occurring in the CBR-specimen is a combination of elastic and plastic deformation. Since these two types of deformation cannot be distinguished in the test and since the ratio of elastic to plastic deformation may differ from one material to another, the standard CBR-test is unsuited for determination of a purely elastic parameter like an elastic modulus.

Repeated load CBR

Under loading granular materials experience deformation that is in part elastic (recoverable) and in part plastic (permanent). Upon multiple repetitions of the same magnitude of loading the material comes to a state in which almost all deformation under a load application is recoverable.

The principle of the repeated load CBR (RL-CBR) test is similar to the standard CBR test but repeated loads are applied until a stabilized state is reached. As reported by different researchers [37, 105-110] the test procedure is straight forward. A CBR test sample is prepared according to the prevailing specifications (AASHTO, BS, EN etc.). Then the CBR test is performed until a penetration of 2.54 mm is obtained. After that the sample is unloaded until the load is zero and then reloaded again until the load that was needed to obtain the 2.54 mm penetration. This sequence is applied a number of times until the elastic deformation reaches a constant value. Normally that occurs after 50 - 60 load cycles.

Opiyo [109] has developed empirical equations to estimate the E-modulus from the applied stress (σ_o), average plunger stress, and the measured vertical resilient (recoverable) deformation (u) in the final load application. He derived two methods to compute the E-modulus: an approximate solution and a solution based on finite element (FE) analyses.

For the approximate solution an assumption is made by Opiyo [109] about how the load is spread over the height of the CBR sample. In that case an estimate has to be made about the angle of load spreading, α. It was assumed that the elastic deformation (u) occurs in two parts of the specimen: a conical and a cylindrical part see Figure 2.20. The total deformation is therefore taken as the sum of elastic deformation from the two parts, equation 2-23.

$$u = \frac{\sigma_o \cdot H \cdot d}{E \cdot D} + \frac{\sigma_o \cdot d^2 (L - H)}{E \cdot D^2} \Rightarrow E = \frac{\sigma_o \cdot d}{u.D}\left[H + \frac{d(L-H)}{D}\right] \qquad 2\text{-}23$$

Where:	u	= elastic deformation	[mm]
	σ_o	= average stress under plunger	[MPa]

d	= plunger diameter = 49.63	[mm]
H	= height of the conical part	[mm]
E	= material elastic modulus	[MPa]
D	= diameter of the CBR mould	[mm]
L	= height of specimen	[mm]

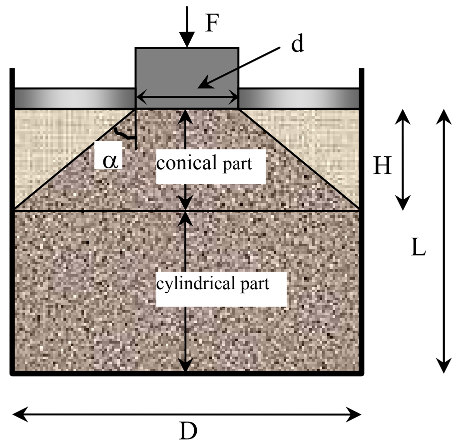

Figure 2.20 Conical and cylindrical deformation parts in the approximate solution of the CBR test

From the finite element (FE) analyses Opiyo computed the magnitude of the deformations of the CBR plunger under applied load assuming linear elastic behavior of the material. His analysis covers a range of stiffness (E) values of 50, 200 and 400 MPa and a range of Poisson's ratio values of 0.35, 0.45 and 0.49. These computations were performed for two extreme cases assuming no-friction and full-friction between the material and the mould. From these analyses equations could be developed, by means of regression, between the elastic modulus of the material tested on one hand and the load and elastic deformation on the other. This relationship is shown in equation 2-24 and 2-25.

No-friction $$E = \frac{1.797(1-\nu^{0.889})\sigma_o\left(\frac{d}{2}\right)}{u^{1.098}}$$ 2-24

Full-friction $$E = \frac{1.375(1-\nu^{1.286})\sigma_o\left(\frac{d}{2}\right)}{u^{1.086}}$$ 2-25

The limitation of this characterization technique to estimate the stiffness modulus at the current state is that to use the approximate method one has to estimate the angle of load spreading, α, and for the FE method one has to specify the friction case and assume the value for the Poisson's ratio, ν.

In this research a huge amount of RL-CBR tests are performed on various coarse UGMs to investigate its suitability as a simple to perform test to estimate the stiffness modulus for base and subbase materials particularly in developing countries. The investigation is carried out on an upgraded or improved version of the CBR test set-up and verification is made by conducting extensive cyclic load triaxial testing on these materials with identical material condition, i.e. grading, degree of compaction and moisture content.

As discussed earlier in chapter 1, the main purpose of this research is to identify a relatively simple test which is capable of estimating the required mechanical properties for input into analytical pavement design, most notably the stiffness modulus, but also resistance to permanent deformation. In the next chapter 3 the approach and methodology followed in the research project in general and the method followed in upgrading and improving the RL-CBR testing will be presented.

2.5 CONCLUSIONS

Despite major advancements in layered theory of pavements and development of sophisticated analytical tools, a gap still exists between actual pavement behavior (practice) and theory.

Almost all standardized flexible pavement design procedures until some 40 years ago were empirical methods. Many countries today, particularly developing countries, still rely on such empirical methods. The disadvantage of an empirical method is that it can be applied only to a given set of environment, material and loading conditions. If these conditions are changed, the design is no longer valid, and a new method must be developed through trial and error to be conformant to the new condition.

A mechanistic-empirical (M-E) method of design is based on the mechanics of materials that relates an input, such as wheel load, to an output or pavement response, such as stresses or strains. The response values are used to predict distress from laboratory-test and field-performance data. Dependence on observed performance is necessary because theory alone has not proven sufficient to design pavements realistically.

Most existing M-E design methods use vertical compressive strain at the top of the subgrade (to minimize rutting) and horizontal tensile strain at the bottom of the asphalt layer (to minimize fatigue failure) as failure criteria. For thin-asphalt surfaced pavements, however, the unbound granular base and subbase layers are the main load bearing layers. Design methods for such pavement structures are required to incorporate performance criteria for the unbound granular layers. The performance criterion that considers the rutting and shear failure of the granular base and subbase layers needs to be characterized in terms of their mechanical parameters such as resilient modulus, permanent deformation and shear strength parameters.

The mechanical behavior of UGMs is highly dependent on material grain property and material condition but also on applied stress conditions. Stress level, moisture content and degree of compaction are some of the most important factors that highly influence the mechanical behavior of UGMs in addition to the nature (crushed or natural) and gradation. A lot of effort has been made to develop models that can describe and predict the non-linear resilient and permanent deformation behavior of unbound granular materials. Many researchers have developed models to describe the stress dependency of these behaviors through laboratory characterization.

On bases of the above summary it can be concluded that the most appropriate laboratory characterization technique, particularly for developing countries, should be evaluated in terms of provision of reasonable estimates of the UGMs mechanical parameters, simplicity and availability or affordability. The CBR test is the most widely used and long established characterization method for soils and granular materials. Although the CBR test has basically an empirical nature it is chosen in this research as a potential candidate to estimate the mechanical behavior of UGMs through repeated load application because of its widely availability, especially in developing countries.

REFERENCES

1. Elliott, R.P. and M.R. Thompson, *Mechanistic design concepts for conventional flexible pavements*. 1985, University of Illinois: Urbana, Illinois.
2. Monismith, C.L., *Evaluation of Long-Lasting Asphalt Pavement design Methodology: A Perspective*. 2004, Distinguished Lecture International Society for Asphalt Pavements; Presented at International Symposium on Design and Construction of Long Lasting Asphalt Pavements: Auburn University, Alabama.
3. De Beer, M., *Aspects of the design and behaviour of road structures incorporating lightly cementitious layers*. 1990, University of Pretoria: Pretoria, South Africa
4. Araya, A.A., *Pavement design for developing countries (PADDEC) and unbound granular materials (UGMs)*, in *Litrature review report*. 2006, Vienna University of Technology, Institute of Road Construction and Maintenance Vienna, Austria.
5. Molenaar, A.A.A. *Are there any lessons to be learned from Pavement Research?* in *Proceedings of the 8th Conference on Asphalt Pavements for Southern Africa*. 2004. Sun City, South Africa.
6. NCHRP, *Guide for Mechanistic-Empirical Design of New and Rehabilitated Pavement Structures*, in *NCHRP 1-37A*, T.R.B. National Cooperative Highway Research Program, National Research Council, Editor. 2004.
7. Porter, O.J., *Foundations for flexible pavements*. Proc. Highway Research Board, 1942. **22**: p. 100-136.
8. Davis, E.H., *The California bearing ratio method for the design of flexible roads and runways*. Géotechnique, 1949. **1**(3): p. 249-263.
9. Jameson, G.W., *Origins of AUSTROADS design procedures for granular pavements, Report ARR 292*. 1996, ARRB Transport Research Ltd.: Victoria, Australia.

10. AASHTO, *Guide for Design of Pavement Structures*. 1993, American Association of State Highway and Transportation Officials: Washington, D.C., USA.
11. AASHTO, *Guide for the Design of Pavement Structures*. 1986, American Association of State Highway and Transportation Officials: Washington D.C.
12. SPDM, *Shell pavement design manual - Asphalt pavements and overlays for road traffic*. 1978, Shell International Petroleum Co. Ltd.: London, UK.
13. Sweere, G.T.H., *Unbound Granular Base for Roads*, in *Faculty of Civil Engineering and Geosciences*. 1990, Delft University of Technology: Delft.
14. Austroads, *Pavement design - A guide to the structural design of road pavements*. 2004, Austroads: Sydney, Australia.
15. NAASRA, *Interim guide to pavement thickness design*. 1979, National Association of Austrian State Road Authorities (NAASRA): Sydney, Australia.
16. MacLean, D.J., *The application of soil mechanics to road and engineering foundations*. J. Inst. of Munic. Eng, 1954. **81**(7): p. 323-339.
17. Leigh , J.V. and D. Croney. *The current design procedure for flexible pavements in Britain*. in *3rd Int. Conf. on Structural Design of Asphalt Pavements*. 1972.
18. Potter, D.W., et al., *A basis for incorporating reliability in the Austroads pavement design procedures WD T196/014*. 1996, ARRB Transport Research: Australia.
19. Austroads, *Technical basis of Austroads pavement design guide AP-T33/04*. 2004, Austroads: Sydney, Australia.
20. Gribble, M. and J. Patrick, *Adaptation of the Austroads pavement design guide for New Zealand conditions* in 2008, Land Transport New Zealand Research Report 305, Opus, Central Laboratories Lower Hutt, New Zealand.
21. Moffat, M.A. and G.W. Jameson, *Characterization of granular material and development of a subgrade strain criterion WD R98-005*. 1998, ARRB Transport Research: Victoria, Australia.
22. TRL, *A Guide to the structural design of bitumen surfaced roads in tropical and subtropical countries*, in *ORN-31*. 1993, Overseas Center Transport Research Laboratory: Crowthorne, Berkshire, UK.
23. BS, *Methods for determination of Ten percent Fines Value (TFV)*, in *BS 812 Part -111*. 1990, Britsh Standards (BS): London, UK.
24. Parsley, L.L. and R. Robinson, *The TRRL road investment model for developing countries (RTIM2)*, in *TRRL Laboratory Report 1057*. 1982, Transport and Road Research Laboratory (TRRL): Crowthorne, UK.
25. Paterson, W.D.O., *Road deterioration and maintenance effects: models for planning and management*. The Highway Design and maintenance Standards Series. 1987: Published for the World Bank [by] the Johns Hopkins University Press, Baltimore.
26. Robinson, R. and B. Thagesen, *Road engineering for development*. Second ed. 2004, London, UK: Taylor & Francis.
27. Rolt, J., et al., *Performance of a full scale pavement design experiment in Jamaica*. Transportation Research Record, 1987. **1117**.
28. Van Vuuren, D.J., E. Otte, and W.D.O. Paterson. *The structural design of flexible pavements in South Africa*. in *the 2nd Conference on Asphalt Pavements in South Africa*. 1974. Durban, South Africa.
29. Walker, R.N., et al. *The South African mechanistic pavement design procedure*. in *the 4th International Conference on the Structural Design of Asphalt Pavements*. 1977. Ann Arbor, Michigan, USA: University of Michigan.

30. Theyse, H.L., *TRH4 Revision (1995) Phase II: Mechanistic design analysis of the pavement structures contained in the TRH4 pavement design catalogue*. 1995, Pretoria: CSIR Transportek.(Service contract report: NSC 24/2): Pretoria, South Africa.
31. Theyse, H.L., et al., *TRH4 Revision Phase I: Updating the transfer functions for the South African mechanistic design method*. 1995, Division for Roads and Transport Technology, CSIR, National Service Contract NSC24/1: Pretoria, South Africa.
32. CSRA, *TRH4: Structural design of interurban and rural road pavements*. 1985, Committee of State Road Authorities (CSRA), Department of Transport: Pretoria, South Africa.
33. Maree, J.H., *Aspects of the design and behaviour of pavements with granular base layers (in Afrikaans)*. 1982, University of Pretoria: Pretoria, South Africa.
34. Theyse, H.L., M. De Beer, and F.C. Rust, *Overview of South African mechanistic pavement design method.* Transportation Research Record: Journal of the Transportation Research Board, 1996. **1539**(-1): p. 6-17.
35. Maree, J.H. and C.R. Freeme, *The Mechanistic Design Method Used to Evaluate the Pavement Structures in the Catalogue of the Draft TRH4 1980*. 1981, National Institute for Transport and Road Research, CSIR.
36. Jooste, F.J. *A re-evaluation of some aspects of the mechanistic-empirical design approach*. in *the 8th Conference on Asphalt Pavements for South Africa (CAPSA'04)*. 2004. Sun City, South Africa.
37. Van Niekerk, A.A., *Mechanical Behavior and Performance of Granular Bases and Subbases in Pavements*, in *Road and Railway Engineering, Faculty of Civil Engineering* 2002, Delft University of Technology: Delft.
38. Araya, A.A., *Estimation of maximum strains in road bases and pavement performance prediction*, in *Transport and Road Engineering (TRE)*. 2002, International Institute for Infrastructural, Hydraulic and Environmental Engineering (IHE): Delft.
39. Van Gurp, C.A.P.M., *Characterization of seasonal influence on asphalt pavement with the use of Falling Weight Deflectometer*, in *Road and Railway Engineering, Faculty of Civil Engineering* 1995, Delft University of Technology: Delft.
40. Thom, N., J.P. Edwards, and A. Dawson, *A Practical Test for Laboratory Characterization of Pavement Foundation Materials*, in *International Center for Aggregate Research Conference (ICAR)*. 2005: Austin, Texas.
41. Brown, S.F., *36th Rankin Lecture: Soil mechanics in pavement engineering.* Géotechnique, 1996. **46**(3): p. 383-426.
42. Seed, H.C., C.C. K., and L.C. E. *Resilient Characteristics of Subgrade Soils and Their Relation to Fatigue Failures in Asphalt Pavements*. in *International Conference on the Structural Design of Asphalt Pavements*. 1962. University of Michigan.
43. Thom, N.H. and S.F. Brown, *The effect of grading and density on the mechanical properties of a crushed dolomitic limestone*, in *14th ARRB Conference*. 1988. p. 94-100.
44. Adu-Osei, A., D.N. Little, and R.L. Lytton, *Structural Characterisitics of Unbound Aggregate Bases to Meet AASHTO 2002 Design Requirements: Interim Report*. 2001, Texas Transportation Institute, The Texas A&M University System.

45. Lekarp, F., U. Isacsson, and A. Dawson, *State of the Art. I: Resilient Response of Unbound Aggregates*. Journal of Transportation Engineering, ASCE, 2000. **126**(1): p. 66-75.
46. Lekarp, F., *Resilient and Permanent Deformation Behaviour of Unbound Aggregates under Repeated Loading*. 1999, Kungliga Tekniska Högskolan (KTH): Stockholm.
47. Uthus, L., *Deformation Properties of Unbound Granular Aggregates*, in *Department of Civil and Transport Engineering*. 2007, Norwegian University of Science and Technology: Trondheim.
48. Hicks, R.G. and C.L. Monismith, *Factors Influencing the Resilient Response of Granular Materials*. Highway Research Record: Highway Research Board, 1971. **354**: p. 15-31.
49. Uzan, J. *Characterization of Granular Material*. in *Transportation Research Records 1022*. 1985. Washington DC: Transportation Research Board.
50. Kolisoja, P., *Resilient Deformation Characteristics of Granular Materials*. 1997, Tampere University of Technology: Tampere.
51. Witczak, M.W. and J. Uzan, *The Universal Airport Pavement Design System Report I of V: Granular Material Characterization*. 1988, University of Maryland, Department of Civil Engineering.
52. Huurman, M., *Permanent deformation in concrete block pavements*, in *Faculty of Civil Engineering and Geosciences*. 1997, Delft University of Technology: Delft.
53. Huurman, M., et al., *The upgraded dutch design method for concrete block road pavements*, in *Int. Conf. on Concrete Block Paving*. 2003: Sun City.
54. Hornych, P., *Prediction of permanent deformation of unbound granular materials and application to pavement modelling and design*, in *Workshop on Pavement Engineering from A Geotechnical Presp[ective-57*. 2004: Quebec, Canada.
55. Paute, J.L., P. Hornych, and J.P. Benaben. *Cyclic load triaxial testing of granular materials in the french network of Laboratoires des Ponts et Chausses (LCPC)*. in *the European Symposium Euroflex*. 1993. Lisbon, Portugal: Balkema.
56. Boyce, J.R. *A non linear model for the elastic behavior of granular materials under repeating loading*. in *Int. Symposium on Soils under Cyclic and Transient Loading*. 1980. Swansea, U.K.: Balkema.
57. Hornych, P., A. Kazai, and J.M. Piau. *Study of the resilient behaviour of unbound granular materials*. in *Bearing Capacity Roads, Railways & Airfields*. 1998. Norweigan Univ. of Science and Technology,Trondheim, Norway.
58. Tutumluer, E. and U. Seyhan, *Laboratory Determination of Anisotropic Aggregate Resilient Moduli Using a New Innovative Test Device* in *78th Annual Meeting of the Transportation Research Board Specialty Session on "Determination of Resilient Modulus for Pavement Design"*. 1999: Washington DC.
59. Desai, C.S., H.J. Siriwardane, and R. Janardhanam, *Interaction and Load Transfer in Track Support Structures, Part 2: "Testing and Constitutive Modeling of Materials and Interfaces"*. 1983, US Department of Transportation, Office of University Research: Washington D.C.
60. Semmelink, C.J. and M. de Beer. *Rapid Determination of Elastic and Shear Properties of Road-Building Materials with the K-Mould*. in *Unbound Aggregates in Roads (UNBAR4) Symposium*. 1995. Nottingham, UK.

61. Chazallon, C., P. Hornych, and S. Mouhoubi, *An elasto-plastic model for the long term behaviour modelling of unbound granular materials in flexible pavements.* International Journal of Geomechanics, ASCE, 2006. **6**(4): p. 279-289.
62. Barksdale, R.D. *Laboratory Evaluation of Rutting in Base Course Materials*. in *3rd International Conference on the Structural Design of Asphalt Pavements*. 1972. London.
63. Lashine, A.K.F., S.F. Brown, and P.S. Pell, *Dynamic properties of soils*. 1971, Department of Civil Engineering, University of Nottingham: Nottingham.
64. Lekarp, F. and A. Dawson, *Modelling permanent deformation behavior of unbound granular materials.* Construction and Building Materials, 1998. **12**(1): p. 9-18.
65. Pappin, J.W., *Characteristics of a granular material for pavement analysis*. 1979, University of Nottingham: Nottingham.
66. Werkmeister, S., A. Dawson, and F. Wellner, *Permanent Deformation Behavior of Granular Materials and the Shakedown Concept.* Transportation Research Record: Journal of the Transportation Research Board, 2001. **1757**(-1): p. 75-81.
67. Arnold, G., et al. *Serviceability design of granular pavement materials*. in *6th Int. Conf. on Bearing Capacity of Roads and Airfields*. 2002. Lisbon, Portugal.
68. Werkmeister, S., *Permanent deformation behaviour of unbound granular materials in pavement constructions*, in *Faculty of Civil Engineering*. 2003, Dresden University of Technology: Dresden.
69. Paige-Green, P., *A comparative study of the grading coefficient, a new particle size distribution parameter.* Bulletin of Engineering Geology and the Environment, 1999. **57**(3): p. 215-223.
70. Strahan, C.M., *A Study of Gravel, Top Soil and Sand-Clay Roads in Georgia.* Public Roads, 1929. **10**(7): p. 117-136.
71. Semmelink, *The effect of material properties on the compactability of some untreated roadbuilding materials*, in *Department of Civil Engineering Faculty of Engineering*. 1991, University of Pretoria: Pretoria.
72. Molenaar, A.A.A., *Road Materials I: Cohesive and Non-cohesive Soils and Unbound Granular Materials for Bases and Sub-bases in Roads*, in *Lecture Note*. 2005, Faculty of Civil Engineering and Geosciences, Delft University of Technology: Delft.
73. Barksdale, R.D. and S.Y. Itani, *Influence of aggregate shape on base behavior.* Transportation Research Record, 1989(1227).
74. Kuo, C.Y., et al., *Three-dimensional image analysis of aggregate particles from orthogonal projections.* Transportation Research Record: Journal of the Transportation Research Board, 1996. **1526**(-1): p. 98-103.
75. Molenaar, A.A.A. and M. Huurman. *Estimation of Resilient and Permanent Deformation Behavior of Granular Bases from Physical Parameters*. 2006. Atlanta, Georgia, USA: ASCE.
76. Allen, J.J. and M.R. Thompson, *Resilient Response of Granular Materials Subjected to Time-Dependent Lateral Stresses.* Transportation Research Record: Journal of Transportation Research Board 1974. **510**: p. 1-13.
77. Uthus, L., et al., *Influence of grain shape and surface texture on the deformation properties of unbound aggregates in pavements.* International Journal of Pavements, 2007. **6**(1): p. 74-87.

78. Janoo, V., *Quantification of shape, angularity, and surface texture of base course materials*. 1998, US Army Corps of Engineers, Cold Regions Research and Engineering Laboratory: Hanover, NH.
79. Thompson, M.R. and Q.L. Robnett, *Resilient properties of subgrade soils.* Transportation Engineering Journal, 1979. **105**(1): p. 71-89.
80. Rada, G. and M.W. Witczak, *Comprehensive evaluation of laboratory resilient moduli results for granular material.* Transportation Research Record, 1981. **810**: p. 23-33.
81. Raad, L., G.H. Minassian, and S. Gartin, *Characterization of saturated granular bases under repeated loads.* Transportation Research Record, 1992(1369): p. 73-73.
82. Marek, C.R. *Compaction of Graded Aggregate Bases and Subbases*. in *The American Society of Civil Engineers*. 1977.
83. Barksdale, R., *The Aggregate Handbook*. 1991, Washington DC: National Stone Assiociation.
84. Edwards, J.P., *Laboratory Characterisation of Pavement Foundation Materials*, in *Centre for Innovative and Collaborative Engineering (CICE)*. 2007, Loughborough University: Loughborough.
85. Kim, I. and E. Tutumluer, *Unbound Aggregate Rutting Models for Stress Rotations and Effects of Moving Wheel Loads.* Transportation Research Record: Journal of the Transportation Research Board, 2005. **1913**(-1): p. 41-49.
86. Chan, F.W.K., *Permanent deformation resistance of granular layers in pavements*. 1990, University of Nottingham.
87. Saeed, A., J.W. Hall Jr, and W. Barker, *Performance-related tests of aggregates for use in unbound pavement layers*. 2001, National Cooperative Highway Research Program (NCHRP): Washington DC.
88. Lee, D.H., et al., *Mechanical behavior of Tien-Liao mudstone in hollow cylinder tests.* Canadian Geotechnical Journal, 2002. **39**(3): p. 744-756.
89. Saada, A.S. and A.K. Baah. *Deformation and failure of a cross anisotropic clay under combined stresses*. in *3rd Pan-American Conference on Soil Mechanics and Foundation Engineering*. 1967. Caracas, Venezuela.
90. Lade, P.V. *Torsion shear tests on cohesionless soil*. in *5th Pan-American Conference on Soil Mechanics and Foundation Engineering*. 1975. Buenos Aires, Argentina.
91. Hight, D.W., A. Gens, and M.J. Sumes, *The development of a new hollow cylinder apparatus for investigating the effects of principal stress rotation in soils.* Géotechnique, 1983. **33**(4): p. 335-383.
92. Saada, A.S., ed. *Hollow cylinder torsional devices: their advantages and limitations, ASTM STP 977.* American Society for Testing and Materials, ed. R.T. Donaghe, R.C. Chaney, and M.L. Silver. 1988: Philadelphia, Pa. 766-795.
93. Seed, H.B., C.K. Chan, and C.L. Monismith. *Effects of repeated loading on the strength and deformation of a compacted clay*. in *Highway Research Board*. 1955.
94. AASHTO, *Standard specifications for transportation materials and methods for sampling and testing. Part 2. Methods for sampling and testing*, in *AASHTO T 274-82*. 1978, American Association of State Highway and Transportation Officials: Washington D.C.
95. CEN, *Unbound and hydraulically bound mixtures - Part 7: Cyclic load triaxial test for unbound mixtures*, in *EN 13286-7*. 2004, European Committee for Standardization (CEN): Brussels.

96. TRB, *Test procedures for characterizing dynamic stress-strain properties of pavement materials*. 1975, Transportation Research Board: Washington D.C.
97. Donbovand, J., *The results obtained from cyclic load triaxial tests*. 1987, Pavement Research Group, University of Nottingham.
98. Thom, N., *Design of road foundations*, in *Department of Civil Engineering*. 1988, University of Nottingham: Nottingham.
99. Brown, S.F. and A.F.L. Hyde, *Significance of cyclic confining stress in cyclic load triaxial testing of granular materials.* Transportation Research Record: Journal of the Transportation Research Board, 1975. **537**: p. 49-58.
100. Muraya, P.M., *Permanent Deformation of Asphalt Mixtures*, in *Road and Railway Engineering, Faculty of Civil Engineering* 2007, Delft University of Technology: Delft.
101. Handy, R.L. and D.E. Fox. *K-Tests for subgrade and base evaluation*. in *Annual Transportation Convention (ATC)*. 1987. Pretoria.
102. Semmelink, C.J., *The use of the DRTT K-mould to determine the elastic and shear properties of pavement materials*. 1991, Division of Roads and Transport Technology, CSIR: Pretoria.
103. Ter Huerne, H.L., *Compaction of Asphalt Road Pavements*, in *CT&M Department*. 2004, Universiteit Twente: Twente.
104. Hveem, F.N. and H.E. Davis, *Some concepts concerning triaxial compression testing of asphaltic paving mixtures and subgrade materials*, in *A compilation of papers Presented at the First Pacific Area National Meeting, San Francisco, 10 october 1949 and Fifty-Third Annual Meeting, Atlantic City 28 june, 1950*. 1950, ASTM: Philadelphia. p. 25-54.
105. Awaje, T.Y., *Repeated Load CBR Testing on Granular Base Course Material*, in *Faculty of Civil Engineering and Geosciences*. 2007, Delft University of Technology: Delft.
106. Bokan, G.L., *Mechanical Behavior of a Clay Subgrade Material for Mechanistic Pavement Design*, in *Faculty of Civil Engineering and Geosciences*. 2007, Delft University of Technology: Delft.
107. Molenaar, A., *Characterization of Some Tropical Soils for Road Pavements.* Transportation Research Record: Journal of the Transportation Research Board, 2007. **1989**(-1): p. 186-193.
108. Molenaar, A.A.A., *Repeated Load CBR Testing, A Simple but Effective Tool for the Characterization of Fine Soils and Unbound Materials*, in *Transportation Research Board TRB 2008 Annual Meeting* 2008: Washington DC.
109. Opiyo, T.O., *A Mechanistic Approach to Laterite-based Pavements*, in *Transport and Road Engineering (TRE)*. 1995, International Institute for Infrastructure, Hydraulic and Environment Engineering (IHE): Delft.
110. Osman, S.A., *Searching for a Fundamental Characterisation of Unbound Materials using CBR Testing*, in *Transport and Road Engineering (TRE)*. 1995, International Institute for Infrastructure, Hydraulic and Environment Engineering (IHE): Delft.

CHAPTER 3

THE RESEARCH DESIGN AND MATERIALS USED

3.1 INTRODUCTION

This research project aims to investigate, develop and validate a laboratory experimentation technique that can measure the mechanical behavior of unbound granular materials (UGMs) by using equipment commonly available in most road engineering laboratories. A research project design is useful to organize the desired activities within the research project because it states what has to be done and how it will be organized [1].

The research design is made up of two components:
a) the conceptual design: the concept or the idea; it indicates what should be achieved during the research and why;
b) the technical research method: the methodology followed in the research; this indicates how the conceptual design can be achieved, the where, the when and the how.

In addition to the research design and methodology this chapter also deals with the range of test materials used in the research and presents the preliminary material characterization carried out for these materials.

3.2 CONCEPTUAL DESIGN AND THE RESEARCH APPROACH

The literature review in chapter 2 revealed the existence of a gap between research and industry based practice in general and absence of appropriate characterization techniques for developing countries in particular. Previous laboratory characterization techniques developed for research purposes, see section 2.4, have economical and practical limitations that prevent their widespread use.

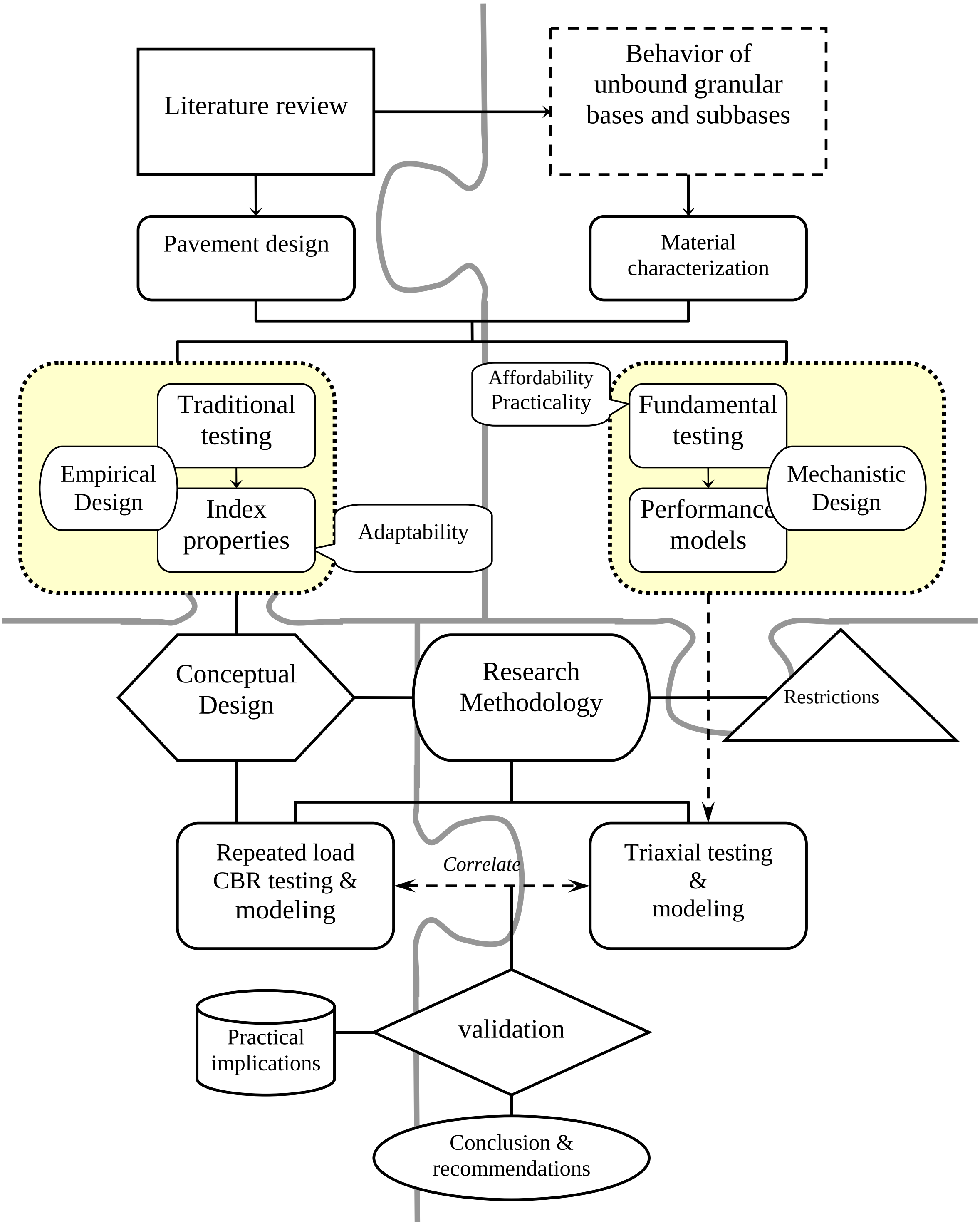

Figure 3.1 A general overview of the research approach

As Edward [2] recognized these barriers include level of complexity, skills or trainings required prior to use, availability and affordability (i.e. capital cost and cost of testing). On the other hand index tests such as CBR, being too empirical, have technical limitations to be used in the M-E design methods despite their worldwide acceptance and existence for a long time.

The research focus is therefore to develop an intermediate testing mechanism that bridges the gap between the purely empirical index tests and the advanced more complex fundamental tests which can bring mechanistic design methods into practice. The research approach, see Figure 3.1, is based on using the widespread availability and the already existing expertise and techniques as a spring board and develop a new technique in order to deliver a good estimate of the desired output.

The design or development of any new testing system requires the input and assessment of a wide range of varying considerations. Figure 3.2 shows the range of considerations that were taken forward into the conceptual design.

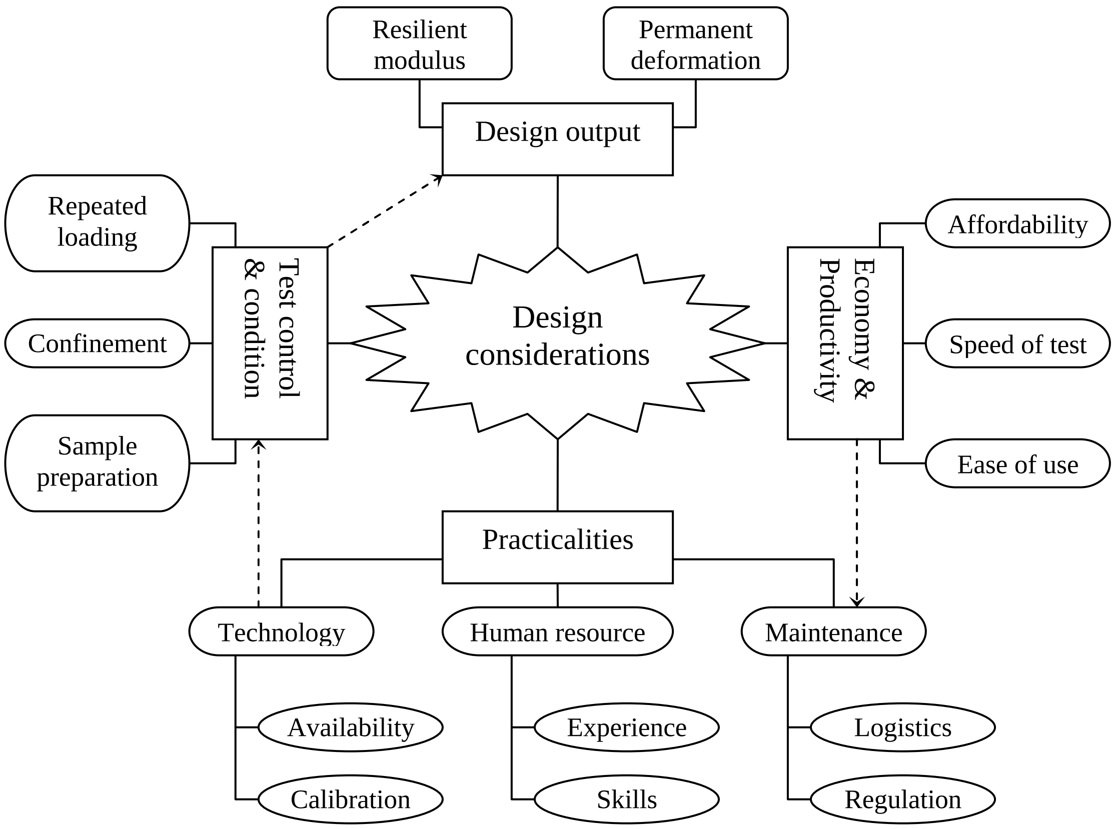

Figure 3.2 Factors and test requirements considered in the design

Some aspects of the test conditions and requirements overlap while others can be argued to be exclusive. Therefore, it was clear from the outset that any equipment design would include a degree of compromise.

3.3 RESEARCH METHODOLOGY

The research consists of three components. Firstly the fundamental behaviors of UGMs were characterized using the standard well accepted triaxial testing techniques. Then the characterization was carried out with the testing technique developed in the concept design i.e. the repeated load

CBR test. Finally this development was validated with support of finite element modeling and performance model results from the triaxial test.

The previous chapters indicate the role of granular materials in pavement structures and provide a review of testing and modeling of the mechanical behavior of granular materials. The information from these chapters and literature review provide the basis for the selection and acquisition of the materials to be investigated and on the other hand the requirements of the testing equipment and facilities to be used.

The selection and acquisition of the granular base and subbase materials used in this research are described in the next section. The experimental requirements and implication hereof for the testing equipment are described herewith.

3.3.1 Requirements for testing equipment and facilities

Two major testing equipment, the triaxial and the repeated load CBR equipment, are used in the study to characterize the mechanical behavior of UGMs. In addition some other preliminary characterization testing equipment and preparation facilities such as sieving and compaction facilities are utilized.

As the research design and approach demonstrated, this research aims to develop a new testing system that is relatively simple and which can be realistically practiced in most road engineering laboratories in general and laboratories in developing countries in particular. Moreover, in the setting up of the research methodology due consideration is taken to effectively utilize available testing equipment and facilities in the Road and Railway Engineering Laboratory (RREL) of Delft University of Technology. For this purpose most of the testing facilities such as the triaxial set-up, repeated load CBR loading frame, the vibratory compaction and large scale aggregate sieving facilities are existing facilities which are well established and developed long time ago and used by different researchers [3-5].

Characterizing the mechanical behavior of coarse grained granular material has an implication in the selection and utilization of the type of test equipment and the scale and size of the testing facilities. The materials used in the study are coarse granular base and subbase aggregates in a range of 0/45 and 0/63 mm grading. Details of the nature and characteristics of the materials are elaborated in the sections 3.4 and 3.5.

Triaxial equipment

In this research the triaxial test set-up and facilities are implemented in the same manner as has been used by Van Niekerk in his research study and the equipment description below is similar to as reported in his dissertation [5].

In chapter 2 of the literature review it is discussed to which stresses granular materials are subjected in pavements. The vertical and horizontal stresses that come from the deadweight of the overlying materials are constant at any point in the pavement. The traffic induced stresses are the variable vertical, horizontal and shear stresses which occur in a pavement as a consequence of repeated application of moving wheel loads. The variable horizontal and shear stresses develop as an element of material is loaded and deformed against the neighboring material. These stresses are thus a function of the applied stresses and of the material response or behavior.

It is further discussed that in a constant confining pressure (CCP) triaxial test it is only possible to apply a cyclic vertical stress at an adjustable but static horizontal stress. In a variable confining pressure (VCP) triaxial test it is possible to apply cyclic variable both vertical and horizontal stresses.

In a triaxial test (a true axi-symmetric triaxial) the applied vertical and horizontal stresses are by definition principal stresses. The rotation of principal stresses under a moving wheel load and the resulting shear stresses experienced by a material element in a pavement structure cannot be simulated. A CCP (cyclic load) triaxial test provides a simulation of a (repeated) circular non-moving wheel load unlike the hollow cylinder triaxial (HCT) test discussed in chapter 2. Through VCP triaxial test only a fixed orthogonal rotation of principal stress axes are possible to handle by applying radial pulse stresses exceeding the vertical ones. The HCT test is able to simulate this rotation of principal stresses or the reversed shear stresses for moving wheel loads by applying torsion (cyclically) to a specimen shaped as a thin-walled hollow cylinder.

For establishing the mechanical material behavior it is further necessary to very accurately measure specimen deformations under the applied stress directions and magnitudes. This requires measurement of deformations on the specimen over the uniformly stressed middle part of the specimen. Consequently, specimens should have a height to diameter ratio of 2 (or friction reducing measures should be applied). This requirement in combination with the requirement of having a specimen diameter to maximum grain size ratio of 5 to 10 dictates the dimensions of triaxial specimens.

In large scale CCP triaxial facilities the confining stress is often realized by applying an internal vacuum to the specimen. This greatly simplifies the equipment, but also the instrumentation of the specimen and the execution of the test. For applying the cyclic confining stress in the VCP apparatus the specimen is enclosed in a (fluid filled) cell which greatly complicates the instrumentation of the specimen and the execution of the test (specimen and instrumentation not directly accessible).

The use of the vacuum-confinement has the disadvantage that only CCP triaxial tests can be performed, since the variation of the internal sub-atmospheric pressure in the specimen is not feasible at the required frequency of, for instance, 1 Hz. Another disadvantage is that the confining stress σ_3 can be varied over a limited range only. Theoretically, σ_3 is limited to 100 kPa (absolute vacuum) but in practice it is limited to around 80 kPa. A third disadvantage of vacuum confinement lies with the fact that due to the suction of water from the specimen, in some cases it is difficult to maintain constant moisture content during long lasting tests such as permanent deformation tests.

From the reviewed literature and extensive experience in the RREL it was concluded that triaxial testing is required for establishing the mechanical behavior of the base and sub-base materials in this research. It also serves as validation reference for the newly developed repeated load CBR testing.

The large amount of triaxial tests required to establish the different types of mechanical behavior (strength, resilient and permanent deformation) in relation to the different influencing factors (material and condition related) allow for CCP testing for the coarse grained base and subbase materials. Establishing of the stress dependent mechanical behavior of the base course materials, even by CCP testing, is considered already a major improvement especially for materials from the (sub)tropics because very little information is available of the mechanical characteristics of these materials determined by triaxial testing.

The functional specifications of the triaxial facilities used in this research are given below. The reader is referred to chapter 4 for detailed descriptions of the equipment and tests.

<u>Large scale CCP triaxial apparatus</u>, Figure 3.3:

- Specimen dimensions: 300 × 600 mm (diameter × height).
- Cyclic vertical stress: wave shapes (haversine), magnitudes (up to 2000 kPa) and loading frequencies (up to 10 Hz) dependent on the type of test.
- Confining stress: applied by internal vacuum (up to 80 kPa).
- On specimen deformation measurement by means of Linear Variable Displacement Transducers (LVDTs), accuracy and measuring range dependent on the type of test.

Compaction equipment

The literature review in chapter 2 demonstrated that compaction is among the most important condition related influence factors affecting the mechanical behavior of granular materials. Consequently the triaxial and repeated load CBR specimens needed to be tested over a wide range of degree of compaction (DOC) and the compaction mechanism was to resemble well the field compaction.

Figure 3.3 Cyclic load triaxial apparatus (300 mm specimen diameter)

Different specifications prescribe different compaction standards. In most (sub)tropical countries the degree of compaction is specified in terms of maximum modified Proctor density (MMPD). Most common ones use a target of 100% MMPD for base course materials and 95 – 98% MMPD for subbase materials. The South African standard specification [6] specifies the high quality Grade 1 (G1) and Grade 2 (G2) base course materials in terms of their apparent relative density (ARD) 86 – 88% ARD which is estimated to be equivalent to 106 – 108% MMPD [7, 8].

Therefore, to investigate and demonstrate the effect of both under and over compaction, the compaction equipment was required to compact the triaxial and RL-CBR specimens over a range of 98% to 105% (the high quality crushed stone base material) and 95% to 100% of MMPD (all the other materials except the mix granulate). The mix granulate is compacted to 97 - 105% of the standard maximum Proctor density (MPD) as shown in section 3.4.

To best simulate the field compaction of unbound granular bases and subbases and achieve the required ranges of DOC, a vibratory compaction mechanism was chosen. The vibratory compaction apparatus, Figure 3.4, in RREL of Delft University of Technology has been designed and built based on the principle of applying vibration from above to a material contained in a mould. For the detailed descriptions of the compaction apparatus, the moulds and operating procedures reference is made to chapter 4 and 5 for compaction of triaxial and RL-CBR specimens respectively.

Figure 3.4 TU Delft vibratory compactor during compaction

Repeated load CBR apparatus

The repeated load CBR test apparatus is expected to be the same as the common standard CBR test equipment. The common CBR testing devices have three buttons, "up", "stop", "down" and by pushing them in the right order, repeated loading can be achieved. This methodology has already been used and proven to be effective Opiyo [9], Osman [10] and Awaje [11]. This way of testing however is rather time consuming and because a very large number of tests has to be performed it was decided to apply the load with a multi purpose hydraulic actuator loading frame, maximum capacity 100 kN, with MTS (Material Testing System) controller, Figure 3.5. The MTS controller is convenient to maneuver and adapt to a required testing system such as the standard CBR test as well as repeated load CBR test. This testing apparatus is also equipped with a data acquisition system and PC so that test results can be digitally stored and processed.

As elaborated in chapter 2 material gradation and maximum grain size have a significant influence on the mechanical behavior of UGMs. In order to represent the in-situ material gradation and grain size in the laboratory, a large size CBR mould and a bigger penetration plunger is used for the RL-CBR. In the standard CBR mould, 152.4 mm diameter, according to the European standard [12] or ASTM standard [13] only aggregates finer than 22.4 mm or 19 mm respectively can be tested. This implies for coarse base and subbase aggregates of 0/45 mm or 0/63 mm that a significant portion of the material (according to the European standard the portion 22.4/45 or 22.4/63) has to be removed and replaced by aggregates between 5.6 and 22.4 mm. A limited study on recycled crushed masonry subbase materials [14, 15] shows a significant effect on the resilient modulus obtained from the standard CBR and larger mould sizes. Scaling down the aggregates significantly affects the mechanical behavior of the material not only by the change of the maximum grain size but also by a complete change of the gradation.

The repeated load CBR test is upgraded into a large scale RL-CBR by manufacturing the extra large mould size, referred as mould C in the European standard [16] i.e. 250 mm diameter and 200 mm height with an extension collar of 75 mm for the research to avoid downgrading of these coarse materials and represent their full gradation as used in the field. Moreover the size of the penetration plunger is changed to a larger size i.e. its diameter d_2 to 81.5 mm so that the ratio of plunger penetration area to mould area will be constant for both the standard CBR and RL-CBR test set-ups, see equation 3-1 and Figure 3.6.

Figure 3.5 RL-CBR loading actuator (left), mould & plunger (right-top) and MTS controller (right-bottom)

$$\frac{d_1}{D_1} = \frac{d_2}{D_2} \qquad \text{3-1}$$

Where:	d_1	= standard CBR plunger diameter	= 49.64 mm
	D_1	= standard CBR mould diameter	= 152.4 mm
	d_2	= RL-CBR plunger diameter	= 81.5 mm
	D_2	= RL-CBR mould diameter	= 250 mm

In the second part of the repeated load CBR testing strain gauges were glued at the external surface of the mould to measure the tangential strain of the mould during the testing. This tangential strain deformation of the mould gives an indication of the lateral confinement developed by the mould in response to the loading. Further detailed descriptions of the test principle, testing facilities and methods followed are presented in chapter 5. It is recognized that although gluing strain gauges to the mould allows obtaining more information, it also makes the test more complicated and less attractive for use in simple laboratories.

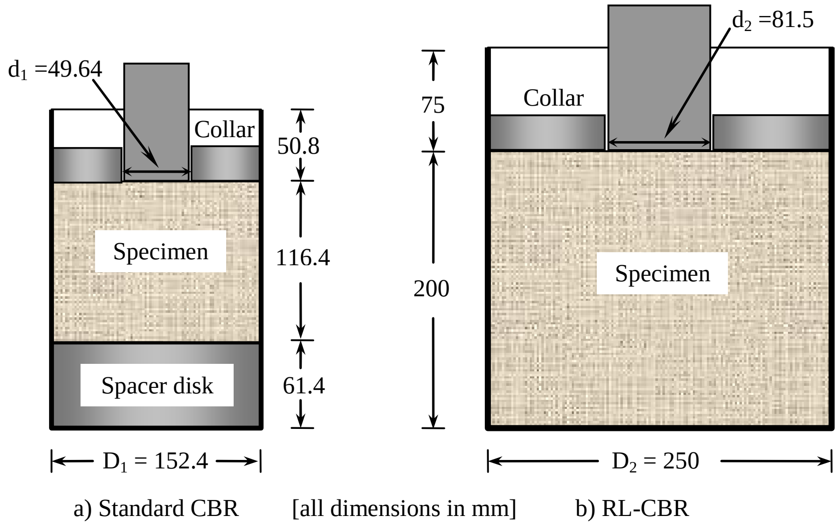

Figure 3.6 Standard CBR and adopted RL-CBR mould & plunger

Compaction of RL-CBR Specimen

The compaction method and equipment used to prepare the RL-CBR specimens is similar to the one used to compact the triaxial specimens. The same vibratory compactor is used by modifying only the head of the compaction to fit into the RL-CBR mould. The vibratory compactor was first designed to compact a 300 mm diameter triaxial specimen with a full face compaction plate. A similar compaction head is designed to fit into the 250 mm diameter RL-CBR mould with a full face compaction plate so that the same compaction machine can be used.

Other compaction methods have also been considered during the study, such as:

i) Compaction by vibrating table – where a mould containing the material is placed on a vibrating table while a full face force, deadweight mass, is applied to the top of the specimen to prevent segregation and de-densification. The amplitude, frequency and duration of the vibration can be controlled.
ii) Compaction under the actuator of the triaxial facilities – where specimens can be compacted by applying a compression load with dynamic and/or static components through the triaxial actuator of which the magnitude of load, frequency of the dynamic load cycles and duration can be controlled.
iii) Compaction by means of a Kango-hammer – where specimens can be compacted through a manually operating vibrating Kango-hammer by means of vibration compaction; this method has been successfully applied in earlier researches by Gebre-egziabher [17], Bokan [18], Awaje [11] etc.

The compaction of the RL-CBR specimen by the vibratory compactor however is preferred for many reasons:

- trial compactions by both the vibrating table and triaxial actuator demonstrated, in line with earlier researches, that the DOC achieved is limited;
- equipment availability: new specimens cannot be compacted during long running triaxial tests, considering the extensive amount of triaxial testing in the research;
- excessive straining of the expensive triaxial equipment;
- compaction using Kango-hammer is feasible but high compaction levels are difficult to achieve in this way; furthermore this method is tedious and time consuming;
- more importantly to compact the RL-CBR specimens in the same way as the triaxial specimens, so that variation in the method of preparation is avoided for verification and comparison.

3.3.2 Experimental design

The literature review shows that the factors influencing the mechanical behavior of UGMs are:
- material grain properties such as grading, particle shape and texture, aggregate source or mineralogical composition;
- material condition properties such as moisture content, degree of compaction, stress level etc.

In order to be able to investigate the relative importance of these material properties and validate the RL-CBR testing mechanism for different materials it is necessary to consider various types of materials in the research. To this end, large quantities greatly varying base and subbase granular materials were collected and transported to the RREL from different countries as described in section 3.4.

All the material grain and condition properties are believed to have an influence on the mechanical behavior of the granular materials but not all are equally significant. Within the scope of this study the most important factors have been chosen as variables in the experimental design based on the literature review and earlier research [4, 5]. Among these aggregate source, moisture content, degree of compaction and stress level are considered as the most important factors that can be varied in the triaxial and RL-CBR experiments. An overview of the overall test program is shown in Figure 3.7. The detailed test programs for the triaxial and RL-CBR are provided in their respective chapters 4 and 5.

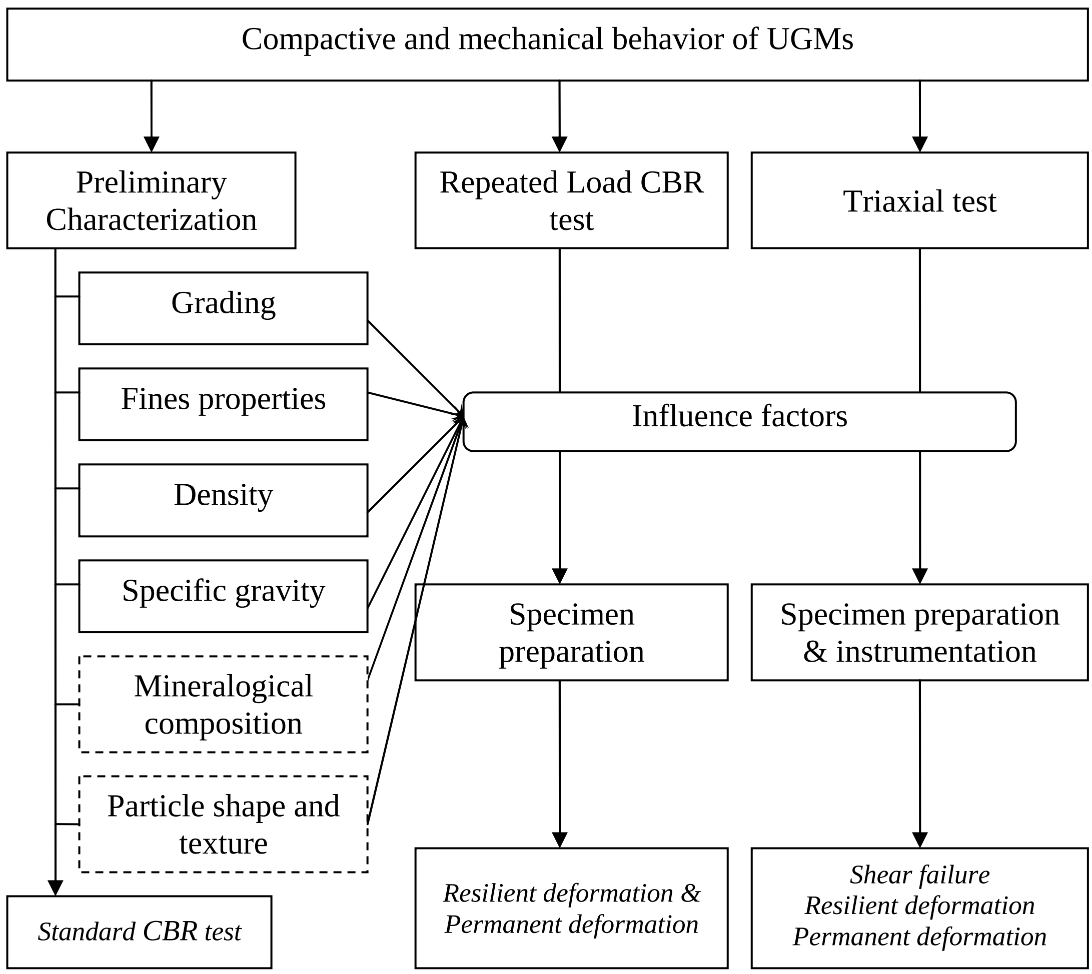

Figure 3.7 An overview of the testing program

Practical restrictions

- Permanent deformation triaxial tests are excluded from the test program later during the experimentation period, mainly due to shortage of test materials as re-shipping the main (sub)tropical materials is not practical feasible but also to complete the extensive test program within a given time frame.
- Though the gradation is also an important factor, practically it was not possible to consider the gradation as a variable for the same reasons mentioned above. However through recomposing, the grading of each specimen per material was the same, see section 3.5.1.
- Again for similar reasons the RL-CBR testing with the strain gauges is limited only to the two South African materials, i.e. the crushed stone and ferricrete.

3.4 MATERIALS USED IN TEST PROGRAM

Chapter 4 of this dissertation will deal in great detail with fundamentally sound testing techniques, i.e. both monotonic and cyclic load triaxial testing.

Following to that the proposed RL-CBR testing will be dealt within an extensive testing program in chapter 5. These two testing programs will follow the preliminary characterization testing which assesses the influencing factors as presented in the next section. To identify the most influential factors on the mechanical behavior of UGMs and more importantly to assess the applicability of the proposed RL-CBR test, a wide variation of materials are incorporated in the test program.

The materials investigated can be broadly categorized into two groups. The (sub)tropical base and subbase materials consist of weathered basalt from Ethiopia, crushed stone and ferricrete from South Africa. The second group is temperate zone road materials and consists of recycled mix granulate from the Netherlands and base course and frost protection granular material from Austria.

The main emphasis of the research described here lays with the (sub)tropical unbound granular materials for two reasons. First, although an extensive study on fundamental properties has been carried out for road materials from temperate zones, only limited studies can be found for materials from (sub)tropical zones. Second, for economical reasons the proposed RL-CBR testing is believed to be more important and highly applicable in developing countries; therefore its verification and validation based on materials from these areas is preferred.

In total about 35 tons of base and subbase granular materials were transported from the (sub)tropics to RREL Delft, the Netherlands. The origin and natural characteristics of the six materials will be described in this section and a code will be given for each material to distinguish the materials throughout this dissertation.

3.4.1 South African crushed rock

The base material, crushed from hard Hornfels rocks, is obtained from a quarry in South Africa. Hornfels are a fine-textured metamorphic rock formed by contact metamorphism [19]. The South African Hornfels is a type that is formed by contact metamorphism of a Greywacke sedimentary rock of mechanical origin. Mechanical origin refers to those sedimentary rocks that are formed by erosion of previously existing rocks (igneous or metamorphic) and their eventual deposition at some point from where they can no further be transported (lake bottoms, plains, ocean floors) [20].

The 8 ton hard crushed rock delivered from South Africa is one of the best quality road base materials that is classified as Granular class 1 crushed stone base course material according to the South African specifications [6]. The crushed rock base course aggregate is produced from a hard rock and the fines are also crushed from the same sound rock. As this material is an aggregate crushed from sound rock the particles are characterized with angular spherical shape and rough surface texture, see Figure 3.8. According to the South African specification the Granular class 1 aggregate shall not contain any deleterious material such as weathered rock, clay, shale or mica. The name of this crushed rock material from now on in this dissertation is labeled as G1 after its classification as Granular class 1 (G1) in the South African specification.

Figure 3.8 South African crushed stone as delivered in bags and material details

3.4.2 South African ferricrete

The ferricrete is a natural gravel obtained from a borrow pit in South Africa. The term ferricrete was coined by Lamplugh [21] for material cemented by iron oxides. The cement is ferruginous and the cemented material is usually iron-rich and can range from ferruginous concretions to non-ferruginous material [22]. The word ferricrete is derived from the combination of *ferruginous* and *concrete*. By this definition ferricrete can be considered as a lateritic material.

Laterite, first defined by Buchanan [23] as “a massive, vesicular or concretionary ironstone formation” is mainly found in wet tropical and sub-tropical areas. It is a group of highly weathered soils formed by the concentration of hydrated oxides of iron and aluminum. This concentration may be by residual accumulation or by solution, movement and chemical precipitation. In all cases it is the result of secondary physico-chemical processes and not of the normal primary process of sedimentation, metamorphism, volcanism or photoism [24]. The accumulated hydrated oxides are sufficiently concentrated to affect the character of the deposit in which they occur.

This iron-rich subtropical ferricrete is characterized as a mineral conglomerate consisting of surficial sand and gravel cemented into a hard mass by iron oxides derived from the oxidation of percolating solutions of iron salts. Ferricrete is widely used in South Africa as subbase material or to create roads in rural areas. It is better known in these regions by its Afrikaans name “Koffieklip” (coffee stone). The South African ferricrete is natural aggregate relatively susceptible to crushing where its particles are characterized by a porous spherical shape and rough surface texture, see

Figure 3.9. In the dissertation this material is labeled as FC after its name ferricrete (FC).

Figure 3.9 South African ferricrete as delivered in bags and material details

3.4.3 Ethiopian weathered basalt

The weathered basalt investigated in this study is a natural gravel obtained from a borrow pit in Ethiopia. Beaven et. al [25] in their study on weathering of basalt in Ethiopia presented a detailed analysis of the formation and weathering of basalt. In their study they described basalts as the most common form of volcanic rock which are widely used in the production of crushed aggregates from quarries. However, where the rock has been weakened by physical disintegration or chemical weathering basalt gravels can be dug from pits. The composition can vary both within a pit and between pits, the most important features being the size and strength of the aggregates and the quantity and plasticity of the fines.

Typical weathered basalts in Ethiopia are predominantly gravel with a low portion of sand [26]. In practice it is difficult to find materials which, when excavated, meet the specification requirements for grading. This limitation is treated by crushing the oversized cobbles, coarser than 45 mm, and mix the crushed material to the natural gravel.

The material shipped from Ethiopia to RREL Delft is from a quarry source in the Bole suburban area of Addis Ababa, Figure 3.10, used as a subbase material for a road construction project in Addis Ababa city. To satisfy the Ethiopian road material specification [27] for gradation, as explained above, the oversize cobbles are mixed with the natural gravel after run through a crusher.

The material particles are characterized by their elongated and flaky shape so that they can be easily crushed during compaction. The fine grains, which can also be influenced by the surrounding soil nature as they are dug pit material, are characterized by a high plasticity index as shown in section 3.5. This material is labeled as WB after its nature of formation i.e. from weathered basalt.

Figure 3.10 Ethiopian Weathered Basalt source and material details

3.4.4 Other materials

Austrian base course and frost protection

An Austrian limestone gravel material which is used as base course and as lower frost protection layer is also investigated to a certain extent in this research. The materials from both the base course and frost protection layers are delivered from a road project under construction. Both materials are identical in nature and characteristics i.e. both are natural gravel from the same source of weathered limestone but differ in gradation as shown in section 3.5.1.

These materials are delivered in their in-situ mix condition i.e. their gradation and moisture content as constructed. In order to protect moisture loss due to evaporation they were sealed in plastic bags of about 20 kg size each. The two types of construction materials differ by their gradation, mainly their maximum grain size i.e. the base course is 0/63 mm and the frost protection 0/32 mm as per the Austrian specification [28]. The two materials are labeled as ZKK63 and ZKK32 respectively where ZKK (Zusammensetzung Kornklassen) in German means grain composition class.

Netherlands recycled mix granulate

The Netherlands crushed concrete and crushed masonry recycled mix granulate is investigated in this study only to a limited extent in the repeated load CBR testing. Many characterization studies have already been carried out on these materials by different researchers [3-5], mainly by Van Niekerk. The purpose of including these materials in this research is basically to characterize them by the use of the RL-CBR and compare the obtained test results with the triaxial test results from Van Niekerk.

The mix granulate composition and gradation for this study is chosen based on the fact that most extensive material test data is available from Van Niekerk's PhD dissertation [5]. It is a composition of recycled crushed concrete and crushed masonry produced by impact crusher with mix proportion of 65% concrete and 35% masonry by weight as described in his dissertation. It is with gradation of average limit (AL) as used by him according to the Dutch Specification [29] for such base materials. This material is labeled in this dissertation as MG to indicate it is a mixed granulate (MG) of recycled concrete and masonry.

3.5 PRELIMINARY TESTING ON THE MATERIALS

Investigation into the basic physical properties is necessary in order to understand their basic behaviors and characteristics and establish practical methods and test conditions for other tests based on their properties. Understanding the physical properties of materials is believed to provide better understanding of the materials character in relation to density, particle and bulk strength and its behavior towards moisture, compaction and loading. For this reason, investigation of the preliminary physical properties of the materials is included in the test program.

3.5.1 Sieving and material gradation

In section 3.3 it is explained that it was perceived that one of the important influencing factors for the mechanical behavior of UGMs is the particle size distribution. The particle size distribution is traditionally determined by sieving the material through a nest of sieves with apertures typically between 63 μm and 63 mm. The actual sieve sizes used depend on the standard test method followed. In this research the European standard [30, 31] sieve sizes are adopted.

Sieving is conducted in this research for two main purposes at two different scales.

<u>Large scale sieving</u>
A large scale sieving is carried out for the three (sub)tropical materials, which are the main constituents in the research. The purpose of this sieving is to acquire and recompose an identical and consistent gradation in the entire test program of the research. For this purpose each of the three materials G1, FC and WB are sieved, using a large scale sieve apparatus, into 7 fractions: *0-2 mm, 2-4 mm, 4-8 mm, 8-16 mm, 16-22.4 mm, 22.4-31.5 mm and 31.5-45 mm*. These 7 fractions of the granular materials make it possible to manipulate the grading and compose it in a consistent way. Each time a sample is prepared for any testing the grading is composed by weighing the required portion from each of the 7 fraction sizes.

The large scale equipment, shown in Figure 3.11, was used in earlier research projects [4, 5]. The large scale sieving equipment consists of two vibrating sieving units with inclined parallel sieves with sieve sizes that range from 45 mm to 2 mm. The sieves are arranged in order of decreasing sieve size with the largest sieve being placed at the top and the smallest sieve at the bottom. The aggregates are delivered to the sieving units by means of a conveyer belt. The material storage in the laboratory after sieving is also shown in Figure 3.11.

Figure 3.11 Large scale sieving equipment [5] and storage

<u>Standard sieving</u>

Another form of sieving which is carried out is the standard sieving using a standard sieve apparatus. Its purpose is to investigate the particle size distribution of the materials received and to check whether these materials satisfy the gradation specification for their respective purpose.

Two standard methods of sieving have been used: dry sieving and wet sieving. In both cases sieve sizes within the range 0.063 – 45 mm were used. The first method is by oven-drying the sample at 110°C, then cooling to room temperature and sieve through the standard nest of sieves. The results from this dry sieving show for some of the materials that the percentage passing 0.063 mm is nearly zero. On the other hand it is observed that a significant portion of the fine fractions stick to the coarse aggregates. Therefore, the second method, wet sieving, is carried out for G1, FC and WB by saturating the aggregate in a water bath, wash and sieve through the standard nest of sieves with water. During the wet sieving 33 g/liter sodium polyphosphate crystals was mixed to the water as a dispersing agent to avoid coagulation of the fine cohesive materials. As shown in Figure 3.12 the particle size distribution between the wet and dry sieving of the three materials differs significantly in the range finer than 2 mm. Figure 3.13 shows the dry gradation of all materials used in the entire test program of the research.

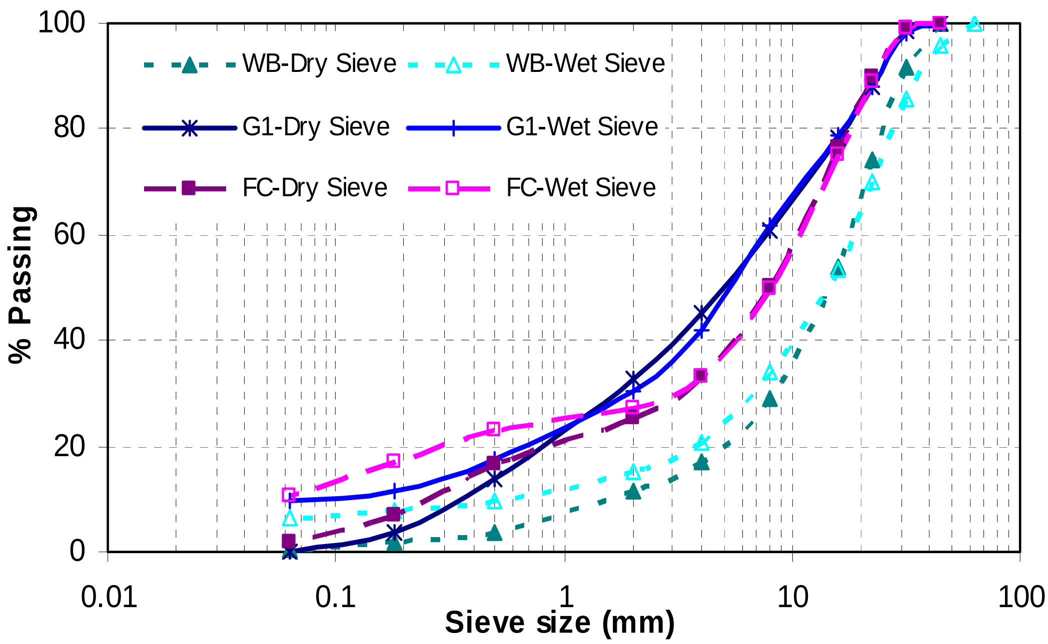

Figure 3.12 Gradation of the materials as received, dry and wet sieving

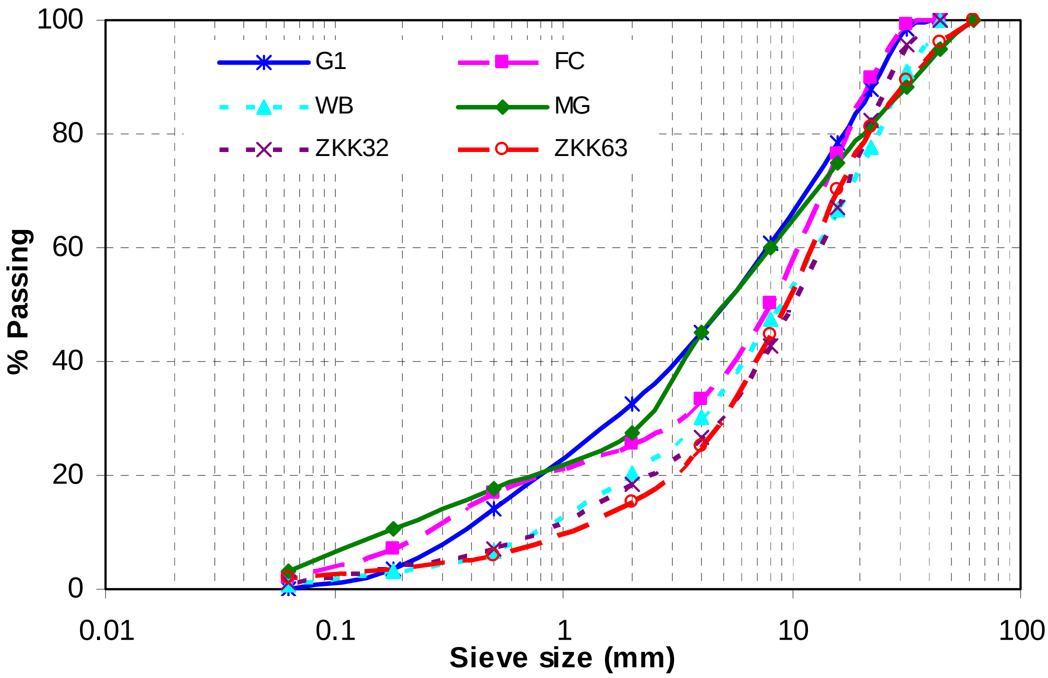

Figure 3.13 Materials gradation used in the test program, dry sieving

3.5.2 Properties of fine grains

Properties of the fine grains such as plasticity characteristics are important factors in influencing the mechanical behavior of the granular mixtures. The behavior of the fine grains in relation to the amount of water available in the system is characterized by the plasticity and water absorption properties.

Water molecules, being bi-polar, are attached to the particle surface and orient themselves on the surface like tiny magnets as shown in Figure 3.14. Adjacent to the mineral surface the water molecules are held so firmly that a layer of solid water is attached to the soil particle. As the distance from the soil-particle surface increases, the water molecules are less tightly held and form a relatively thick layer (viscous or cohesive layer) of water attached to the soil particle. This cohesive water layer between the soil particles is responsible for the plasticity of the soil [32].

The chemical and mineral composition, the size and shape of the soil particles considerably control the amount of absorbed water films on the particles. Among the factors affecting the plasticity of soil are: the clay content, platy or sheet-like nature of the soil particles, chemical composition of the colloidal, nature of exchangeable cations and organic matters.

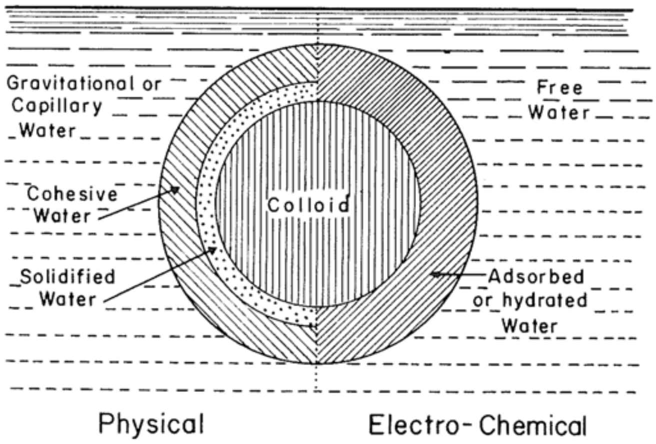

Figure 3.14 Types of soil moisture [32, 33]

Properties such as compressibility, permeability and more importantly strength are dependent on the water films and hence on the Atterberg limits. Knowledge of the Atterberg limits of the fine grain particles of the granular mixtures has been considered important in the research to characterize the plasticity of the materials. Since the fine grains of G1 are purely crushed fines from hard rock they are not expected to contain any clay minerals and have plasticity problems. Therefore, the plasticity characterization is made only for the two (sub)tropical natural gravels FC and WB.

Plasticity characteristics: Atterberg limits

The plasticity characteristics of the fine grains are evaluated from the Atterberg limits, i.e. the liquid and plastic limits and the plasticity index.

The liquid limit (LL) of the WB is determined by the 'fall cone penetration method' according to the European standard technical specification [34] using a standard cone of 80 g mass with an apex angle of 30°. The liquid limit is the moisture content that corresponds to 20 mm penetration after 5 s by free fall of the cone on a mixture. The LL is determined by drawing a line on penetration [mm] vs. moisture content [%], as shown in Figure 3.15, for three to five specimens at different moisture content.

The plastic limit (PL) is determined by rolling out a thread of the moist soil on a glass plate. Three replicate determinations are made of the minimum moisture content at which the fine grains can be rolled into a thread of 3 mm in diameter without breaking. The minimum moisture content is the plastic limit of the fine materials.

The plasticity index (PI) is defined as the difference between the liquid limit (LL) and plastic limit (PL).

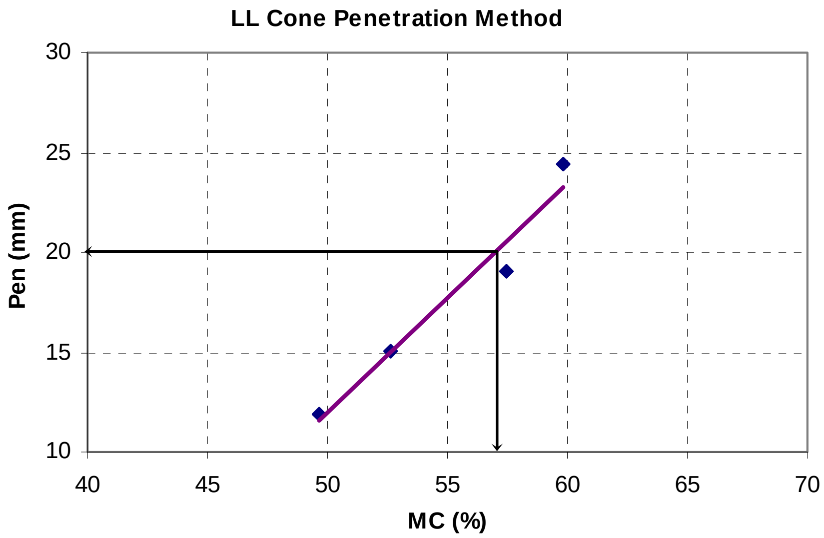

Figure 3.15 WB liquid limit by cone penetration method

The results for these tests can be summarized. Though the FC exhibits a liquid limit of 26%, by means of the Casagrande method, it was not possible to determine the plastic limit for the fact that the fine materials of the ferricrete are non plastic. The WB comes out with a liquid limit of 57%, as shown in Figure 3.15, and a plastic limit of 33% which gives a plasticity index of 24%. From the result it can be said that the Ethiopian weathered basalt contains fine materials with high plasticity. It is also important to recognize that the weathered basalt is a natural gravel dig out of a quarry site abundantly covered by a clay soil surface. It is possible that during quarrying a certain amount of surface soil is mixed with the basalt gravels.

For further verification and understanding whether these granular materials contain clay soils, which are highly plastic with high exchangeable cations, a methylene blue adsorption test has been carried out.

<u>Methylene blue adsorption</u>
From a geotechnical point of view the ability to swell and shrink and the possibility of clays to be chemically active by exchanging ions is important. In many minerals an atom of lower positive valence replaces one of higher

valence, resulting in a deficit of positive charge or, in other words, an excess of negative charge. This excess negative layer charge is compensated by the adsorption of a layer of cations which are too large to be accommodated in the interior of the crystal. The interpretation of the results of the analysis of the chemical composition of the clay minerals was first proposed by Marshall in 1935 [35].

In the presence of water, the compensating cations on the layer surface may be easily exchanged by other cations when available in solution; hence they are called "exchangeable cations" [36]. The total amount of these cations can be determined analytically. This amount, expressed in milli-equivalents per 100 g of clay, is called the cation exchange capacity (CEC) of the clay.

Methylene blue (Dimethylamino phenazothium chloride) is an organic material which is built up of benzene rings with molecular formula $C_{16}H_{18}N_3ClS$ and the ring structure is shown in Figure 3.16. Looking at the structural formula it can be seen that the molecule actually contains a negative charged (Cl) ion and a large positively charged ion. A study by Hang and Brindley [37] was specifically undertaken to examine the determination of surface areas and CEC by methylene blue adsorption. Careful experimenting with clay suspensions showed that the clay suspensions started to flocculate at a specific concentration of methylene blue (MB). This point was interpreted as the amount of MB needed to cover the clay surfaces with MB cations.

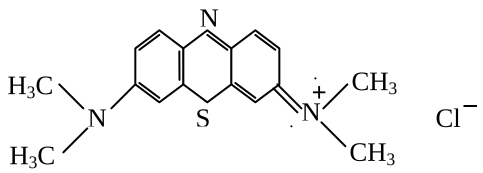

Figure 3.16 Methylene blue structural formula

Two test methods have been used extensively, i.e. the "spot method" and the "turbimetric method". The spot method is adopted in the Engineering Geology laboratory of the Delft University of Technology. It is a simplified titration technique. A 3 g/l of concentration of MB solution is used, which is added in definite volumes (0.5 ml) to a suspension of fine grained soil or grinded rock particles (finer than 63 μm). A 2 g of oven dried mineral particles is suspended in 30 ml distilled water and the suspension is thoroughly shaken by a magnetic rod stirrer for 4 minutes.

Drops of the suspension are placed on filter paper. When MB is adsorbed, the fluid migrating in the filter paper from the droplet outwards is colorless. MB is added to the suspension again. Another droplet is placed on the filter paper and the migrating halo around the droplet is examined. This process is continued until the migrating fluid is blue colored by an excess MB resting in solution when MB is adsorbed, Figure 3.17. By using this method, the MB that is adsorbed by the mineral particles corresponds with total coverage of the surface areas of the particle layers. When titrating a particle suspension the amount adsorbed is related to the cation exchange capacity of the soil or rock particles.

The methylene blue adsorption (MBA) value is computed in grams MB adsorbed by 100 g of sample according to equation 3-2:

$$MBA = \frac{c \cdot p}{A/100} \qquad [g/100g] \qquad 3\text{-}2$$

The adsorption expressed in milli-equivalent (M_f) can also be computed using equation 3-3:

$$M_f = \frac{100 \cdot N \cdot p}{A} \qquad [meq/100g] \qquad 3\text{-}3$$

Where MBA = methylene blue adsorption value (V_B in French literature)
c = concentration methylene blue solution [g/ml] *= 0.003*
p = measured amount of MB adsorbed [ml]
A = weight of soil or rock powder [g] *= 2*
N = normality of the MB solution [meq/l] *= 0.0094*

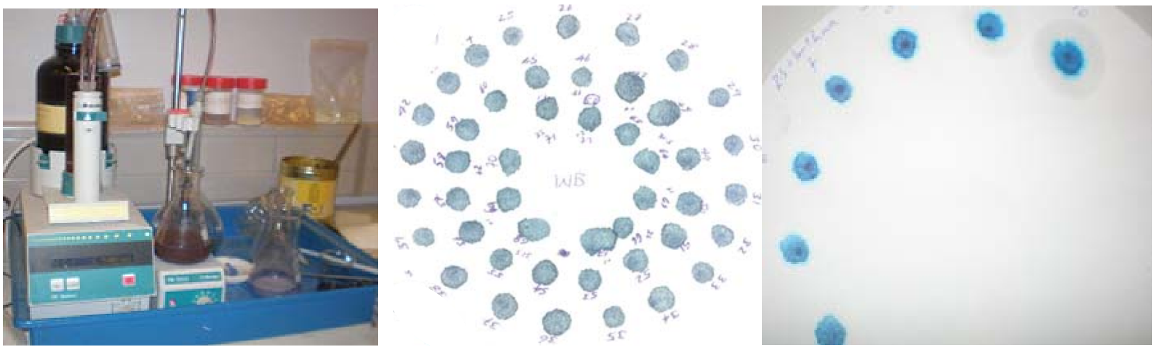

Figure 3.17 Methylene blue testing apparatus and sample of droplets

The result of the test for the three materials G1, FC and WB as summarized in table 3-1 shows that the fines from G1 which is crushed from sound Greywacke Hornfels rock has the lowest MBA as expected. The WB has the highest MBA value in which its cation exchange capacity is comparable with clay minerals such as illite or bentonites clay minerals based on data found from literature [35-38]. The presence of clay minerals in the WB and the highest cation exchange capacity comparing to the G1 and FC also perfectly agrees with the high plasticity characteristics obtained from the Atterberg limit tests.

Table 3-1 Methylene blue adsorption test results

	p (added MB) [ml]	MBA [g/100g]	M_f [meq/100g]
G1	2.5	0.4	1.2
FC	5.5	0.8	2.6
WB	36	5.4	16.9

3.5.3 Particle density and water absorption

Apparent relative density

In some countries specification, such as South Africa's [6], the compaction requirement is specified in terms of apparent relative density (ARD) instead of the usual maximum dry density of the mixture. Particularly for very high quality base materials such as the G1, the compaction specification in terms of ARD is preferred for the reason that:

i) such materials can be compacted to the highest possible degree without damaging the material;
ii) such specification avoids confusion during quality control of a construction when gradation can be varied between the field and the laboratory test due to downgrading of materials, for instance by removing particles coarser than 31.5 mm in Modified Proctor tests in the laboratory.

The apparent relative density (apparent specific gravity) for "solid" road building materials is the ratio of apparent density of the aggregate, *the mass per unit volume of the impermeable portion of the aggregate particles*, to the density of distilled water at a stated temperature. The apparent relative density of the (sub)tropical materials is determined for the fractions 0 – 2, 2 – 16 and 16 – 31.5 mm separately and a weighted average according to their gradation in a given mix is considered per material. This determination is done according to ASTM and CEN standard procedures [39, 40], which involves determination of the sample volume using a gas pycnometer.

The pycnometer is designed to measure the volume and true density of solid objects by employing Archimedes's principle of fluid displacement, Boyle's law to determine the volume and the theory of gas expansion. The displaced fluid is a Nitrogen gas which can penetrate into the finest pores, assuring maximum accuracy. The relative density is then computed by dividing the dry sample mass by the sample volume.

The test results given in table 3-2 show that the ferricrete has the biggest relative density despite the highly porous nature of the aggregates of the material, see section 3.4, due to the high concentration of iron minerals.

Table 3-2 Apparent relative density by gas pycnometer

Particle size (mm)	Apparent relative density (10^3 kg/m^3)		
	G1	FC	WB
0 – 2	2.727	2.736	2.575
2 – 16	2.720	2.911	2.585
16 – 31.5	2.720	2.911	2.541
Wt. Avg.	2.722	2.866	2.570

Water absorption capacity

The water absorption capacity of soil and granular materials is an important factor in studying their mechanical behavior. Curing of compacted specimens is a very important factor for mechanical behavior of materials with a self-cementing nature such as the recycled mix granulates (MG). Moreover, the strength and stiffness of some natural gravel materials may be affected by curing due to variation of their water absorption nature. Therefore the water absorption capacity of the FC and WB is tested and compared to the MG to know whether sample preparation and handling can have an influence on the strength behavior of the natural gravels. This is in order to take sufficient care of sample preparation and consider mainly the time gap (curing) between specimen preparation and testing periods.

The water absorption capacity of aggregates with time is determined for the fractions 0.063 – 2, 2 – 8, 8 – 22.4 and 22.4 – 45 mm separately and then its weighted average according to their gradation is calculated. The water absorption test is carried out by a wire basket method. The test is carried out for oven dry aggregates of known mass. The aggregate is immersed in a clean water bath, using a wire basket for the coarse aggregates and a container for the fine portions, attached to a balance. The mass of the aggregate sample in water is measured after a few minutes. The aggregates are removed and their surface dried using a clean and dry cloth; then the surface dry mass of the aggregates is measured in air and the aggregates are immersed in the water again. This cycle continues at short interval for the first two hours and after that the aggregates remain immersed for 24 hours. The saturated surface dry mass and oven dry mass is measured afterwards.

In comparison to MG both the FC and WB are less sensitive for water absorption as shown in Figure 3.18. Relative to WB the FC absorbs more water. It is also observed that for all the materials, similar to FC, the finer particles have a high absorbing capacity compared to the coarse aggregates, see Figure 3.19. This is also in line with the apparent density observations i.e. the lower the ARD of the fine particles the higher the water absorption.

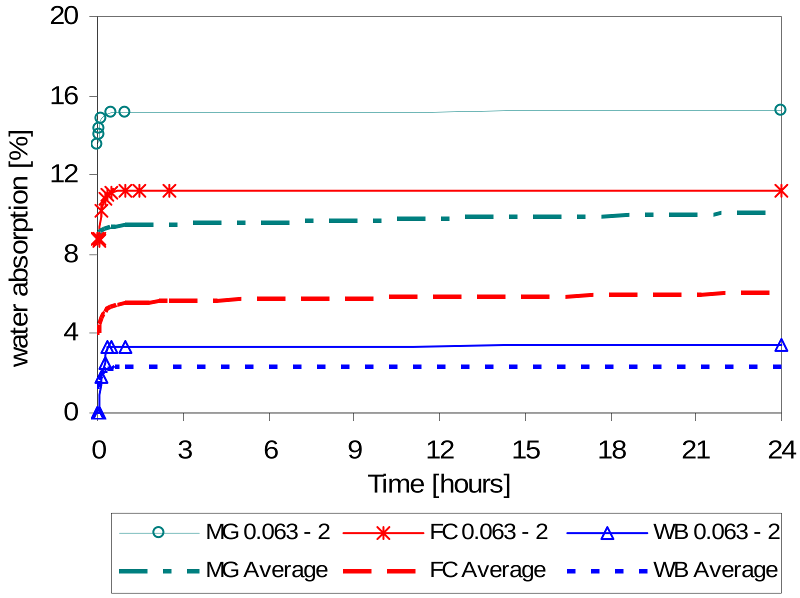

Figure 3.18 Water absorption curve for three materials MG, FC and WB

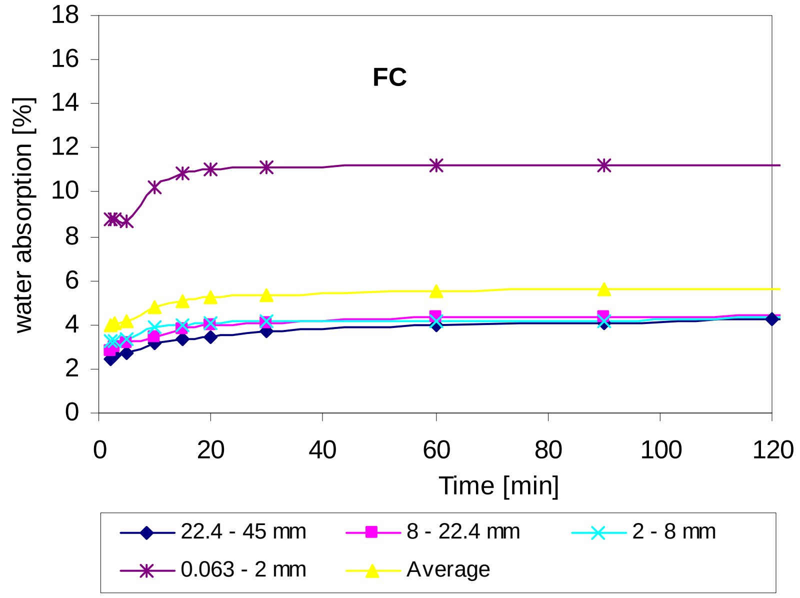

Figure 3.19 Water absorption curve for Ferricrete

3.5.4 XRF spectrometer assessment

The mineralogical composition or nature of its parent rock has an influence on the performance of aggregate with respect to strength and stiffness of the material. For this purpose the research comprises various types of aggregate materials ranging from crushed rock, recycled and different natural gravels. At the beginning of the research, especially for the Austrian base course and frost protection aggregates it was not known whether they are from limestone or granite origin. XRF spectrometer analysis is carried out to assess the main chemical components of the materials and identify their type or origin.

X-ray fluorescence (XRF) is an analytical method to determine the chemical composition of all kinds of materials, where its traditional use has roots in geology. Spectrometer systems can be divided into two main groups: energy dispersive systems (EDXRF) and wavelength dispersive systems (WDXRF). In energy dispersive spectrometers, the detector allows the determination of the energy of the photon (x-ray) when it is detected. In wavelength dispersive spectrometers the photons are separated by diffraction on a single crystal before being detected.

When materials are exposed to X-rays, ionization of their component atoms may take place. Ionization consists of the ejection of one or more electrons from the atom, and may take place if the atom is exposed to radiation with energy greater than its ionization potential. The term fluorescence is applied to phenomena in which the absorption of higher-energy radiation results in the re-emission of lower-energy radiation.

An atom consists of a nucleus with positively charged protons and non-charged neutrons, surrounded by electrons grouped in shells or orbits. The innermost shell is called K-shell, followed by L-shells, M-shells etc. X-rays can be energetic enough to expel tightly held electrons from the inner orbitals of the atom. The removal of an electron in this way renders the electronic structure of the atom unstable, and electrons in higher orbitals "fall" into the lower orbital to fill the hole left behind, see Figure 3.20. In falling, energy is released in the form of a photon, the energy of which is equal to the energy difference of the two orbitals involved. Thus, the material emits radiation, which has energy characteristics of the atoms present.

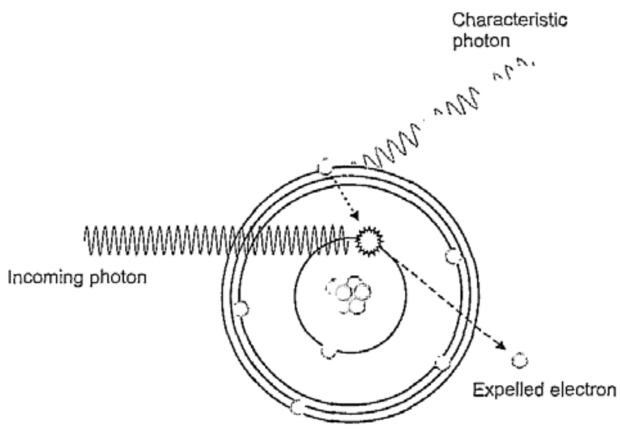

Figure 3.20 Production of characteristic radiation [41].

The XRF spectrometer analysis test for each material is done on coarse (above 2 mm) and fine (below 2 mm) particles both grinded into a very fine powder. A small amount, a sample of about 50 g of the powder, is used for the test. As mentioned above the collection of emitted radiation is characteristic for the element and is more or less a fingerprint of the element. Based on this principle the charts in Figure 3.21 and Figure 3.22 show the main chemical components of the material FC and ZKK obtained from the XRF spectrometer. In these figures the peak profiles are clearly visible. The first peak at zero energy (keV) is just from the system and not relevant. The positions of the peaks determine the elements present in the sample, while the height of the peaks determines the concentrations. The three lines in black (1), blue (2) and red (3) are results from three radiation targeting three different element target groups. The first target group (1) is for the heavy elements called as Mo (Molybdenum) or secondary target groups for excited elements ranging from Cr to Y and Pr to U. The second target group (2) is for very heavy elements group called AL2O3 or Barkla for excited elements ranging from Zr to Ce. The third target group (3) is for light elements group called HOPG (Highly Oriented Pyrolytic Graphite) or Bragg for excited elements ranging from Na to V.

As the name indicates, the ferricrete contains large amount of Iron with a high amount of Silicon-dioxide these chemical component are shown in Figure 3.21. It also clearly identifies that the ZKK material with a high percentage of Calcium carbonate is a limestone origin.

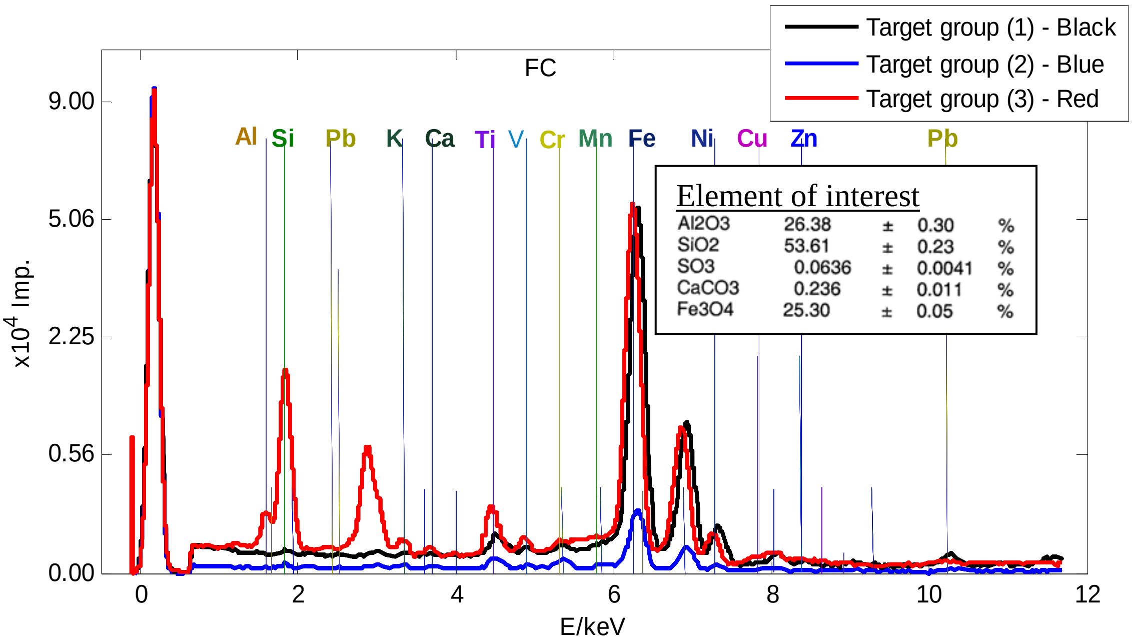

Figure 3.21 XRF spectrum of FC mineralogical components

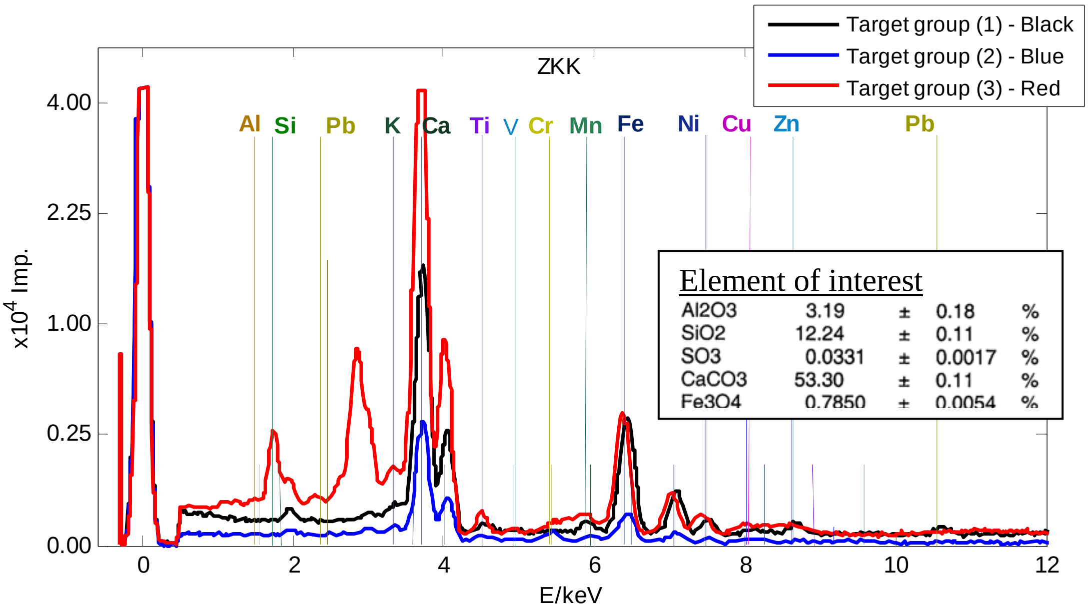

Figure 3.22 XRF spectrum of ZKK mineralogical components

3.5.5 Compaction properties

The level of compaction to be achieved in the field during construction of granular layers is commonly specified as a percentage of the maximum dry density obtained in a compaction test in the laboratory. The traditional laboratory tests are the standard and the modified AASHTO compaction tests. They are also known as standard and modified Proctor tests after the person who invented the laboratory compaction tests seventy years ago.

Although the standard and modified Proctor compaction methods are the most universally used compaction tests, engineers have realized since the late fifties that these tests are not suitable to determine the maximum dry density of all types of materials, for example for coarse granular materials. For unbound granular materials vibratory compaction methods were found to be suitable [42]. It is appropriate to note the relative distinctive difference between density and compaction [43]. Two granular materials may have the same density, but different degrees of compaction. Good compaction always results in good performance, whereas high density may or may not result in good performance depending on the degree of compaction achieved. The degree of compaction of any material can only be measured in terms of the material's density after compaction relative to the "maximum" density attainable for the same material, utilizing specific equipment and procedures.

To use as a reference two types of compaction tests were performed on the various materials: the single point modified Proctor compaction and the single point normal Proctor compaction test. All the compaction tests have been carried out on the large Proctor mould of 152.4 mm diameter in accordance with the European standard [16]. The procedure followed is similar to ASTM standards for modified and standard Proctor efforts [44, 45], the main difference being that the European standard prescribes testing of material with particle diameter less than 31.5 mm in this mould, whereas the ASTM standards prescribe testing of material with particle diameter less than 19 mm. The discarded material greater than 31.5 mm is replaced by material size 4 to 31.5 mm diameter.

<u>Single point modified Proctor compaction</u>
The single point modified Proctor compaction test from the European standard [16], Annex B, is used in the Netherlands as part of the compaction control of granular base courses. The moisture content is chosen rather subjectively by gradually adding water to the material until all grains are wet and shiny after thorough mixing and a 'plastic' grains–water mixture is obtained without excess water.

The single point modified Proctor compaction test was performed on all the materials except the MG and the value of the single point modified Proctor dry density SMPD is obtained for G1, FC, WB, ZKK63 and ZKK32 at their respective moderate moisture content, see table 3-3.

<u>Single point Proctor compaction</u>
The Dutch specifications for granular bases [29] specify compaction of bases in terms of the single point Proctor density SPD. The single point Proctor compaction is the same as the single point modified Proctor compaction discussed above except that the compaction effort is the standard Proctor effect instead of the modified Proctor effort. Another reason for compacting the MG using this single point Proctor density is to be consistent with the degree of compactions used by Van Niekerk in his PhD dissertation [5] since some reference will be made from his data for these materials.

In general for all tests carried out in this research the following dry density are considered as reference dry density at 100% MMPD, except for the MG in which 100% MPD, for the degree of compaction in all the CBR, RL-CBR as well as the triaxial tests. And the moisture content at which these densities were obtained are taken as moderate moisture content i.e. the dry and wet side compactions are referred to with respect to these moisture contents.

Table 3-3 Reference compaction densities

	Moisture Content [%]	Dry Density [kg/m^3]	Dry density reference	ARD [kg/m^3]
G1	4	2293	MMPD	2.722
FC	7.5	2173	MMPD	2.866
WB	7	1950	MMPD	2.570
ZKK32	3	2260	MMPD	-
ZKK63	3	2236	MMPD	-
MG	8	1735	MPD	-

3.5.6 California Bearing Ratio

CBR tests are often conducted in combination with Proctor compaction tests to obtain a dry density – moisture content – CBR relation. In many (sub)tropical countries CBR tests are conducted on specimens compacted to modified Proctor density. In many of these countries the test method is the most widely used test for controlling the quality of base and subbase layers.

For the FC and WB materials specimens are compacted of particles passing 22.4 mm sieve in accordance to European standard [12]. The CBR mould has a diameter of 152.4 mm. Specimens are compacted in 5 layers in the same way as the modified Proctor compaction. The test is carried out on both soaked and unsoaked specimens. The moisture content and dry density (DD) in the Figures 2.23 and 2.24 for the soaked specimens is the MC and DD of the compacted specimen before soaking.

As discussed in chapter 2 the CBR test is a penetration test in which a piston of 49.6 mm diameter penetrates the specimen at a prescribed (slow) rate of 1.27 mm/min (0.05 inch/min). The force required for 2.54 mm (0.1 inch) and 5.08 mm (0.2 inch) penetration are expressed as a percentage of the force required for achieving the same penetrations for a reference crushed rock. The larger of the two percentages is normative. Surcharge weight(s) are placed on the specimen to simulate the deadweight of overlying layers.

In Figures 3.23 and 3.24 it is shown that the dry densities for the soaked and unsoaked samples vary to some extent for both FC and WB materials. This is especially significant for the WB; such variation could arise from inconsistency of sample preparation. On the other hand, it can be observed that soaking has a big influence on the CBR values, despite the fact that the soaked specimens have a higher density.

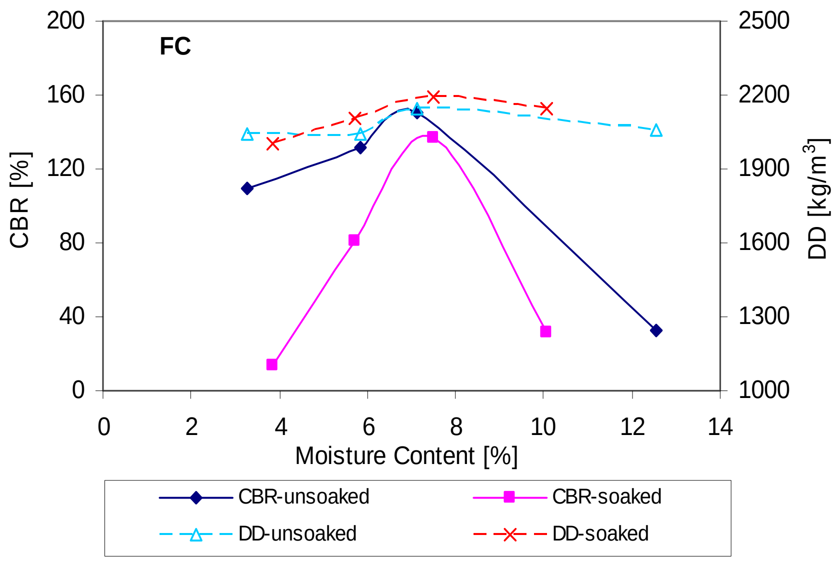

Figure 3.23 Moisture – density – CBR for FC

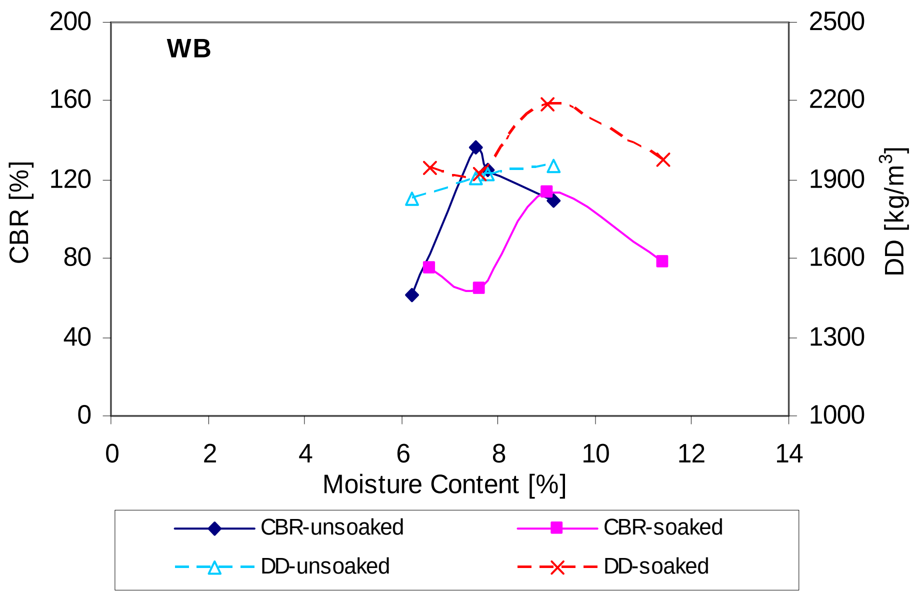

Figure 3.24 Moisture – density – CBR for WB

Based on the preliminary investigation carried out on the basic physical characteristics of the test materials the following remarks can be made.

- As most of the test materials are received directly from road site under construction their gradations satisfy their respective specification in the countries they originate. Only the weathered basalt didn't satisfy the ERA [27] or TRL ORN-31 [46] specification for subbases. In this case modification is made by removing some of its coarse portion to bring the gradation into the specification.

- The investigation on the fine portion of the natural gavel materials such as the WB and FC reveals that:
  - in dealing with the fine portion of the WB with a LL 57% and PI 24%, which can be classified as A-7-5 (clayey soils) according to the AASHTO soil classification system, one has to be careful with these materials as they may cause problems;
  - with the relative high water adsorptive capacity of the FC, one has to take care in mixing, compacting and curing time of mixtures of the materials. In the laboratory characterization to be conducted in this research, chapter 4 and 5, an extended period of sample preparation, instrumentation and testing might become more sensitive for such material.

- The moisture sensitivity of the cohesive FC material is also reflected on the CBR measurements of the soaked CBR test. For the FC the soaked CBR at the extreme (dry and wet) compaction moisture contents is much lower than the unsoaked CBR at these moisture, while near to the optimum moisture content the difference is minimal.

REFERENCES

1. Verschuren, P. and H. Doorewaard, *Het ontwerpen van een onderzoek (The design of a research)*. 1995: Lemma, Utrecht.
2. Edwards, J.P., *Laboratory Characterisation of Pavement Foundation Materials*, in *Centre for Innovative and Collaborative Engineering (CICE)*. 2007, Loughborough University: Loughborough.
3. Huurman, M., *Permanent deformation in concrete block pavements*, in *Faculty of Civil Engineering and Geosciences*. 1997, Delft University of Technology: Delft.
4. Sweere, G.T.H., *Unbound Granular Base for Roads*, in *Faculty of Civil Engineering and Geosciences*. 1990, Delft University of Technology: Delft.
5. Van Niekerk, A.A., *Mechanical Behavior and Performance of Granular Bases and Subbases in Pavements*, in *Road and Railway Engineering, Faculty of Civil Engineering* 2002, Delft University of Technology: Delft.
6. CEAC, *Standard Specifications for Road and Bridge Works for State Road Authorities*. 1998, Civil Engineering Advisory Council (CEAC), Committee of Land Transport Officials (COLTO): South Africa.
7. Mahoney, J.P., M.D. Pietz, and K.W. Anderson, *Summary Report on the State Pavement Technology Consortium.* 2000, Washington state department of transportation: Washington DC.
8. Theyse, H.L., *Stiffness, Strength and Performance of Unbound Aggregate Material: Application of South Africa HVS and Laboratory results to California Flexible Pavements.* 2002, CSIR Transportek: Pretoria, South Africa.
9. Opiyo, T.O., *A Mechanistic Approach to Laterite-based Pavements*, in *Transport and Road Engineering (TRE)*. 1995, International Institute for Infrastructure, Hydraulic and Environment Engineering (IHE): Delft.
10. Osman, S.A., *Searching for a Fundamental Characterisation of Unbound Materials using CBR Testing*, in *Transport and Road Engineering (TRE)*. 1995, International Institute for Infrastructure, Hydraulic and Environment Engineering (IHE): Delft.
11. Awaje, T.Y., *Repeated Load CBR Testing on Granular Base Course Material*, in *Faculty of Civil Engineering and Geosciences*. 2007, Delft University of Technology: Delft.
12. CEN, *Unbound and hydraulically bound mixtures - Part 47: Test method for the determination of California bearing ratio, immediate bearing index and linear swelling*, in *EN 13286-47*. 2004, European Committee for Standardization (CEN): Brussels.
13. ASTM, *Standard test method for CBR (California Bearing Ratio) of laboratory-compacted soils*, in *ASTM D 1883-94*. 1978, American Society for Testing and Materials: Philadelphia.
14. Molenaar, A.A.A., *Repeated Load CBR Testing, A Simple but Effective Tool for the Characterization of Fine Soils and Unbound Materials*, in *Transportation Research Board TRB 2008 Annual Meeting* 2008: Washington DC.
15. Osman, S.A., *Searching for a fundamental characterisation of unbound materials using CBR testing*, in *TREND - Transport and Road Engineering for Development*. 1995, International Institute for Infrastructural, Hydraulic and Environmental Engineering (IHE): Delft.
16. CEN, *Unbound and hydraulically bound mixtures - Part 2: Test methods for the determination of the laboratory reference density and water content - Proctor*

compaction, in *EN 13286-2*. 2004, European Committee for Standardization (CEN): Brussels.
17. Gebre-egziabher, E., *Stabilisation of Cinder with Foamed Bitumen and Cement and Its Use as (Sub) Base for Roads*, in *Transport and Road Engineering (TRE)*. 2000, International Institute for Infrastructure, Hydraulic and Environment Engineering (IHE): Delft.
18. Bokan, G.L., *Mechanical Behavior of a Clay Subgrade Material for Mechanistic Pavement Design*, in *Faculty of Civil Engineering and Geosciences*. 2007, Delft University of Technology: Delft.
19. Enotes. *World of Earth Science | Hornfels*. 2008 [cited; Available from: http://www.enotes.com/earth-science/hornfels.
20. Northstone. *Basic Geological Classification*. ref. 2010 [cited; Available from: http://www.northstone-ni.co.uk/about-us/education/basic-geological-classification//.
21. Lamplugh, G.W., *Calcrete*, in *Geological Magazine* 1902. p. 575.
22. Ollier, C.D. and R.W. Galloway, *The laterite profile, ferricrete and unconformity*. CATENA, 1990. **17**(2): p. 97-109.
23. Buchanan, F., *A Journey from Madras through the Countries of Mysore, Kanara and Malabar*. 1807, London: East India Co.
24. Molenaar, A.A.A., *Road Materials I: Cohesive and Non-cohesive Soils and Unbound Granular Materials for Bases and Sub-bases in Roads*, in *Lecture Note*. 2005, Faculty of Civil Engineering and Geosciences, Delft University of Technology: Delft.
25. Beaven, P.J., R. Robinson, and K. Aklilu, *The performance of weathered basalt gravel roads in Ethiopia*. 1988, Overseas Unit Transport and Road Research Laboratory, Department of Transport: Berkshire.
26. Sahlu, A.M., *The upgrading of weathered basalt gravel for use as a road base in Ethiopia*, in *Transport and Road Engineering for Development (TREND)*. 2001, International Institute for Infrastructure, Hydraulic and Environmental Engineering (IHE): Delft.
27. ERA, *Pavement Design Manual: Volume I Flexible Pavements and Gravel Roads*. 2002, Ethiopian Roads Authority (ERA): Addis Ababa, Ethiopia.
28. RVS, *Guidelines and specifications for road construction. (in German) Richtinien und Vorschriften fur den strassenbau*. 2005, Austrian Research Association for Transportation Engineering: Vienna, Austria.
29. CROW, *RAW Standard Bepalingen 2005 (in Dutch)*. CROW, Editor. 2005: Ede, The Netherlands.
30. CEN, *Tests for geometrical properties of aggregates - Part 7: Determination of particle size distribution: Test sieves, nominal size apertures*, in *EN 933-2*. 1995, European Committee for Standardization (CEN): Brussels.
31. CEN, *Tests for geometrical properties of aggregates - Part 7: Determination of particle size distribution: Sieving method*, in *EN 933-1*. 2005, European Committee for Standardization (CEN): Brussels.
32. Gidigasu, M.D., *Laterite Soil Engineering: pedogenesis and engineering principles*. Development in geotechnical Engineering. Vol. 9. 1976, Amsterdam: Elsevier scientific publishing company.
33. Hegentogler, C.A., *Engineering Properties of Soils*. 1937, New York: McGraw-Hill.

34. CEN, *Geotechnical investigation and testing - Laboratory testing of soil - Part 12: Determination of Atterberg limits*, in *CEN ISO/TS 17892-12*. 2004, European Committee for Standardization (CEN): Brussels.
35. Van Olphen, H., *An introduction to clay colloid chemistry : for clay technologists, geologists, and soil scientists / H. van Olphen*. 1977, New York :: Wiley.
36. Verhoef, P.N.W., *The methylene blue adsorption test applied to geomaterials*, in *GEOMAT.02 Memoirs of the Center of Engineering Geology in the Netherlands, 101*. 1992, Delft University of Technology: Delft. p. 36.
37. Hang, P.T. and G.W. Brindley, *Methylene blue absorption by clay minerals-Determination of surface areas and cation exchange capacities.* Clays and Clay Minerals, 1970. **18**(4): p. 203-212.
38. Stapel, E.E. and P.N.W. Verhoef, *The use of the methylene blue adsorption test in assessing the quality of basaltic tuff rock aggregate.* Engineering Geology, 1989. **26**(3): p. 233-246.
39. ASTM, *Standard test method for Density, Relative Density (Specific Gravity), and Absorption of Coarse Aggregate*, in *ASTM C 127 – 07*. 2007, American Society for Testing and Materials: Philadelphia.
40. CEN, *Tests for mechanical and physical properties of aggregates - Part 6: Determination of particle density and water absorption*, in *EN 1097-6*. 2000, European Committee for Standardization (CEN): Brussels.
41. Brouwer, P., *Theory of XRF: Getting acquainted with the principles*. 2003, The Netherlands: PANalytical BV.
42. Semmelink, *The effect of material properties on the compactability of some untreated roadbuilding materials*, in *Department of Civil Engineering Faculty of Engineering*. 1991, University of Pretoria: Pretoria.
43. Marek, C.R. and T.R. Jones. *Compaction - an essential ingredient for good base performance*. in *Conference on Utilization of Graded Aggregate Base Materials in Flexible Pavements* 1974: Oak Brook.
44. ASTM, *Standard Test Methods for Laboratory Compaction Characteristics of Soil Using Modified Effort (56,000 ft-lbf/ft3(2,700 kN-m/m3))*, in *ASTM D 1557 – 07*, A.S.f.T.a. Materials, Editor. 2007: Philadelphia.
45. ASTM, *Standard Test Methods for Laboratory Compaction Characteristics of Soil Using Standard Effort (12 400 ft-lbf/ft3 (600 kN-m/m3))*, in *ASTM D 698 – 07*, A.S.f.T.a. Materials, Editor. 2007: Philadelphia.
46. TRL, *A Guide to the structural design of bitumen surfaced roads in tropical and subtropical countries*, in *ORN-31*. 1993, Overseas Center Transport Research Laboratory: Crowthorne, Berkshire, UK.

CHAPTER 4

MECHANICAL BEHAVIOR OF UNBOUND GRANULAR MATERIALS

4.1 INTRODUCTION

This chapter presents the results of the extensive triaxial testing performed into the mechanical behavior of the granular base and subbase materials.

From the literature review in chapter 2 it is elaborated that the mechanical behaviors (the strength, stiffness, and resistance to permanent deformation) of coarse unbound granular base and subbase materials are better characterized in the laboratory with triaxial testing. As noted in section 2.4.2, the purpose of the triaxial test is to simulate in the laboratory as closely as possible the situation within the pavement structure with respect to grading, moisture content, density and applied stresses. The strains resulting from the application of stresses are measured and fundamental material parameters are determined from the values of stresses and strains.

The objective of this triaxial test program is to:

- characterize the failure and deformation behavior of unbound granular materials (UGMs);
- assess the influence of material and condition properties, mainly material type, moisture content (MC) and degree of compaction (DOC);
- assess the suitability of existing resilient deformation mathematical models for the materials under consideration;
- use the results for validation of the newly developed repeated load CBR (RL-CBR) test technique.

In the triaxial test program the permanent deformation test is not included for two main reasons:

i) despite the large amount of materials transported from South Africa and Ethiopia, there was no sufficient material left for the permanent deformation tests;
ii) due to the extensive testing program of the monotonic and resilient deformation triaxial tests and the RL-CBR tests, which are the primary objective of the research project as discussed in chapter 1 and 3, it was

not possible to include permanent deformation tests within the limited research period.

The structure of this chapter is given below. It serves not only to outline the components of the results of the tests which were performed for the various materials, but also to guide the reader looking for a specific aspect of the behavior of coarse granular materials, for instance the resilient deformation behavior.

In section 4.2 a detailed description of the large scale triaxial apparatus and specimen preparation procedures is given. In section 4.3 and 4.4 the results of the monotonic failure tests and cyclic load resilient deformation tests are presented followed by the modeling of the resilient deformation behavior in section 4.5. The effect of MC, DOC and material type on the mechanical behavior is discussed in section 4.6 and conclusive remarks are given in section 4.7.

4.2 LARGE SCALE TRIAXIAL APPARATUS AND SPECIMEN PREPARATION

Performing a triaxial test includes three main components: the preparation of the specimen, the instrumentation of the specimen and the main testing procedure i.e. the loading and measuring process. Of these components the preparation of the specimen is identical for all triaxial tests in the project. In this section a detailed description of the main components of the large scale constant confining pressure (CCP) triaxial apparatus in the Road and Railway Engineering Laboratory (RREL) of Delft University of Technology, the compaction apparatus and the specimen preparation is given. The specimen instrumentation and testing procedures are presented in the respective section of the different triaxial tests.

The large scale CCP triaxial apparatus consists of the following items [1, 2]:

1. A loading frame, a hydraulic actuator, a load cell and a controller for application and measurement of displacement or force controlled monotonic and cyclic axial loading, Figure 4.1. The hydraulic actuator has a capacity of 250 kN. Closed loop servo control is effectuated by a MTS controller, which feeds back on the signals of the load cell and the internal displacement transducer for force and displacement control, respectively.

Figure 4.1 Large scale CCP triaxial apparatus, control and data acquisition unit

2. A vacuum regulator, analogue vacuum gauges and electronic vacuum transducers for application and measurement of the internal vacuum, which is applied to the specimen. The level difference between the adjustable constant (i.e. non-cyclic) internal vacuum and the atmospheric air pressure effectuates a confining stress to the specimen. The level can be adjusted by means of a vacuum regulator. Outlets at the top and the bottom plate of the specimen allow for analogue and continuous electronic measurement and recording of the level of vacuum.

3. A Control and Data Acquisition System consisting of a PC and a multi-programmer. On the PC tailored software generates the required loading signals and stores the acquired data signals to the hard disk. The multi-programmer provides the memory and the required digital to analogue (D/A) conversion for the control system and the required A/D conversion for the data acquisition on up to 16 channels. Out of these, 13 channels are in use for:
   - the load cell and the actuator LVDT (Linear Variable Differential Transformer),
   - the 2 electronic confining pressure transducers,
   - the 6 radial and 3 axial LVDTs.

4. For measurement of resilient deformations LVDTs are used with a total range of 1 mm. The use of this type of smaller deformation range LVDTs increases the accuracy of the measurement.

Compaction apparatus

The compaction apparatus consists of [1, 2] a steel frame mounted on four air bellows, supporting two reinforced concrete slabs, Figure 4.2. The frame and air bellows provide a semi-static system that vibrates at a much lower resonance frequency than the frequency at which the eccentric engines vibrate. This provides a base for the compaction while vibrations are not transmitted to the floor.

The vibrating part of the apparatus consists of two eccentric engines that are mounted on two mounting plates. Oversized bushes in the mounting plates prevent horizontal drifting of this “vibrating part” by guiding it along the shaft. The rotors of the eccentric engines rotate in opposite direction at an exact phase difference. As the masses simultaneously reach opposite horizontal positions, the horizontal centripetal forces are eliminated. As the masses simultaneously reach identical vertical positions the vertical centripetal forces add up introducing pure vertical vibrations, which compact the material in the mould.

The frequency at which the engines rotate can be controlled by means of a frequency regulator. To raise the mounting plates, an automated crane is used. Upon raising, the mounting plates can be locked to the guiding shaft by means of pins and turned away to have access to the specimen. The details of the split mould and the pedestal used to compact triaxial specimens will be discussed in the next subparagraph. The pedestal and the split mould are bolted on a metal plate, which is rigidly connected to the semi-static concrete block.

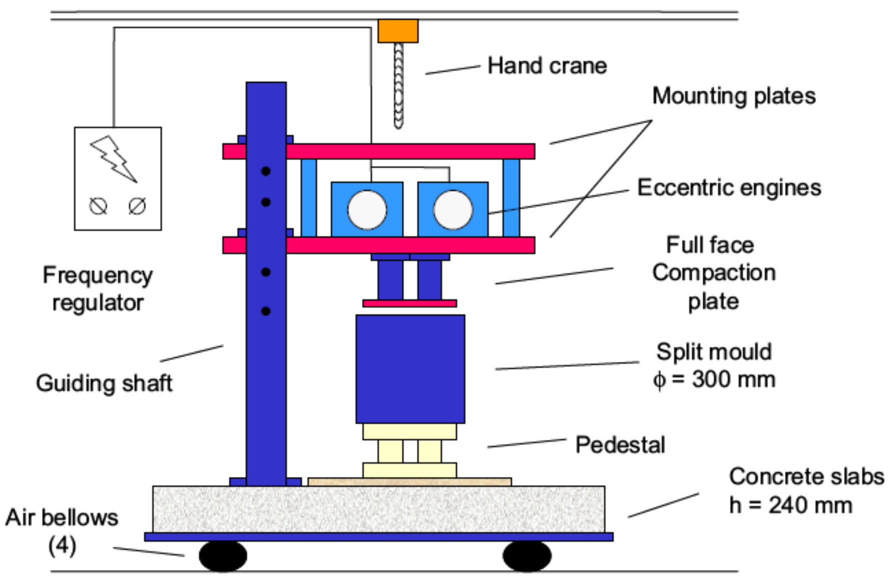

Figure 4.2 Schematic representation of TU Delft Compaction apparatus [2]

From the above description it follows that the compactive effort which can be applied by this specific apparatus is thus dependent on the frequency of rotation of the engines and the duration of vibration.

Preparation of specimen

The procedure for preparation of the 300 x 600 mm triaxial specimens is described as follows [1, 2]:

1. The unbound granular materials at required grading are obtained by recombination of various fractions of sieved materials to their respective target grading. The moisture content of the bulk material is pre-determined and the required quantity of water to bring the material to

the required level of moisture content is added and mixed with a mechanical mixer, Figure 4.3. Having obtained the sample material at the target moisture content, the triaxial specimen is then built in a split mould Figure 4.4.

Figure 4.3 Mechanical mixer, weighing, pouring and hand tamping

2. Specimens are prepared in a split mould which holds a membrane. The membrane is made of “weldable” low-density polyethylene (LDPE) sheet (0.4 mm thick), which is shaped into a cylinder with a slight barrel shape. This prevents the membrane from inducing uncontrolled confinement to the specimen in case of significant radial deformation of the specimen during the test. The first membrane is stretched around the bottom plate. To ensure an airtight seal the side of the plate is greased and O-rings are stretched over the membrane which is kept in place by two groves. The membrane has to be stretched to line the split mould with as little folds as possible and kept in place to obtain a smooth surfaced specimen. To prevent fine materials from being sucked out of the specimen a perforated PVC plate and a geotextile are placed between the bottom plate and the specimen.

Figure 4.4 A layer after compaction and scarification, the split mould assembly, specimen ready for instrumentation and testing

3. The required quantity of sample material, pre-determined from the specimen volume and wet density to achieve a target DOC, is divided into 8 equal portions. Specimens are compacted in 4 layers, each layer consisting of two portions. For each layer the exact amount of material is weighed to obtain a layer thickness of 150 mm after compaction.

4. Half the material of the first layer (one portion) is poured and pre-compacted by hand tamping, Figure 4.3. Then the material of the second portion is poured and pre-compacted in the same way. Subsequently the two portions are compacted by means of the vibratory compactor to the required density, which is controlled by determining the achieved layer thickness. The same procedure is followed for the remaining three layers. The surface of each layer is mechanically scarified, Figure 4.4, before adding the next layer on top to obtain a good layer interlock and a homogeneous sample.

5. It is important to ensure that the top of the last layer is as much as possible parallel to the bottom plate (horizontal). A non horizontal top of the specimen may lead to a non-truly vertical load application and will introduce shear stress in the specimen during the triaxial test. After compaction of the last layer the specimen is covered in the same way with a geotextile, a perforated PVC plate, a top-plate, and sealed with grease and O-rings. Prior to removal of the split mould a partial vacuum is applied to the specimen to support and minimize disturbance to the specimen. A second membrane is then placed over the specimen in order to seal the specimen from any leaks that may develop in the first membrane caused by the compaction process and due to the coarse and granular nature of the material. The second membrane is again sealed by means of grease and O-rings. The specimen is now ready for instrumentation or testing.

4.3 MONOTONIC FAILURE TRIAXIAL TEST

4.3.1 Test principle

In the monotonic (static) failure (MF) triaxial test a granular material is subjected to a controlled constant confining pressure. Apart from the all-around confining stress the material is also subjected to an increasing additional axial (vertical) stress which leads to failure. Failure is defined as the level at which no further increase in axial stress is required to obtain an increase of axial deformation or strain. At failure, the axial stress can be expressed as a shear stress (τ_f) or a major principal stress ($\sigma_{1,f}$) and the confining stress as a normal stress (σ_n) or a minor principal stress (σ_3).

By performing a failure test at a minimum of two or three confining stress levels the stress dependency of the failure behavior of a granular material can be established. This is described by the well-known Mohr-Coulomb failure criterion in equations 4-1:

$$\tau_f = c + \sigma_{n,f}.\tan\phi \qquad 4\text{-}1$$

Where:

τ_f	=	shear stress at failure	[kPa]
$\sigma_{n,f}$	=	normal stress at failure	[kPa]
c	=	cohesion	[kPa]
ϕ	=	angle of internal friction	[°]

The Mohr-Coulomb failure criterion can be expressed in principal stresses as in equation 4-2 and schematically illustrated for constant confining pressure (CCP) in Figure 4.5:

$$\sigma_{1,f} = \frac{(1+\sin\phi)\sigma_{3,f} + 2c\cos\phi}{(1-\sin\phi)} = A.\sigma_{3,f} + B \qquad 4\text{-}2$$

Where:

$\sigma_{1,f}$	=	major principal stress at failure [kPa]
$\sigma_{3,f}$	=	minor principal stress at failure [kPa]

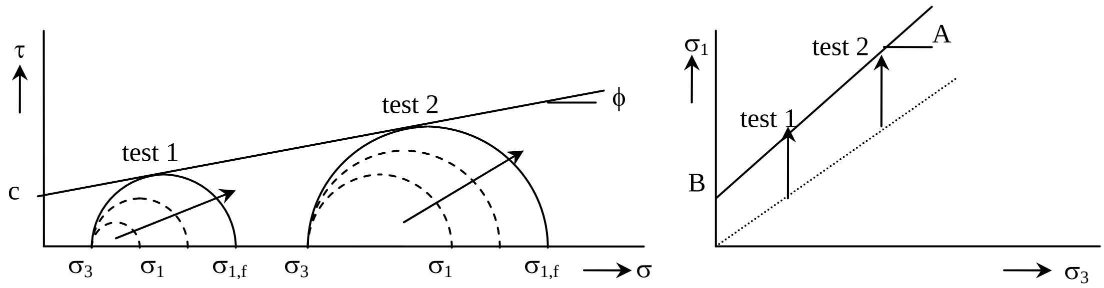

Figure 4.5 Mohr stress circles and stress path in CCP failure tests

4.3.2 Test program

The monotonic failure (MF) triaxial test is carried out in the large scale CCP triaxial apparatus (diameter * height = 300 mm * 600 mm) described in section 4.2, see also Figure 4.6. The failure test is performed in the displacement controlled mode at a fast constant displacement rate of $\Delta\varepsilon_p/\Delta t$ = 0.33%/sec (118.8 mm per minute or 1.98 mm per sec) to simulate failure loading rates under moving wheel loads. This displacement rate was also applied in earlier performed monotonic failure tests [2, 3]. In the displacement controlled mode the load magnitude is applied which is required to maintain a constant displacement rate. This has the advantage over force controlled test that the load reduces as the specimen fails while the test extends after failure.

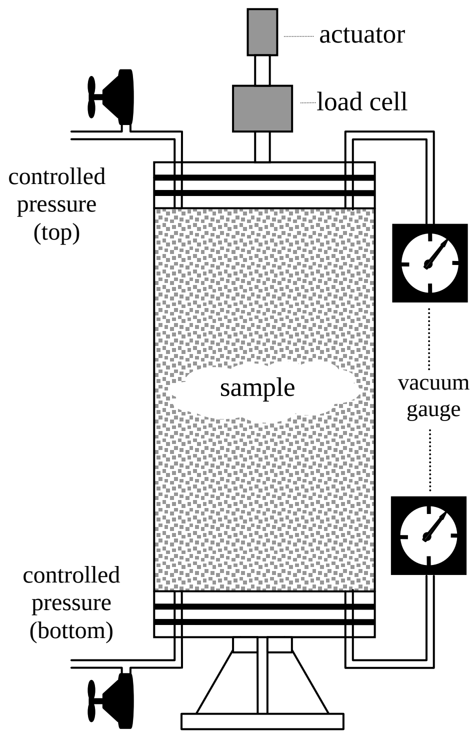

Figure 4.6 The large scale (300 mm * 600 mm) CCP triaxial test set-up

The software and data acquisition system allows to continuously record:
- the axial load and displacement measured by the load cell and the internal LVDT respectively;
- confining stress from the upper and lower vacuum sensors.

From this the maximum levels of σ_1 for the applied levels of σ_3 can be determined to establish the c and ϕ, according to equation 4-2.

The reliability of the obtained c and ϕ values can not be established from failure tests at only two confining stress (σ_3) levels. For this reason, in this research, failure tests are carried out at three σ_3-levels per material, DOC and MC condition. First failure tests are conducted at two σ_3-levels (20 kPa and 80 kPa) on virgin specimens, in which the result is also used to establish the load levels for the resilient deformation (RD) tests. Due to time and effort required for building a large base course sample, a third failure test is conducted at an intermediate σ_3-level (50 kPa) on a non-virgin specimen but after the resilient deformation test is carried out at stress levels far below the failure stress level.

The monotonic failure (MF) triaxial test is carried out for five materials FC, WB, G1, ZKK63 and ZKK32 at different mix and compaction conditions that range from 95% to 105% DOC and dry to wet MC. DOC is measured as percentage of the modified Proctor dry density of each material. Similarly MC is measured relative to the moderate (Mod.) MC measured in the modified Proctor compaction as given in table 3-3. The test conditions for the MF tests are shown in table 4-1. Within the scope of the research project and material limitation for the ZKK materials, only moderate moisture content is targeted for the G1 and ZKK materials.

Table 4-1 MF triaxial target test conditions

Material	Target DOC (%)	Target MC (% by mass)	Target σ_3 (kPa)	Test code	Specimen
FC	95	Mod. (7.5)	20	MF-FC-95-20	virgin
			50	MF-FC-95-50	after RD*
			80	MF-FC-95-80	virgin
	98	Dry (5)	20	MF-FC-98dr-20	virgin
			50	MF-FC-98dr-50	after RD
			80	MF-FC-98dr-80	virgin
		Mod. (7.5)	20	MF-FC-98-20	virgin
			50	MF-FC-98-50	after RD
			80	MF-FC-98-80	virgin
		Wet (9.5)	20	MF-FC-98wt-20	virgin
			50	MF-FC-98wt-50	after RD
			80	MF-FC-98wt-80	virgin
	100	Mod. (7.5)	20	MF-FC-100-20	virgin
			50	MF-FC-100-50	after RD
			80	MF-FC-100-80	virgin
WB	95	Mod. (7)	20	MF-WB-95-20	virgin
			50	MF-WB-95-50	after RD
			80	MF-WB-95-80	virgin
	98	Dry (5)	20	MF-WB-98dr-20	virgin
			50	MF-WB-98dr-50	after RD
			80	MF-WB-98dr-80	virgin
		Mod. (7)	20	MF-WB-98-20	virgin
			50	MF-WB-98-50	after RD
			80	MF-WB-98-80	virgin
		Wet (9)	20	MF-WB-98wt-20	virgin
			50	MF-WB-98wt-50	after RD
			80	MF-WB-98wt-80	virgin
	100	Mod. (7)	20	MF-WB-100-20	virgin
			50	MF-WB-100-50	after RD
			80	MF-WB-100-80	virgin
G1	98	Mod. (4)	20	MF-G1-98-20	virgin
			50	MF-G1-98-50	after RD
			80	MF-G1-98-80	virgin
	100	Mod. (4)	20	MF-G1-100-20	virgin
			50	MF-G1-100-50	after RD
			80	MF-G1-100-80	virgin
	102	Mod. (4)	20	MF-G1-102-20	virgin
			50	MF-G1-102-50	after RD
			80	MF-G1-102-80	virgin
	105	Mod. (4)	20	MF-G1-105-20	virgin
			50	MF-G1-105-50	after RD
			80	MF-G1-105-80	virgin
ZKK32	100	Mod. (3)	20	MF-ZKK32-100-20	virgin
			50	MF-ZKK32-100-50	after RD
			80	MF-ZKK32-100-80	virgin
ZKK63	100	Mod. (3)	20	MF-ZKK63-100-20	virgin
			50	MF-ZKK63-100-50	after RD
			80	MF-ZKK63-100-80	virgin

* RD = Resilient Deformation triaxial test

Moisture contents in the entire research are taken as the average of the mixture MC measured before compaction and after testing. It was observed that in most cases the MC before and after testing was almost identical. Only in a few cases, especially for wet mixtures, a lower MC (up to 15% less e.g. MC went down from 8% to 6.8%) was found after compaction due to drying out during compaction and testing. In a very unique case a strange MC measurement was recorded i.e. the MC after testing is larger than before compaction. This of course cannot be true; it is only a result of variation in sampling. It was noted that such sampling variation can happen for two practical reasons: i) in the case where the sample for MC determination before compaction is taken from a mixture exposed to air for a significant time ii) in the case where a significant portion of the sample for MC determination after testing is taken from the wet part (usually towards the bottom) despite the careful procedure of removing and remixing for obtaining a representative sample.

4.3.3 Failure behavior

The strength of an UGM depends primarily on the confining pressure applied on the material, see equation 4-2.

As discussed in sections above the failure behavior of unbound (sub)base materials is characterized in terms of the cohesion (c) and the angle of internal friction (ϕ). The coarse nature of these (sub)base materials and their loading history dependency require careful consideration of how to obtain representative c- and ϕ-values. These considerations are discussed in the following paragraphs prior to the presentation of the obtained c- and ϕ-values.

The failure tests are conducted, as shown in table 4-1, in part on “virgin” (not previously loaded) specimens prepared exclusively for the MF test and in part on specimens after completion of resilient deformation (RD) tests in which its load levels are far below the failure level. The intention for doing the MF test after RD test is basically to economize on specimen preparation, but in the mean time it also gives an opportunity to take account of the fact that the failure behavior of granular materials is affected by the loading history. This applies both to materials in-service under traffic loading and in cyclic load triaxial tests.

The use of the virgin and pre-loaded types of specimens along with the unavoidable specimen preparation variation, despite of the efforts made for consistent and careful monitoring during preparation, yields in some cases unexpected results. Though for most cases the use of a pre-loaded specimen doesn’t affect the test result significantly, see Figure 4.7 to 4.9, there are instances that due to pre-loading the specimen gains strength from post-compaction by the cyclic load of the RD test, Figure 4.10, especially for lower DOC. In such cases the other two confining stress (σ_3) levels are considered for the regression in the analysis of the c- and ϕ-values. Repeating the test with a virgin specimen was considered prohibitively elaborated.

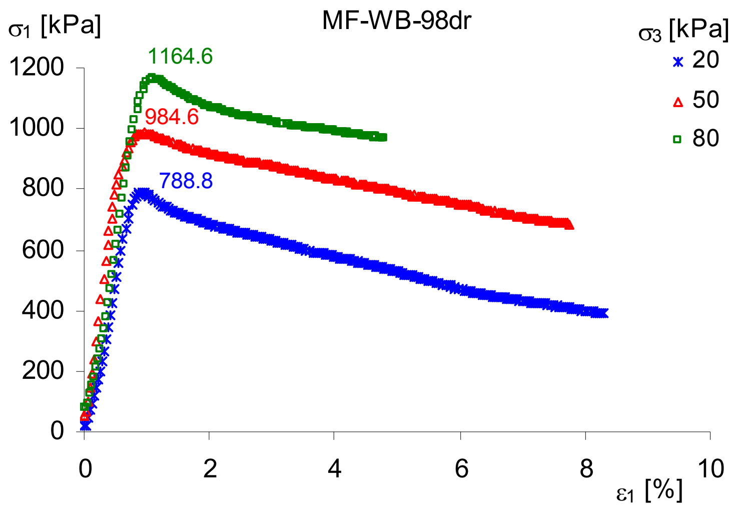

Figure 4.7 Stress-strain in MF test for WB at 98% DOC and Dry MC

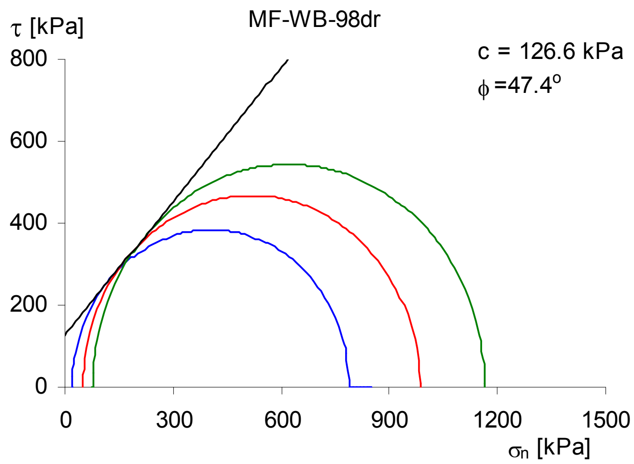

Figure 4.8 Mohr-Coulomb failure criterion for WB at 98% DOC and Dry MC

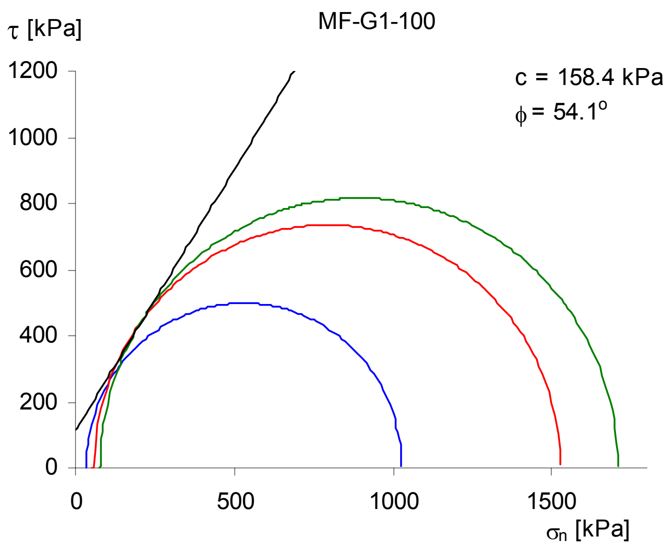

Figure 4.9 Mohr-Coulomb failure criterion for G1 at 100% DOC and Mod. MC

Huurman [3] obtained suitable MF test results on different sands. However, as Werkmeister [4] reported, for coarse granular base materials, particularly for crushed aggregates such as G1, it is not always possible to define failure so readily. An example of the results obtained for G1 is given in Figure 4.11. In such cases the strength parameters c and ϕ are determined from a failure line that is determined as an average of the regression results of the three possible combinations of failure lines.

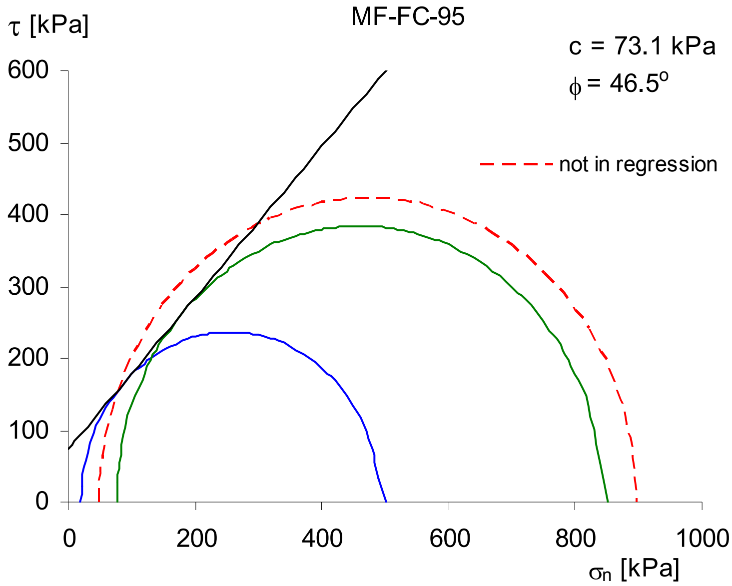

Figure 4.10 Mohr-Coulomb failure criterion for FC at 95% and Mod. MC

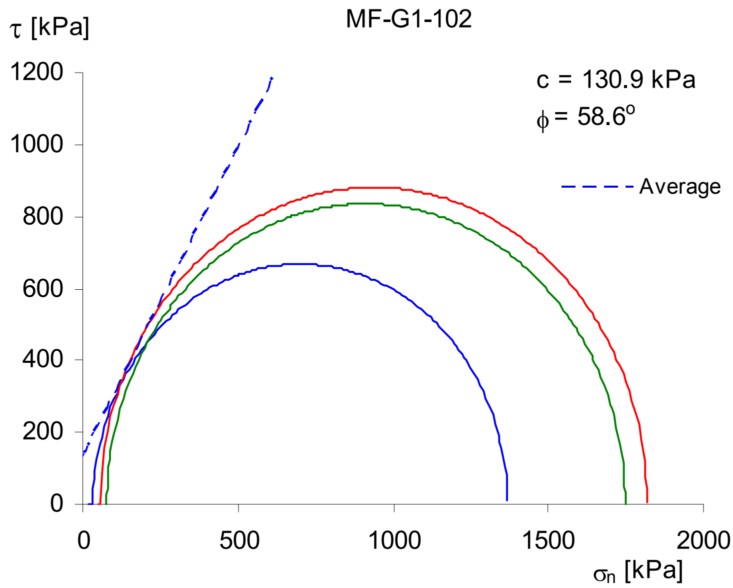

Figure 4.11 Mohr-Coulomb failure criterion for G1 at 102% and Mod. MC

The strength properties of the materials can be compared in terms of c and ϕ. The comparison for the five materials at 100% DOC and Moderate MC is shown in Figure 4.12. While the angle of internal friction in general increases from FC to G1 the cohesion property is dependent on the compaction conditions such as the DOC and MC. In general high cohesion is observed for FC and WB probably due to the cohesive and plastic properties of the natural fine grains in these materials. The effect of DOC and MC on the strength properties of the materials is discussed in section 4.3.4.

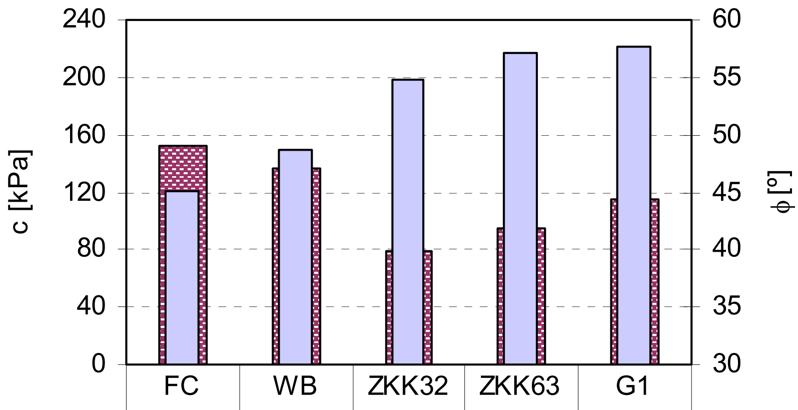

	FC	WB	ZKK32	ZKK63	G1
c [kPa]	152.8	136.1	79.0	94.1	114.3
Φ [°]	45.0	48.6	54.7	57.1	57.6

Figure 4.12 c- and ϕ-values for 100% DOC and moderate MC

4.3.4 Effect of moisture content and degree of compaction on failure behavior

In this research the MF triaxial test results serve different purposes. The failure axial stresses ($\sigma_{1,f}$) at different confining stress (σ_3) levels are used primarily to define the axial stress ratio ($\sigma_1/\sigma_{1,f}$) for the RD cyclic triaxial tests. For a number of models, used to describe the stress dependency of the resilient deformation behavior, the stress needs to be expressed as failure stress ratio thus requiring representative c- and ϕ-values, see also section 4.4.

As the strength properties of the materials apparently change as a result of the influence factors, the effect of these influence factors will be demonstrated in this section for the three materials FC, WB and G1. The obtained c- and ϕ-values are presented in bar charts showing the c- and ϕ-values plotted against the specific influence factor under consideration i.e. MC and DOC. However, as it is not always possible to define failure lines so readily for coarse grain granular materials, the reported c- and ϕ-values may lack consistent trends in such cases. Moreover, these strength parameters may also be influenced through the mode of failure. Shear failure is observed on most of specimens, however in some cases plastic and compression failure is observed. The plastic failure particularly occurred in the cohesive material FC at high moisture content. The compression failure, a failure similar to concrete cube compression test failure, is observed for the coarsest material ZKK63. Figure 4.13 shows typical examples of the various modes of failure observed during the MF testing.

The influence of the DOC on the c- and ϕ-values is investigated for the FC, WB and G1 materials. The influence of MC is investigated only for FC and WB. In the following paragraphs the effect of the two influence factors DOC and MC is demonstrated for each material.

Shear failure | Plastic failure | Compression failure

Figure 4.13 Various modes of failure observed during the MF triaxial tests

Ferricrete

Figure 4.14 shows that for the ferricrete for moderate MC (7.5%) the internal angle of friction values slightly decreases from 46.5° to 45° with an increase of DOC from 95% to 100%. The cohesion c-value significantly increases from 73 to 153 kPa with the increment of the DOC.

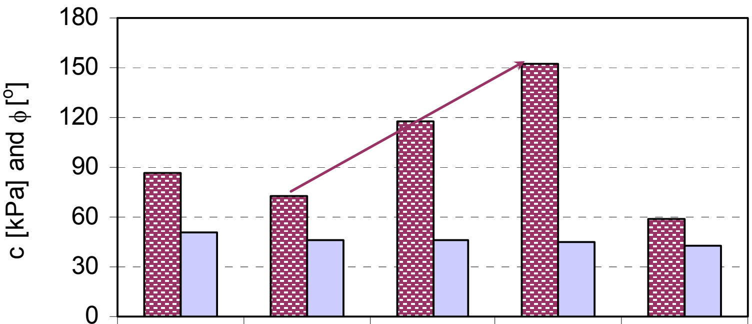

	Dry (5) - 98	Mod.(7.5) - 95	Mod.(7.5) - 98	Mod.(7.5) - 100	Wet (9.5) - 98
c [kPa]	87.0	73.1	117.4	152.8	58.7
Φ [°]	50.9	46.5	45.7	45.0	42.5

Moisture content [%] - Degree of compaction [%]

Figure 4.14 c- and ϕ-values for FC

Figure 4.14 also shows that the FC is sensitive to the moisture content too i.e. for 98% DOC the ϕ-value decreases from 51° to 42° with an increase in moisture from dry to moderate to wet. For the same 98% DOC the c-value is highest (117 kPa) at the moderate moisture content compared to the dry and wet conditions. Overall the strength behavior of the ferricrete is the best at moderate moisture content (7.5%) and high degree of compaction (100%).

Weathered basalt

For the weathered basalt for moderate MC (7%) the ϕ-value increases from 40° to 49° with an increment of the DOC from 95% to 98% to 100%. This is shown in Figure 4.15. The cohesion value is highest at the medium compaction level, i.e. 98% DOC compared to both the 95% and 100% DOC. The smaller c-value for the 100% DOC compared to the 98% DOC is expected to be the result of damaging and crushing of the coarse aggregates due to over-compaction. The aggregate crushing strength of weathered basalt particles seems to be stronger than the strength of the ferricrete particles, however due to their flaky and elongated shape the WB particles are more susceptible to crushing than the ferricrete particles in addition to having a coarser gradation.

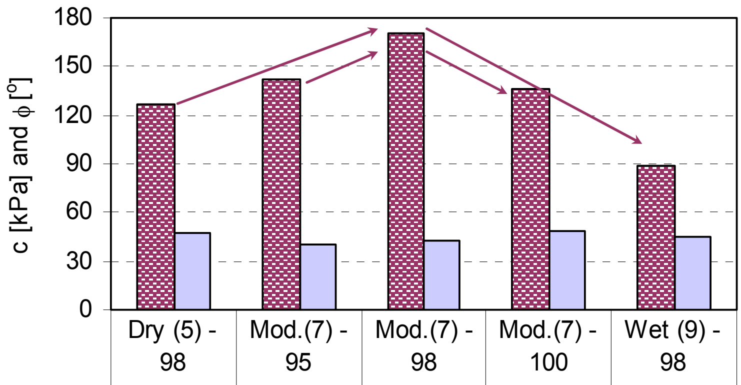

	Dry (5) - 98	Mod.(7) - 95	Mod.(7) - 98	Mod.(7) - 100	Wet (9) - 98
c [kPa]	126.6	142.2	171.0	136.1	88.5
Φ [°]	47.4	40.1	43.1	48.6	45.2

Moisture content [%] - Degree of compaction [%]

Figure 4.15 c- and ϕ-values for WB

Figure 4.15 also shows a similar trend for the cohesion c-value as a function of the moisture content. For 98% DOC the c-value is highest at moderate MC compared to the dry and wet moisture conditions. On the other hand the ϕ-value is somewhat smaller at the moderate moisture content compared to the dry and wet conditions.

Crushed stone

As mentioned earlier it is not always possible to define failure lines easily for coarse granular aggregates. Moreover, the mechanical behavior of crushed aggregates is less sensitive to moisture compared to natural gravels. For that reason both the monotonic and cyclic triaxial test of the G1 is carried out at moderate moisture content, varying only the degree of compaction.

Figure 4.16 shows that for G1 with moderate moisture content (4%) both the internal angle of friction and cohesion generally increase with an increment of the DOC except that the cohesion value decreases for 105% DOC.

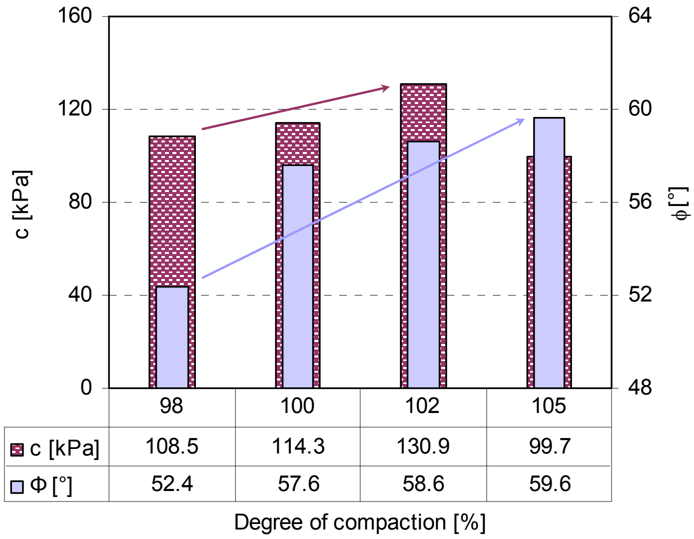

Figure 4.16 c- and ϕ-values for G1 for moderate (4%) MC

Concluding remarks

In general the monotonic failure triaxial tests are capable of providing the overall failure (strength) behavior of the granular materials and trends of the influence factors material type, DOC and MC. However, there are limitations in order to precisely quantify the stress dependency of the strength behavior. One of the major limitations is the small magnitude of the maximum possible confining stress (80 kPa) that can be applied by the system compared to high levels of the failure stress ranging to 1800 kPa. The difference in magnitude between 20, 50 and 80 kPa confining stress is very small compared to the magnitude of the failure stresses.

Another limitation of the triaxial testing is a problem related to the uniform distribution of the confining stress along the height of the specimen. During triaxial testing observations have been made that raise the question whether the vacuum pressure (confining stress), which is induced through inlets at the top and bottom of the specimen, is uniformly distributed throughout the specimen. For further details about this limitation the reader is referred to chapter 7.

4.4 RESILIENT DEFORMATION CYCLIC LOAD TRIAXIAL TEST

4.4.1 Test principle

The cyclic load triaxial compression test is currently the most commonly used method to measure the resilient (elastic) deformation characteristics of aggregates for use in pavement design [5]. The resilient deformation test is performed on a cylindrical specimen subjected to a cyclic axial compressive stress, σ_d, and a constant all-around confining stress, σ_3. A schematic representation of the triaxial loading system is shown in Figure 4.17. The resilient properties, resilient modulus M_r and Poisson's ratio ν, describe the relation between the resilient deformation of a specimen, ε_{1r} and ε_{3r}, and the applied stresses, σ_1 and σ_3, (equations 4-3 and 4-4):

$$\Delta\varepsilon_{1r} = \frac{1}{M_r}[\Delta\sigma_1 - 2\nu\Delta\sigma_3] \qquad 4\text{-}3$$

$$\Delta\varepsilon_{3r} = \frac{1}{M_r}[\Delta\sigma_3(1-\nu) - \nu\Delta\sigma_1] \qquad 4\text{-}4$$

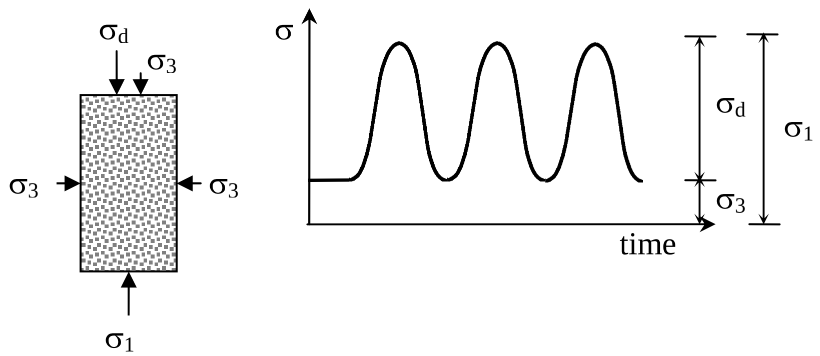

Figure 4.17 Schematic representation of triaxial stress system

For a cylindrical axial symmetrical triaxial specimen the lateral (radial) confining stress (σ_3) and strain (ε_3) are the minor principal stress and strain and the vertical axial stress (σ_1) and strain (ε_1) are the major principal stress and strain. For a constant confining pressure (CCP) resilient deformation test, at any applied stress combination σ_3 = constant and thus $\Delta\sigma_3 = 0$. Equations 4-3 to 4-4 can therefore be simplified to:

$$\Delta\varepsilon_{1r} = \frac{\Delta\sigma_1}{M_r} \qquad 4\text{-}5$$

$$\Delta\varepsilon_{3r} = -\frac{\nu\Delta\sigma_1}{M_r} = -\nu\Delta\varepsilon_1 \qquad 4\text{-}6$$

From equations 4-5 and 4-6 the M_r and ν can thus be expressed as equations 4-7 and 4-8. The M_r determined in this way is in line with the European standard EN 13286-7 [6] for the CCP case:

$$M_r = \frac{\Delta\sigma_1}{\Delta\varepsilon_{1r}} \qquad 4\text{-}7$$

$$\nu = -\frac{\Delta\varepsilon_3}{\Delta\varepsilon_{1r}} \qquad 4\text{-}8$$

4.4.2 Test procedure and test program

The resilient deformation (RD) cyclic triaxial test of the coarse grained (sub)base granular materials is carried out in the large scale CCP triaxial apparatus (300 mm x 600 mm). After the specimen is produced according to the procedure described in section 4.2, the specimen is instrumented as shown in Figure 4.18 for measuring of the deformations.

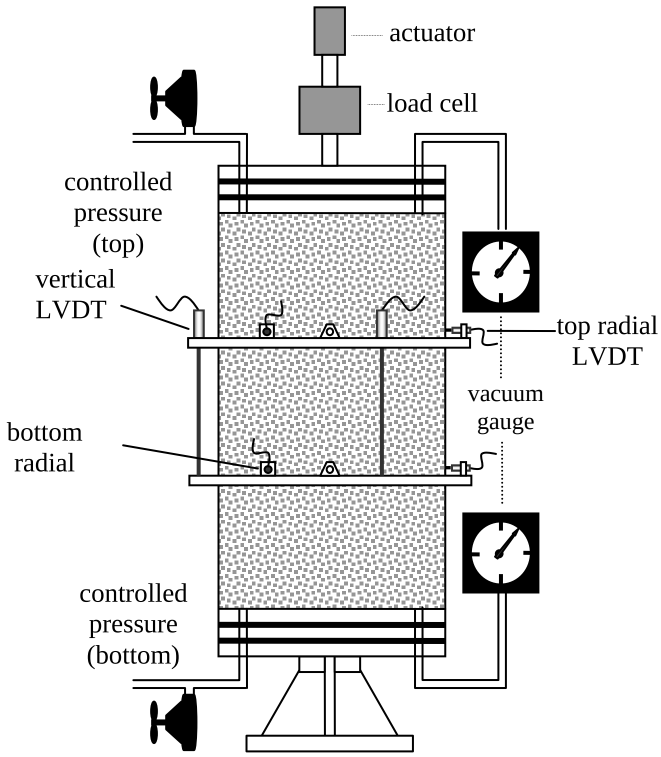

Figure 4.18 CCP resilient deformation triaxial test set up

The instrumentation of the specimen starts with the gluing of especially shaped blocks to the membrane at 1/3 and 2/3 of the specimen height (Figure 4.19). Two measuring rings, upper and lower, are mounted around the specimen supported by the blocks. Each measuring ring is fitted with 3 studs and adjustable springs and with 3 horizontal LVDTs (Linear Variable Differential Transducers) at an equal spacing of 120°. The studs center the ring and the LVDTs measure the radial displacement of the specimen relative to the ring. In addition the upper measuring ring is fitted with 3 vertical LVDTs, at 120° spacing, which extend to the lower ring by means of extenders.

As the specimen deforms under vertical loading the lower and upper ring displace to follow the deformation of respectively the lower 1/3 and 2/3 parts of the specimen. The vertical LVDTs thus measure the difference in deformation of the upper and lower ring. This is the deformation of the middle third part (200 mm) of the specimen where, most likely, a uniform vertical and horizontal stress distribution exists.

Figure 4.19 Fully instrumented triaxial specimen and measuring details

To establish the stress dependency of the resilient modulus M_r and ν the resilient deformation cyclic load triaxial testing was performed at a large number of combinations of the stresses σ_1 and σ_3. The resilient modulus tests were done on virgin specimens with a constant confining stress σ_3.

<u>Conditioning of the specimen</u>
A test starts with a conditioning loading. The conditioning is performed with a stress level corresponding to the maximum stress combination i.e. the maximum confining stress σ_3 and maximum cyclic stress σ_d, applied in the test as per the European standard [6]. In the conditioning phase the cyclic stress σ_d is applied for 20,000 cycles at a frequency of 10 Hz. The 10 Hz frequency for the conditioning phase is chosen to optimize the time required for testing one RD specimen per day starting from preparation of the specimen until removing to take a representative sample for determination of the moisture content. In this way a change in moisture content and a possible curing effect that can result from an extended testing period can be limited. The objective of the cyclic conditioning is to permit the bedding of the end caps of the triaxial apparatus into the specimen, and to allow the stabilization of the permanent strains of the material and attain a practically elastic behavior in the RD test [7].

Measurement readings are taken during conditioning at load cycle numbers 1-20, 50, 100, 200, 400, 1000, 2500, 5000, 10000, 12500, 15000 and 20000. At each selected load cycle number, the readings were recorded for 10 consecutive cycles with the following parameters:

- minimum and maximum axial stress: σ_{1min} and σ_{1max}
- confining stress: σ_3
- resilient and permanent axial strain: ε_{1r} and ε_{1p}
- resilient and permanent radial strain: ε_{3r} and ε_{3p}

Cyclic loading for resilient deformation test

After conditioning the confining stress is reduced to the smallest confining stress level σ_3 and maintained for about 1 hour for strain stabilization. After the confining pressure stabilizes, a constant contact stress, σ_c, is first applied prior to the application of the cyclic stress, σ_d. This small contact stress, 3 to 5 kPa, is only to ensure constant contact between the actuator piston and the top platen during dynamic testing.

When considering the behavior of granular materials under cyclic loading it is useful to compare the magnitude of the vertical stress, σ_1, to the peak vertical stress at failure $\sigma_{1,f}$ obtained from the monotonic failure triaxial tests. The ratio $\psi = \sigma_1/\sigma_{1,f}$ is hence defined for this purpose, with a ψ-value close to one implying that the cyclic loading amplitude approaches the peak strength of a monotonically sheared specimen at the same confining stress σ_3.

The cyclic stress range applied is thus determined based on the ratio of axial stress to their respective failure axial stress, i.e. ψ = 0.05 to 0.6, where the monotonic failure triaxial tests are carried out prior to the cyclic load triaxial tests as reported in section 4.3. At each of the stress combinations, shown in table 4-2, the specimen is loaded for 100 cycles with a haver-sine load shape at a frequency of 1 Hz, see Figure 4.20. Measurement readings are recorded for the last 10 cycles of the 100 load cycles per each load combination i.e. cycles #91 to #100 are recorded. The average stress and strain values of these 10 cycles are used in the analyses.

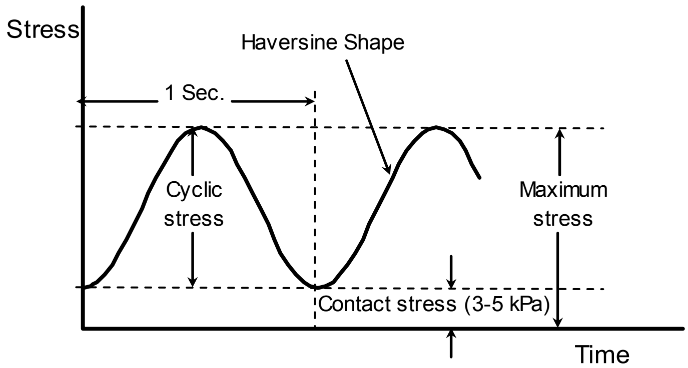

Figure 4.20 Haver-sine curve for RD triaxial test

Test program

Similar to the MF triaxial test the resilient deformation cyclic load triaxial test is also carried out on five materials FC, WB, G1, ZKK63 and ZKK32 at different compaction conditions that ranged from 95% to 105% DOC and dry to wet MC. DOC is measured as percentage of the modified Proctor dry density of each material and similarly MC is measured relative to the moderate (Mod.) moisture content measured in the modified Proctor compaction as given in table 3.3. The test conditions for the RD triaxial tests are shown in table 4-3.

Table 4-2 Stress combination for each cyclic loading RD test specimen

Sequence No.	Confining stress σ_3 (kPa)	Cyclic stress σ_d (kPa) Minimum	Maximum based on $\sigma_1/\sigma_{1,f}$	No. of Load Applications
1	20	0	0.05	100
2	20	0	0.1	100
3	20	0	0.15	100
4	20	0	0.2	100
5	35	0	0.1	100
6	35	0	0.15	100
7	35	0	0.2	100
8	35	0	0.3	100
9	35	0	0.35	100
10	50	0	0.15	100
11	50	0	0.2	100
12	50	0	0.3	100
13	50	0	0.35	100
14	50	0	0.4	100
15	65	0	0.2	100
16	65	0	0.3	100
17	65	0	0.35	100
18	65	0	0.4	100
19	65	0	0.5	100
20	80	0	0.25	100
21	80	0	0.3	100
22	80	0	0.4	100
23	80	0	0.5	100
24	80	0	0.6	100

Table 4-3 RD cyclic load triaxial test program

Material	Target DOC (%)	Target MC (%)	Test code	Specimen
FC	95	Mod. (7.5)	RD-FC-95	virgin
	98	Dry (5)	RD-FC-98dr	virgin
		Mod. (7.5)	RD-FC-98	virgin
		Wet (9.5)	RD-FC-98wt	virgin
	100	Mod. (7.5)	RD-FC-100	virgin
WB	95	Mod. (7)	RD-WB-95	virgin
	98	Dry (5)	RD-WB-98dr	virgin
		Mod. (7)	RD-WB-98	virgin
		Wet (9)	RD-WB-98wt	virgin
	100	Mod. (7)	RD-WB-100	virgin
G1	98	Mod. (4)	RD-G1-98	virgin
	100	Mod. (4)	RD-G1-100	virgin
	102	Mod. (4)	RD-G1-102	virgin
	105	Mod. (4)	RD-G1-105	virgin
ZKK32	100	Mod. (3)	RD-ZKK32-100	virgin
ZKK63	100	Mod. (3)	RD-ZKK63-100	virgin

4.4.3 Resilient modulus

The effect of the confining stress σ_3 and deviatoric stress σ_d on the resilient modulus M_r was assessed by recording bursts of resilient (recoverable) strain and cyclic axial stress data for the last 10 cycles of each 100 cycles in a test. In the study M_r is calculated according to equation 4-7, where $\Delta\varepsilon_{1r}$ is the recoverable portion of axial strain, and $\Delta\sigma_1$ is the difference between the maximum $\sigma_{d,max}$ and minimum $\sigma_{d,min}$ cyclic stress of the actuator as shown in Figure 4.20.

The resilient strain $\Delta\varepsilon_{1r}$ was computed from the resilient deformation which was recorded over the middle third height of the specimen. Figure 4.21 presents a typical example of the response of one of the materials, FC, at moderate MC and 98% DOC (RD-FC-98) during the conditioning phase and a series of short loading (100 cycles each) of the cyclic triaxial test, with a stress level corresponding to typical conditions in a pavement layer. The response of the material is elasto-plastic. It can be observed that during the first load cycles in the conditioning phase the permanent strains increase rapidly. After this initial phase the permanent strains tend to stabilize (or continue to increase at a very slow rate) and the response of the material becomes essentially elastic. This “stable” behavior is generally obtained after several thousands of load cycles. As already mentioned, the conditioning phase includes 20,000 load cycles.

In Figure 4.21 it can also be observed that in the series of short loading phase the stress-strain curve in a full cycle of loading and unloading is smoother (more stable) than in the conditioning phase. In addition to the stabilization of the specimen after conditioning this can also be related to the loading time i.e. the difference in loading frequency 10 Hz during the conditioning phase and 1 Hz for the series of short loadings.

Lekarp et al. [8] reported that loading time/frequency has only a limited effect on the response of granular materials and its influence is not investigated in this study. However a close observation on the stress-strain relation reveals that depending on the accuracy of the loading actuator and nature of the software employed, a higher loading frequency gives less accurate load records in the two extreme ends, the minimum and maximum peaks, of the loading cycle. For instance, in Figure 4.21 the minimum contact stress of the cyclic loading is targeted for about 5 kPa. The series of short loading tested at a frequency of 1 Hz yields a contact stress of 3 to 5 kPa while the contact stress at the conditioning phase with a frequency of 10 Hz shows about 20 kPa.

Similarly the maximum peak of the cyclic stress is less for the conditioning phase compared to the series of short loadings. It is to be noted that such variation is not due to accuracy of the data sampling rate. For all the triaxial tests in this study the sampling rate adopted is 500 samples/sec for the conditioning phase with loading frequency 10 Hz and 100 samples/sec for the series of short loadings with loading frequency of 1 Hz. The sampling rate difference is only by half whereas the recording accuracy variation between the conditioning phase and series of short loadings is significantly high. Consequently in this study for the series of short loadings, where the resilient modulus and Poisson’s ratio are determined, a 1 Hz loading frequency is used consistently.

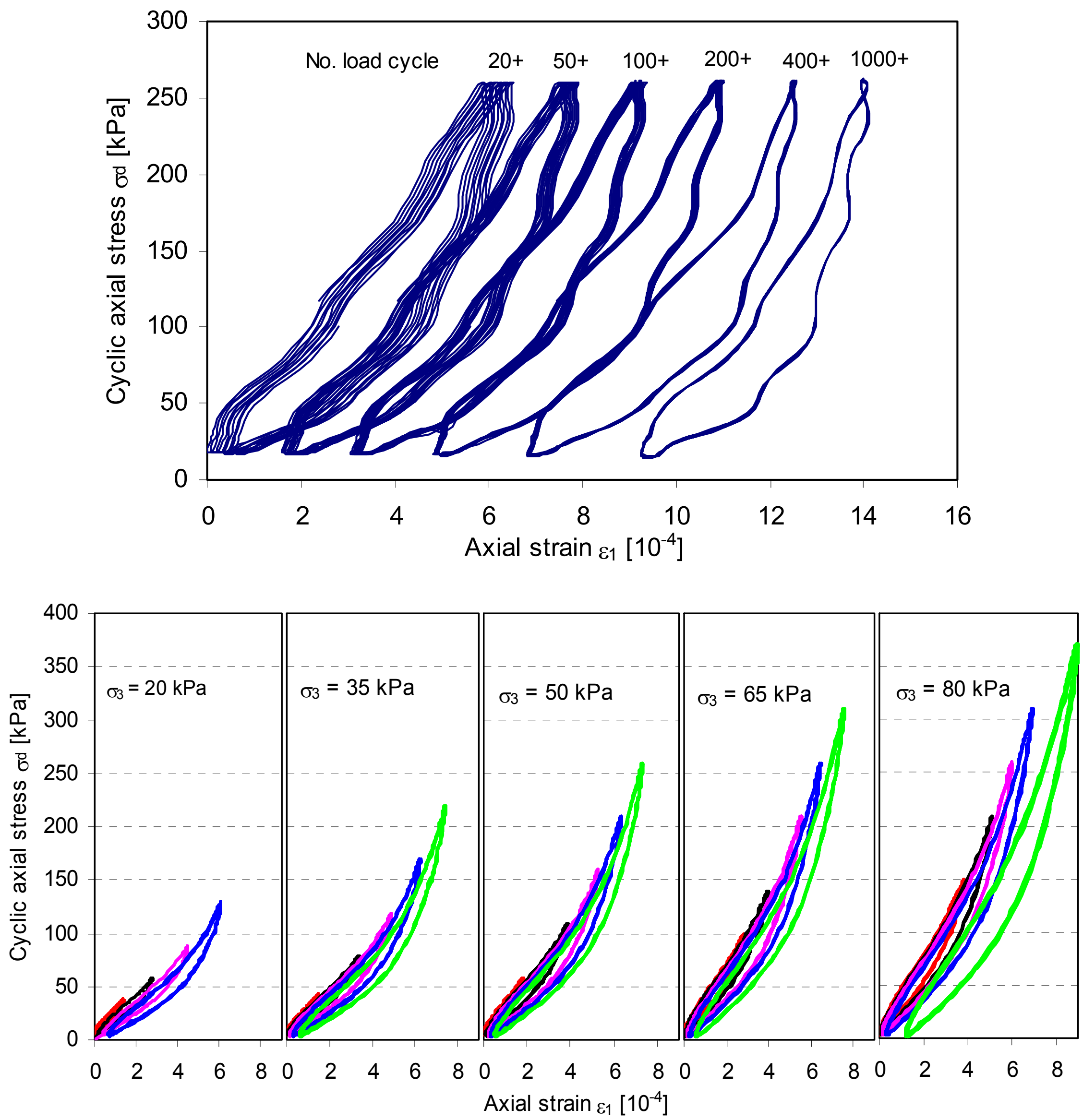

Figure 4.21 Example of stress-strain cycles during conditioning (top) and series of short loading phases (bottom) in a cyclic triaxial test of FC material

Figure 4.22 shows a typical example of M_r-values for two materials, WB and G1, as a function of the confining stress and the sum of principal stress θ. In section 4.4.2 it is explained that a resilient deformation test is performed under increasing confining stress levels. In order to be able to discriminate between the influence of the individual principal stresses σ_1 and σ_3 on M_r, the M_r-values at each σ_3-level are presented with different symbols.

Close examination of Figure 4.22 demonstrates that the M_r-value increases with increasing confining stress, a phenomenon that is called "stiffening". At a particular σ_3-level the M_r-value also increases with increasing σ_d/σ_3 ratio except for the lowest σ_3 for WB where the M_r-value first decreases and then increases with increasing σ_d/σ_3 ratio. The later tendency of decreasing and then increasing M_r-values with an increase of the σ_d/σ_3 ratio is basically observed for relatively less strong materials and/or compacted mixtures tested at less than about 70 kPa cyclic axial stress σ_d.

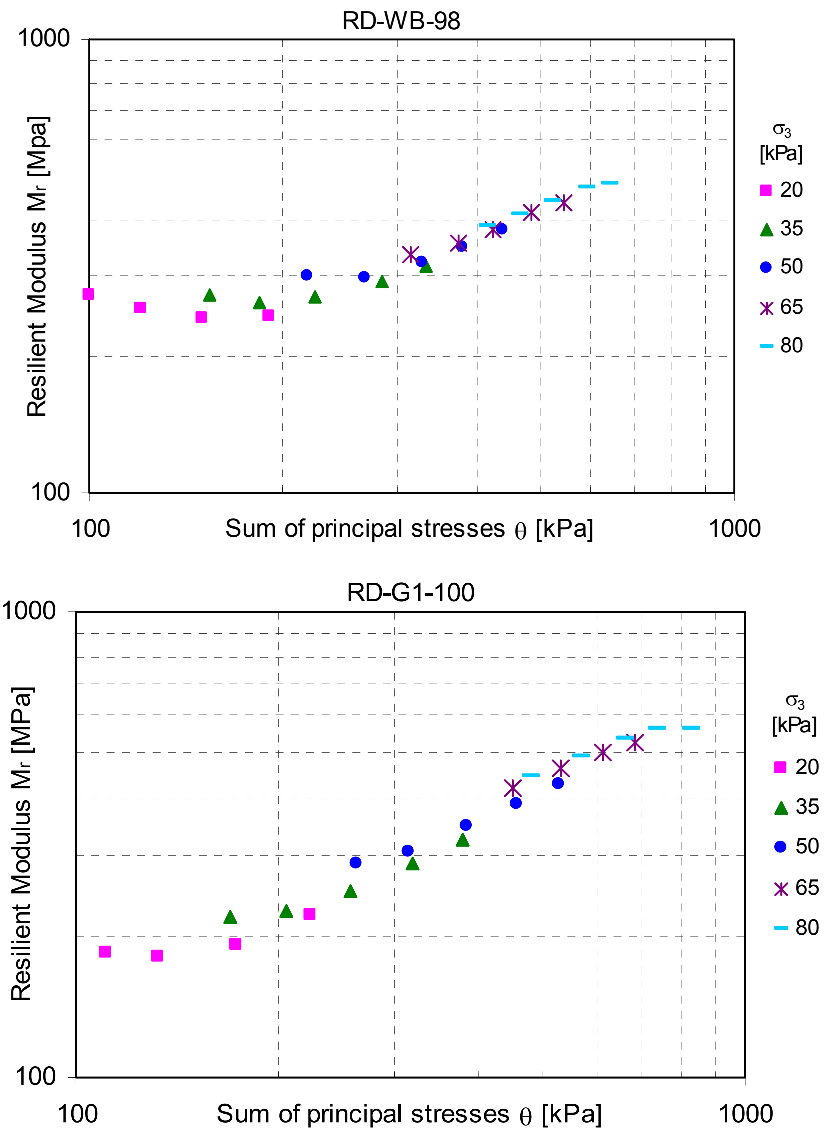

Figure 4.22 Resilient modulus M_r as a function of σ_3 and θ for WB and G1

In Figure 4.22 at low load levels, i.e. 20 kPa confining pressure and low deviator stress, a decreasing trend of M_r with increasing deviator stress is observed i.e. “softening” of the material. When granular materials are subjected to compaction, they rearrange themselves by translating and rotating to become locked in a final position. After the externally applied compaction stress is removed, this final stage is not a stress free state, but rather a residual stress state. The residual stress state includes the effect of both confinement and aggregate interlock. Uzan [13] experimentally demonstrated the residual stress produced in granular bases. With out significant confinement when such compacted specimens are subjected to low deviator stress, the stress causes a disturbance on the aggregate interlock “softening” and cause decrease in M_r.

4.5 MODELING RESILIENT DEFORMATION BEHAVIOR

For cyclic load triaxial tests with constant confining stress, the resilient modulus and Poisson's ratio are defined by equation 4-7 and 4-8 respectively. Among all the factors that affect M_r (density, grading, moisture content, stress history, aggregate type) the most important factor is the stress state [8-10]. Several models have been developed to address the effect of stress state on the resilient response.

A great many models exist for describing the stress dependency of the resilient modulus. In fact these are often quite related. In this research a limited number of models are applied and evaluated which comprises of on the one hand relatively simple, extensively used models and on the other hand more complex but physically more correct models.

4.5.1 $M_r - \Theta$ model

The $M_r - \theta$ model as stated in section 2.3.1.1 is a power relationship between the sum of the first stress invariant θ (bulk stress) and the resilient modulus:

$$M_r = k_1 \left(\frac{\theta}{\sigma_o} \right)^{k_2} \qquad \text{4-9}$$

Where k_1, k_2 are model parameters and σ_o = 1 kPa is the reference stress. This model is widely used for its simplicity. Figure 4.23 to 4.25 show plots of the measured M_r-values versus the sum of principal stresses θ together with their fitted M_r-θ model for FC, G1 and ZKK. As can be seen from the figures and from the value of the correlation coefficients r^2, the M_r-θ model provides a good fit between the measured values of M_r and its model-predicted value.

The real test for a material model lies in its capability to accurately predict both components of strains. The model fit is carried out using a non-linear least square regression technique to predict the axial ε_1 and radial ε_3 resilient strains using the M_r-θ model parameters k_1, k_2 and Poisson's ratio as a constant, see equation 4-10 and 4-11, to fit the measured axial ε_1 and radial ε_3 resilient strains. The measured and model-predicted axial and radial strains are shown along with the M_r-θ plots in Figures 4.23 to 4.25.

$$\varepsilon_1 = \frac{\Delta\sigma_1}{k_1 \left(\frac{\theta}{\sigma_o} \right)^{k_2}} \qquad \text{4-10}$$

$$\varepsilon_3 = -\nu \frac{\Delta\sigma_1}{k_1\left(\dfrac{\theta}{\sigma_o}\right)^{k_2}} \qquad 4\text{-}11$$

In the model fit three parameters including the constant Poisson's ratio have been used in the regression. One of the limitations of this model is the use of a constant Poisson's ratio. As demonstrated by several researchers [2, 3, 11] the Poisson's ratio exhibits to a certain extent stress dependent behavior. In the regression carried out for the test results the constant Poisson's ratio obtained as model parameter is found to be often greater than 0.5. This is an indication of an increasing volume of the specimen. This phenomenon is also explained by the anisotropic K–G model described in section 4.5.3. In addition the model is not capable of discriminating the influence that the confining stress σ_3 and the deviatoric stress σ_d individually have on M_r. It thus predicts equal M_r-values for equal values of θ, irrespective if θ is composed of low σ_3- and high σ_d-values or vice versa. Despite these drawbacks the model shows a good fit with the measured data, see Figure 4.23 to 4.25. For all the materials tested in different conditions the model parameters are summarized in table 4-4. It should be noted that in all analyses in this chapter compression stresses and strains are labeled as positive and tensile stresses and strains as negative.

4.5.2 The Universal model and TU Delft model

<u>The Universal model</u>

May and Witczak [12] noted that the in-situ resilient modulus of a granular layer is a function of not only the bulk stress but also of the magnitude of the shear strain induced mainly by shear or deviator stress. Uzan [13] included the deviatoric stress into the M_r-θ model and wrote the equation as equation 4-12. This classical Universal model is deemed the best compromise between ease of implementation and accuracy as was stated by Andrei et al [14] compared to the modified Universal model shown in section 2.3.1.1.

$$M_r = k_1\left(\frac{\theta}{\sigma_o}\right)^{k_2}\left(\frac{\sigma_d}{\sigma_o}\right)^{k_3} \qquad 4\text{-}12$$

Where k_1, k_2 and k_3 are model parameters, θ is the bulk stress and σ_d is the deviatoric stress.

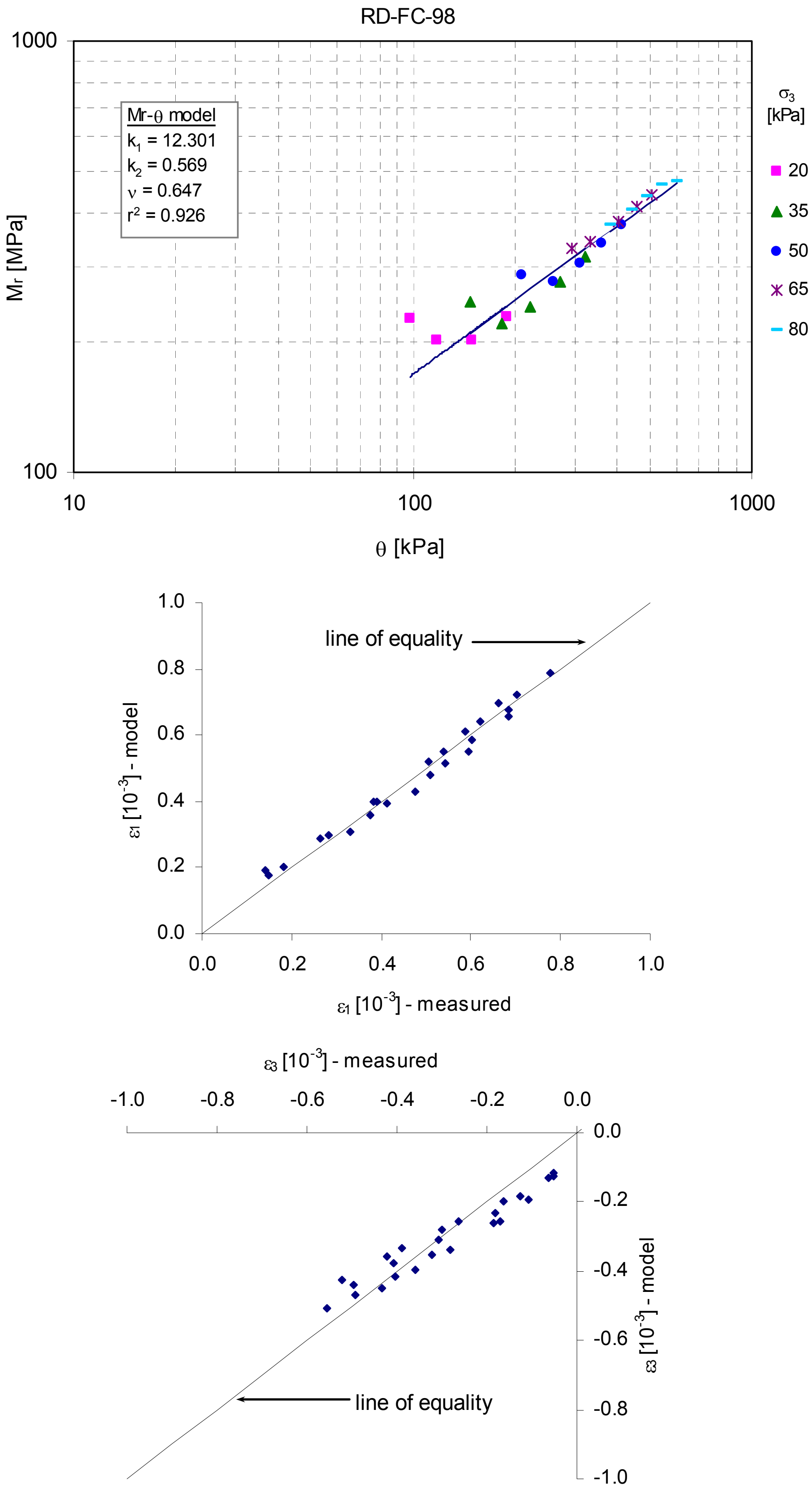

Figure 4.23 M_r vs. θ data, M_r-θ model for FC with 98% DOC, moderate (7.5%) MC and measured vs. model-predicted strains

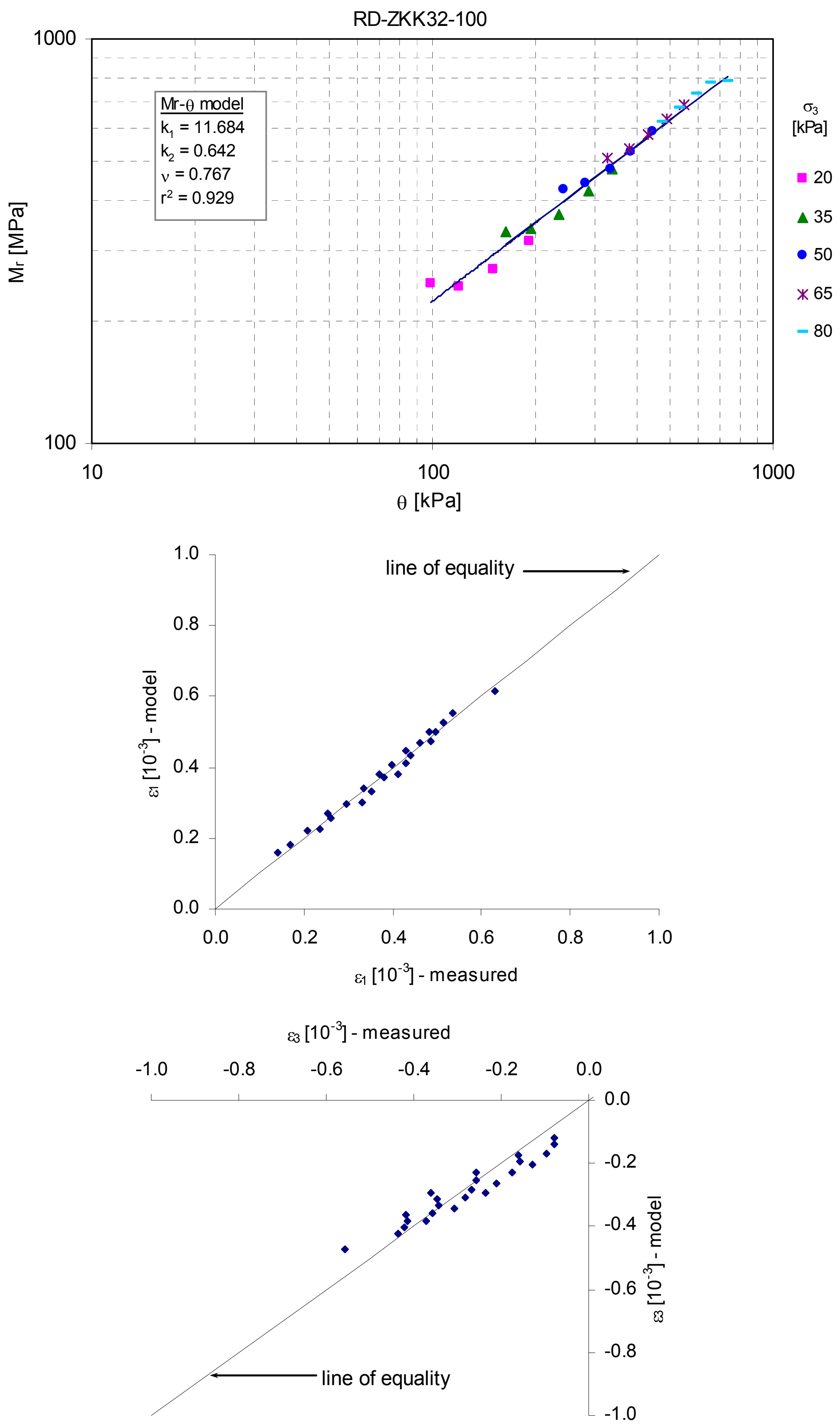

Figure 4.24 M_r vs. θ data and M_r-θ model for ZKK32 with 100% DOC, moderate (3%) MC and measured vs. model-predicted strains

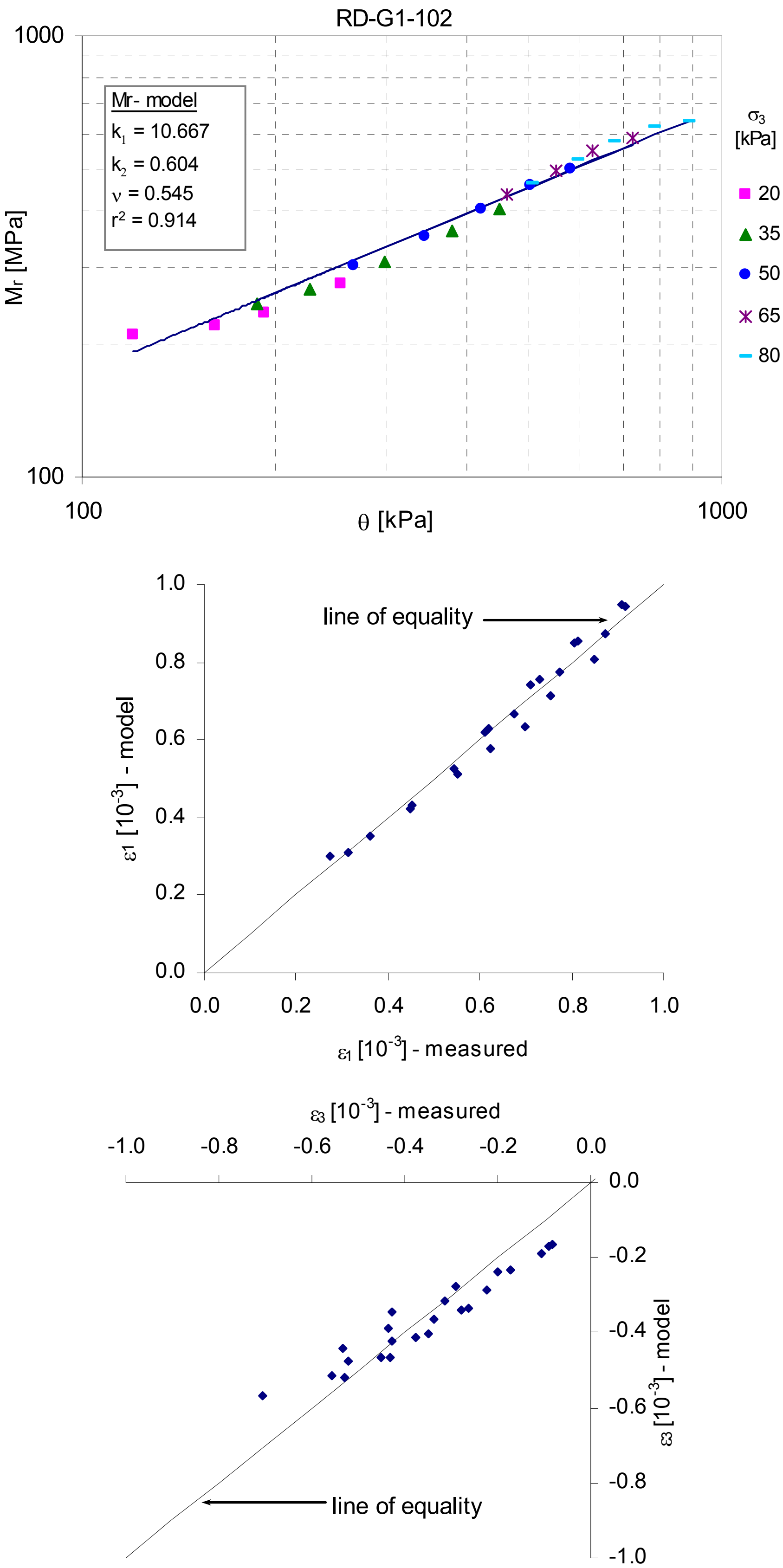

Figure 4.25 M_r vs. θ data and M_r-θ model for G1 with 102% DOC, moderate (4%) MC and measured vs. model-predicted strains

Table 4-4 M_r –θ model prediction parameters for all materials

Test code	DOC (%)	MC (%)	M_r – θ model parameters			
			k_1 [MPa]	k_2 [-]	ν [-]	r^2 [-]
RD-FC-95	95[i] 95.6[ii]	7.5[i] 7.5[ii]	139.7	0.218	0.513	0.976
RD-FC-98dr	98 84.6	5 7	175.9	0.168	0.358	0.953
RD-FC-98	98 98.2	7.5 8.5	12.30	0.569	0.647	0.926
RD-FC-98wt	98 97.9	9.5 9.6	45.52	0.359	0.418	0.928
RD-FC-100	100 100.1	7.5 7.8	33.65	0.425	0.478	0.952
				Average	r^2:	0.947
RD-WB-95	95 94.8	7 7.3	25.58	0.453	0.285	0.956
RD-WB-98dr	98 95.8	5 5.6	24.35	0.430	0.277	0.947
RD-WB-98	98 96.8	7 8.6	35.39	0.394	0.274	0.959
RD-WB-98wt	98 96.7	9 10.5	10.26	0.578	0.276	0.956
RD-WB-100	100 99	7 8.2	20.22	0.479	0.319	0.948
				Average	r^2:	0.953
RD-G1-98	98 97.3	4 4	6.221	0.691	0.433	0.880
RD-G1-100	100 99.4	4 4.1	8.126	0.635	0.719	0.886
RD-G1-102	102 102.0	4 3.9	10.66	0.604	0.545	0.916
RD-G1-105	105 104.1	4 3.8	30.32	0.438	0.782	0.930
				Average	r^2:	0.903
RD-ZKK32-100	100 99.7	3 3.3	11.68	0.642	0.767	0.929
RD-ZKK63-100	100 100.3	3 3.0	10.87	0.684	0.721	0.919

[i]: intended DOC and MC
[ii]: achieved DOC and MC

This model has shown to be superior to the M_r-θ model in some studies [15, 16]. The model is physically better than the M_r-θ model, in the sense that it takes into account the influence of the deviatoric stress σ_d on the M_r-values. The first term of the model describes the increase of M_r with increasing σ_3 and σ_d values, but it can't discriminate between the influence that the stress invariants σ_3 and σ_d individually have on M_r. The second term is therefore introduced to express the role the deviatoric stress can have on the M_r.

The method of regression is similar to the regression used for the M_r-θ model that axial and radial strains are predicted using the model parameters k_1, k_2, k_3 and constant Poisson's ratio to fit the measured strains as shown in the equations 4-13 and 4-14.

$$\varepsilon_1 = \frac{\Delta\sigma_1}{k_1\left(\frac{\theta}{\sigma_o}\right)^{k_2}\left(\frac{\sigma_d}{\sigma_o}\right)^{k_3}} \qquad \text{4-13}$$

$$\varepsilon_3 = -\nu\frac{\Delta\sigma_1}{k_1\left(\frac{\theta}{\sigma_o}\right)^{k_2}\left(\frac{\sigma_d}{\sigma_o}\right)^{k_3}} \qquad \text{4-14}$$

Figure 4.26 shows a model fit to the measured M_r-values along with their measured and model-predicted axial and radial strain plots for WB. From the resulting $r^2 = 0.977$ and the plots of the measured and model-predicted strains it is observed that this model fits better than the M_r-θ model and particularly it perfectly predicts the radial strains ε_3 as can be seen in the measured vs. model-predicted plot of the radial strain. For all the materials tested in different conditions the universal model parameters are summarized in table 4-5.

TU Delft model

As reported in section 2.3.1.1 Huurman [3] has derived a model, equation 4-15, that describes better the resilient behavior of the Netherlands subbase sands, particularly at high stress levels close to failure. The first term of the model describes the increase of M_r for increasing σ_3 values. The second term serves to describe the decrease of M_r as loading approaches failure ($\sigma_1/\sigma_{1,f} \rightarrow 1$). However, since the RD tests in this research are carried out at stress levels far below the failure load (table 4-2) this decreasing M_r as load approaches failure will not appear.

$$M_r = k_1\left(\frac{\sigma_3}{\sigma_0}\right)^{k_2}\left(1-k_3\left(\frac{\sigma_1}{\sigma_{1,f}}\right)^{k_4}\right) \qquad \text{4-15}$$

A similar regression method is employed to determine the model parameters k_1, k_2, k_3, k_4 along with constant Poisson's ratio and to fit the model-prediction to the measured data. Figure 4.27 shows a model fit of G1 to the measured values. For all the materials tested in different conditions the TU Delft model parameters are summarized in table 4-6.

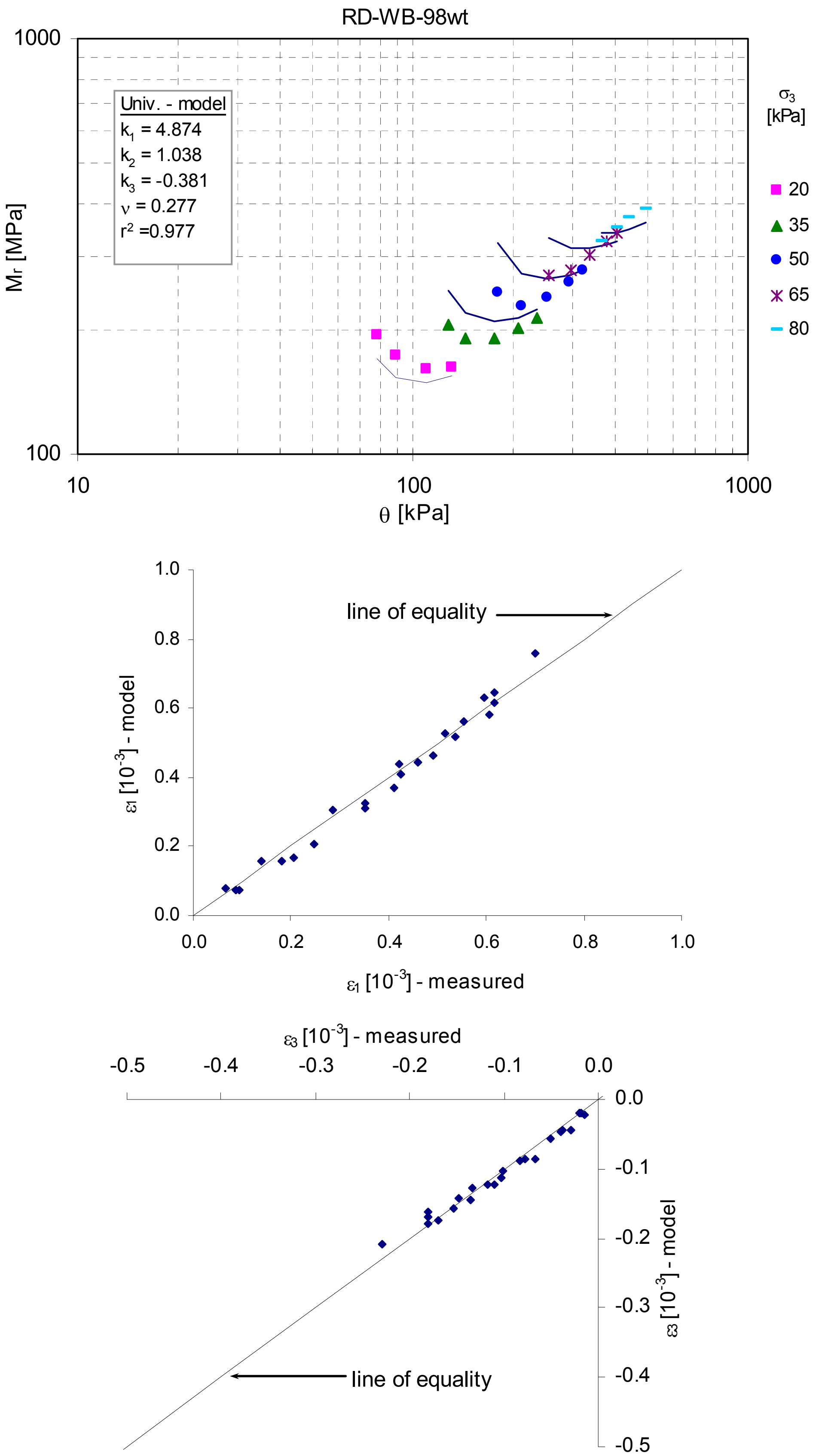

Figure 4.26 M_r vs. θ data and Universal model for WB with 98% DOC, wet (9%) MC and measured vs. model-predicted strains

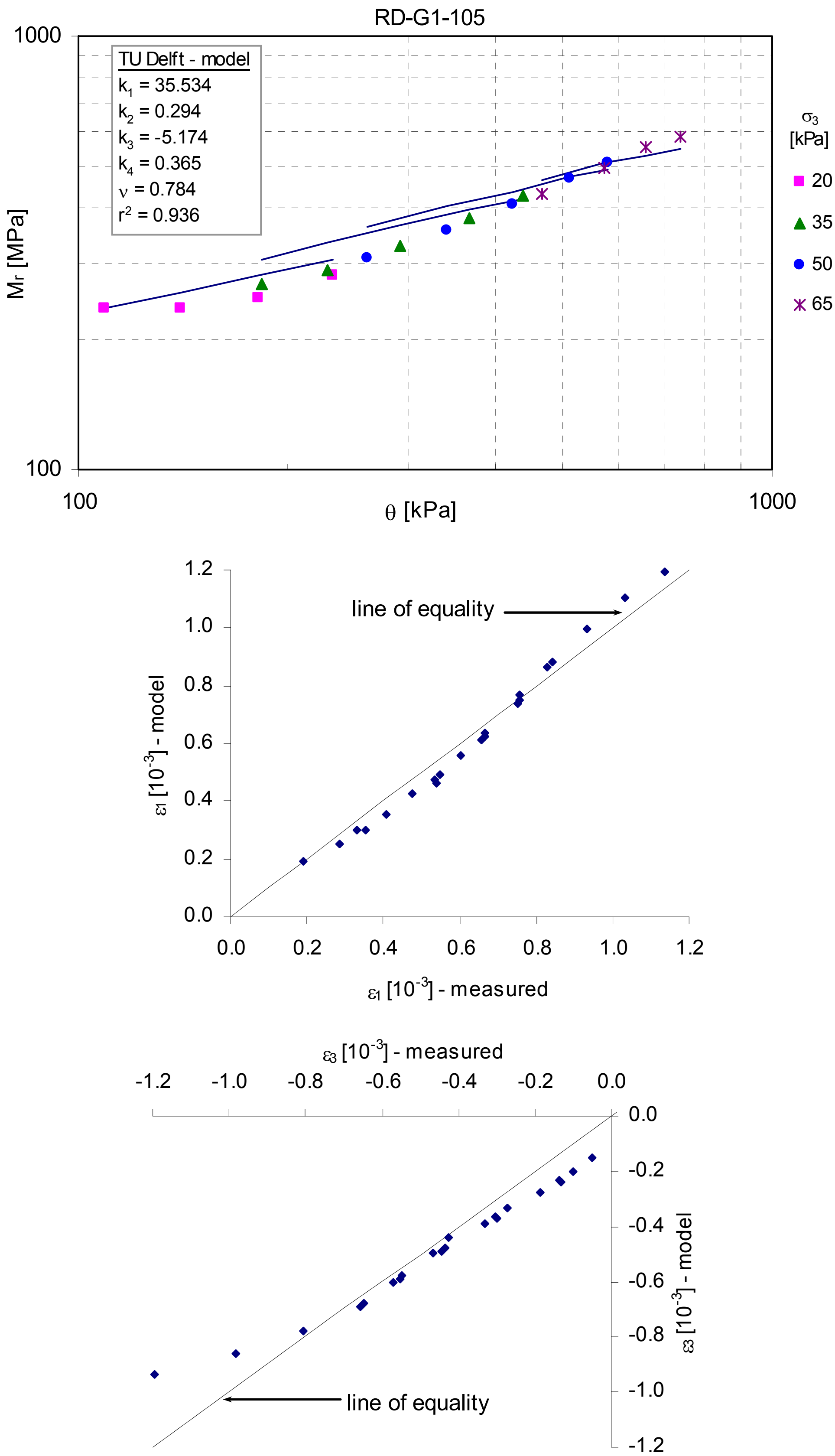

Figure 4.27 M_r vs. θ data and TU Delft model for G1 with 105% DOC, moderate (4%) MC and measured vs. model-predicted strains

Table 4-5 Universal model prediction parameters for all materials

Test code	DOC (%)	MC (%)	Universal model parameters				
			k_1 [MPa]	k_2 [-]	k_3 [-]	ν [-]	r^2 [-]
RD-FC-95	95[i] 96.5[ii]	7.5[i] 7.5[ii]	91.36	0.436	-0.185	0.514	0.982
RD-FC-98dr	98 84.6	5 7	83.91	0.654	-0.403	0.359	0.966
RD-FC-98	98 98.2	7.5 8.5	6.508	1.073	-0.440	0.653	0.960
RD-FC-98wt	98 97.9	9.5 9.6	23.19	0.670	-0.247	0.420	0.939
RD-FC-100	100 100.1	7.5 7.8	21.65	0.784	-0.318	0.480	0.966
					Average	r^2:	0.963
RD-WB-95	95 94.8	7 7.3	13.35	0.929	-0.405	0.287	0.980
RD-WB-98dr	98 95.8	5 5.6	12.97	0.856	-0.354	0.277	0.960
RD-WB-98	98 96.8	7 8.6	20.12	0.790	-0.335	0.275	0.971
RD-WB-98wt	98 96.7	9 10.5	4.874	1.038	-0.381	0.277	0.977
RD-WB-100	100 99	7 8.2	10.89	0.902	-0.357	0.321	0.964
					Average	r^2:	0.970
RD-G1-98	98 97.3	4 4	2.126	1.566	-0.760	0.439	0.955
RD-G1-100	100 99.4	4 4.1	2.408	1.601	-0.826	0.727	0.939
RD-G1-102	102 102.0	4 3.9	5.411	1.198	-0.518	0.549	0.940
RD-G1-105	105 104.1	4 3.8	18.98	0.770	-0.274	0.784	0.933
					Average	r^2:	0.942
RD-ZKK32-100	100 99.7	3 3.3	5.832	1.206	-0.491	0.772	0.966
RD-ZKK63-100	100 100.3	3 3.0	4.943	1.243	-0.473	0.726	0.948

[i]: *intended DOC and MC*
[ii]: *achieved DOC and MC*

4.5.3 Anisotropic K–G model

Boyce's K–G model separates stresses and strains into volumetric and shear components using the equations 2-10 and 2-11 discussed in section 2.3.1.1. The stresses applied to the triaxial specimen are separated into the mean normal stress p and shear (deviatoric) stress q. Their relation with the principal stresses is also presented in section 2.3.1.1. These stresses applied to the triaxial specimen can be plotted in p-q stress space, as shown in Figure 4.28.

Due to the nature of the constant confining pressure (CCP) test, all stress paths are at the same angle, $\Delta q/\Delta p = 1/3$, since the change in deviator stress between beginning and end of the stress path Δq equals $\Delta\sigma_1$ in the triaxial test and the change in mean normal stress Δp equals 1/3*$\Delta\sigma_1$. The fixed angle of the stress paths to the p-q axes demonstrates one of the limitations of the CCP triaxial test i.e. rotation of stress paths is not feasible in such tests.

The confining stresses levels can clearly be recognized in the p-q plots. At each given level of confining stress, the stress paths for all tests at that level of σ_3 plot on the same line. Each stress path starts at q equal to the actuator contact stress and p equal to the respective confining stress plus one third of the contact stress.

Table 4-6 TU Delft model prediction parameters for all materials

Test code	DOC (%)	MC (%)	Universal model parameters					
			k_1 [MPa]	k_2 [-]	k_3 [-]	k_4 [-]	ν [-]	r^2 [-]
RD-FC-95	95[i] 96.5[ii]	7.5[i] 7.5[ii]	20.44	0.299	-4.542	-0.135	0.514	0.981
RD-FC-98dr	98 84.6	5 7	94.72	0.400	39.24	31.41	0.354	0.952
RD-FC-98	98 98.2	7.5 8.5	51.60	0.454	-1.269	1.693	0.653	0.960
RD-FC-98wt	98 97.9	9.5 9.6	60.92	0.411	39.24	31.41	0.419	0.939
RD-FC-100	100 100.1	7.5 7.8	76.37	0.426	39.24	31.41	0.481	0.960
						Average	r^2:	0.958
RD-WB-95	95 94.8	7 7.3	58.19	0.469	-46.25	5.129	0.287	0.980
RD-WB-98dr	98 95.8	5 5.6	57.25	0.403	-0.950	1.677	0.277	0.961
RD-WB-98	98 96.8	7 8.6	90.50	0.340	-2.868	3.115	0.275	0.974
RD-WB-98wt	98 96.7	9 10.5	26.78	0.586	-110.5	5.391	0.277	0.979
RD-WB-100	100 99	7 8.2	59.16	0.421	-3.564	2.848	0.321	0.967
						Average	r^2:	0.972
RD-G1-98	98 97.3	4 4	4.158	0.706	-6.007	0.153	0.439	0.960
RD-G1-100	100 99.4	4 4.1	18.16	0.663	-1.203	0.484	0.728	0.942
RD-G1-102	102 102.0	4 3.9	35.27	0.438	-2.791	0.554	0.549	0.943
RD-G1-105	105 104.1	4 3.8	35.53	0.294	-5.174	0.365	0.784	0.936
						Average	r^2:	0.945
RD-ZKK32-100	100 99.7	3 3.3	31.708	0.516	-2.195	0.433	0.772	0.964
RD-ZKK63-100	100 100.3	3 3.0	31.37	0.542	-2.843	0.504	0.726	0.949

[i]: *intended DOC and MC*
[ii]: *achieved DOC and MC*

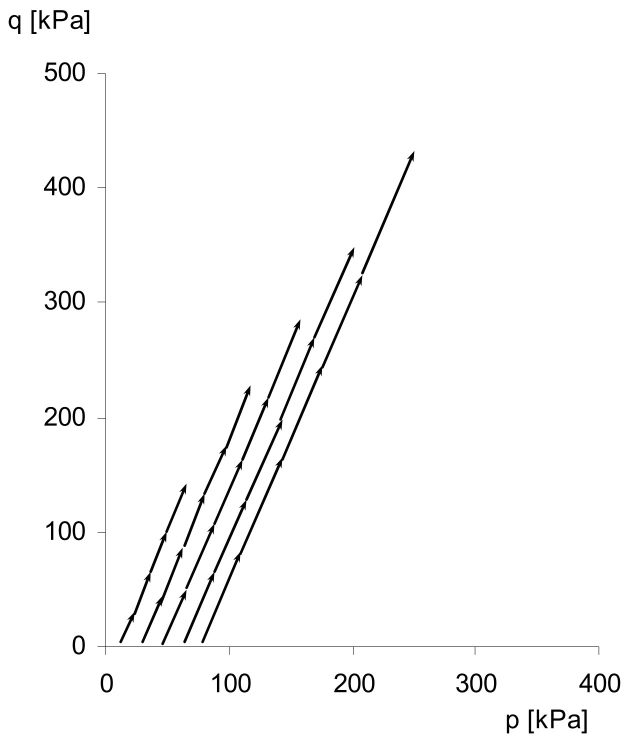

Figure 4.28 p-q stress-space representation of stresses applied in the CCP resilient deformation triaxial testing

Several researchers have concluded from experimental studies on granular materials that the measured horizontal specimen stiffness is typically less than the vertical one [5, 17, 18]. This is primarily due to the preferential orientation of the longest dimension of sand and aggregate particles in the horizontal plane, which occurs during specimen preparation and testing.

As elaborated in the literature review section 2.3.1.1, to account for the anisotropic nature of granular materials in pavements a generalized K–G model for anisotropic material is developed by Hornych et al [19] from the Boyce [20] model. The volumetric and shear strain equations of the model are given in equations 2-16 and 2-17 and presented again in equation 4-16 and 4-17 for convenience. The model is a four parameter model with K_a, G_a, n and the anisotropic coefficient γ which is the ratio of horizontal to vertical stiffness modulus.

$$\varepsilon_v = \frac{p^{*n}}{p_a^{n-1}}\left[\frac{\gamma+2}{3K_a} + \frac{(n-1)}{18G_a}(\gamma+2)\left(\frac{q^*}{p^*}\right)^2 + \frac{\gamma-1}{3G_a}\left(\frac{q^*}{p^*}\right)\right] \qquad \text{4-16}$$

$$\varepsilon_q = \frac{2}{3}\frac{p^{*n}}{p_a^{n-1}}\left[\frac{\gamma-1}{3K_a} + \frac{(n-1)}{18G_a}(\gamma-1)\left(\frac{q^*}{p^*}\right)^2 + \frac{2\gamma+1}{6G_a}\left(\frac{q^*}{p^*}\right)\right] \qquad \text{4-17}$$

It should be noted that the anisotropic nature of granular materials can be better characterized in the laboratory by using a true triaxial testing device with a variable confining pressure (VCP). In a consistent laboratory approach for investigating the anisotropic behavior, it is important to individually account for the resilient response of aggregates to both radial and vertical pulse loadings [5, 21]. Cycling the radial load is not accomplished in this research with the CCP nature of the triaxial apparatus. Nevertheless, test results from the CCP cyclic load triaxial test employed in the generalized anisotropic K–G model give an insight of such anisotropic behavior of the granular materials.

Figures 4.29 and 4.30 show plots of measured values of the volumetric strain ε_v and the shear strain ε_q vs. the mean normal stress p for ZKK63 and WB materials. As can be seen from the plots and the values of the correlation coefficient r^2, the anisotropic K–G model shows for these figures a very good fit between the measured and predicted volumetric and shear strains.

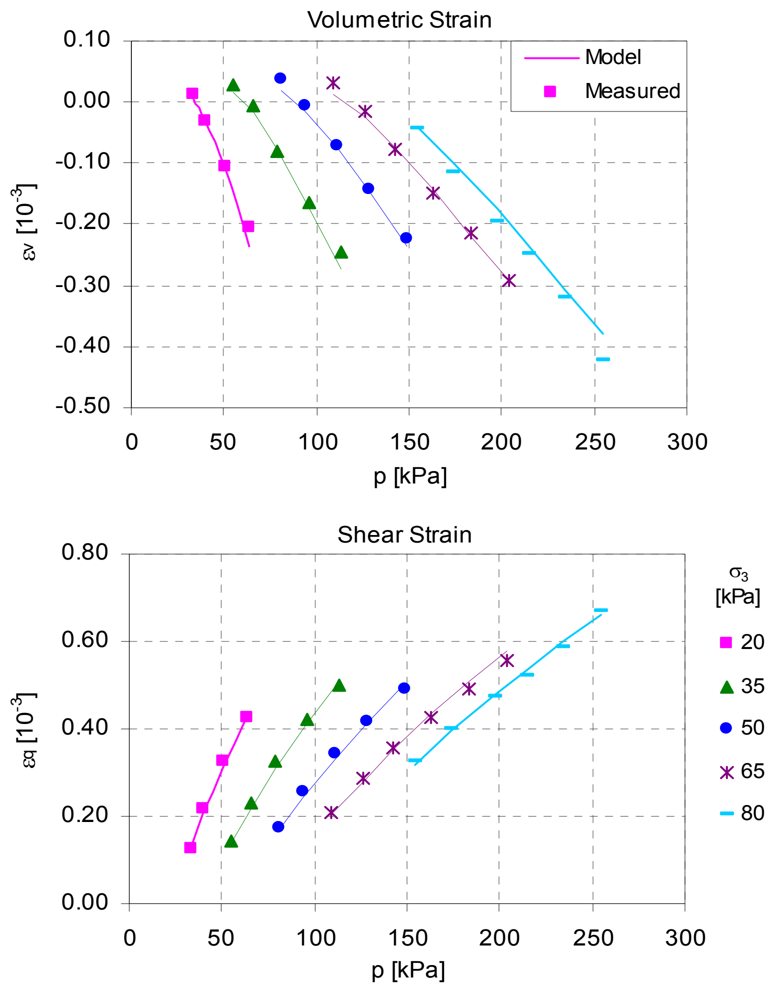

K_a	G_a	n	γ	r^2
13.2	33.6	0.254	0.262	0.989

Figure 4.29 Measured volumetric* and shear strains and anisotropic K–G model for ZKK63 with 100% DOC and moderate (3%) MC

* In the stress and strain measurements compression is positive and tension negative; negative volumetric strain indicates expansion/increase in volume of specimen

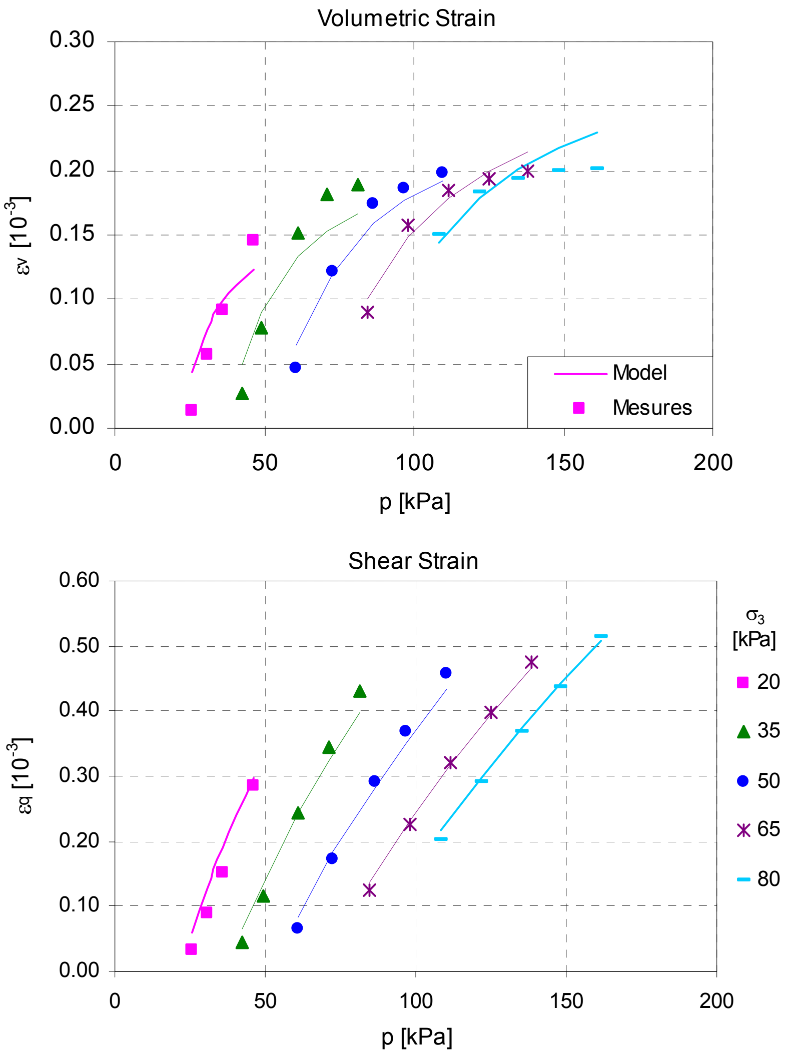

K_a	G_a	n	γ	r^2
24.7	55.1	0.428	0.532	0.953

Figure 4.30 Measured volumetric and shear strains and anisotropic K–G model for WB with 95% DOC and moderate (7%) MC

The good performance of the anisotropic K–G model in predicting the shear strain better than the volumetric strain is due to the fact that the definition of both strain components is in terms of principal strains. The small coefficient of anisotropy γ=0.26 for the most coarse graded ZKK63 material in Figure 4.29 indicates that the resilient modulus in the horizontal direction is one fourth of the resilient modulus in the vertical direction. This low stiffness in horizontal direction compared to the vertical direction along with practical limitations of the test set-up, discussed in chapter 7, results in a relatively high radial strain compared to the vertical strain. The higher (tensile) radial strain with smaller (compressive) vertical strain gives a negative volumetric strain or specimen volume increase (sometimes referred to as dilatancy). The WB in Figure 4.30 on the other hand shows a specimen volume decrease (total volume compression).

For all the materials tested in different conditions the model parameters are summarized in table 4-7.

Table 4-7 Anisotropic K–G model prediction parameters for all materials

Test code	DOC (%)	MC (%)	Anisotropic K – G model parameters K_a [MPa]	G_a [MPa]	n [-]	γ [-]	r^2 [-]
RD-FC-95	95[i] 96.5[ii]	7.5[i] 7.5[ii]	3237	131.9	0.891	0.90	0.688
RD-FC-98dr	98 84.6	5 7	21.60	64.90	0.313	0.503	0.677
RD-FC-98	98 98.2	7.5 8.5	10.60	12.60	0.590	0.233	0.965
RD-FC-98wt	98 97.9	9.5 9.6	9.60	15.00	0.520	0.253	0.835
RD-FC-100	100 100.1	7.5 7.8	4.00	6.20	0.629	0.143	0.886
					Average	r^2:	0.810
RD-WB-95	95 94.8	7 7.3	24.70	55.10	0.428	0.532	0.953
RD-WB-98dr	98 95.8	5 5.6	12.90	60.20	0.217	0.627	0.874
RD-WB-98	98 96.8	7 8.6	26.40	85.60	0.299	0.770	0.913
RD-WB-98wt	98 96.7	9 10.5	19.60	59.10	0.315	0.619	0.963
RD-WB-100	100 99	7 8.2	15.40	72.40	0.197	0.685	0.791
					Average	r^2:	0.899
RD-G1-98	98 97.3	4 4	29956390	67.40	0.221	0.287	0.934
RD-G1-100	100 99.4	4 4.1	421370937	67.90	0.245	0.528	0.892
RD-G1-102	102 102.0	4 3.9	13868192	67.60	0.266	0.327	0.945
RD-G1-105	105 104.1	4 3.8	13868192	84.00	0.506	0.749	0.859
					Average	r^2:	0.908
RD-ZKK32-100	100 99.7	3 3.3	18.00	33.00	0.308	0.306	0.990
RD-ZKK63-100	100 100.3	3 3.0	13.20	33.60	0.254	0.262	0.989

[i]: *intended DOC and MC* [ii]: *achieved DOC and MC*

4.6 EFFECT OF INFLUENCE FACTORS ON RESILIENT DEFORMATION BEHAVIOR

In the same way as the failure tests, described in section 4.3, the resilient deformation test program is designed systematically to be able to investigate the influence of factors such as material, moisture content and degree of compaction on the resilient deformation behavior of the granular materials. These effects are best shown graphically in charts in which M_r-θ relations are grouped for the influence factors under consideration. The M_r-θ model is chosen over the others for the following reasons:

i. the M_r-θ model is the most widely used and simplest model;
ii. the M_r-θ model is the model adopted to verify and validate the RL-CBR stiffness modulus in chapter 6;
iii. through single lines plotted in log scale charts it is much more convenient to compare the (relative) effect of the influence factors.

In the following paragraphs the (relative) effect of the investigated influence factors moisture content, degree of compaction and material nature are presented and discussed. It is deemed that a careful selected number of charts elucidate effects better than an excessive amount of charts in which each influence factor is presented explicitly for each investigated variant of the extensive RD tests performed. For such explicit numerical references the reader is referred to the summary of the M_r-θ model results in table 4-4.

4.6.1 Moisture content

The effect of moisture content on the resilient modulus M_r is presented here for two materials WB and FC. The analyzed tests are carried out with a "homogenous" test series i.e. all the above mentioned influencing factors are kept identical, only the influence of moisture content is investigated. In these series the DOC is kept 98% for both the WB and FC and the moisture effect is studied by testing at three varying target moisture contents i.e. dry, moderate and wet.

<u>Weathered Basalt</u>
Figure 4.31 gives the M_r-θ relation for different MCs: dry (5%), moderate (7%) and wet (9%) for the WB with 98% target DOC. The figure shows that the stiffness modulus M_r is higher for the moderate moisture content in the entire testing load range compared to both the dry and wet moisture conditions.

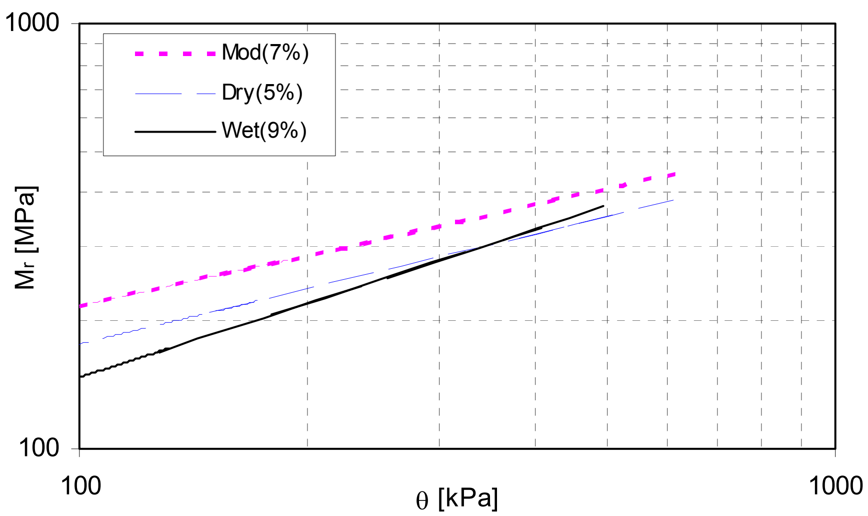

Figure 4.31 M_r-θ relations as a function of MC for WB with 98% target DOC

The good performance of the moderate moisture content is consistent with expectation since dry as well as wet granular materials in general result in poor performance. Comparing the dry and wet conditions, the dry condition performs relatively better than the wet one for the major part of the loading range. The wet mix gains some stiffness at higher loading range which can be a result of further compaction by the load cycles

Ferricrete

Figure 4.32 presents the M_r-θ relation for different MCs: dry (5%), moderate (7.5%) and wet (9.5%) for the FC with 98% target DOC. Opposite to the WB the figure shows that the stiffness modulus of the FC at moderate moisture content is less compared to both the dry and wet condition. The high stiffness of the dry mix is attained despite of its extremely low achieved DOC (84.6%) which is far from the intended 98% DOC and the obtained DOC 98.2% for the moderate and 97.9% for the wet conditions. The high performance of the dry mix can be explained by the high resistance to overall deformation of the dry cohesive ferricrete.

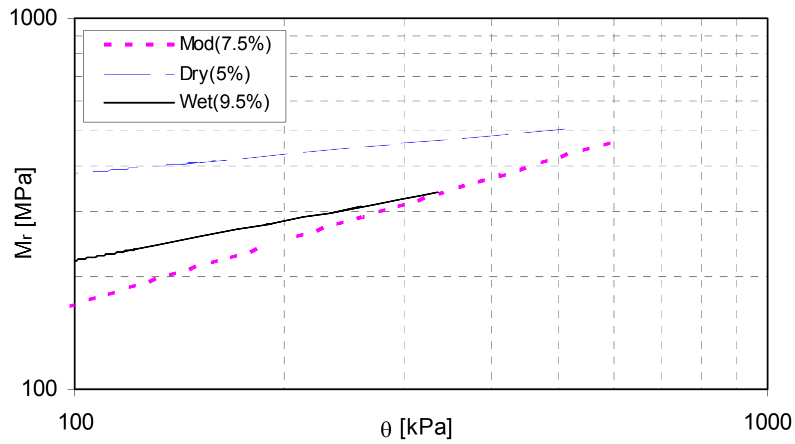

Figure 4.32 M_r-θ relations as a function of MC for FC with 98% target DOC

On the other hand, the wet mix also seems to perform better, at least at the initial loading levels, compared to the moderate moisture condition. This is an unexpected result as the wet mix is very weak in resisting overall deformation. The RD test for the wet mix is carried out for limited load levels. This is due to the fact that high permanent deformation was observed during testing, as shown in Figure 4.33 for one of the vertical LVDTs, and the test had to be aborted at earlier stage (at σ_3 = 65 kPa and σ_d = 130 kPa) as the specimen had to be used for further monotonic failure (MF) test.

The better performance observed for the wet mix compared to the moderate at the initial loadings is also attributed to the high modulus results due to actuator and/or perhaps LVDTs accuracy limitations at very small load levels, in general terms explained in section 4.4.3. Furthermore, the moderate mix has high slopes of the M_r-θ line compared to both the dry and wet conditions.

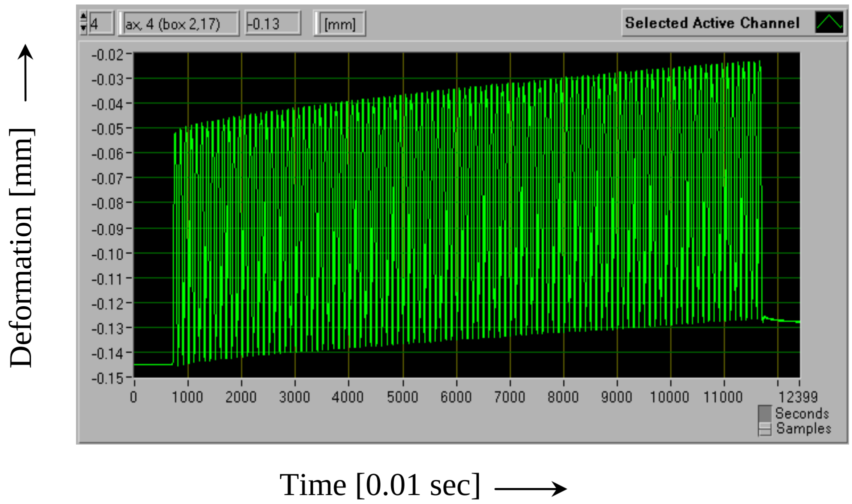

Figure 4.33 Permanent deformation observed on one of the vertical LVDTs for RD-FC-98wt

4.6.2 Degree of compaction

The effect of DOC on the resilient modulus M_r is presented here for three materials G1, WB and FC. The investigated tests are carried out with a "homogenous" test series, all influence factors are kept identical only the influence of DOC is investigated. In these series the target MC is kept at moderate moisture content for each respective material (4% MC for G1, 7% MC for WB and 7.5% MC for FC) and the effect of DOC is investigated by testing at four target DOC's i.e. 98%, 100%, 102% and 105% for the G1 and three target DOC 95%, 98% and 100% for the WB and FC materials.

<u>Crushed stone (G1)</u>
Figure 4.34 presents the M_r-θ relation for DOC (target value): 98%, 100%, 102% and 105% for the G1 with moderate (4% target) MC. Except for the 100% DOC which is slightly below the 98% DOC, the stiffness modulus increases with an increase of DOC for the major part of the loading range before they all converge to a similar modulus at higher stress levels. There is no sufficient explanation for the better performance of the 98% DOC compared to the 100% except that this can be a typical example of a variation in sample preparation and its effect on material performance.

<u>Weathered basalt</u>
Figure 4.35 gives the M_r-θ relation for DOC (target value): 95%, 98% and 100% for the WB with moderate (7% target) MC. From the figure it can be concluded that the effect of DOC on the stiffness modulus of WB is not very significant. The difference in stiffness modulus of the three compaction conditions is negligible except that contrary to the expectation the 100% DOC is performing less than the other two DOC. The poor performance of the higher DOC can be related to the effect of over-compaction which affects the gradation through crushing of the elongated and flaky coarse particles of the WB.

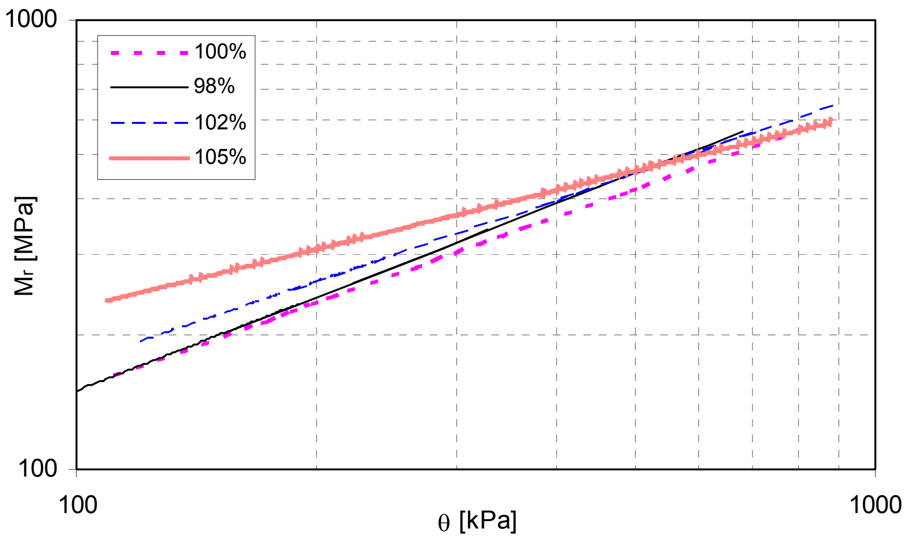

Figure 4.34 M_r-θ relations as a function of DOC for G1 with moderate (4% target) MC

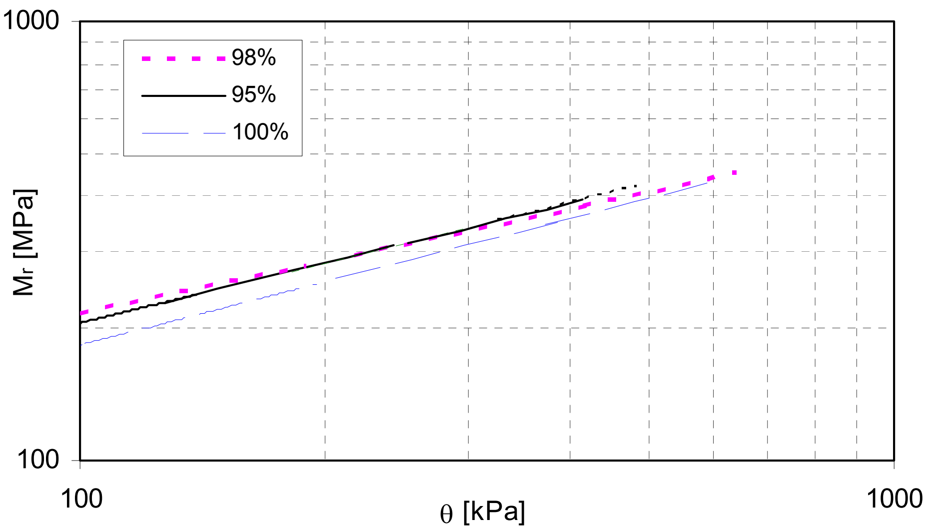

Figure 4.35 M_r-θ relations as a function of DOC for WB with moderate (7% target) MC

<u>Ferricrete</u>

Figure 4.36 shows the M_r-θ relation for DOC (target value): 95%, 98% and 100% for the FC with moderate (7.5% target) MC. Here it is better to compare only the 98% and 100% target DOC as the test condition for the 95% is different from the others. The 95% DOC test is the ever first RD test carried out in this research and it was conducted at 10 Hz frequency unlike all the other tests where the series of short loading for the RD test is conducted with 1 Hz loading frequency. Similar to the explanation given in section 4.4.3 for the conditioning load cycles using 10 Hz frequency along with the actuator and LVDT accuracy limitation at low load level the result for the FC with 95% DOC is rated as not reliable. Excluding the 95% DOC for the ferricrete, the figure shows that an increase in DOC form 98% to 100% results in an increase of the stiffness modulus.

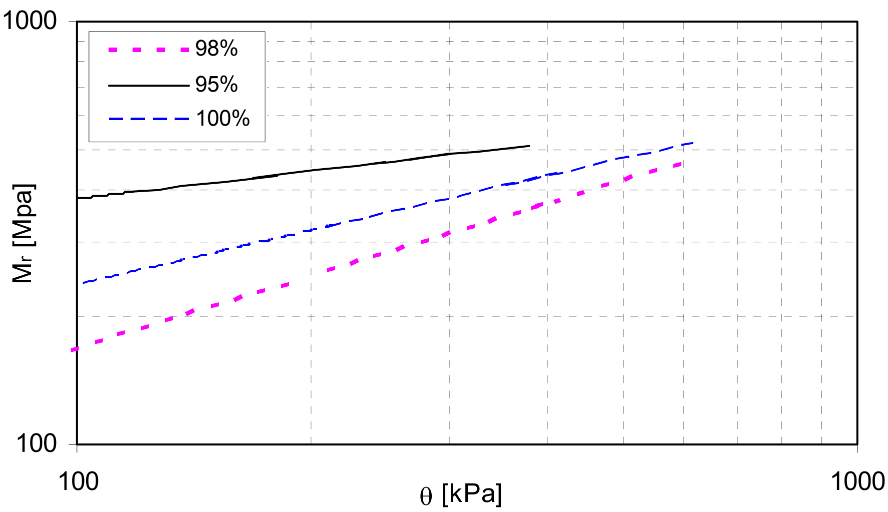

Figure 4.36 M_r-θ relations as a function of DOC for FC with moderate (7.5% target) MC

4.6.3 Material type

The effect of nature and type of material on the resilient modulus M_r is presented here for all the materials considered in the research. Here it has to be noted that the investigated tests are not carried out with a "homogenous" test series anymore. Varying material type incorporates several varying influence factors such as gradation, particle shape and texture, mineralogical composition, strength of particles etc. Therefore all influence factors are varying along with the material type except two, the target DOC and the category of moisture content.

The influence of material type is investigated in a condition that the category of moisture is kept moderate for all, but one has to keep in mind that the target moderate moisture condition for each material is different. That is 3% target MC for ZKK32 and ZKK63, 4% target MC for G1, 7% target MC for WB and 7.5% target MC for FC. Moreover the influence of material type is compared for two targets of DOC i.e. 98% for G1, WB and FC and 100% for G1, ZKK63, ZKK32, WB and FC materials.

Figure 4.37 shows the M_r-θ relation for the five materials considered in the research study at 100% target DOC and their respective target moderate moisture content. From the figure it can be observed that the two coarse graded natural limestone aggregates ZKK63 and ZKK32 show a higher stiffness modulus in all stress ranges. In comparison to WB and FC too, the G1 has a lower stiffness modulus at lower stress levels but a higher stiffness modulus at higher stress levels. As explained in the previous section 4.6.2 this low performance of the G1 at 100% DOC can be a result of poor sample preparation or test set up.

However, on the other hand, observing the performance of the G1 in Figure 4.34, for instance at $\theta = 500$ kPa the stiffness modulus M_r for all DOC is in a range of 420 to 450 MPa, which is very small compared to the M_r values of 650 and 750 MPa at similar $\theta = 500$ kPa for the ZKK32 and ZKK63 respectively shown in Figure 4.37. This demonstrates that very high quality crushed rock materials such as the G1, having a very good performance in the real pavement field, does not mean by definition that they have a high stiffness (resilience) modulus as determined by means of CCP triaxial testing. The high performance of such crushed rock aggregates is attributed mainly to their high resistance to permanent deformation and shear failure as illustrated in section 4.3.3, particularly in the Figures 4.9, 4.12 and 4.16. This is illustrated in chapter 5 when dealing with modified CBR (MCBR) and repeated load CBR (RL-CBR) results.

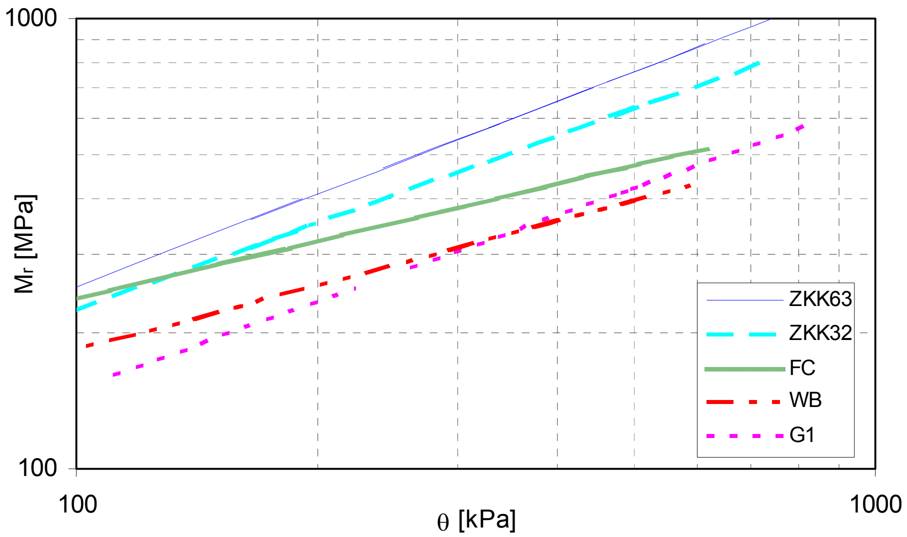

Figure 4.37 M_r-θ relations as a function of material type with 100% target DOC and moderate MC

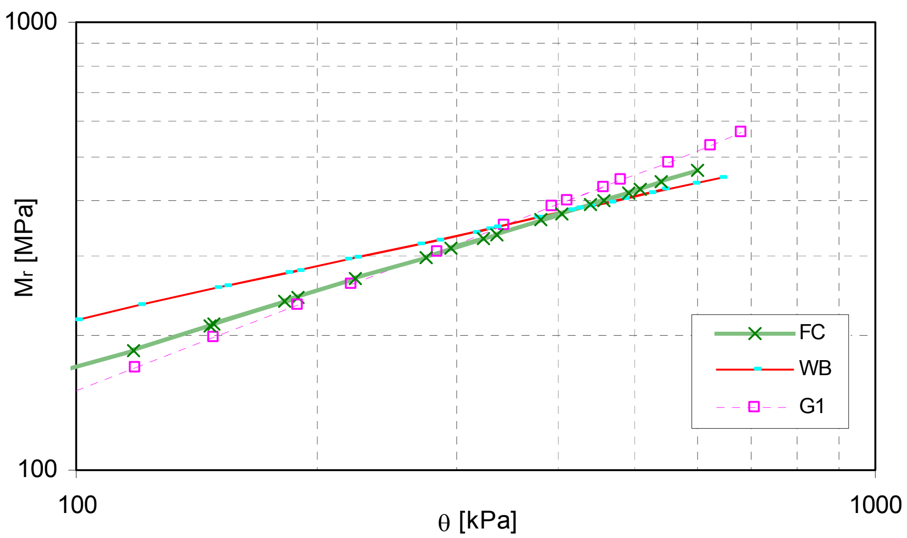

Figure 4.38 M_r-θ relations as a function of material type with 98% target DOC and moderate MC

Figure 4.38 shows the M_r-θ relation for three materials (G1, FC and WB) at 98% target DOC and their respective target moderate moisture content. From the figure it can be observed that the WB is performing better than the other two materials at low stress levels whereas the G1 achieves a higher stiffness modulus than the other two at high stress levels.

4.7 CONCLUSIONS

This chapter has dealt with the laboratory characterization of the mechanical behavior of various coarse granular materials. The granular base and subbase materials range from a solid crushed rock Greywacke Hornfels G1, natural limestone to a rather marginal ferricrete and weathered basalt gravels. A number of these materials were tested at three degrees of compaction and three moisture contents.

The mechanical behavior, failure and resilient properties, of all the materials were determined in monotonic (static) and cyclic load triaxial tests. The most important conclusions related to the mechanical behavior derived from the extensive amount of large-scale triaxial tests performed on the coarse granular materials are summarized below. These conclusions are presented structured along each type of material behavior, i.e. shear failure and resilient deformation behavior. For each type of material behavior the conclusions relate to testing, modeling and materials behavior in relation to the investigated influence factors, DOC (degree of compaction) and MC (moisture content).

Failure behavior

The failure tests are conducted in part on “virgin” (not previously loaded) specimens prepared exclusively for the MF test and in part on specimens after completion of resilient deformation (RD) test in which its load levels are far below the failure level. Though for most cases the use of a pre-loaded specimen doesn’t affect the test result significantly there are instances that due to pre-loading the specimen gains strength from post-compaction by the cyclic load of the RD test, especially for lower DOC. Although it is recognized for coarse aggregates, especially crushed rocks, that it is not always possible to define failure readily, from the large amount of tests the strength parameters c and ϕ are determined and assessed per the main influence factors.

The c-values increase in general with increasing DOC for most of the materials at moderate MC. However it is observed that for the WB with weak or flaky coarse particles the c-value tends to decrease after the optimum DOC 98%. This might be due to damage occurred from over compaction.

As a consequence of the application of internal vacuum in the triaxial facility the MC during testing is changing and the actual MC is not known.

For both the FC and WB both the c-value and ϕ-value are higher at the moderate MC than the dry and wet mixtures. This shows that moisture control in the field, especially, for natural gravel layers is remarkably important.

Resilient deformation behavior

The resilient deformation tests are conducted on "virgin" (not previously loaded) specimens prepared exclusively for the RD tests. However, in order to economize on specimen preparation and to use the same specimen for MF tests, the RD tests are carried out at load levels far below the failure level.

Among all factors that affect Mr (density, moisture content, aggregate type etc.) the most important factor is the stress state. Several models have been developed to address the effect of stress state on the resilient response. All the four models used (M_r-θ, Universal, TU Delft and anisotropic K-G models) describe fairly well the stress dependency of the resilient modulus. One of the limitations of the first three models is the use of a constant Poisson's ratio. On the other hand, the strong side of the anisotropic K-G model is the insight it provides regarding the anisotropic nature of the UGM specimens.

In modeling the resilient behavior of the coarse granular materials significant number of the material mixtures shows anisotropic behavior. In addition to the possible actual specimen volume increment (dilatancy) at higher loadings the effect of this anisotropy, along with other material and test conditions discussed in chapter 7, is also reflected in the large value (>0.5) of the constant Poisson's ratio.

The resilient modulus of the granular base and subbase materials was, generally, shown to be less affected by moisture content, degree of compaction and material type. Relatively the effect of moisture content is larger compared to the effect of degree of compaction and material type.

In real pavement construction in South Africa the G1 is known for its very good performance, in contrary to the measured lower resilience modulus from the laboratory characterization. The high performance of such crushed rock aggregates is attributed mainly to their high resistance to permanent deformation and shear failure rather than resilient modulus. The better performance of the G1 with respect to shear failure behavior is described in section 4.3 particularly its higher internal angle of friction is illustrated in Figure 4-12. However, resilience modulus is not the best representative for the quality of coarse granular aggregates especially for crushed rocks.

REFERENCES

1. Houben, L.J.M. and S. Molenaar, *Triaxial Testing of Askøy Granular Aggregate*, in *SINTEF-Contract GARAP-Delft*. 2005, Delft University of Technology: Delft.

2. Van Niekerk, A.A., *Mechanical Behavior and Performance of Granular Bases and Subbases in Pavements*, in *Road and Railway Engineering, Faculty of Civil Engineering* 2002, Delft University of Technology: Delft.
3. Huurman, M., *Permanent deformation in concrete block pavements*, in *Faculty of Civil Engineering and Geosciences*. 1997, Delft University of Technology: Delft.
4. Werkmeister, S., *Permanent deformation behaviour of unbound granular materials in pavement constructions*, in *Faculty of Civil Engineering*. 2003, Dresden University of Technology: Dresden.
5. Tutumluer, E. and U. Seyhan, *Laboratory Determination of Anisotropic Aggregate Resilient Moduli Using a New Innovative Test Device* in *78th Annual Meeting of the Transportation Research Board Specialty Session on "Determination of Resilient Modulus for Pavement Design"*. 1999: Washington DC.
6. CEN, *Unbound and hydraulically bound mixtures - Part 7: Cyclic load triaxial test for unbound mixtures*, in *EN 13286-7*. 2004, European Committee for Standardization (CEN): Brussels.
7. AS, *Method for Sampling and testing Aggregates. Method 6.8.1: Soil Strength and Condition Tests - Determination of the Resilient Modulus and Permanent Deformation of Granular Unbound Pavement Materials*, in *AS 1289.6.8.1-1995*. 1995, Australia Standards: Sydney, NSW, Australia.
8. Lekarp, F., U. Isacsson, and A. Dawson, *State of the Art. I: Resilient Response of Unbound Aggregates.* Journal of Transportation Engineering, ASCE, 2000. **126**(1): p. 66-75.
9. Gonzalez, A., et al. *Nonlinear finite element modeling of unbound granular materials*. in *Advanced Characterisation of Pavement and Soil Engineering Materials*. 2007. Athens, Greece: Taylor & Francis.
10. Hicks, R.G. and C.L. Monismith, *Factors Influencing the Resilient Response of Granular Materials.* Highway Research Record: Highway Research Board, 1971. **354**: p. 15-31.
11. Sweere, G.T.H., *Unbound Granular Base for Roads*, in *Faculty of Civil Engineering and Geosciences*. 1990, Delft University of Technology: Delft.
12. May, R.W. and M.W. Witczak, *Effective granular modulus to model pavement responses.* 1981.
13. Uzan, J. *Characterization of Granular Material*. in *Transportation Research Records 1022*. 1985. Washington DC: Transportation Research Board.
14. Andrei, D., et al., *Harmonized Resilient Modulus Test Method for Unbound Pavement Materials.* Transportation Research Record: Journal of the Transportation Research Board, 2004. **1874**(-1): p. 29-37.
15. Kolisoja, P. *Simple automatic stress path control system for triaxial testing*. in *The 13th International Conference on Soil Mechanics and Foundation Engineering*. 1994. New Delhi, India.
16. Lade, P.V. and R.B. Nelson, *Modelling the elastic behaviour of granular materials.* International journal for numerical and analytical methods in geomechanics, 1987. **11**(5): p. 521-542.
17. Lo, S.-C.R. and I.K. Lee, *Response of Granular Soil along Constant Stress Increment Ratio Path.* Journal of Geotechnical Engineering, 1990. **116**(3): p. 355-376.

18. Semmelink, C.J. and M. de Beer. *Rapid Determination of Elastic and Shear Properties of Road-Building Materials with the K-Mould*. in *Unbound Aggregates in Roads (UNBAR4) Symposium*. 1995. Nottingham, UK.
19. Hornych, P., A. Kazai, and J.M. Piau. *Study of the resilient behaviour of unbound granular materials*. in *Bearing Capacity Roads, Railways & Airfields*. 1998. Norweigan Univ. of Science and Technology,Trondheim, Norway.
20. Boyce, J.R. *A non linear model for the elastic behavior of granular materials under repeating loading*. in *Int. Symposium on Soils under Cyclic and Transient Loading*. 1980. Swansea, U.K.: Balkema.
21. Lo, K.Y., G.A. Leonards, and C. Yuen, *Interpretation and Significance of Anisotropic Deformation Behavior of Soft Clays*. 1977, Norwegian Geotechnical Institute: Oslo.

CHAPTER 5

REPEATED LOAD CBR TESTING AND MODELING

5.1 INTRODUCTION

This chapter covers the research undertaken to achieve objectives O2 and O3 set in section 1.3. The research approach and conceptual design considered for the research requirement are outlined in section 3.2.

Developments on Mechanistic-Empirical (M-E) pavement design procedures and material specifications demand for fundamental material properties in order to predict pavement responses (section 1.2). The M-E design procedures require fundamental inputs, for which the lack of a suitable and affordable laboratory test(s) and the production of data sets that can be used as a direct design input is a major constraint.

The design inputs, for unbound granular materials, are strength, resilient modulus and resistance to permanent deformation. It is recognized that testing under laboratory conditions is not always ideal, in terms of being directly representative of a material's field behavior, but it is required to give confidence (in the absence of case study data sets) that a material will perform adequately in a certain application. The literature review, on the other hand, shows a gap between the relatively fundamental research tests and a simpler approach that could provide a routine design input for the road industry. Therefore, the need for developing a simplified laboratory test, capable of estimating mechanical properties of unbound pavement granular materials is identified.

The principle of the repeated load CBR (RL-CBR) test and the experimental research undertaken to fulfill this requirement is detailed in sections 5.2 to 5.4. Its finite element modeling and results are discussed in section 5.5 and 5.6 and at the end conclusive remarks are given in section 5.7.

5.2 THE PRINCIPLE OF REPEATED LOAD CBR TEST

The standard California Bearing Ratio (CBR) test, discussed in section 2.4.2.3, is a long established extensively applied test that yields an empirical strength property of granular road materials. The RL-CBR test is developed to take the advantage of the widespread familiarity of the standard CBR test and excel the already developed extensive experience.

The principle of the RL-CBR test is similar to the standard CBR test but repeated loads are applied. Upon multiple repetitions of the same magnitude of loading granular materials come to a state in which almost all strain under a load application is recoverable. The permanent (plastic) strain ceases out to exist or becomes negligible and the material behaves basically elastic i.e. with stable recoverable deformation. This is represented in Figure 5.1. From the applied stress and the measured recoverable strain an elastic modulus can be estimated. Details of the test set-up and test procedure are presented in sections 5.3 to 5.5 and the estimation of the E-modulus from the test is discussed in section 5.6.

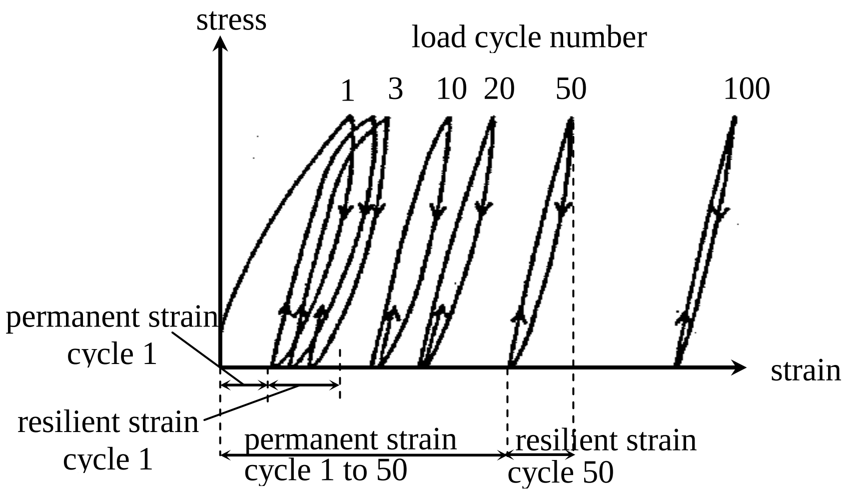

Figure 5.1 Stress-strain behavior of a granular material under repeated loading

By recording the load and displacement and plot in x-y axes, a graph similar to Figure 5.1 is obtained from which load levels and total, elastic (recoverable) and plastic (permanent) deformations under the penetration plunger can be obtained. The elastic modulus (E) is computed from the applied plunger stress (σ_p) and the elastic deformation of the specimen (u) in the final load application. The stress σ_p can be calculated from the applied plunger force (F) and the contact area of the plunger (A).

$$\sigma_p = \frac{F_{penetration}}{A_{plunger}} = \frac{F_{penetration}}{\pi \cdot \left(d/2 \right)^2} \qquad 5\text{-}1$$

The standard CBR test is initially developed to determine strength properties of fine subgrade soils. Through time it is accepted as a standard test for base and subbase materials finer than 22.4 mm. In this research, as presented in chapter 3 in detail, by scaling up the mould and the plunger sizes the test is adopted to characterize materials as coarse as 0/45 mm. Moreover, it is attempted to determine the stiffness modulus of coarse granular materials by repeating the load application. As discussed in chapter 3 the purpose of this approach is to estimate the stiffness modulus of granular materials, that normally have to be determined from a cyclic load triaxial test, from a simplified test.

It is known that the stiffness modulus of unbound granular base and subbase materials is stress dependent. Therefore, one of the drawbacks to use the CBR test for determination of the fundamental material properties such as the stiffness modulus is its non-uniform complex stress distribution compared to the triaxial test. In general in a triaxial test system, for specimens with their diameter to maximum grain size ratio being at least 5, it is assumed that the material is homogenous and the stress distribution is uniform throughout the material excluding the contact effects at the top and bottom end of the sample. This holds true, however, depending on the scale and level of detail one is interested in.

Figure 5.2 is considered to evaluate the effect of grain size and loading condition on the stress distribution in unbound granular specimens and to compare between triaxial and CBR specimens. In this figure three cases are presented, i.e. coarse aggregate triaxial specimen, coarse aggregate in CBR mould and sand in CBR mould. In these three cases let’s consider that the coarse aggregates are materials that are used in this research thus 0/45 mm base and subbase aggregates. The specimen sizes are also the sizes adopted throughout this research i.e. 300 mm diameter with 600 mm high triaxial specimens and 250 mm diameter and 200 mm high CBR specimens.

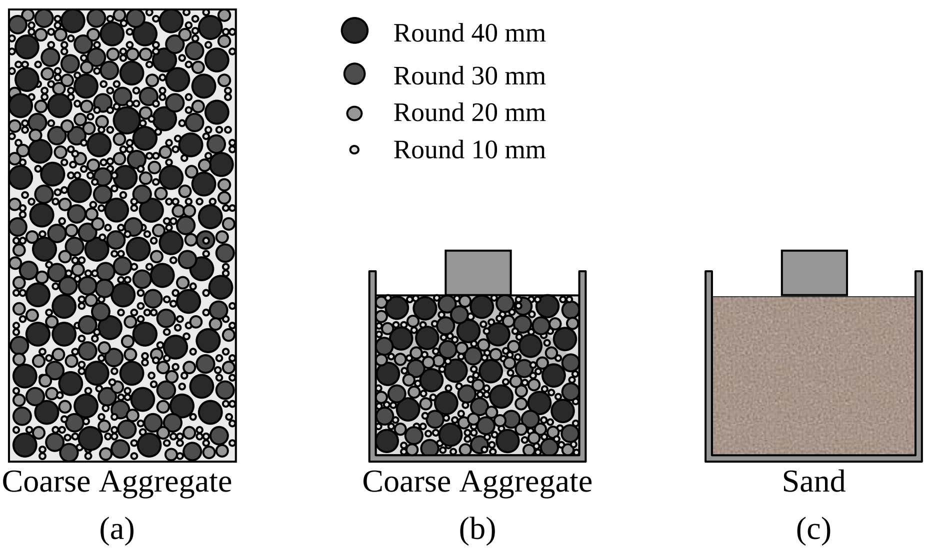

Figure 5.2 Coarse aggregate triaxial specimen and coarse aggregate and sand filled CBR samples

This implies that, say at a macro-scale, see Figure 5.3 (a), the unwritten rule that says the minimum specimen dimension should be at least 5 times the maximum grain size in order to consider the specimen as a bulk and homogenous material, is satisfied for the coarse aggregate triaxial specimen. The enclosed volume of the coarse aggregate and sand in the CBR mould may just be considered as a bulk. However, when the dimension of the loading plunger is taken into account this is surely no longer the case for the coarse aggregate in the CBR test despite the use of an enlarged plunger. Moreover, the penetration plunger load in the CBR results in a non-uniform stress distribution in the specimen as shown in Figure 5.3 (a). Therefore it can be concluded that at macro-scale the assumed homogenous material results in a uniform stress distribution for the triaxial specimens, at least at the mid-height of the specimen, and hence a uniform stress dependent stiffness modulus known as "resilient modulus". For the CBR specimen, however, it gives a non-uniform stress distribution and hence the specimen will exhibit a non-uniform material stiffness modulus.

If we observe the stress condition at a more detailed scale, say meso-scale, the random grain pattern and the grain to grain contact will play a significant role in the stress distribution, see Figure 5.3 (b). The grain to grain contacts result in a significant stress distribution variation for the coarse aggregate materials for both the triaxial as well as the CBR specimen as shown in Figure 5.3 (c). In the sand filled CBR mould the grain to grain contact doesn't influence much the stress and hence the stress dependent stiffness modulus. It should be clear that the intention is not to make an argument that both triaxial and CBR specimens are equally inaccurate or approximations. It is to give a good picture that considering a given granular specimen as a bulk is rather dependent on the scale one is looking at and the detail and level of accuracy one is interested in.

It should also be clear that the purpose of RL-CBR testing is not to determine a pin point accurate stiffness modulus of granular materials but to get an approximate estimate of acceptable accuracy from a simpler characterization technique. The research starts from the concept that the cyclic triaxial test is too complex for the purpose of, say, pavement design in developing countries. Thus, instead of zooming-in from macro-scale $\rightarrow$ meso $\rightarrow$ micro $\rightarrow$ nano-scale in Materiomics*, the approach goes in opposite direction zooming-out to a more general say "global" scale, as shown in Figure 5.4. Where the macro-scale is the scale that most conventional soil mechanics and pavement engineering applications are dealt with.

* Materiomics is defined as the study of the material properties of natural and synthetic materials by examining fundamental links between processes, structures and properties at multiple scales, from nano to macro, by using systematic experimental, theoretical or computational methods. [1. Wikipedia. *Materiomics*. [cited 2010 August 17]; Available from: http://en.wikipedia.org/wiki/Materiomics.

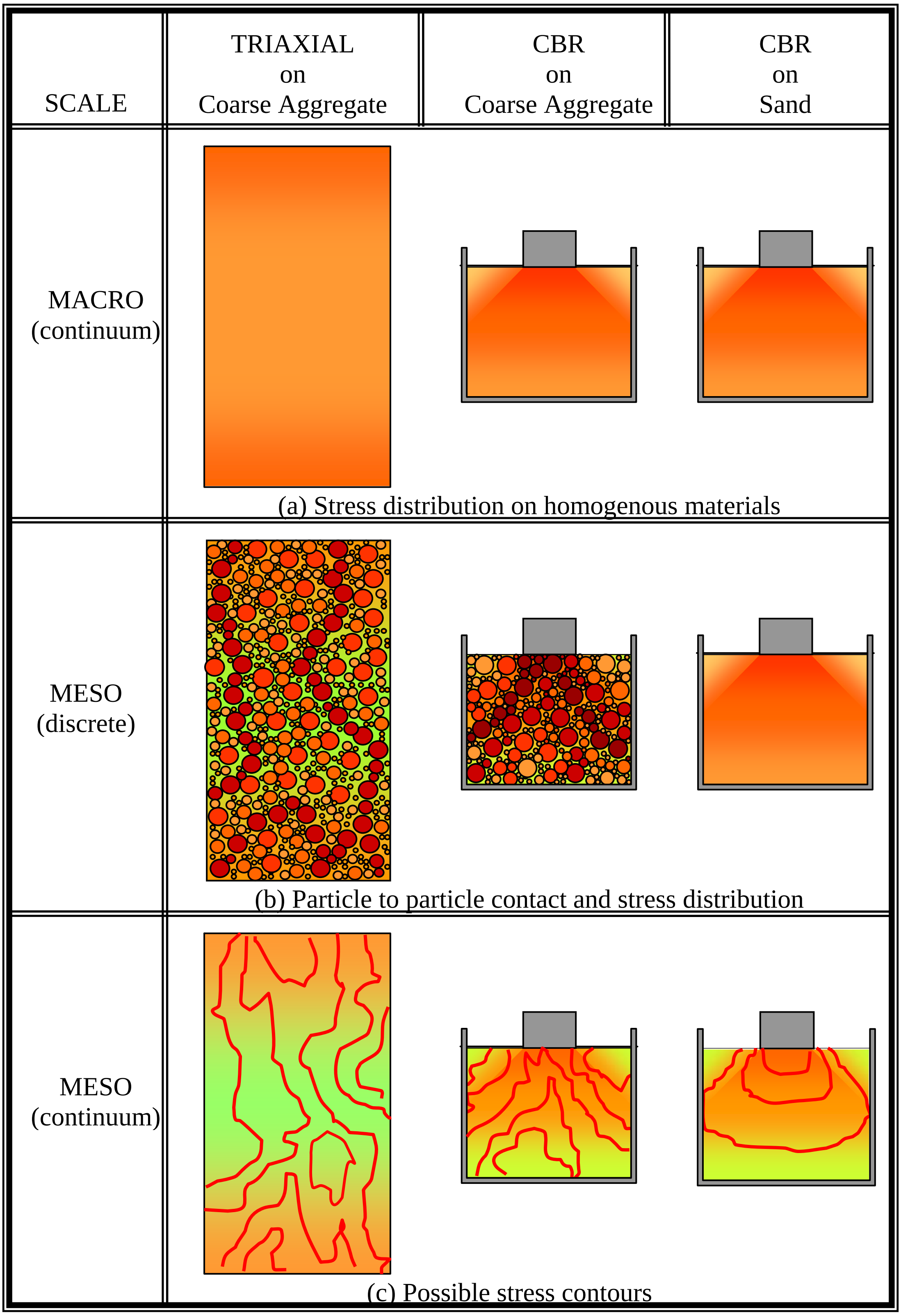

Figure 5.3 Scale of investigation, particle to particle contact and stress distribution in triaxial and CBR specimens

Figure 5.4 From macro to "Global" scale for RL-CBR characterization

At the 'global' scale the variation of the stiffness modulus of the material in the CBR test is replaced by an average, representative or equivalent modulus for the bulk sample. In other words, this averages not only the stress variation due to the grain pattern but also due to the variation of stress distribution from the penetration load. To reflect the scale deviation from the common macro-scale, the conventional term "Resilient Modulus" of the granular material is replaced with an "Equivalent Modulus" for the material stiffness property investigated by the RL-CBR. From this onwards the term "equivalent modulus" in this study refers to the stiffness modulus estimated by the RL-CBR testing.

In this research RL-CBR tests are performed on all the materials discussed in section 3.4 to investigate its suitability as a simple to perform test to estimate mainly the equivalent modulus and to a certain extent the resistance to permanent deformation for unbound granular materials. The laboratory investigation is carried out in two test techniques: without and with strain gauges. The characterization technique and investigation of the resilient and permanent deformation behavior of the extensive RL-CBR testing without strain gauge is reported in section 5.3 and that of with strain gauges in section 5.4.

5.3 REPEATED LOAD CBR TESTING TECHNIQUE

5.3.1 Specimen preparation and measuring apparatus

Specimen preparation

In testing unbound granular materials the ratio of mould (specimen) size to maximum particle size of the material to be tested is an important factor. As discussed in section 3.3.1, in order to use the coarse granular material at their full gradation the RL-CBR tests are carried out with a large size CBR mould and accordingly a bigger plunger. The large RL-CBR mould used is 250 mm in diameter, 200 mm in height with an extension collar of 75 mm and the penetration plunger is 81.5 mm in diameter.

The method used for the preparation of RL-CBR test specimens is similar to the method adopted for the 300 x 600 mm triaxial specimens reported in section 4.2. The RL-CBR test specimens are compacted using the same vibratory compactor apparatus and the same compaction principle discussed in section 4.2 but with a new compaction head that fits into the 250 mm diameter RL-CBR mould. The procedure followed for the preparation of the RL-CBR specimens is as follows:

1. 25 kg of unbound granular materials at required grading are obtained by recombination of various fractions of sieved materials to their respective target grading. The moisture content (MC) of the bulk material is pre-

determined and the required quantity of water to bring the material to the required level of moisture content is added and mixed with a mechanical mixer, Figure 5.5. Having obtained the sample material at the target moisture content, the specimen is then built in the RL-CBR mould.

2. The required quantity of sample material, pre-determined from the specimen volume and wet density to achieve a target degree of compaction (DOC), is divided into 3 equal portions. Specimens are compacted in 3 layers. For each layer the exact amount of material is weighed to obtain a layer thickness of 1/3 of the specimen height after compaction for the targeted DOC or density.

3. The first layer of material is poured and pre-compacted by hand tamping, and then compacted by means of the vibratory compactor to the required density. This has been done by increasing the frequency of the vibratory compaction step by step each minute until the required layer thickness, 1/3 of the specimen height, is attained, Figure 5.5. The compacted layer thickness is controlled by measuring the level of the compaction head with respect to a chosen reference point. The same procedure is followed for the remaining two layers. The surface of each layer is mechanically scarified before adding the next layer on top to obtain a good layer interlock and a homogenous sample.

4. A static compressive load ranging from 50 – 140 kN depending on the material and DOC (i.e. the smaller load for the weak material mixtures at low DOC and the higher load for high quality material such as the G1 compacted with high DOC) is applied to improve the compactness of the top surface of the specimen. This top surface improvement is necessary as vibratory compaction is good in compacting unbound granular layers at a lower depth but weak at the top surface. On the other hand, at least the initial penetration load of the (RL-)CBR is mainly dependent on the condition of the top surface.

5. Lastly, after measuring the top end surface level of the compacted specimen to determine the actual density, the specimen is ready for testing.

Figure 5.5 Mechanical mixer and vibratory compactor during compaction

RL-CBR testing apparatus

The overall objective of this research is to develop a simplified testing mechanism that makes use of available testing equipment in most standard road engineering laboratories. It is also indicated in section 5.2 and discussed in detail in section 5.3.2 that the RL-CBR test set-up is similar to the standard CBR test but with repeated loadings. In day to day practice the RL-CBR test is therefore meant to be carried out in a standard CBR test machine with repeated loading of the specimen obtained by pushing the button “plunger down” on the control unit for loading and pushing the “plunger up” button for unloading.

To facilitate the extensive experimental research in this project, however, a more advanced testing facility with a hydraulic actuator similar to the one for the large scale triaxial apparatus presented in section 4.2 is used. The TU Delft Road and Railway Engineering (RL-) CBR test apparatus consists of:

1. A loading frame, a hydraulic actuator, a load cell and a controller for application and measurement of displacement or force controlled static and cyclic axial loading with a capacity of 100 kN, Figure 5.6. Closed loop servo control is effectuated by an MTS controller, which feeds back on the signals of the load cell and the internal displacement transducer for force and displacement control, respectively.

2. A Control and Data Acquisition System consisting of a PC and a multi-programmer. The control unit generates the required loading signals and stores the acquired data signals to the hard disk. The multi-programmer provides the memory and the required digital to analogue (D/A) conversion for the control system and the required A/D conversion for the data acquisition.

3. For measurement of resilient and permanent deformations an external LVDT attached to the load cell or loading piston in the vertical direction is used with a total range of 10 or 20 mm. The external LVDT has a better accuracy than the internal actuator displacement measurement and is attached to the vertical piston with a magnetic stand.

4. The data acquisition system has up to 16 channels. Out of these 3 or 7 channels are in use:
   - 2 for load cell and the internal actuator displacement measurement,
   - 1 for external vertical deformation LVDT,
   - 4 for radial strain of the mould measured by strain gauges in the case of RL-CBR test with strain gauges, see section 5.4.

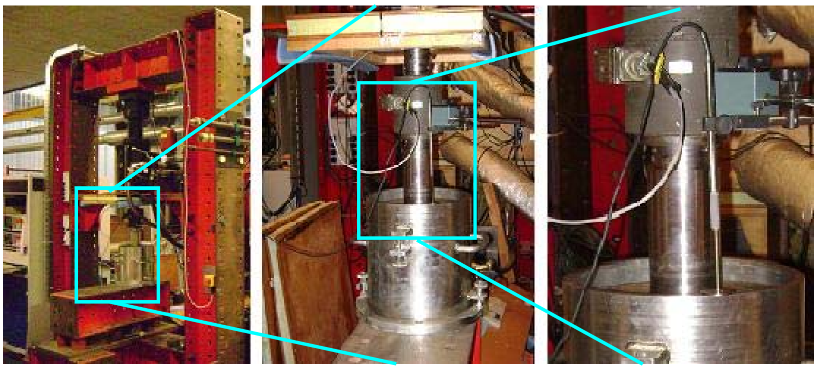

Figure 5.6 TU Delft (RL-) CBR test apparatus and LVDT detail

5.3.2 Testing procedure and test program

Repeated load CBR test set-up and procedure

The RL-CBR is carried out in the test apparatus described in section 5.2.2 with a specimen mould, diameter 250 mm and height 200 mm with a penetration plunger of diameter 81.5 mm. A schematic diagram of the RL-CBR test set-up is shown in Figure 5.7. The test is performed in the displacement controlled mode at a constant displacement rate of 1.27 mm/min (0.05 inch/min) = 0.021 mm/sec similar to the standard CBR test loading specification [2].

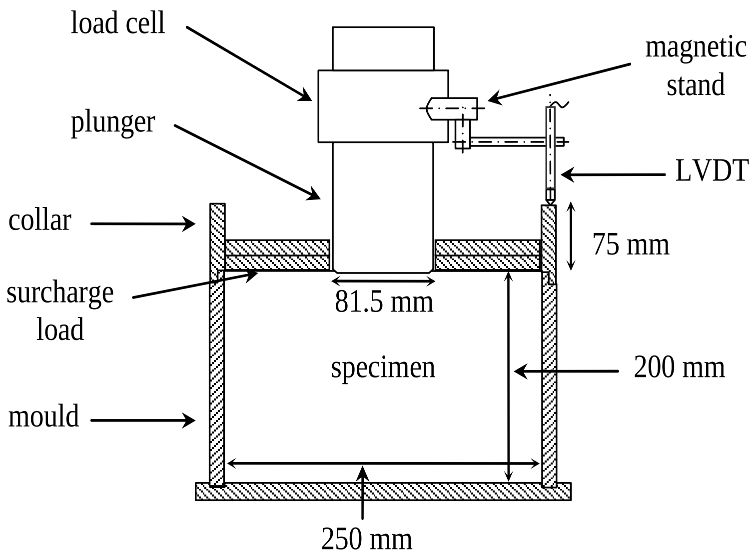

Figure 5.7 Schematic diagram of the repeated load CBR test set-up

To simulate the repeated load application in the standard CBR test, the following procedure is adopted [3-7]:

- Throughout the RL-CBR test program a 16 kg of surcharge load metal discs are used to reproduce approximately the weight equivalent to an 80 mm thick asphalt surface layer.

- The specimen is loaded, at the standard CBR displacement rate (1.27 mm/min), to a predetermined deformation (e.g. 2.54 mm) or load level. The load is recorded and unloaded with the same rate (1.27 mm/min) to a minimum contact load of 0.5 to 1 kN (0.1 to 0.2 MPa).
- The specimen is re-loaded to the same load at the same displacement rate of 1.27 mm/min, and released once more to the minimum contact load. The maximum and minimum load levels for each cycle are therefore kept constant.
- These cycles are generally repeated for 50 – 100 load cycles at which the permanent deformation due to the last 5 loading cycles will be less than 2% of the total permanent deformation at that point. The load and deformation can be recorded at a required reasonable accuracy rate (10 data points per sec is adopted). The resilient (recoverable) and permanent (unrecoverable) deformation is then measured as shown in Figures 5.1 and 5.8.
- In this research the loading and unloading cycles are automated, by using the MTS controlling unit provided with the testing facility, in two ways:
  i. The test is carried out at a load level which gives a predetermined deformation level (usually 2.54 mm); after recording the load level required to reach the deformation the test is re-run for the repeated load cycles by feeding the controller this load as maximum load and the contact load usually 0.15 MPa as minimum load.
  ii. The test is carried out at a predetermined load level usually for stress dependent behavior, the test is run by putting this load as a maximum and the contact load as a minimum and run continuously for the required number of load repetitions.
- Therefore it was convenient to run the test of all the specimens for at least 100 cycles and to consider the 100th cycle as standard for all resilient deformation analyses. Depending on the testing load or deformation level and material response the 100 load cycles mostly last from half an hour to two hours.
- Testing has also been carried out for few specimens for much more than 100 cycles, say up to 2000 cycles, by running the test overnight to investigate the permanent deformation after such a large number of load applications.

Once the load and deformation data per unit time is recorded it is possible to compute the resilient and permanent deformation for each cycle and the total deformation after a certain number of cycles. Figure 5.8 elaborates in detail the RL-CBR test and the method of determining the different deformation components.

Figure 5.8A shows the deformation with time indicating the constant 1.27 mm/min loading and unloading displacement rate and it also illustrates the resilient and permanent deformation for a typical load cycle drawn in pink color and the cumulative or total permanent deformation after some load cycles.

Figure 5.8B presents similarly the load with time. The shape of the curve depends on the material response for the defined displacement rate of loading and unloading. The shape is generally found to be similar for all unbound granular materials investigated in the study. It is to be noted that the transition from loading to unloading and vice versa is made sudden which is controlled by a program of two events: one event for the loading to end when it reaches the maximum load and the other for unloading which ends when it reaches the minimum load.

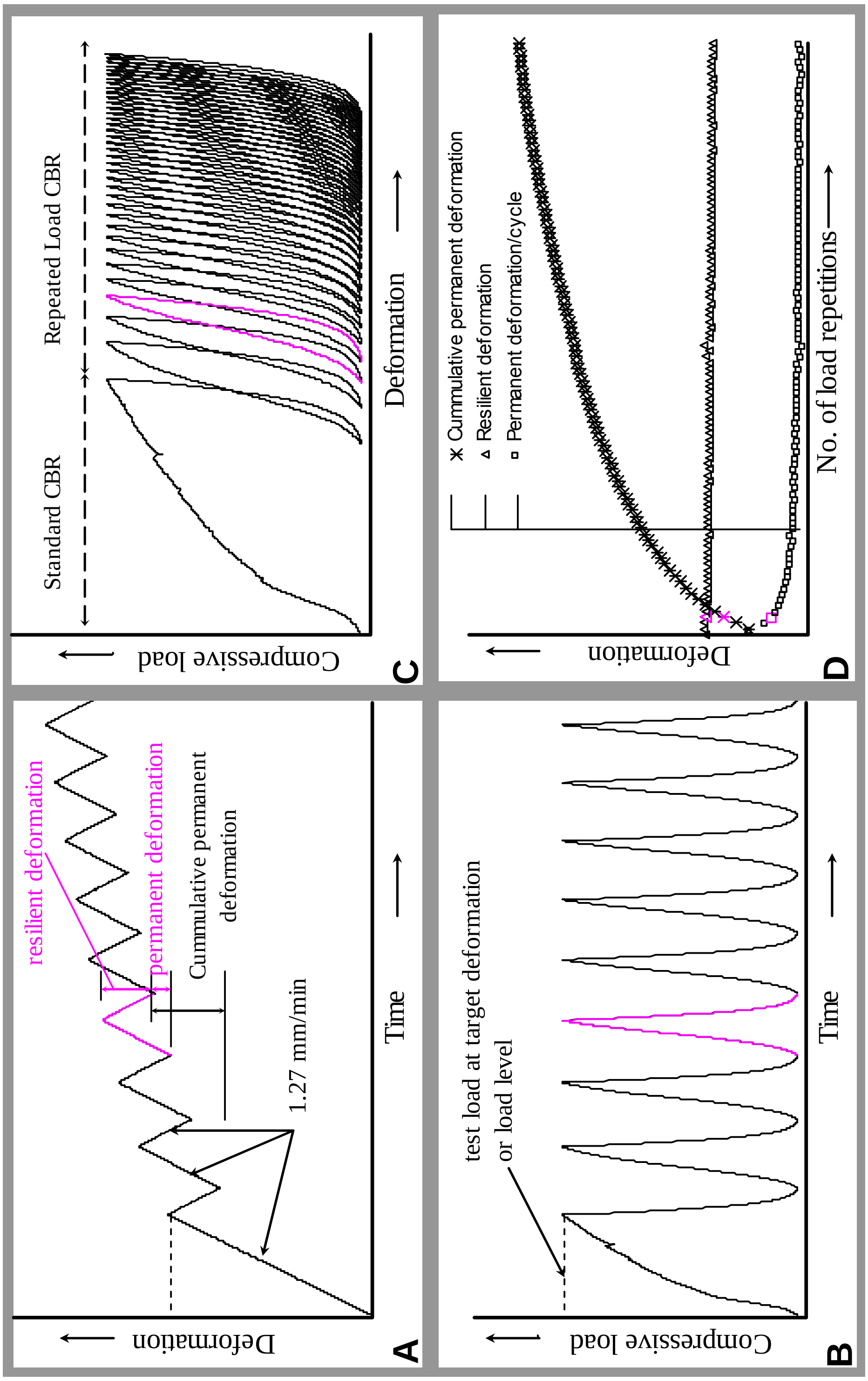

Figure 5.8 RL-CBR test and typical load - deformation measurements

Figure 5.8C illustrates the load – deformation relation for both the initial loading, i.e. standard CBR loading, and the repeated load cycles. It also shows the hysteresis loop between the loading and unloading curves and how the permanent deformation per cycle decreases as the number of loading cycles progresses. This figure demonstrates the fundamental stress – strain behavior of unbound granular materials under repeated loading similar to Figure 5.1.

Figure 5.8D shows the development of the main deformation outputs, i.e. the resilient and permanent deformations, of the RL-CBR test versus the number of load repetitions.

The load and deformation can also be monitored on the computer screen while running the test by choosing the appropriate data channel. Figure 5.9 shows the load in kN and deformation in mm during the test versus number of samples. One sample number is equivalent to 1/10 sec. for a sampling rate taken at 10 data points per second. The load progresses downward during loading as compressive forces are programmed as negative loads. The plunger is also displacing in the downward direction resulting in compression of the LVDT, therefore decreasing the LVDT reading from +10 mm towards the -10 mm end.

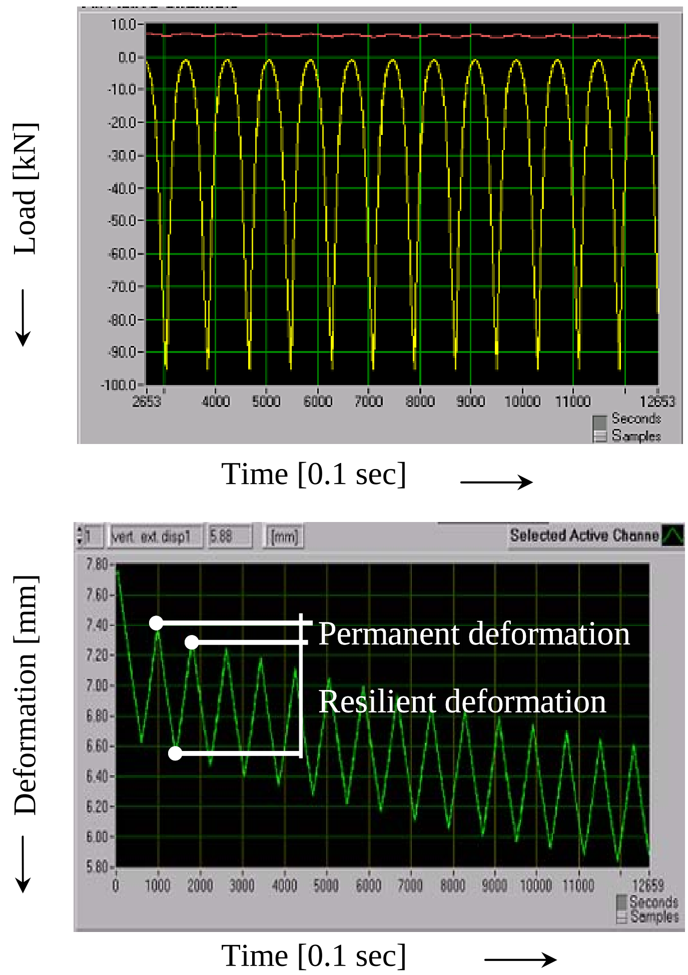

Figure 5.9 Load and deformation signals during RL-CBR testing

Test program

The RL-CBR test is carried out for all the six granular materials characterized in this research, so the FC, WB, G1, ZKK63, ZKK32 and MG at various compaction conditions that range from 95% to 102% DOC and dry to wet MC. Similar to the triaxial test program reported in chapter 4 the DOC is measured as percentage of the modified Proctor dry density of each material except the MG. For the MG the DOC is measured as percentage of normal Proctor dry density as has been used by Van Niekerk [7]. Similarly the MC is measured relative to the moderate (Mod.) moisture content measured in the modified Proctor compaction as given in table 3.3. The MG is exceptional as it is tested at one MC of 8% as adopted by Van Niekerk [7] in most of his resilient deformation (RD) triaxial tests on the same material.

The test program is designed in two series.

The first test series is conducted with a target initial plunger penetration deformation of 2.54 mm (0.1 inch) and continuing the test at the plunger load level recorded to obtain this deformation. The empirical nature of the CBR test and unavoidable sampling and compaction variations, for instance random arrangement and position of the coarse aggregates with respect to the plunger, results in a varying plunger load for identically prepared specimens and penetrated to the same initial deformation level of 2.54 mm.

The second series is performed with a predetermined but varying plunger load level. This experimental series is carried out to widen the test stress range applied in the first test series and to obtain a stress dependent behavior of the granular materials from RL-CBR testing.

The test conditions for the RL-CBR tests without strain gauge for the five materials (FC, WB, G1, ZKK32 and ZKK63 are shown in table 5-1. Each test that is listed in table 5-1 with its unique test code is conducted on a virgin specimen. Some of the specimens tested with a predetermined plunger stress level (mainly those with low load level) are however used for multi-stage testing i.e. testing with multiple varying load levels per specimen, to investigate the influence of pre-loading on their resilient and permanent deformation behavior.

In chapter 3 it is noted that for the mix granulates (MG) only RL-CBR tests are performed in this research to compare the results with the triaxial test results reported by Van Niekerk [7]. Therefore the test program was designed in an identical way to the most representative material composition, grading and compaction condition of Van Niekerk's triaxial testing. These test conditions performed in this research are summarized separately in table 5-2.

Table 5-1 Test program for RL-CBR test without strain gauge

Material	Target DOC (%)	Target MC (% by mass)	Target initial deformation or predetermined plunger stress level: Target initial deformation (mm)	Target initial deformation or predetermined plunger stress level: Predetermined plunger stress level (MPa)	Test code
FC	95	Dry (5)	2.54		RLCBR-FC-95dr
		Mod. (7.5)	2.54		RLCBR-FC-95a
			2.54		RLCBR-FC-95b
			2.54		RLCBR-FC-95c
				2.78	RLCBR-FC-95_s1
				10.54	RLCBR-FC-95_s2
		Wet (9.5)	2.54		RLCBR-FC-95wt
			2.54		RLC-FC-95wt
	98	Dry (5)	*2.54*♣		RLCBR-FC-98dr
				10.54	RLCBR-FC-98dr_s1
				24.92ψ	RLCBR-FC-98dr_s2
		Mod. (7.5)	2.54		RLCBR-FC-98a
			2.54		RLCBR-FC-98b
			2.54		RLCBR-FC-98c
			2.54		RLC-FC-98
				2.78	RLCBR-FC-98_s1
				8.05	RLCBR-FC-98_s2
				12.46	RLCBR-FC-98_s3
		Wet (9.5)	2.54		RLCBR-FC-98wt
			2.54		RLC-FC-98wt_a
			2.54		RLC-FC-98wt_b
			2.54		RLC-FC-98wt_c
				3.83	RLCBR-FC-98wt_s1
	100	Dry (5)	2.54		RLCBR-FC-100dr
		Mod. (7.5)	2.54		RLCBR-FC-100a
			2.54		RLCBR-FC-100b
			2.54		RLCBR-FC-100c
				2.78	RLCBR-FC-100_s1
				10.54	RLCBR-FC-100_s2
		Wet (9.5)	2.54		RLCBR-FC-100wt
			2.54		RLC-FC-100wt
WB	95	Dry (5)	2.54		RLCBR-WB-95dr_a
			2.54		RLCBR-WB-95dr_b
		Mod. (7)	2.54		RLCBR-WB-95a
			2.54		RLCBR-WB-95b
			2.54		RLCBR-WB-95c
				4.79	RLCBR-WB-95_s1
				8.05	RLCBR-WB-95_s2
		Wet (9)	2.54		RLCBR-WB-95wt_a
			2.54		RLCBR-WB-95wt_b
	98	Dry (5)	2.54		RLCBR-WB-98dr_a
			2.54		RLCBR-WB-98dr_b
			2.54		RLCBR-WB-98dr_c
				2.78	RLCBR-WB-98dr_s1
				10.54	RLCBR-WB-98dr_s2
		Mod. (7)	2.54		RLCBR-WB-98a
			2.54		RLCBR-WB-98b
			2.54		RLCBR-WB-98c
			2.54		RLCBR-WB-98d
			2.54		RLCBR-WB-98e
				2.78	RLCBR-WB-98_s1
				8.05	RLCBR-WB-98_s2
				10.54	RLCBR-WB-98_s3

Material	Target DOC (%)	Target MC (% by mass)	Target initial deformation or predetermined plunger stress level		Test code
			Target initial deformation (mm)	Predetermined plunger stress level (MPa)	
WB	98	Wet (9)	2.54		RLCBR-WB-98wt_a
			2.54		RLCBR-WB-98wt_b
			2.54		RLCBR-WB-98wt_c
				6.13	RLCBR-WB-98wt_s1
	100	Dry (5)	2.54		RLCBR-WB-100dr_a
			2.54		RLCBR-WB-100dr_b
		Mod. (7)	2.54		RLCBR-WB-100a
			2.54		RLCBR-WB-100b
			2.54		RLCBR-WB-100c
				2.78	RLCBR-WB-100_s1
				10.54	RLCBR-WB-100_s2
		Wet (9)	2.54		RLCBR-WB-100wt_a
			2.54		RLCBR-WB-100wt_b
G1	98	Dry (2)	2.54		RLCBR-G1-98dr
		Mod. (4)	2.54		RLCBR-G1-98
			2.54		RLC-G1-98
				8.05	RLCBR-G1-98_s1
				18.21	RLCBR-G1-98_s2
		Wet (6)	2.54		RLCBR-G1-98wt
	100	Dry (2)	2.54		RLCBR-G1-100dr
			2.54♣		RLC-G1-100dr
				8.05	RLCBR-G1-100dr_s1
				24.92ψ	RLCBR-G1-100dr_s2
		Mod. (4)	2.54		RLCBR-G1-100a
			2.54		RLCBR-G1-100b
			2.54♣		RLCBR-G1-100c
			2.54		RLC-G1-100a
			2.54♣		RLC-G1-100b
			2.54		RLC-G1-100c
				8.05	RLCBR-G1-100_s1
				10.54	RLCBR-G1-100_s2
				24.92 ψ	RLCBR-G1-100_s3
		Wet (6)	2.54		RLCBR-G1-100wt
			2.54		RLC-G1-100wt
				16.24	RLCBR-G1-100wt_s1
	102	Dry (2)	2.54		RLCBR-G1-102dr
		Mod. (4)	2.54		RLCBR-G1-102
			2.54♣		RLC-G1-102
				10.54	RLCBR-G1-102_s1
				24.92 ψ	RLCBR-G1-102_s2
		Wet (6)	2.54		RLCBR-G1-102wt
ZKK32	100	Mod. (3)		2.78	RLCBR-ZKK32_s1
				4.79	RLCBR-ZKK32_s2
				8.05	RLCBR-ZKK32_s3
				10.54	RLCBR-ZKK32_s4
ZKK63	100	Mod. (3)		2.78	RLCBR-ZKK63_s1
				6.75	RLCBR-ZKK63_s2
				10.54	RLCBR-ZKK63_s3
				16.24	RLCBR-ZKK63_s4

♣ *the target initial penetration deformation is not achieved due to limitation of the loading capacity (100 kN = 20 MPa) of the RL-CBR testing machine, thus tested at 95 kN = 18.2 MPa plunger load.*

ψ *tests on specimens with more than 20 MPa plunger stress levels are performed on the triaxial loading frame with similar test set-up to the RL-CBR and the loading and unloading is operated manually by means of loading-pause-unloading-pause-loading etc.*

Table 5-2 Test program for MG for RL-CBR test without strain gauge

Material	Target DOC (%)	Target MC (% by mass)	Target initial deformation or predetermined plunger stress level		Test code
			Target initial deformation (mm)	Predetermined plunger stress level (MPa)	
MG	97	Mod. (8)	2.54		RLC-MG-AL-97-4
	100	Mod. (8)	2.54		RLC-MG-AL-97-4a
			2.54		RLC-MG-AL-97-4b
			2.54		RLC-MG-AL-97-4c
	105	Mod. (8)	2.54		RLC-MG-AL-105-4

Prior to these extensive RL-CBR testing programs a standard CBR test is performed, section 3.5.6, on two materials FC and WB. This along with the compaction properties of the materials provides some information about their strength and resistance to deformation. Similar to the standard CBR test a static CBR test with the large mould and large plunger (modified CBR) is performed on three materials G1, FC and WB. This provides an insight into the material strength and resistance to deformation and helps in planning the test program.

Modified CBR

A modified CBR (MCBR) test is performed to observe and understand the reaction of the different materials with varying compaction conditions to the penetration loading. The name modified CBR is used since the test is similar to the standard CBR but using a big mould and plunger size. This test gives an overview of the development of deformation with loading and what magnitude of load is expected to deform say the 2.54 mm or 5.08 mm etc using the big plunger. Further the test demonstrates the influence of material type, moisture content and DOC on the resistance to penetration or strength properties of the granular materials.

The value of MCBR in percent is defined similar to the definition of the standard CBR as a ratio of plunger stress to the reference stresses 6.75 MPa and 10.18 MPa at 2.54 mm and 5.08 mm penetration respectively. One has to note that the results from the MCBR test can't be expressed in terms of CBR loads. The reference loads are for the standard plunger size, in the case of the modified CBR a larger plunger size is adopted.

Figure 5.10 shows the effect of DOC and MC on the relation between plunger stress and penetration. Generally for most of the granular materials an increase to MC results in a decrease of the deformation resistance while increasing DOC improves it. However, as shown in Figure 5.11, the resistance to penetration of FC decreases after an optimum compaction degree. For weak aggregates such as FC excessive compaction has a significant negative impact on the performance. This has to do with crushing of the aggregates and weakening the specimen by over-compaction, this phenomenon is further elaborated in chapter 7. The performance of the high quality G1, on the other hand, increases with increasing DOC and decreasing MC as shown in Figure 5.12 [8].

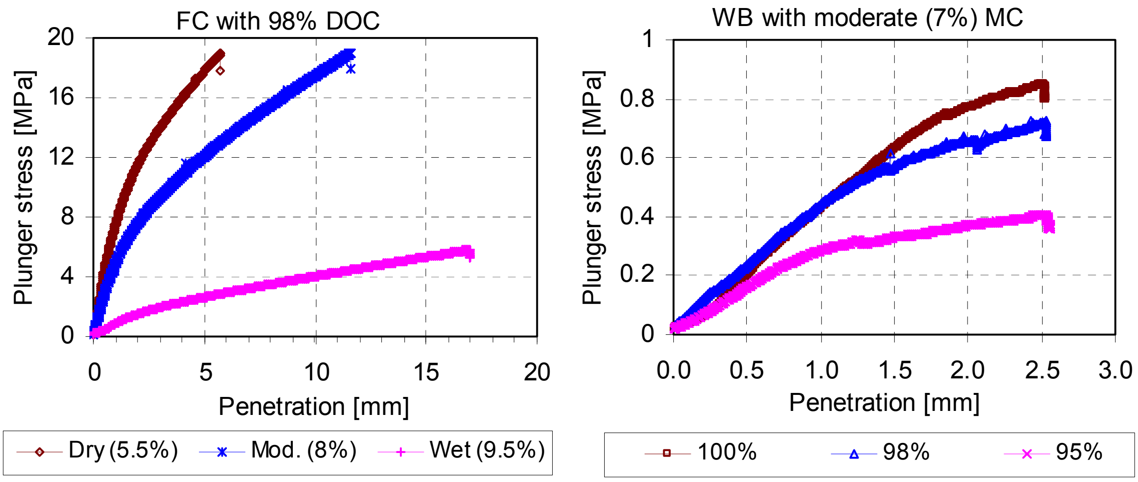

Figure 5.10 Plunger stress vs. penetration for FC and WB

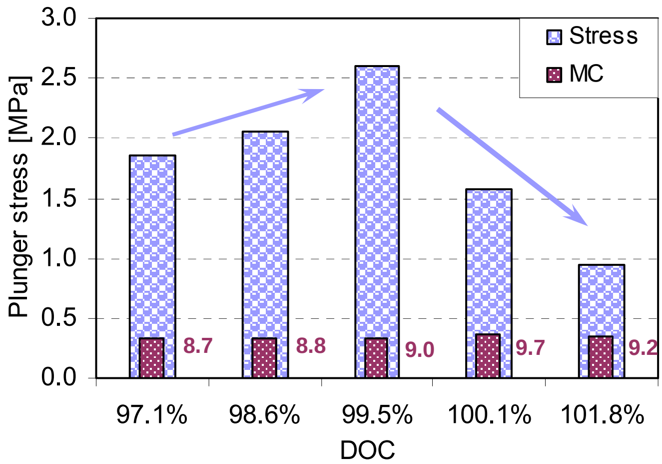

Figure 5.11 Plunger stress for 2.54 mm penetration for FC

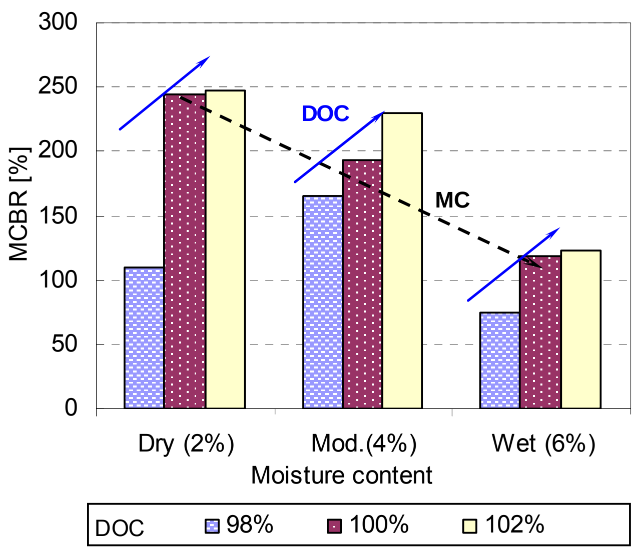

Figure 5.12 Modified CBR values for G1 with varying DOC and MC

In the RL-CBR tests without strain gauge the first series is carried out for all materials with initial target penetration of 2.54 mm. The repetition of loading cycles is then performed with this plunger stress. However, due to unavoidable inhomogeneity of the specimens a varying plunger stress is obtained for the same 2.54 mm penetration of similar mixtures. For such varying plunger stress, an example of a varying resilient and permanent deformation is shown in Figure 5.13 for three WB specimens tested at the same condition (moderate MC and 95% DOC) and initial penetration of 2.54 mm.

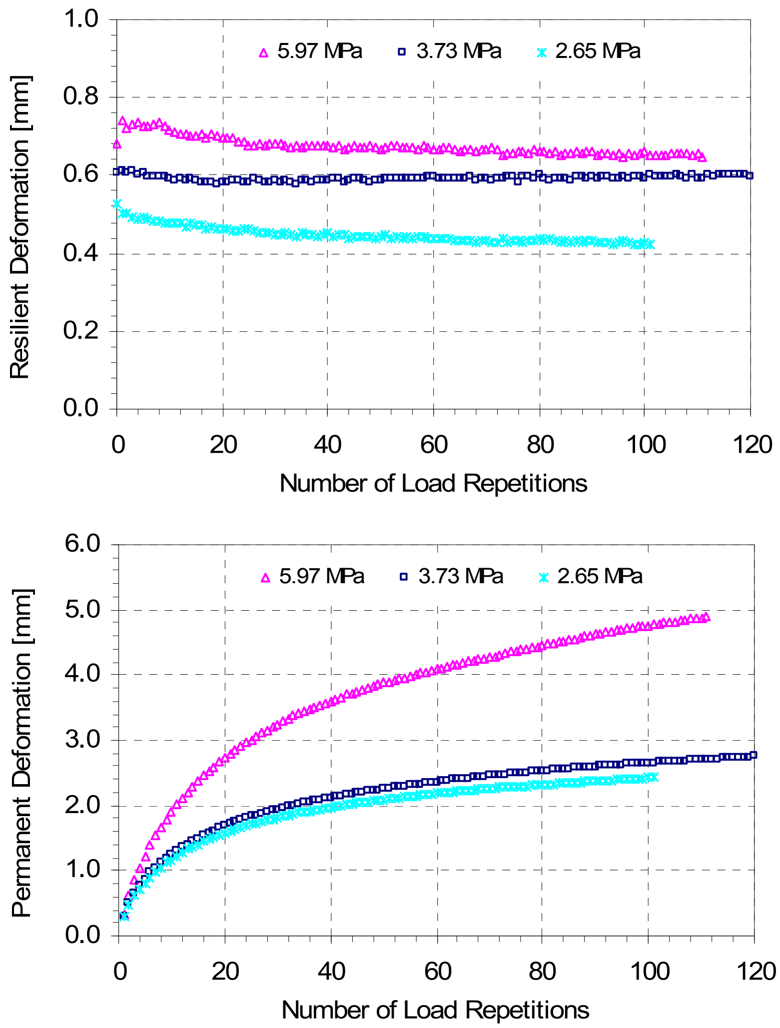

Figure 5.13 Plunger stress effect on WB at moderate MC and 95% DOC

In addition to the stress level the deformation properties of the materials apparently change as a result of other influence factors. In the same way as the triaxial tests, described in chapter 4, the RL-CBR test program is designed systematically to be able to investigate the influence of factors such as moisture content and degree of compaction on the resilient and permanent deformation behavior of the granular materials. These effects are best presented graphically in carefully selected charts showing their development along the number of load cycles grouped for the influence factor under consideration.

5.3.3 Effect of moisture content on resilient and permanent deformation

Selected cases are presented below to investigate the effect of moisture content on the resilient and permanent deformation of granular materials. Similar to the triaxial tests the investigated tests are carried out with a "homogenous" test series i.e. all the above influencing factors are kept identical, only the influence of the moisture content is investigated. In these series the DOC is kept 100% and 98% for G1 and WB respectively and the moisture effect is studied by testing at three different target moisture contents i.e. dry, moderate and wet.

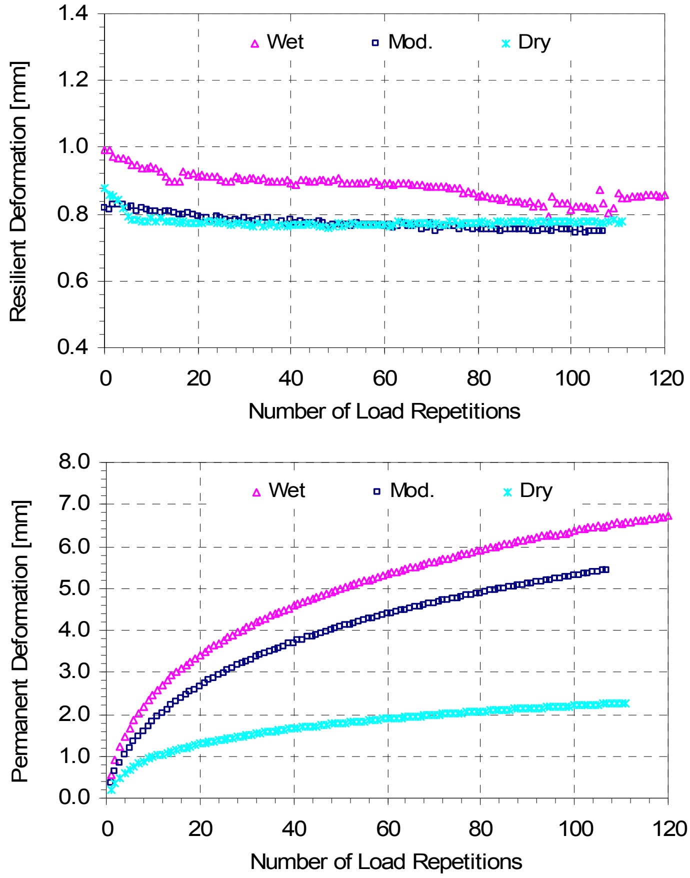

Figure 5.14 Resilient and permanent deformation of G1 at 100% DOC at around 16 MPa plunger stress

The influence of the moisture content is illustrated with Figures 5.14 and 5.15. Figure 5.14 presents a test series conducted on G1 at 100% DOC at around 16 MPa plunger stress for three target MCs and Figure 5.15 presents a test series on WB at 98% DOC at around 6 MPa plunger stress. It is recalled that at these stress levels a penetration of 2.54 mm was obtained. It is expected that the effect of the moisture content is more pronounced on the permanent deformation than on the resilient deformation.

In both Figures 5.14 and 5.15 the increase in permanent deformation with an increase of moisture content is clearly shown for both G1 and WB. The wet mix of the G1 shows a higher resilient deformation compared to the moderate and dry mixes. Contrary, the wet mix of WB shows less resilient deformation with increasing number of load repetitions compared to the moderate and dry mixes.

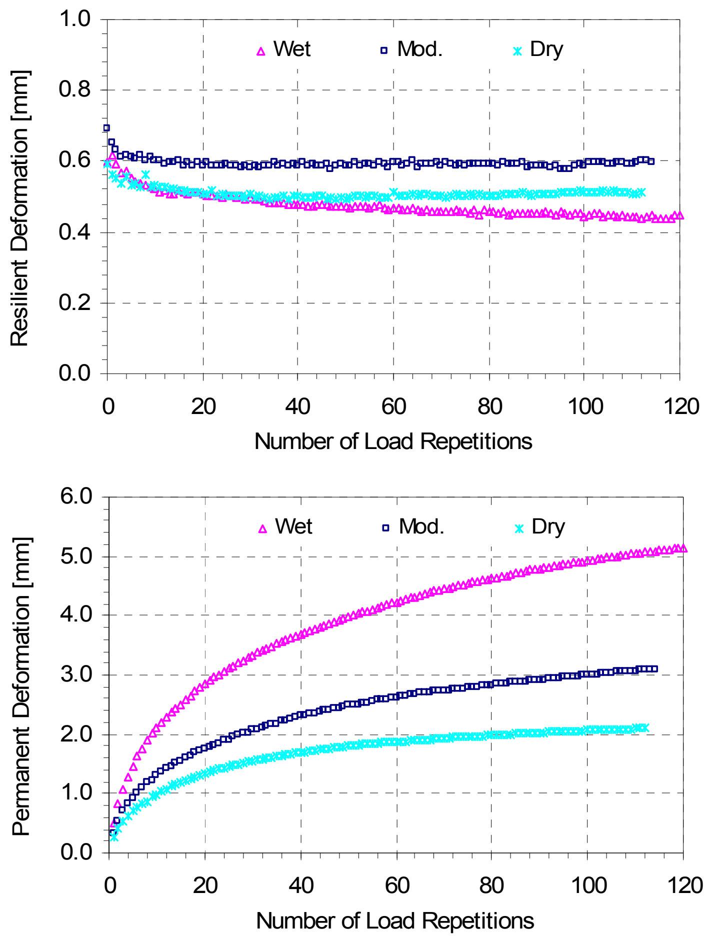

Figure 5.15 Resilient and permanent deformation of WB at 98% DOC at around 6 MPa plunger stress

5.3.4 Effect of degree of compaction on resilient and permanent deformation

The effect of DOC on the resilient and permanent deformation is presented here for two materials FC and WB. The tests are carried out with a "homogenous" test series, all influence factors are kept identical only the influence of DOC is investigated. In these series the target MC is kept at moderate moisture content for each respective material (7.5% MC for FC and 7% MC for WB) and the effect of DOC is investigated by testing at three target DOC 95%, 98% and 100% for both materials.

Figure 5.16 shows the resilient and permanent deformation of FC at moderate (7.5%) target MC and around 5.5 MPa plunger stress. Similar to the effect of the MC the effect of the DOC is more pronounced on the permanent deformation development. That is the resistance to permanent deformation increases with an increase of DOC. The resilient deformation is however smaller for the 98% DOC compared to the 95% and 100% DOC. This agrees with the stiffness behavior of the ferricrete observed in the triaxial test. Both under-compaction and over-compaction of the ferricrete relative to the 98% DOC decreases its stiffness. The ferricrete is a material with porous and weak coarse aggregates which can be easily crushed. Over-compaction thus results in crushing the coarse aggregates and changes the gradation of particle package as demonstrated in chapter 7. Of course under-compaction also results in a less dense and thus less stiff specimen.

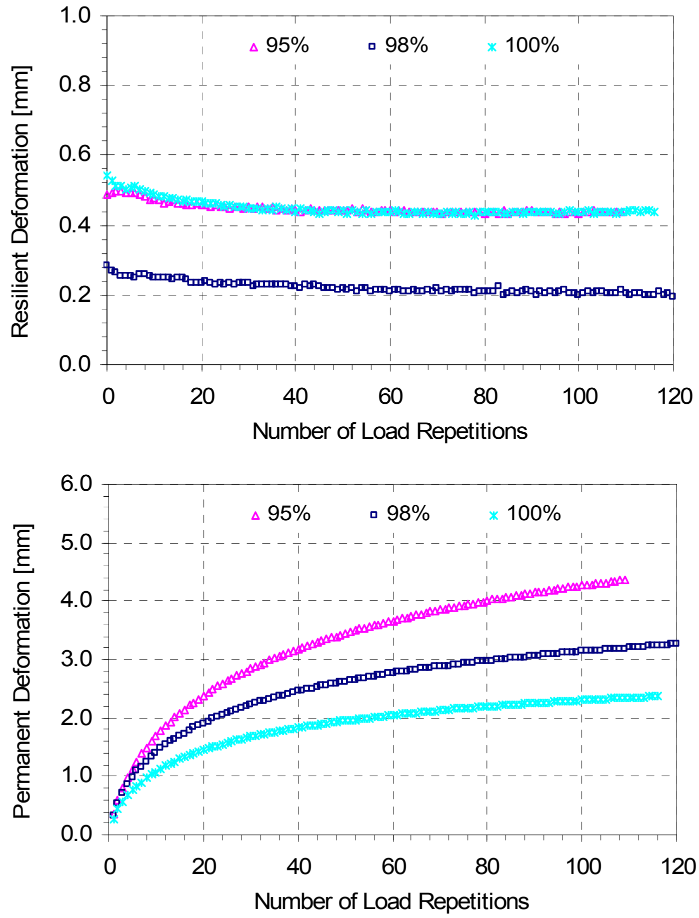

Figure 5.16 Resilient and permanent deformation of FC at moderate MC at around 5.5 MPa plunger stress

Figure 5.17 shows the resilient and permanent deformation of WB at moderate (7%) target MC and around 6 MPa plunger stress. At these conditions both the resilient and permanent deformations decrease with an increase of the DOC from 95% to 100%. During the triaxial testing however a lower stiffness was found for the samples compacted at 100% DOC (Figure 4.35). This difference is attributed to the fact that a 100% DOC compaction level in the 200 mm thick CBR mould is with much less damage to the flaky coarse particles compared to the compaction of the 600 mm thick triaxial specimen to the same 100% DOC.

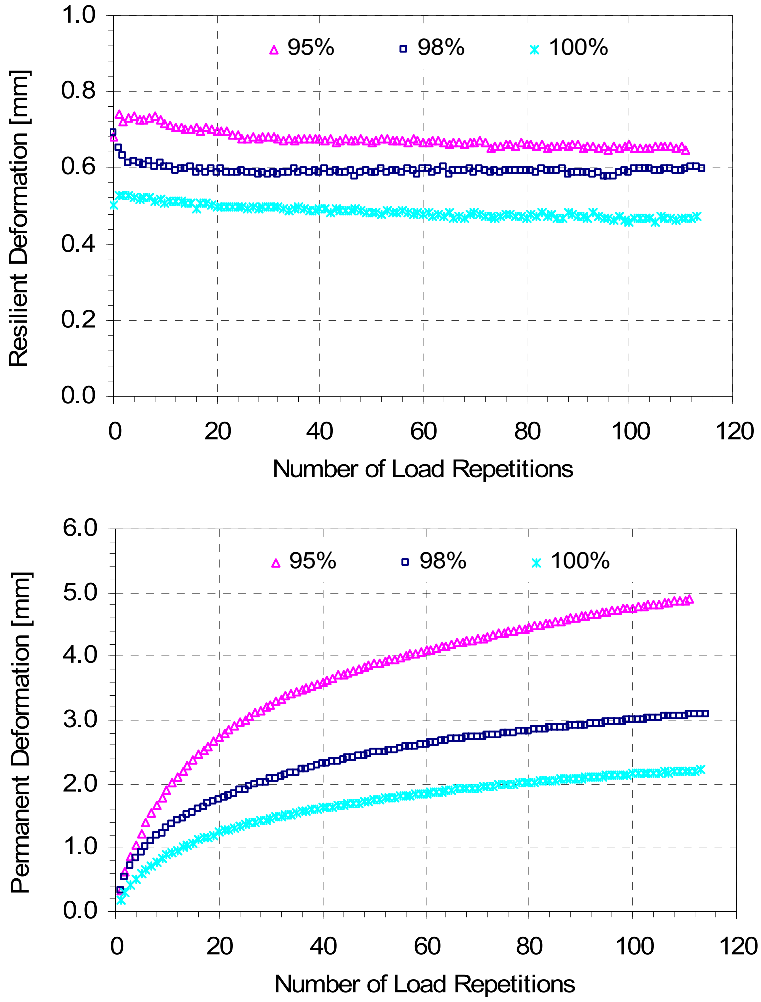

Figure 5.17 Resilient and permanent deformation for WB at moderate MC at around 6 MPa plunger stress

5.4 REPEATED LOAD CBR TEST WITH STRAIN GAUGES

5.4.1 Test principle

The principle of repeated load CBR testing with strain gauges is similar to the principle elaborated in section 5.2: by repeating the CBR load elastic properties can be determined. With the RL-CBR test with strain gauges, however, the confining condition and hence the stress state of the specimen is estimated through mould deformation measurements.

It is well known that the stiffness modulus of unbound granular materials is stress dependent and the effect of the confining stress is significant. On the other hand, the confining pressure is not readily measurable due to the complex nature of the stress state in the CBR mould. However, the compacted specimen will apply a load on the steel mould when loaded. This will result in a deformation of the mould which can be measured by means of strain gauges. The degree of confinement and its effect on the elastic properties of the specimen can then be investigated.

5.4.2 Measuring apparatus and test procedure

Measuring apparatus

The specimen preparation, measuring apparatus and testing procedure of the RL-CBR with strain gauges is exactly the same as for the RL-CBR without strain gauge which was discussed in detail in section 5.3. The only exception is that strain gauges are glued at the exterior of the mould to measure the mould's lateral deformation. It is preferred to glue the strain gauges at the exterior of the mould rather than at the inside. The reason is the fact that if they are positioned at the internal surface of the mould the sensitive strain gauges will be easily damaged by the high vibratory compression of the compactor and the friction from the granular specimen.

Four strain gauges (60 mm long and 120 ohm resistance TML polyester wire P- series PL-60-11 Quarter bridge application [9]) capable of measuring in micro-strains are glued at the external surface of the mould, see Figure 5.18. Two of them are positioned at mid height of the mould, where maximum deformation is expected, and the other two near to the top (40 mm below top edge) for comparison. The schematic and real test set-up of the RL-CBR is shown in Figure 5.19. The lateral deformations measured at the mid height of the mould during the loading and unloading cycles were considered as main data for analysis. For each strain gauge a similar type of gauge is also connected in vertical alignment for temperature compensation.

Figure 5.18 Strain gauges glued to the RL-CBR mould

The strain gauges are glued by special adhesive material (CN – Cyanoacrylate) to a polished surface of the mould. It is then coated by special coating material (N-1 chloroprene rubber system) for moisture proofing and other physical protection. These strain gauges are connected to the digital data acquisition system through amplifiers.

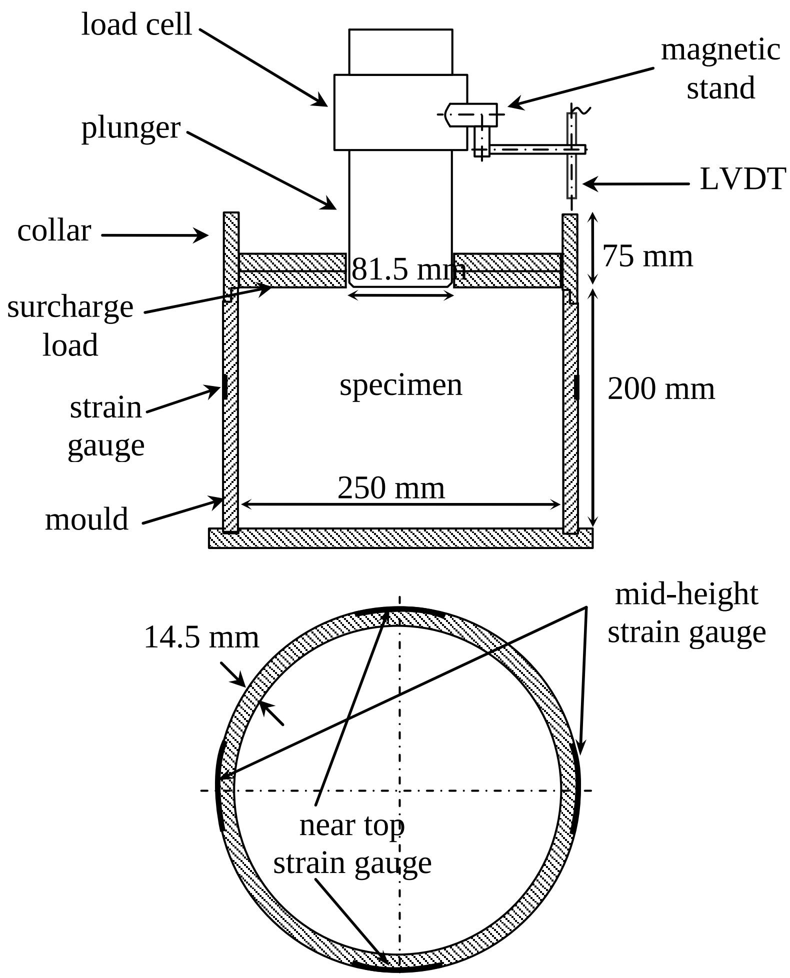

(a)

(b)

Figure 5.19 Repeated load CBR with strain gauges (a) schematic diagram (b) test set-up

Test procedure

The testing procedure of the RL-CBR with strain gauges is the same as the RL-CBR tests without strain gauge. Thus it is not necessary to repeat the entire procedure here. The only addition in the procedure is that lateral mould strain readings were recorded during the test. Prior to the start of compaction the strain gauge readings were continuously recorded or set to zero as a reference. Initially it was intended to record the strain gauge measurements throughout the compaction period in order to measure and evaluate the pre-confining effect by the compaction process. However, this is not followed after observing the highly varying results due to the high vibration effect from the vibratory compactor set-up and sensitivity of the strain gauges to such vibration noise. Moreover, the equipment handling for recording the strains during compaction was complicated with respect to power and amplifier connections. Instead the strain gauge readings before the start of the compaction and after the compaction just before application of the plunger test load were recorded.

The mould lateral strains were recorded for each loading and unloading cycle during the test. Figure 5.20 shows RL-CBR with strain gauge measurements for the mid-height strain gauges for G1 material. In this figure both the mid-height strain gauges (Mid-SG 1 and Mid-SG 2) measured a similar range of magnitude of elastic (recoverable) lateral strain between the minimum and maximum loads in a given load cycle.

In some other instants, as shown in Figure 5.21 for the FC material, the measurement between the two strain gauges at the same height (mid-height) varies significantly for unknown reasons. To a certain extent a measurement difference among the two gauges can be expected as a result of the arrangement and location of the coarse aggregates within the mould. However, such a huge difference perhaps is a consequence of test set-up problems that can result in an unbalanced load transfer. For instance, when the load alignment is not vertical or centered, the overall equipment set-up is not leveled. Also the sensitivity of the volt amplifiers could play a role. In all cases the average of the two mid-height strain gauges is considered for analysis unless either of the strains is considered erroneous and therefore should be disregarded.

Generally the mould strain follows closely the load curve, and when plotted against the plunger deformation they show similarity. Figure 5.22 shows the general trend of the load – deformation and mould strain – deformation patterns. However, for small load levels the mould strain – deformation curve appears to be irregular and more scattered as these strains are too small. Figure 5.23 gives an example of the load – deformation and mould strain – deformation patterns for low level loading.

The RL-CBR test with strain gauges is carried out for the two South African materials G1 and FC. Within the scope of this research the test is conducted at a specific compaction condition for each material. The G1 is characterized at moderate MC (4%) and 100% DOC and the FC at moderate MC (7.5%) and 98% DOC. All the tests are performed with a predetermined but varying plunger load level. It is attempted to cover a wide range of plunger loads per material to obtain a stress dependent behavior of the granular materials. A load range of 8 – 95 kN is used for both G1 and FC materials. However, at very low load levels the strain levels were too small for accurate measurement.

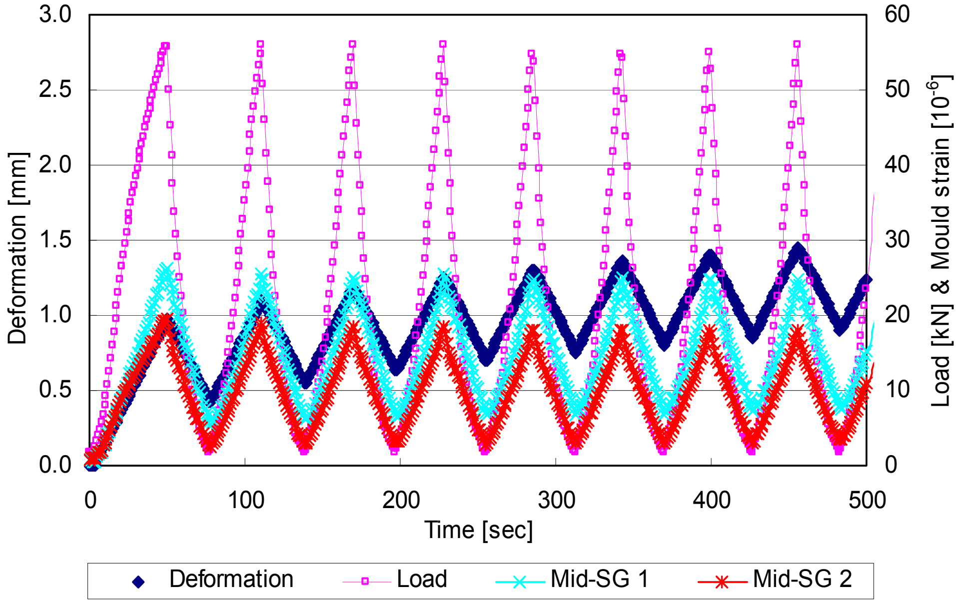

Figure 5.20 RL-CBR measurements on G1 at 55 kN plunger load with two mid-height strain gauges

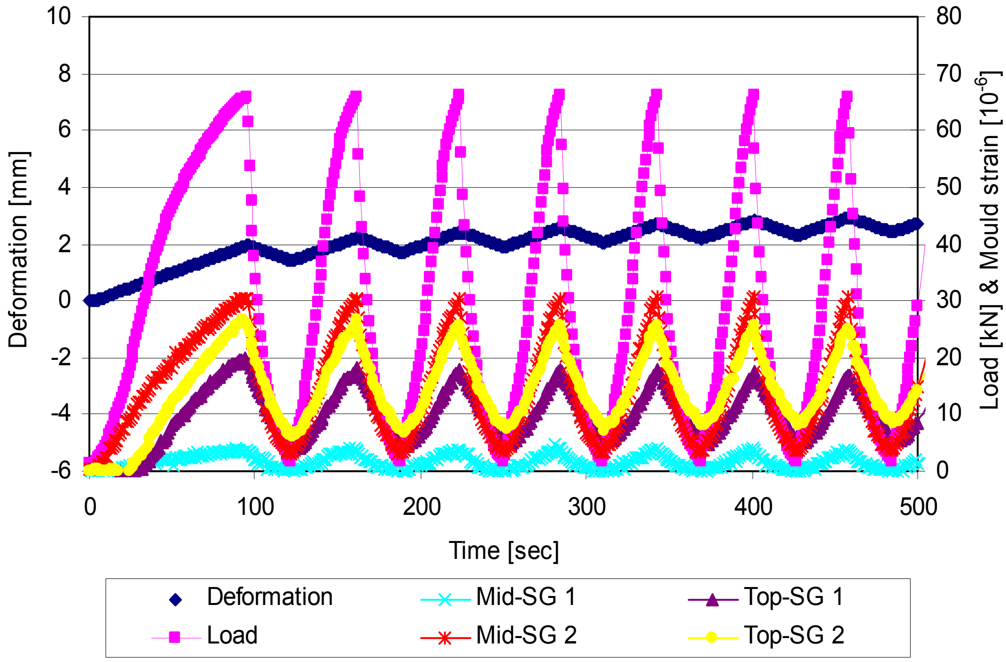

Figure 5.21 RL-CBR measurements on FC at 65 kN plunger load with four strain gauges two mid-height and two near the top

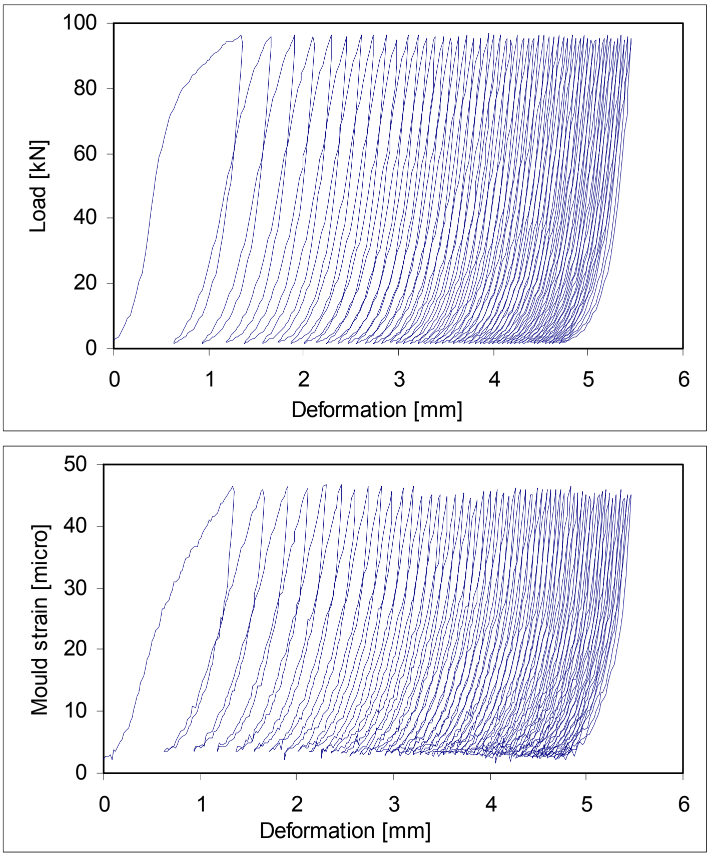

Figure 5.22 Load – deformation and mould strain – deformation pattern

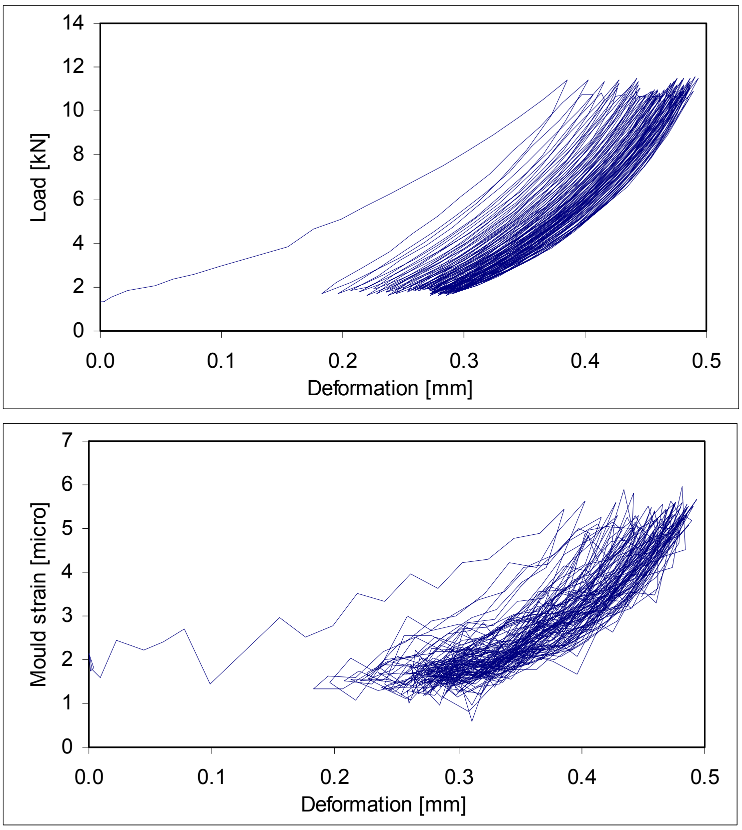

Figure 5.23 Load – deformation and mould strain – deformation pattern for small loads

5.5 FINITE ELEMENT MODELING

The finite element method (FEM) has been extensively used in research to model pavement structures as has been reported by several researchers [10-12]. In this research finite element modeling of granular materials under repeated load CBR is carried out.

ABAQUS [13], a commercially available finite element modeling program, has been widely applied for pavement analysis. Chen et al [14] did a comprehensive study of various pavement analysis programs and showed that the results from the ABAQUS program were comparable to those from other programs. Zaghloul and White [15], Kim et al [11] simulated responses of flexible pavements using three-dimensional dynamic analysis in ABAQUS. The main capabilities of ABAQUS in solving pavement engineering problems include linear and nonlinear elastic, visco-elastic, elasto-plastic etc material modeling. ABAQUS also provides two-dimensional, three-dimensional and axisymmetric calculations and interface modeling with friction.

5.5.1 Modeling the repeated load CBR test

The main purpose of the finite element modeling in this research is to simulate the RL-CBR test through finite element analysis. That is to develop a simplified relation between the unbound granular material elastic properties, mainly the stiffness modulus, with the stresses and deformations obtained. For this purpose a simple linear elastic material property is used in modeling both the granular material and the steel mould confining the granular specimen. For modeling the RL-CBR set-up the ABAQUS axisymmetric FEM code is utilized.

The finite element mesh used for the analysis and its 3D visualization are shown in Figure 5.24(a) and 5.24(b). The number of elements and nodes in the mesh are 730 and 2437 respectively. A three-dimensional response is simulated by using 8-node biquadratic axisymmetric quadrilateral reduced integration (CAX8R) elements. These were used because of their ability to accurately predict the response of axially symmetric loaded models. They are used to give a simulated three-dimensional response by revolving a two-dimensional surface around the centerline of symmetry. The use of CAX8R elements increases the efficiency of the model, when compared to a true three-dimensional model while still maintaining accurate results [16].

The structure is modeled as consisting of a rigid plunger, the steel mould and the granular material. The plunger is modeled as a rigid body and the steel mould has been assigned an elastic modulus of 210 GPa and Poisson's ratio of 0.2. The granular base and subbase materials considered in this study vary from high quality crushed stone to a rather marginal ferricrete and recycled mix granulate. Thus the elastic properties, elastic modulus and

Poisson's ratio, of the granular material included in the modeling cover a wide range as shown in table 5-3.

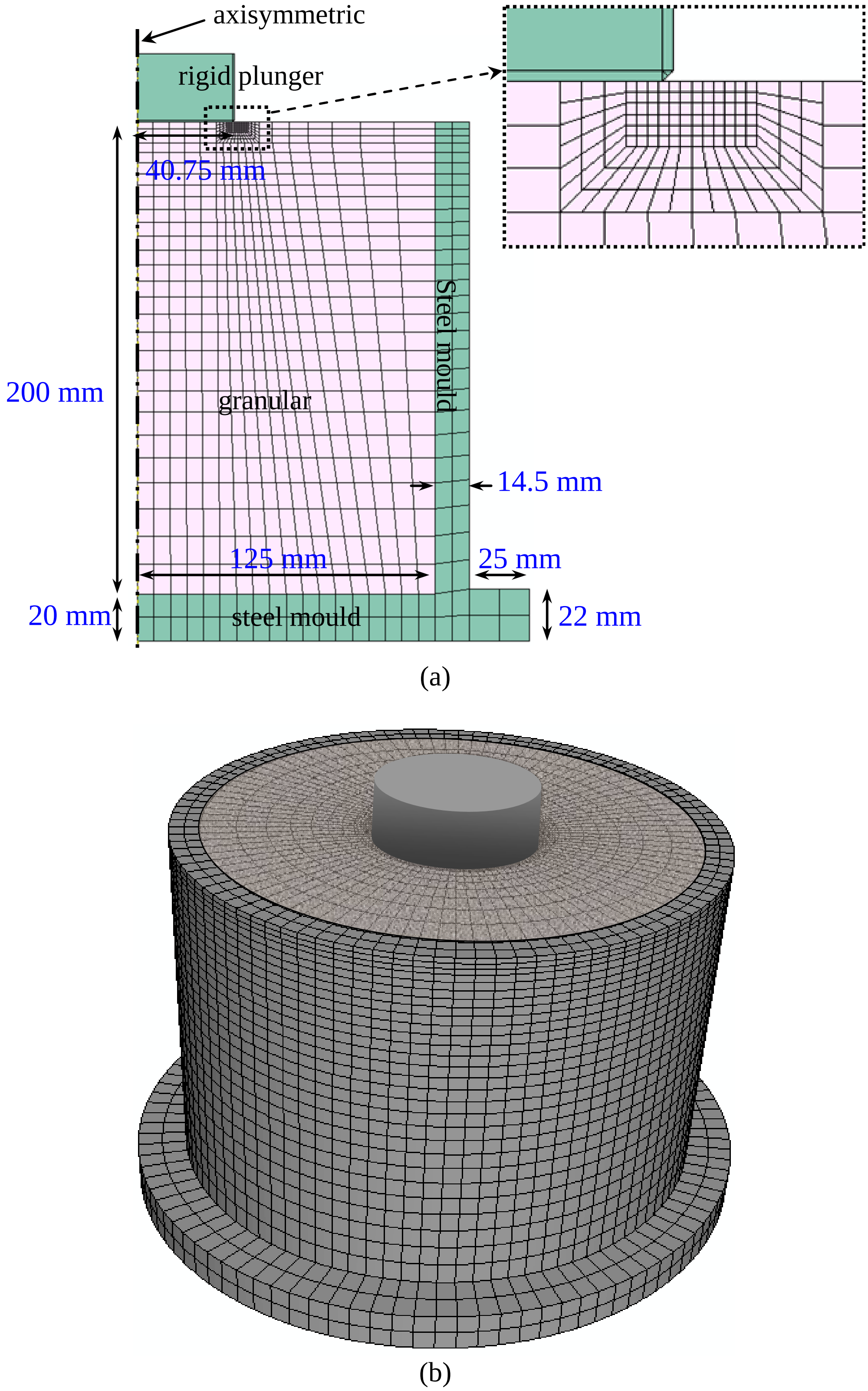

Figure 5.24 (a) Finite element mesh used in modeling the axisymmetric RL-CBR (b) its 3D visualization

Table 5-3 Granular material properties used in the FE analysis

Poisson's ratio [-]	Elastic modulus [MPa]
0.15	100
0.25	200
0.35	300
0.45	400
	500
	600
	800
	1000

Modeling of the mould-granular material and plunger-granular material interface is important for proper analysis of the contact condition between the mould or plunger and the granular material. ABAQUS [13] provides a number of advanced models for contact behavior. Surface-based contact, which allows modeling of contact between two deformable bodies that undergo small or finite sliding, was used in the analyses presented here. The mechanical contact simulation of the interaction between two bodies in Abaqus includes a model for the contact pressure-overclosure relationship (i.e. behavior normal to the contact surfaces) and a friction model that defines the force resisting relative tangential motion of the surfaces.

The most common contact pressure-overclosure relationship is "hard" contact. This type of contact is defined for the plunger-material contact surface. When surfaces are in contact, any contact pressure can be transmitted between them. The surfaces separate if the contact pressure reduces to zero. Separated surfaces come into contact when the separation between them reduces to zero. The contact condition between the mould and the granular material is defined with a "softened exponential pressure-overclosure" along with frictional behavior to model the tangential stress transmitted across the interface. The softened contact allow separation (provide clearance), the particularity is that you will have a contact pressure even if the surfaces are opened. This way of provision of clearance prevents the nodes and elements at the interference penetration to each other in addition to the simulation of the frictional/sliding behavior at the mould and granular material contact.

The boundary conditions have a significant influence in predicting the response of the model, the model is constrained only at the bottom as a simple support. It is constrained against displacement in the vertical direction. The lateral confinement for the granular material is realized by the factual response of the steel mould to the applied loadings.

In the simulation, for given linear-elastic properties of the granular material, a vertical displacement is applied on the rigid plunger. The surcharge weights are modeled as uniformly distributed loads at the surface of the granular material. The resulting stresses, strains and displacements, are determined throughout the granular material and steel mould. These data sets can be recorded for each node or element and the total load applied by the plunger for an applied vertical displacement can be determined. For each different possible combination of the granular material properties a simulation is run for a wide range of plunger displacements, i.e. 0.5 mm to 5.08 mm.

Through regression analysis on the output data relations are developed among the material properties and the resulting model response i.e. stresses, strains and displacements. These relations are developed using different approaches for the two different laboratory test set-ups without and with strain gauges.

5.5.2 Model analysis for tests without strain gauge

For the repeated load CBR test set-up without strain gauge a similar approach to previous work by Opiyo [6] is used to relate the elastic modulus of the granular material with displacement measurement. From elastic theory, the surface deflection, u, of a quasi-static infinite half-space under a circular load can be computed by equation 5-2.

$$u = \frac{f(1-\nu^2)\sigma_o r}{E} \qquad \text{5-2}$$

Where
- ν = the Poisson's ratio
- σ_o = the stress at the surface
- r = the radius of the circular load
- E = the elastic modulus of the material
- f = a factor which is: 2 for a uniformly distributed load; $\pi/2$ for a stiff plate stress distribution

The steel plunger gives the same stress distribution as that of the stiff plate, because the deflection at every point under the plunger is the same. The equation for the CBR test would therefore take the same form as equation 5-2, but with a different factor f, and a different exponent for the Poisson's ratio and the displacement. This difference arises for the reason that, unlike the infinite half-space, the CBR test is conducted on specimens of limited dimensions while the tested material is confined with stiff steel that gives high confinement stress. Therefore, the appropriate equation was considered to be of the form given in equation 5-3. The constants k_1 to k_3 were determined by regression analysis on the results of the finite element model presented in section 5-5-1.

$$E = \frac{k_1(1-\nu^{k_2})\sigma_o \cdot r}{u^{k_3}} \qquad \text{5-3}$$

By means of regression analyses performed on a huge set of data points obtained from the finite element analysis with various combination of E and ν and load levels, the values of k_1 to k_3 have been determined with $r^2 = 0.997$. Equation 5-3 is then rewritten as equation 5-4. This equation between, on the one hand, the plunger stress σ_p (MPa) and displacement u (mm) in the RL-CBR test and, on the other hand, the modulus E (MPa) of the material, makes it possible to estimate the equivalent modulus E_{equ}-values from RL-CBR test results.

$$E_{equ} = \frac{1.513(1-\nu^{1.104})\sigma_p \cdot r}{u^{1.012}} \qquad 5\text{-}4$$

The developed equivalent modulus relation (equation 5-4) is similar in structure to the earlier work of Opiyo (equations 2-24 and 2-25). However, the three constants k_1, k_2 and k_3 in equation 5-4 resulting from the pressure-overclosure contact model shows close to the averages of their respective constants in the no-friction and full-friction equations of 2-24 and 2-25.

The estimation of the equivalent modulus for RL-CBR tests without strain gauge can thus be determined from the displacement, u, measured in the RL-CBR test provided that one specifies the value of the Poisson's ratio, ν.

In this research RL-CBR tests without strain gauge are performed on all materials in the research project with various mix conditions as shown in table 5-1 and 5-2. This large scale test program is performed to investigate its suitability as a simple to perform test to estimate the equivalent modulus for various materials. These results are reported in section 5.6.1 and their validation with triaxial test results is presented in section 6.2.

5.5.3 Model analysis for tests with strain gauges

The stress and strain condition inside the CBR specimen was not considered in developing equation 5-4 for tests without strain gauge. Moreover, determination of the equivalent modulus from the RL-CBR test without strain gauge requires assumption of the Poisson's ratio. To develop a more fundamental relation between the material properties and the material response, knowledge of the stress-strain condition in the CBR specimen and the degree of confinement by the mould is important.

It is very difficult and not practicable to measure the complex stress-strain condition of the material in RL-CBR testing. However, the degree of confinement exerted by the mould can be estimated from the mould deformations. For this purpose strain gauges were used to measure the mould lateral deformation from which the confining stress can be approximated. In this section it is explained how the finite element model analysis is used to develop transfer functions that relate material properties to material response. The test set-up and procedure of the RL-CBR with strain gauges is already presented in section 5.4.

The approach of the model analysis is set to develop transfer functions that can predict material properties from laboratory measured parameters. The parameters that can be measured from a RL-CBR test with strain gauges are: the plunger load, plunger displacement and the lateral strain at the mould exterior. The approach starts with the assumption that the granular materials under the plunger are carrying most of the load, thus the stresses along the central axis are considered as representative stresses for analysis of the specimen as a bulk.

The vertical, σ_v, and radial (horizontal), σ_h, stresses of the bulk granular specimen are approximated by the weighted average of the vertical, $\sigma_{v,i}$, and horizontal, $\sigma_{h,i}$, stresses of each element, i, along the central axis (the axis of symmetry). These stresses are weighted by the vertical displacements of each element along the depth of the sample (equation 5-5). As the vertical plunger displacement is the governing parameter for all the stresses and strains in the specimen, the vertical displacement, $u_{v,i}$, of each element is used as weighting factor for both the vertical and horizontal stresses.

$$\sigma_V = \frac{\sum \sigma_{v,i} u_{v,i}}{\sum u_{v,i}} \qquad \sigma_h = \frac{\sum \sigma_{h,i} u_{v,i}}{\sum u_{v,i}} \tag{5-5}$$

The stress-strain condition along the axis of symmetry in the CBR specimen is considered in developing the transfer functions. The approach departs from isotropic linear elastic theory for a three-dimensional system, which is then reduced to axisymmetric condition, and develops empirical transfer functions by regression from the finite element analysis data.

For a three-dimensional stress state the stress-strain matrix in Cartesian coordinates can be written as:

$$\begin{bmatrix} \varepsilon_x \\ \varepsilon_y \\ \varepsilon_z \\ \gamma_{xz} \\ \gamma_{xy} \\ \gamma_{yz} \end{bmatrix} = \frac{1}{E} \begin{bmatrix} 1 & -\nu & -\nu & 0 & 0 & 0 \\ -\nu & 1 & -\nu & 0 & 0 & 0 \\ -\nu & -\nu & 1 & 0 & 0 & 0 \\ 0 & 0 & 0 & 2(1+\nu) & 0 & 0 \\ 0 & 0 & 0 & 0 & 2(1+\nu) & 0 \\ 0 & 0 & 0 & 0 & 0 & 2(1+\nu) \end{bmatrix} \begin{bmatrix} \sigma_x \\ \sigma_y \\ \sigma_z \\ \tau_{xz} \\ \tau_{xy} \\ \tau_{yz} \end{bmatrix} \tag{5-6}$$

For a general axisymmetric case, with the z-axis representing the central axisymmetric axis, r-axis the radial axis and the θ-axis any rotational angle θ in polar coordinates, equation 5-6 can be reduced to four independent components. Figure 5-25 illustrates and defines these strains and the associated stresses in bodies of revolution (axisymmetric solids) under axisymmetric loading. Therefore the stress-strain analysis in the axisymmetric CBR can be expressed in polar coordinates as:

$$\begin{bmatrix} \varepsilon_z \\ \varepsilon_r \\ \varepsilon_\theta \\ \gamma_{rz} \end{bmatrix} = \frac{1}{E} \begin{bmatrix} 1 & -\nu & -\nu & 0 \\ -\nu & 1 & -\nu & 0 \\ -\nu & -\nu & 1 & 0 \\ 0 & 0 & 0 & 2(1+\nu) \end{bmatrix} \begin{bmatrix} \sigma_z \\ \sigma_r \\ \sigma_\theta \\ \tau_{rz} \end{bmatrix} \quad 5\text{-}7$$

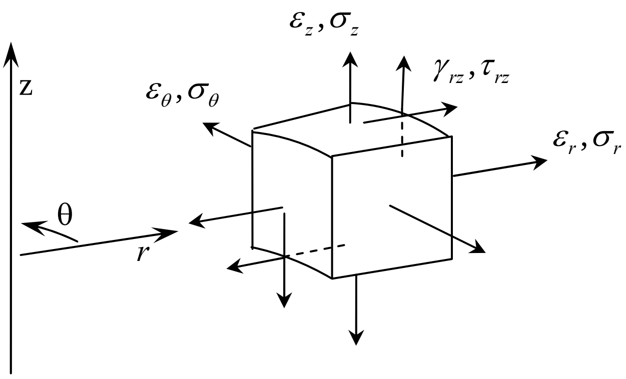

Figure 5.25 Stress and strain involved in axisymmetric solids

If we consider the special case in the points along the central axis (axisymmetric line) of the CBR model, the stresses and strains are the principal stresses and strains. As noted earlier these stresses and strains along the central axis are assumed to represent the stress and strain condition of the specimen as a bulk, and ε_θ, σ_θ will be equal to ε_r, σ_r when $\theta = 90^o$. These components can be expressed in the Cartesian coordinate system as vertical and horizontal components, i.e.:

$\varepsilon_z = \varepsilon_1 = \varepsilon_v$
$\sigma_z = \sigma_1 = \sigma_v$
$\varepsilon_r = \varepsilon_2 = \varepsilon_h = \varepsilon_3 = \varepsilon_\theta$
$\sigma_r = \sigma_2 = \sigma_h = \sigma_3 = \sigma_\theta$

Equation 5-7 can be reduced to equation 5-8 and further to equation 5-9.

$$\begin{bmatrix} \varepsilon_1 \\ \varepsilon_2 \\ \varepsilon_3 \end{bmatrix} = \frac{1}{E} \begin{bmatrix} 1 & -\nu & -\nu \\ -\nu & 1 & -\nu \\ -\nu & -\nu & 1 \end{bmatrix} \begin{bmatrix} \sigma_1 \\ \sigma_2 \\ \sigma_3 \end{bmatrix} \quad 5\text{-}8$$

$$\begin{bmatrix} \varepsilon_v \\ \varepsilon_h \end{bmatrix} = \frac{1}{E} \begin{bmatrix} 1 & -2\nu \\ -\nu & 1-\nu \end{bmatrix} \begin{bmatrix} \sigma_v \\ \sigma_h \end{bmatrix} \quad 5\text{-}9$$

From equation 5.9 the elastic modulus E can be expressed as a function of the vertical strain ε_v:

$$E = \frac{\sigma_v - 2\nu\sigma_h}{\varepsilon_v} \tag{5-10}$$

From the FE analysis illustrative stress, strain and displacement distributions along the depth of the specimen at the axis of symmetry are developed which are shown in Figure 5.26. Moreover stress and strain distributions from the FE analysis are illustrated in Figures 5.27 and 5.28 for a quarter of the CBR specimen. By means of regression analysis on large data sets of the finite element analyses the vertical and horizontal stress-strain components and the Poisson's ratio and the modulus are estimated in terms of three parameters the vertical plunger displacement, the average plunger stress and the mould lateral strain.

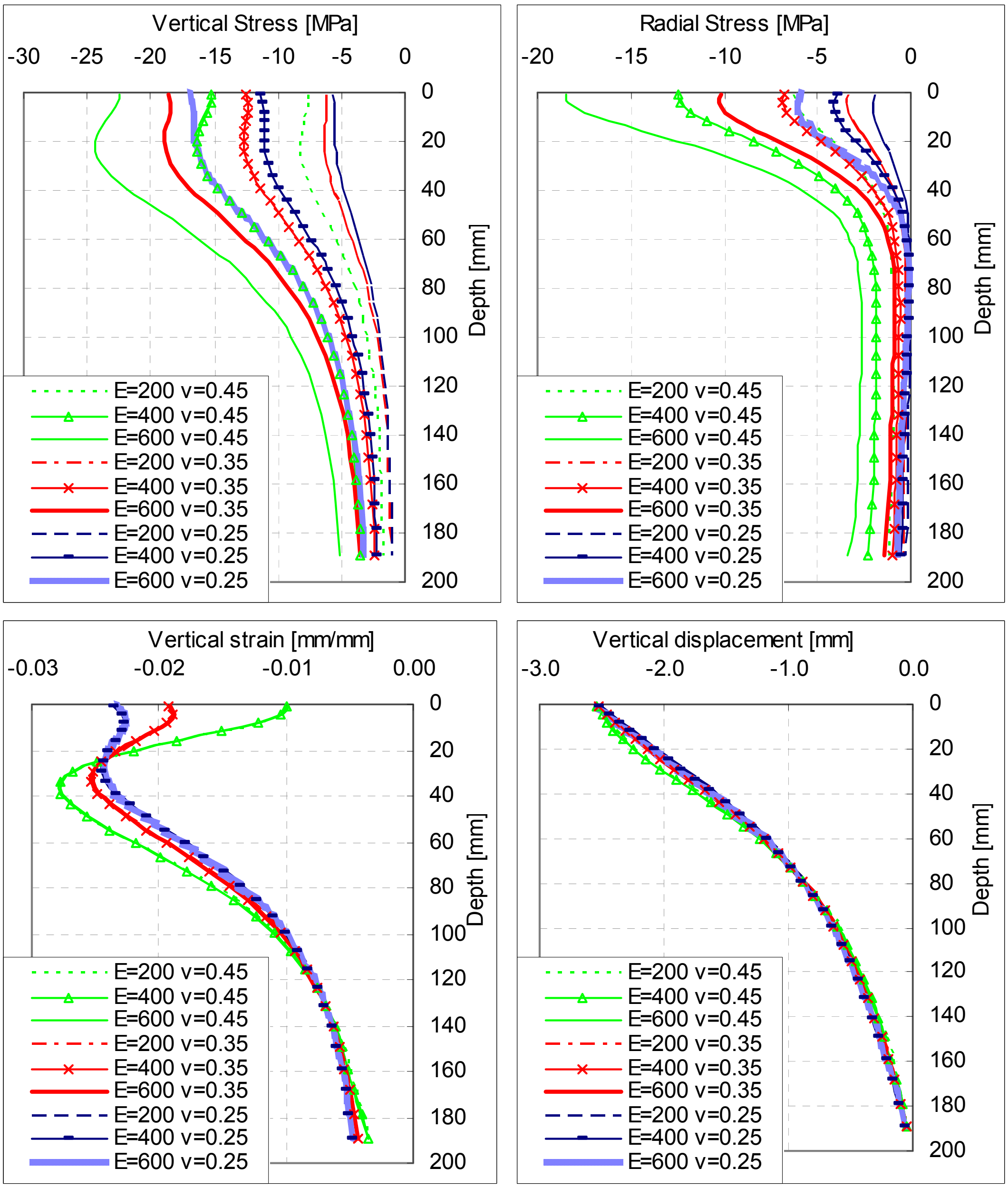

Figure 5.26 Illustrative stress and strain distribution along the axis of symmetry for a 2.5 mm plunger displacement

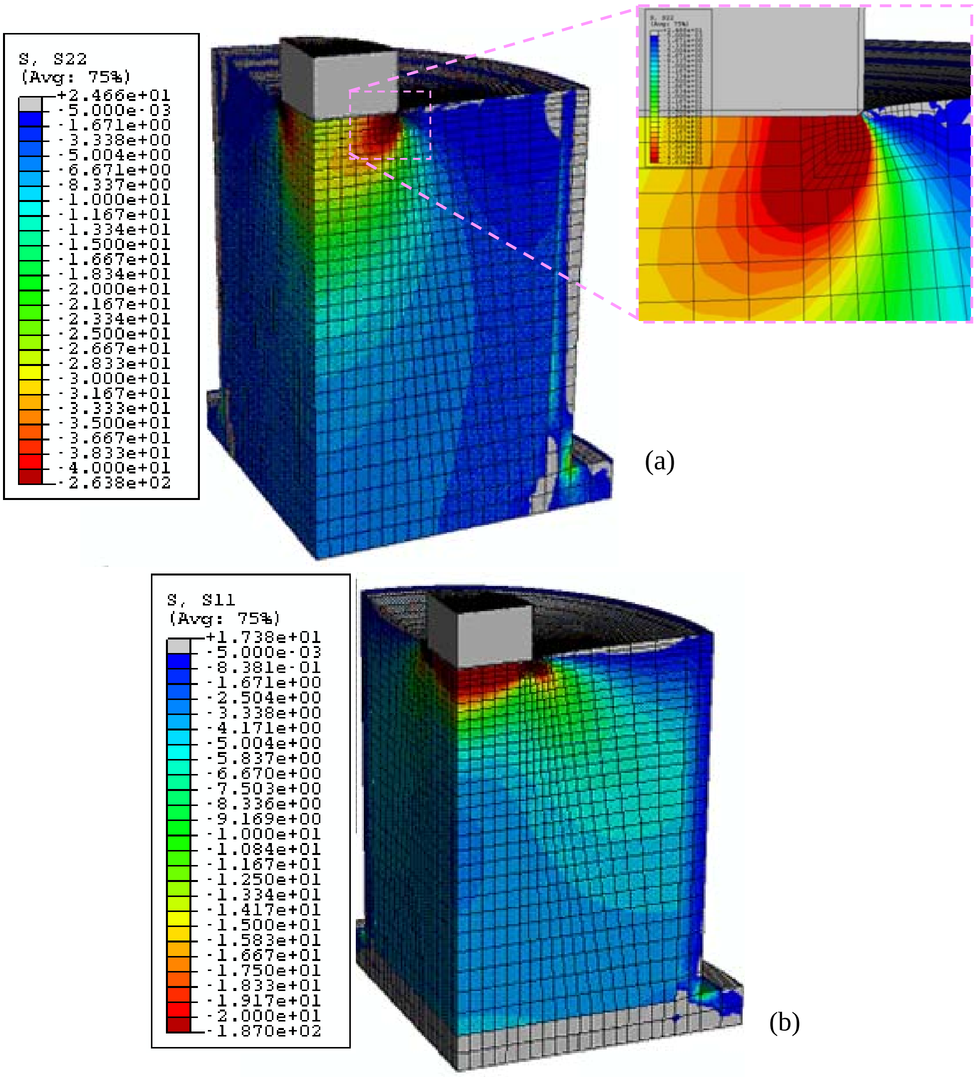

Figure 5.27 Example of (a) vertical and (b) radial stress distribution through the RL-CBR specimen

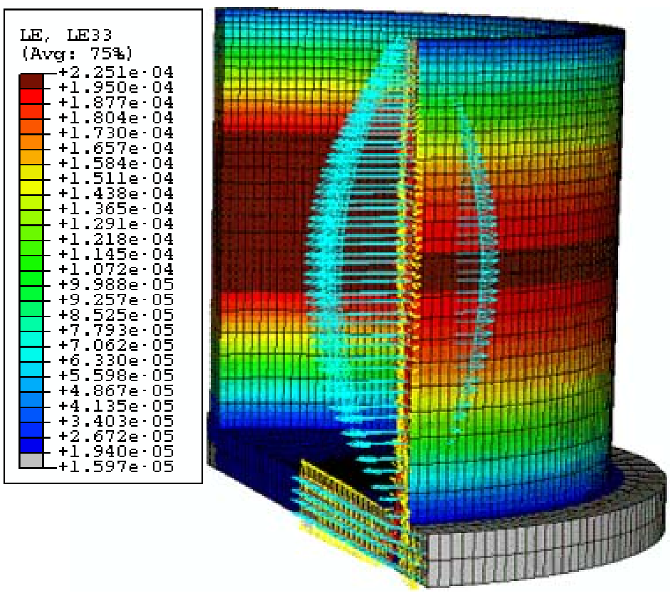

Figure 5.28 Lateral strain distribution on the steel mould

The equivalent (average) vertical strain ε_v along the central axis is related to the vertical plunger displacement, *u*, per a certain linear dimension, thus $\varepsilon_v \approx u/k$. The vertical and horizontal stresses in equation 5-10 are the weighted average stresses, equation 5-5, in which the vertical stress is mainly related to the average plunger stress, σ_p, thus $\sigma_v \approx k^*\sigma_p$. The Poisson's ratio and the horizontal stress are related mainly to the mould strain and the plunger stress and fitted by regression. Finally the four transfer functions, equations 5-11 to 5-14, are developed by means of least square regression fitting on the finite element analyses data with a total of five model parameters k_1 to k_5.

The four transfer functions are:

$$\sigma_V = k_1 \sigma_p \qquad \nu = k_2 \left(\frac{\varepsilon_{lm}}{\sigma_p} \right) \qquad \text{5-11 \& 5-12}$$

$$\sigma_h = k_3 \varepsilon_{lm} \exp\left({k_4}/{\nu} \right) \qquad E_{equ} = \frac{k_5 \left(\sigma_V - 2\nu\sigma_h \right)}{u_v} \qquad \text{5-13 \& 5-14}$$

Where
σ_v = vertical stress [kPa]
σ_h = horizontal stress [kPa]
σ_p = vertical plunger stress [kPa]
= plunger load / plunger area
ν = Poisson's ratio [-]
E_{equ} = equivalent modulus [MPa]
ε_{lm} = lateral strain at mid-height of the mould exterior [micro-strain]
u_v = vertical plunger displacement [mm]
k_1 - k_5 = model parameters
k_1 = 0.368 [-] k_2 = -120.927 [kPa]
k_3 = 43.898 [kPa] k_4 = -0.072 [-]
k_5 = 0.144 [mm]

The regressions for the above four relations in equations 5-11 to 5-14 show a good fit: $r^2 > 0.99$, see Figure 5-29. This fit is of course an indication of relations of the parameters presented in the finite element model through the stiffness matrix (force and displacement relation), the kinematic compatibility (strain and displacement relation) etc under the given boundary conditions.

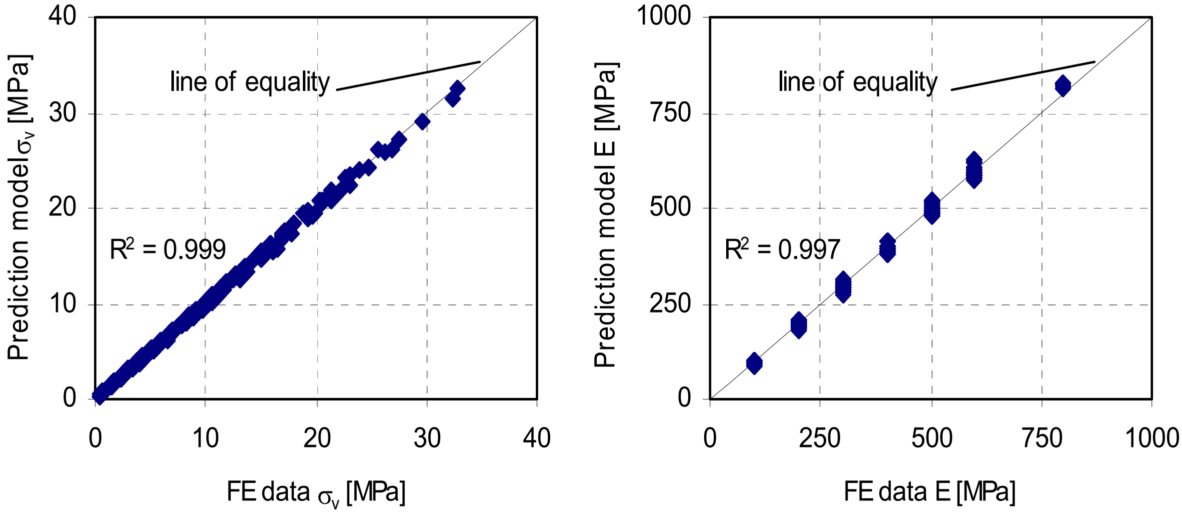

Figure 5.29 Model prediction fit for transfer functions σ_v and E

In this research RL-CBR tests with strain gauges are performed for the two South African materials G1 and FC. The test is performed to investigate whether the mould confinement effect can be determined by the use of strain gauges. Moreover it is to study the role of the confinement on the stiffness behavior and to adopt a better approach in estimating the stiffness modulus of granular base and subbase materials. The results of this testing are reported in section 5.6.2 and their validation with triaxial test results is presented in section 6.3.

5.6 EQUIVALENT MODULUS FROM REPEATED LOAD CBR TEST

As already stated in section 1.3 one of the main objectives of this research is to develop a simplified characterization technique for the mechanical behavior of unbound granular materials. One of the most important parameters that can be used for pavement analysis and design is the stiffness modulus.

In section 5.2 a new terminology "Equivalent Modulus" is introduced as a representative stiffness modulus of UGMs determined by the method of repeated load CBR testing. As it is explained earlier this term is used to indicate that the modulus is an average or representative value of the material in the mould as a bulk in a more general or global scale. The equivalent modulus of the various materials characterized by the RL-CBR test without and with strain gauges is elaborated in section 5.6.1 and 5.6.2 respectively.

5.6.1 Tests without strain gauge

From RL-CBR tests without strain gauge, discussed in section 5.3, the only parameters that can be measured in the laboratory are the plunger load (average plunger stress) σ_p and the plunger displacement *u*.

Based on linear elastic finite element analyses equation 5-4 has been developed that relates the equivalent modulus to the plunger stress and displacement. Equation 5-4 is replicated below in equation 5-15 for convenience.

$$E_{equ} = \frac{1.513(1-\nu^{1.104})\Delta\sigma_p \cdot r}{\Delta u^{1.012}} \qquad 5\text{-}15$$

Where:

- E_{equ} = equivalent modulus [MPa]
- ν = Poisson's ratio [-]
- $\Delta\sigma_p$ = change in plunger stress between maximum and minimum in a loading cycle [MPa]
- r = radius of plunger [mm]
- Δu = change in elastic (recoverable) displacement between maximum and minimum in a loading cycle [mm]

When using this equation one has to make an estimate for the Poisson's ratio ν. The choice depends on the type of material (fine grained soil or granular materials) and moisture conditions [5]. For all the granular materials characterized in this research a value of 0.35 is assumed.

The equivalent modulus is computed based on the full cycle of loading and unloading. The equivalent modulus is the secant modulus of the unloading path (see Figure 5.8). For the equivalent modulus the plunger stress and plunger displacement are computed as the difference between the maximum loading and minimum unloading.

In addition to the adopted Poisson's ratio of 0.35, the results obtained for Poisson's ratio of 0.25 are presented in table 5-4 for comparison. In this table either the initial penetration or plunger stress values written in bold are the target values set to conduct the test. In table 5-4 the values with shaded area are considered to be unrealistic as they highly deviate from the general trends and observations. At these lower initial penetration levels it is doubted whether it is tested the material skeleton of the specimen, this can be an effect from the accumulation of fines at the surface. Therefore they are not considered for further analysis and the calibration with the triaxial test results in chapter 6. Though it is not definitely clear for such results to happen, it is generally believed to be due to the low plunger stress level resulting in an extremely low initial penetration.

Table 5-4 Equivalent modulus results from RL-CBR tests without strain gauge

Test code	Target DOC (%)	Achieved DOC (%)	Target MC (% by mass)	Achieved MC (%)	Initial penetration (mm)	Elastic def. ♣ u (mm)	Plunger stress $^{\psi}$ σ_p (MPa)	Equivalent Modulus ν=0.25	Equivalent Modulus ν=0.35
RLCBR-FC-95dr	95	94.6	Dry (5)	5.73	*2.58*	0.274	5.99	1074	940
RLCBR-FC-95_s1		94.8	Mod. (7.5)	7.70	0.47	0.097	**2.74**	1405	1231
RLCBR-FC-95b		94.5		7.80	**2.60**	0.372	3.69	484	423
RLCBR-FC-95a		95.0		7.64	**2.59**	0.436	5.87	656	575
RLCBR-FC-95c		95.0		7.60	**2.59**	0.426	6.65	763	668
RLCBR-FC-95_s2		95.4		7.29	4.34	0.296	**10.43**	1729	1541
RLC-FC-95wt		97.1	Wet (9.5)	8.75	**2.60**	0.192	1.74	446	391
RLCBR-FC-95wt		95.5		9.44	**2.61**	0.326	2.01	301	264
RLCBR-FC-98dr	98	98.3	Dry (5)	5.51	**2.54**	0.534	18.10	1650	1445
RLCBR-FC-98dr_s2		97.4		5.46	12.16	0.727	**24.92**	1662	1456
RLCBR-FC-98_s1		98.8	Mod. (7.5)	6.78	0.33	0.071	**2.73**	1929	1689
RLCBR-FC-98c		97.4		8.29	**2.60**	0.445	5.36	587	514
RLC-FC-98		95.2		7.22	**2.58**	0.207	5.31	1263	1106
RLCBR-FC-98b		98.2		7.57	**2.57**	0.474	7.38	759	664
RLCBR-FC-98_s2		98.9		7.09	2.03	0.150	**7.93**	2608	2284
RLCBR-FC-98a		98.9		6.84	**2.57**	0.492	10.32	1022	895
RLCBR-FC-98_s3		99.3		7.01	12.51	0.335	**12.34**	1804	1580
RLC-FC-98wt_b		98.6	Wet (9.5)	9.72	**2.63**	0.199	1.25	311	272
RLCBR-FC-98wt		98.3		9.61	**2.59**	0.225	1.39	304	266
RLC-FC-98wt_a		98.6		8.76	**2.62**	0.203	1.93	468	410
RLC-FC-98wt_c		99.5		9.05	**2.62**	0.202	2.51	612	536
RLCBR-FC-98wt_s1		99.6		9.44	5.01	0.193	**3.74**	957	838
RLCBR-FC-100dr	100	98.1	Dry (5)	5.28	**2.54**	0.698	13.69	952	834
RLCBR-FC-100_s1		100.3	Mod. (7.5)	7.59	0.31	0.105	**2.69**	1276	1117
RLCBR-FC-100b		98.5		8.33	**2.61**	0.399	4.80	587	514
RLCBR-FC-100c		99.2		8.11	**2.59**	0.437	5.07	566	495
RLCBR-FC-100a		100.1		7.32	**2.57**	0.480	7.59	771	675
RLCBR-FC-100_s2		101.2		7.61	2.16	0.206	**10.16**	2429	2127
RLC-FC-100wt		100.1	Wet (9.5)	9.70	**2.89**	0.287	1.04	178	156
RLCBR-FC-100wt		99.9		9.23	**2.62**	0.273	1.36	245	214
RLCBR-WB-95dr_b	95	94.6	Dry (5)	5.50	**2.56**	0.346	2.88	408	357
RLCBR-WB-95dr_a		94.9		5.18	**2.59**	0.367	3.08	410	359
RLCBR-WB-95b		94.9	Mod. (7)	7.17	**2.65**	0.427	2.65	303	265
RLCBR-WB-95c		94.6		7.48	**2.70**	0.595	3.73	304	267
RLCBR-WB-95_s1		95.0		7.22	2.88	0.318	**4.68**	721	631
RLCBR-WB-95a		96.2		7.25	**2.83**	0.654	5.97	443	338
RLCBR-WB-95_s2		94.0		8.93	10.22	0.416	**7.96**	933	817
RLCBR-WB-95wt_b		94.8	Wet (9)	9.27	**2.64**	0.465	3.70	388	340
RLCBR-WB-95wt_a		97.0		9.01	**2.61**	0.480	4.34	440	385
RLCBR-WB-98dr_s1	98	98.4	Dry (5)	5.85	0.15	0.078	**2.67**	1709	1496
RLCBR-WB-98dr_a		98.4		4.60	**2.57**	0.513	6.82	648	568
RLCBR-WB-98dr_b		98.3		4.87	**2.62**	0.637	7.35	560	491
RLCBR-WB-98dr_c		98.4		4.60	**2.60**	0.699	8.02	557	487
RLCBR-WB-98dr_s2		98.2		6.23	2.97	0.475	**10.39**	1065	933
RLCBR-WB-98_s1		100.6	Mod. (7)	5.53	0.26	0.107	**2.70**	1250	1095
RLCBR-WB-98c		97.4		7.10	**2.60**	0.540	4.74	427	374
RLCBR-WB-98d		98.4		6.32	**2.67**	0.584	6.14	511	448
RLCBR-WB-98e		98.1		6.68	**2.61**	0.694	6.27	439	384
RLCBR-WB-98a		97.8		7.26	**2.64**	0.527	6.67	616	539
RLCBR-WB-98b		99.0		5.95	**2.62**	0.574	7.18	608	533
RLCBR-WB-98_s2		99.3		6.00	4.01	0.275	**7.95**	1419	1243
RLCBR-WB-98_s3		99.8		6.44	5.29	0.334	**10.43**	1530	1340

Test code	Target DOC (%)	Ach. DOC (%)	Target MC (%)	Ach. MC (%)	Initial pen. (mm)	Elastic def. ♣ u (mm)	Plunger stress ψ σ_p (MPa)	Equivalent Modulus ν=0.25	Equivalent Modulus ν=0.35
RLCBR-WB-98wt_b		97.7		9.41	**2.89**	0.498	2.74	268	235
RLCBR-WB-98wt_c	98	98.0	Wet (9)	9.08	**2.60**	0.530	3.28	301	264
RLCBR-WB-98wt_a		98.5		8.46	**2.78**	0.552	4.58	403	353
RLCBR-WB-98wt_s1		96.9		10.39	3.69	0.449	**6.02**	653	572
RLCBR-WB-100dr_a		99.6	Dry (5)	5.45	**2.60**	0.588	9.05	749	656
RLCBR-WB-100dr_b		101.0		4.55	**2.49**	0.783	15.74	974	853
RLCBR-WB-100_s1		100.7		6.70	0.64	0.146	**2.73**	924	810
RLCBR-WB-100b		99.3	Mod.	7.23	**2.61**	0.476	5.20	533	467
RLCBR-WB-100a	100	100.1	(7)	6.88	**2.53**	0.465	6.08	637	558
RLCBR-WB-100c		99.4		7.45	**2.64**	0.822	7.88	464	406
RLCBR-WB-100_s2		99.3		8.12	11.20	0.499	**10.41**	1017	891
RLCBR-WB-100wt_b		100.9	Wet (9)	9.13	**2.60**	0.583	5.68	474	415
RLCBR-WB-100wt_a		99.9		9.08	**2.60**	0.689	6.56	462	405
RLCBR-G1-98dr		98.0	Dry (2)	2.18	**2.55**	0.571	7.24	617	540
RLCBR-G1-98_s1		98.3		3.50	0.88	0.197	**7.96**	1988	1741
RLCBR-G1-98	98	98.0	Mod.	3.95	**2.57**	0.801	11.00	665	582
RLC-G1-98		98.4	(4)	3.52	**2.56**	0.717	16.58	1121	982
RLCBR-G1-98_s2		98.6		3.38	3.41	0.812	**18.15**	1083	948
RLCBR-G1-98wt		98.5	Wet (6)	5.45	2.60	0.654	4.97	369	323
RLCBR-G1-100dr_s1		99.2		2.20	0.95	0.610	**7.97**	635	557
RLCBR-G1-100dr		99.2	Dry (2)	2.07	**2.55**	0.778	16.49	1027	899
RLC-G1-100dr		99.4		2.65	**2.10**	0.797	18.14	1103	966
RLCBR-G1-100dr_s2		98.9		2.33	4.74	0.676	**24.79**	1781	1560
RLCBR-G1-100_s1		100.0		3.83	1.10	0.183	**7.92**	2130	1865
RLCBR-G1-100_s2		99.9		3.97	1.06	0.224	**10.44**	2288	2004
RLCBR-G1-100a		100.2		3.58	**2.58**	0.697	11.40	794	695
RLCBR-G1-100b	100	99.8	Mod.	3.69	**2.56**	0.866	12.75	713	624
RLC-G1-100c		99.9	(4)	3.82	**2.57**	0.752	16.14	1040	911
RLCBR-G1-100c		100.2		3.79	**2.63**	0.886	17.16	934	818
RLC-G1-100b		100.4		3.68	**2.56**	0.758	17.78	1137	996
RLC-G1-100a		100.4		3.11	**2.55**	0.738	18.50	1222	1070
RLCBR-G1-100_s3		99.8		3.89	4.44	0.729	**24.74**	1645	1441
RLC-G1-100wt		101.8		5.53	**2.58**	0.524	6.83	634	555
RLCBR-G1-100wt		100.5	Wet (6)	5.03	**2.59**	0.617	7.88	620	543
RLCBR-G1-100wt_s1		100.5		5.11	4.97	0.834	**16.17**	939	823
RLCBR-G1-102dr		98.7	Dry (2)	2.17	**2.55**	0.784	16.56	1024	897
RLCBR-G1-102_s1		103.1		3.77	1.14	0.493	**10.47**	1035	906
RLCBR-G1-102	102	102.1	Mod.	3.68	**2.58**	0.796	15.37	936	820
RLC-G1-102		102.3	(4)	3.59	**2.72**	0.734	18.10	1197	1048
RLCBR-G1-102_s2		102.5		3.76	2.76	0.578	**24.58**	2067	1810
RLCBR-G1-102wt		102.1	Wet (6)	5.90	**2.60**	0.695	8.21	572	501
RLCBR -ZKK32_s1		100.4		3.96	0.72	0.184	**2.69**	718	629
RLCBR -ZKK32_s2	100	101.2	Mod.	3.23	0.67	0.276	**4.71**	838	734
RLCBR -ZKK32_s3		101.5	(3)	3.47	1.29	0.408	**7.94**	950	832
RLCBR -ZKK32_s4		102.6		2.89	0.72	0.474	**10.45**	1075	942
RLCBR -ZKK63_s1		99.8		3.88	0.28	0.197	**2.70**	674	590
RLCBR -ZKK63_s2	100	100.0	Mod.	3.59	1.14	0.413	**6.61**	782	684
RLCBR -ZKK63_s3		100.6	(3)	3.46	1.61	0.507	**10.44**	1003	878
RLCBR -ZKK63_s4		100.0		3.37	9.23	0.735	**16.20**	1069	936
RLC-MG-AL-97-4	97♠	97.9♠	Mod (8)	8.20	3.15	0.238	**2.00**	412	361
RLC-MG-AL-100-4b		99.9		9.31	**2.62**	0.329	3.86	574	503
RLC-MG-AL-100-4a	100	100.0	Mod.	9.15	**2.61**	0.453	5.02	541	474
RLC-MG-AL-100-4c		101.7	(8)	7.64	0.46	0.408	**5.12**	613	537
RLC-MG-AL-105-4	105	106.3	Mod (8)	8.65	**2.58**	0.631	6.07	468	410

♣ *Average elastic (recoverable) deformation, u, of the last 5 cycles of the 100 load cycles*

ψ *Average plunger stress difference, σ_p, between the max. of loading and min. of unloading of the last 5 cycles of the 100 load cycles*

♠ *DOC for MG is in terms of Max. Proctor Density (MPD) and unlike the others not Max. Modified Proctor Density (MMPD)*

Effect of influence factors on equivalent modulus

In the same way as the resilient and permanent deformation, described in section 5.3, the influence of factors such as moisture content, degree of compaction and material type on the equivalent modulus of the granular materials are elaborated. These effects are best shown graphically in charts in which E_{equ}-values, analyzed for Poisson's ratio of 0.35, are grouped for the influence factor under consideration. The stress dependent E_{equ} is presented as a function of the plunger stress σ_p.

<u>Moisture content</u>
The effect of the moisture content on the equivalent modulus E_{equ} is presented here for three materials WB, FC and G1. In these series the DOC is first kept 98% for the WB and FC and 100% for the G1 and then the results for the entire range of DOC are presented. The moisture effect is studied in both cases by testing at three varying target moisture contents i.e. dry, moderate and wet.

Figure 5.30 shows the stress dependent equivalent modulus of the WB. It is to be noticed that the RL-CBR equivalent modulus is stress dependent and generally the stiffness of the WB increases with decrease in MC, in both the constant 98% DOC and all DOC, with some exceptions that the moderate MC performs better than the dry mix, especially at higher stress levels.

The variation in MC for the FC results in wide range of stress levels and distinction in stress level for the three MCs, see Figure 5.31. This indicates the resistance to penetration or permanent deformation is more sensitive to moisture content than the stiffness does. The ferricrete is sensitive to moisture content due to its cohesive nature compared to the other granular materials.

The equivalent modulus vs. plunger stress relation for G1, shown in Figure 5.32, reveals that although the equivalent modulus is in general increasing with the decrease of MC, the G1 is less sensitive to moisture change. The equivalent modulus is consistently increasing with the plunger stress. It is somewhat more stress dependent than the WB and FC materials.

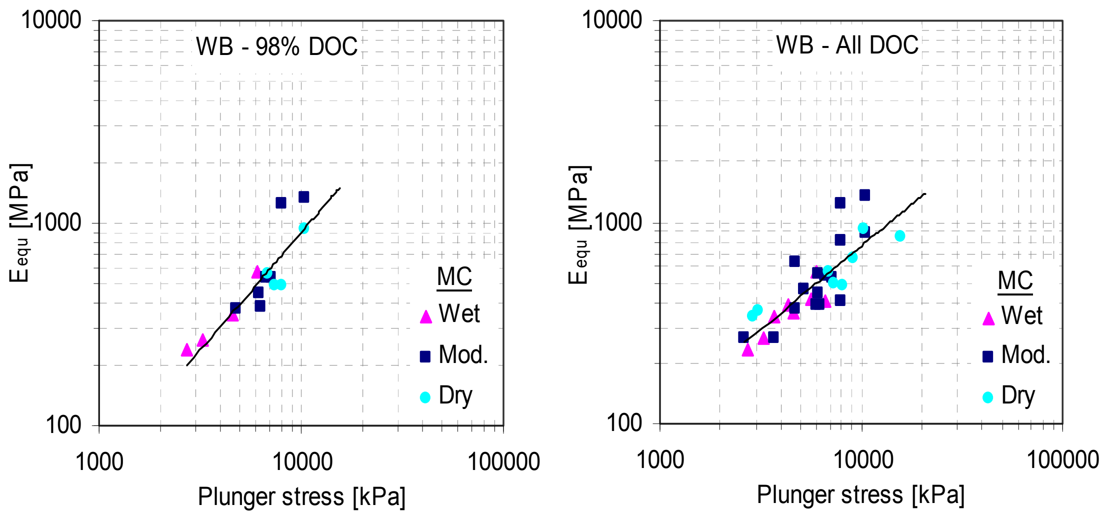

Figure 5.30 Equivalent modulus as a function of plunger stress and moisture content MC for WB

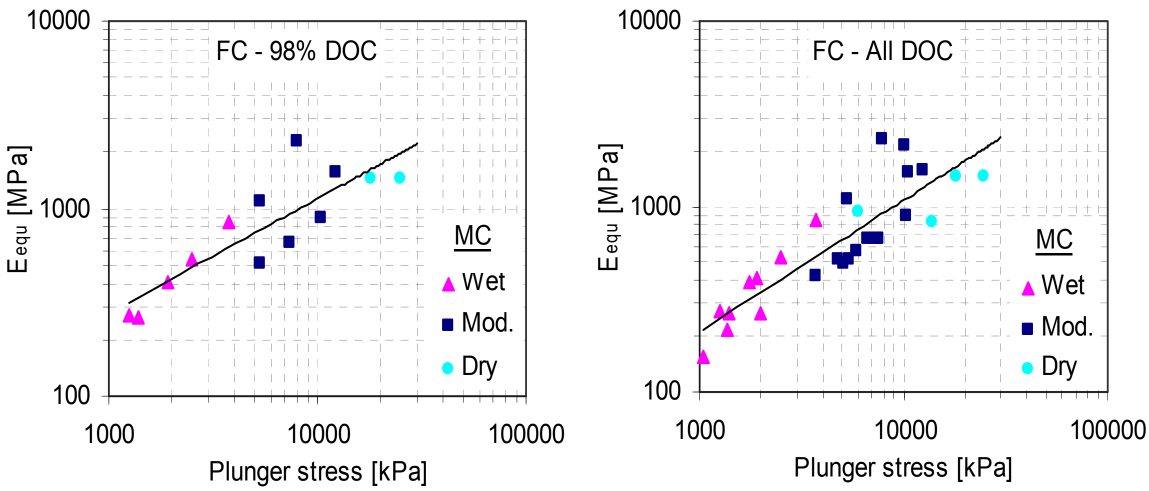

Figure 5.31 Equivalent modulus as a function of plunger stress and moisture content MC for FC

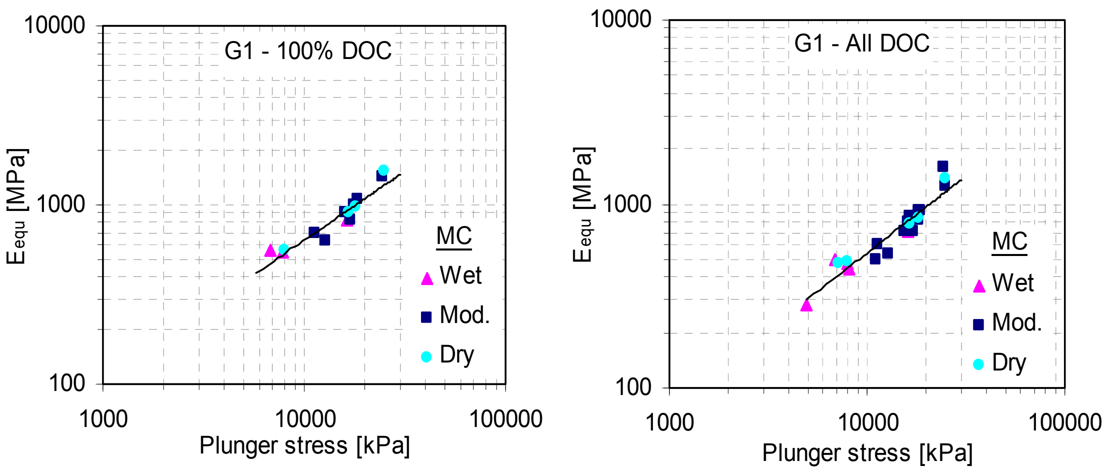

Figure 5.32 Equivalent modulus as a function of plunger stress and moisture content MC for G1

Degree of compaction

Similarly the effect of the degree of compaction on the equivalent modulus E_{equ} is presented here again for the three materials WB, FC and G1. In these series the MC is first kept at moderate level and after that the results for the entire range of MC is presented. The degree of compaction effect is studied in both cases by testing at three varying target DOC i.e. 95%, 98% and 100% for the WB and FC and 98%, 100% and 102% for the G1.

Figures 5.33 to 5.35 are produced to demonstrate the influence of DOC on the equivalent modulus of WB, FC and G1. In general it is difficult to observe the effect of DOC from these results. In order to distinguish the effect of DOC, wide range of plunger stresses has to be applied for each DOC. This can be observed to some extent on the FC. For the FC Figure 5.34, both the low (95%) and high (100%) degree of compaction result in a lower equivalent modulus compared to the medium (98%) degree of compaction. As stated in section 5.3 the ferricrete is highly sensitive to under and over-compaction.

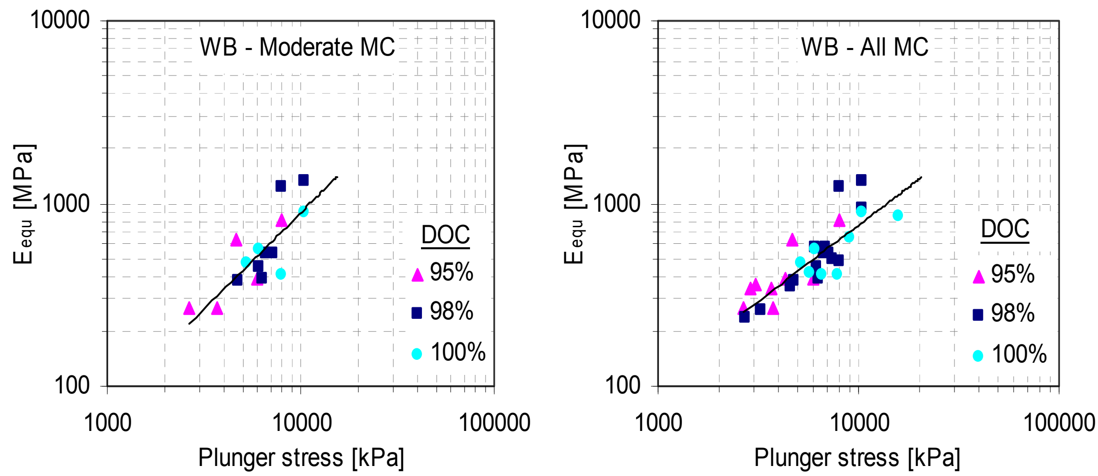

Figure 5.33 E_{equ} as a function of plunger stress and degree of compaction DOC for WB

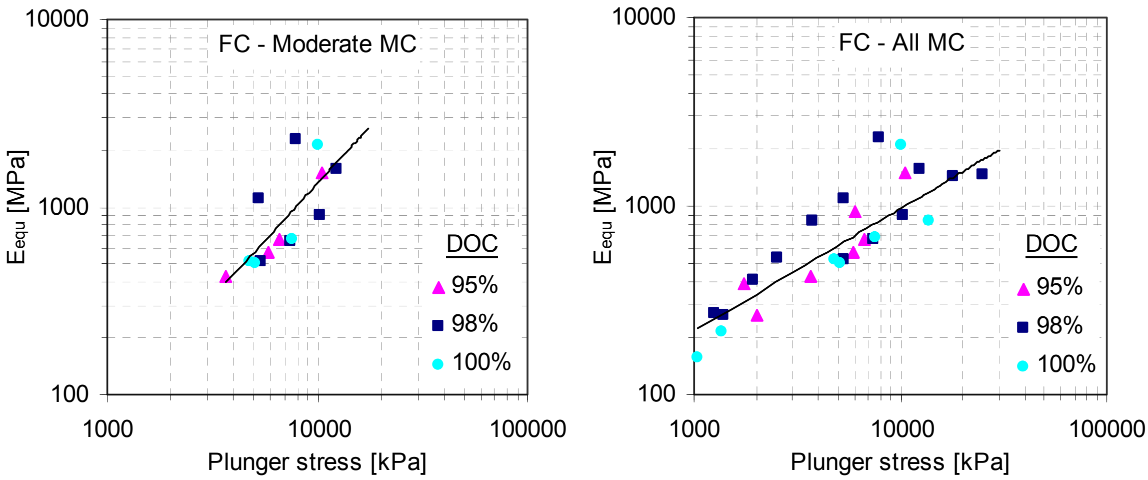

Figure 5.34 E_{equ} as a function of plunger stress and degree of compaction DOC for FC

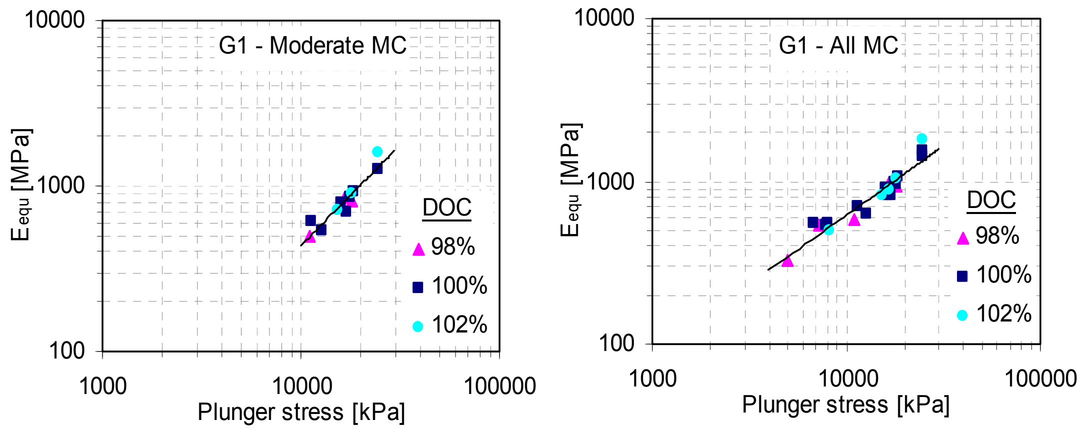

Figure 5.35 E_{equ} as a function of plunger stress and degree of compaction DOC for G1

Material type

As discussed in section 4.6.3 the various material types tested incorporate several varying influence factors such as gradation, particle shape and texture, mineralogical composition, strength of particles etc. Therefore all influence factors are varying along with the material type except the target DOC and the category of moisture content which is kept constant in these series.

The influence of material type is investigated in a condition that the category of moisture is kept moderate for all. However, one has to keep in mind that the target moderate moisture condition for each material is different. That is 3% target MC for ZKK32 and ZKK63, 4% target MC for G1, 7% target MC for WB, 7.5% target MC for FC and 8% for MG. Moreover the influence of material type is compared for two target DOC i.e. 100% for the six materials shown in Figure 5.36 and 98% for the three materials in Figure 5.37.

In Figure 5.36 at 100% DOC the equivalent modulus of the G1 shows a higher stress dependency than all the other materials. The Austrian frost protection (ZKK32) and base material (ZKK63) show better performance compared to the WB, FC and MG while they are less stress dependent compared to G1, FC and WB. Of all the materials MG has the lowest stiffness however one has to note that the 100% DOC for MG is not in terms of MMPD like the others but in terms of MPD.

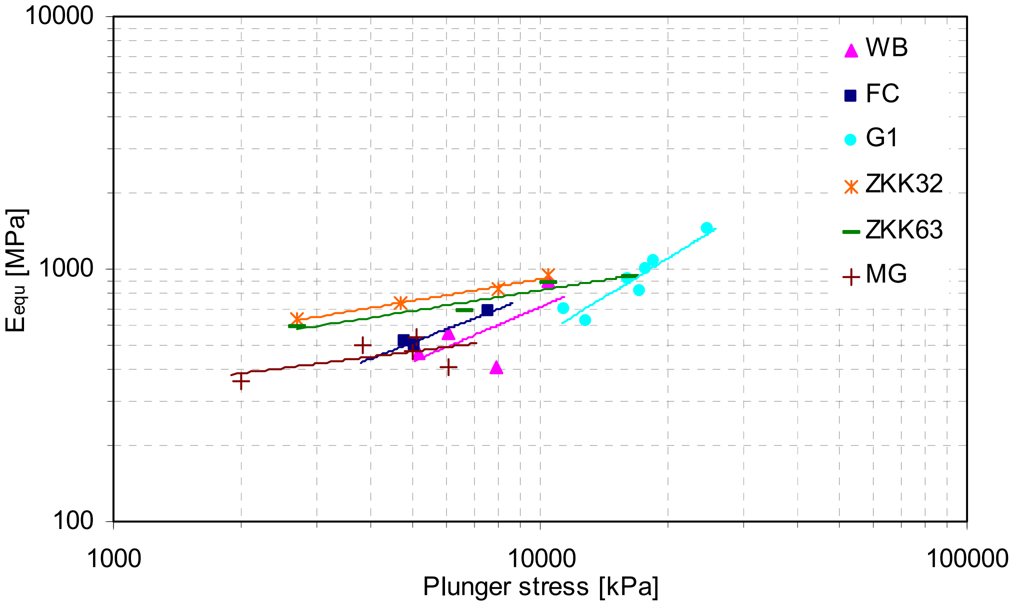

Figure 5.36 E_{equ} as a function of plunger stress and material type for all materials at moderate MC and 100% DOC

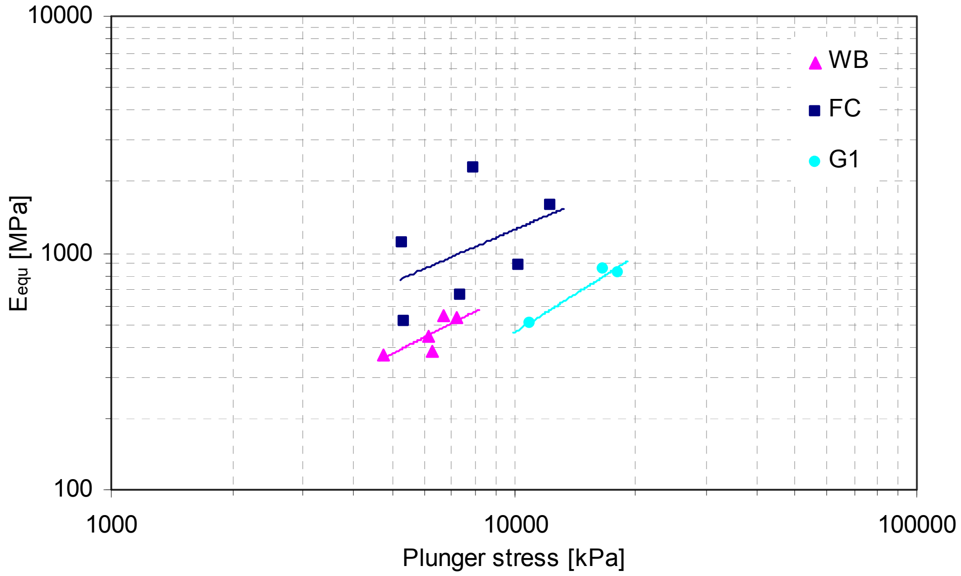

Figure 5.37 E_{equ} as a function of plunger stress and material type for three materials at moderate MC and 98% DOC

At moderate compaction level (98% DOC) and moderate MC the FC exhibits a higher equivalent modulus comparing to both WB and G1 (see Figure 5.37). The reason is that 98% DOC is too low to obtain a dense and stiff G1 specimen and in the most favorable condition for FC moderate DOC and moderate MC the FC performs better than WB. However, in small shift from this condition the FC performs less due to its sensitive nature to both MC and compaction. Even with in this favorable range the FC still shows more scatter than the WB and G1.

5.6.2 Tests with strain gauges

The equivalent modulus of granular materials characterized by means of RL-CBR tests with strain gauges is computed using the mould deformation data from the strain gauges in addition to the plunger stress and its axial deformation.

Based on linear elastic finite element analyses four transfer functions were developed (see section 5.5) that relate the material properties and internal stresses on one hand and plunger stress, displacement and mould strain on the other. These transfer functions are replicated in equation 5-16 to 5-19 for convenience.

$$\sigma_V = k_1 \Delta\sigma_p \qquad 5\text{-}16$$

$$\nu = k_2 \left(\frac{\Delta\varepsilon_{lm}}{\Delta\sigma_p} \right) \qquad 5\text{-}17$$

$$\sigma_h = k_3 \Delta\varepsilon_{lm} \exp\left({k_4}/{\nu} \right) \qquad 5\text{-}18$$

$$E_{equ} = \frac{k_5 \left(\sigma_V - 2\nu\sigma_h \right)}{\Delta u_v} \qquad 5\text{-}19$$

Where
- σ_v = vertical stress [kPa]
- σ_h = horizontal stress [kPa]
- $\Delta\sigma_p$ = change in plunger stress between maximum and minimum in a loading cycle [kPa]
- ν = Poisson's ratio [-]
- E_{equ} = equivalent modulus [MPa]
- $\Delta\varepsilon_{lm}$ = change in lateral strain at mid-height of mould exterior between maximum and minimum in a loading cycle [micro-strain]
- Δu_v = change in recoverable plunger displacement between maximum and minimum in a loading cycle [mm]
- k_1 - k_5 = model parameters

k_1	= 0.368 [-]	k_2	= -120.927 [kPa]
k_3	= 43.898 [kPa]	k_4	= -0.072 [-]
k_5	= 0.144 [mm]		

From the RL-CBR tests with strain gauges three parameters i.e. plunger stress, σ_p, vertical plunger displacement, u_v, and the lateral strain at mid-height of the mould exterior, ε_{lm}, are measured to compute these transfer functions. The equivalent modulus E_{equ} is expressed as a function of the vertical and horizontal stresses, equation 5-19. An equivalent bulk stress, θ, that represent the bulk stress of the whole specimen, can also be expressed as a function of the vertical and horizontal stresses using equation 5-20 at the maximum loading.

$$\theta = \sigma_V + 2\sigma_h \qquad 5\text{-}20$$

The equivalent modulus and the equivalent bulk stress are computed based on the full cycle of loading and unloading. The equivalent modulus is the secant modulus of the unloading path (see Figure 5.8). For the equivalent modulus the plunger stress, plunger displacement and lateral mould strain, in equation 5-19, are computed as the difference between the maximum loading and minimum unloading. For the bulk stress the absolute values of these measurements are considered, in equation 5-20, to represent the stress state of a specimen under testing.

The RL-CBR tests with strain gauges have been conducted on two materials, G1 and FC, at specific material conditions, that are at their respective moderate moisture content and 100% DOC for G1 and 98% DOC for FC.

Seven G1 specimens are tested with the RL-CBR test with strain gauges. On each specimen different loads are applied, see table 5-5. This is a kind of "multi-stage" testing where the plunger load is increasing consecutively. Only on one specimen (RLCBR-G1-100-SG7) the load applications are in reverse order from larger to smaller load level. This is conducted to investigate the effect of a larger load history on the material behavior. For each load level a minimum of 100 load cycles is applied. The equivalent modulus and the bulk stress are computed as the average of the last 5 cycles of the 100 loading cycles. Similarly RL-CBR tests with strain gauges are performed on three FC specimens with multiple loading per specimen.

Table 5-5 summarizes the data and computed bulk stress and equivalent modulus for both G1 and FC. The values in bold letters are data for tests on virgin specimens and the others a result from the multi-stage testing.

<u>Crushed rock - G1</u>

The equivalent modulus determined from the RL-CBR tests with strain gauges can be plotted against the bulk stress similar to the M_r-θ plot of a triaxial test. The results of the tests on the virgin specimens and all loading of the seven specimens are plotted in Figure 5.38. In this figure it is indicated that one of the specimens (RLCBR-G1-100-SG6) has erroneous measurements, resulting in a lower stiffness compared to the other specimens. This mould strain recording error was observed and noted during the experimentation.

Excluding the result of the erroneous measurement on sample RLCBR-G1-100_SG6 the two plots (a) and (b) of Figure 5.38 are re-plotted along with their E_{equ}-θ model fit in Figure 5.39. The models fit, for both the test results on only the virgin specimen and for all specimens subjected to the multi-stage loading, show that both can give a prediction with equal goodness of fit $R^2 = 0.96$. Moreover, the two regression lines are very close to each other, with the slope in log-log plot (the power) is slightly higher for the test data obtained from the virgin specimens. However the difference between the two is negligible, thus it seems that the G1 material behavior can be characterized by the multi-stage testing. This approach will be very useful in cases where only limited specimens have to be tested, such as the three specimens for the ferricrete in this test program.

Table 5-5 Equivalent modulus results from RL-CBR test with strain gauges

Test code	Target DOC (%)	Achi-eved DOC (%)	Target MC (% by mass)	Achi-eved MC (%)	Initial penetra-tion* (mm)	Elastic def. ♣ Δu (mm)	Plunger stress ψ $\Delta\sigma_p$ (MPa)	Bulk stress θ [kPa]	Equ. Modulus E_{equ} [MPa]
RLCBR-G1-100_SG1	100	101.0	Mod. (4)	3.83	**0.856**	**0.343**	**7.63**	**4357**	**1028**
					1.333	0.452	12.46	6787	1298
RLCBR-G1-100_SG2		100.4		3.93	**0.507**	**0.205**	**2.46**	**1297**	**619**
					0.791	0.325	5.50	2631	871
					1.167	0.401	7.74	3642	994
					2.507	0.707	18.00	8853	1267
RLCBR-G1-100_SG3		100.5		3.83	**0.306**	**0.109**	**1.20**	**1018**	**564**
					0.598	0.237	4.58	2711	943
					1.140	0.405	10.21	5450	1241
					1.714	0.560	16.07	7583	1454
RLCBR-G1-100_SG4		101.5		3.94	**0.815**	**0.289**	**4.31**	**2429**	**751**
					1.241	0.387	8.04	3880	1003
					1.763	0.512	7.70	6047	1218
					2.415	0.660	18.00	8854	1353
RLCBR-G1-100_SG5		100.7		3.78	**0.386**	**0.192**	**7.79**	**1043**	**463**
					1.363	0.520	10.20	4470	1025
					2.003	0.598	14.01	6261	1209
RLCBR-G1-100_SG6♠		*100.4*		*3.87*	***2.137***	***0.630***	***12.53***	***8390***	***849***
					2.870	*0.782*	*17.92*	*11661*	*1007*
RLCBR-G1-100_SG7		100.9		3.65	**2.284**	**0.661**	**17.92**	**7705**	**1397**
					2.854	0.525	12.35	5061	1223
					3.257	0.411	7.71	3044	989
					3.582	0.311	4.34	1907	739
					3.729	0.144	1.17	695	422
RLCBR-FC-98_SG1	98	99.3	Mod. (7.5)	6.67	**1.936**	**0.474**	**12.02**	**5528**	**1314**
					5.717	0.65	18.01	8445	1416
RLCBR-FC-98_SG2		99.2		7.31	**0.281**	**0.081**	**1.19**	**668**	**761**
					0.560	0.165	3.32	1506	1099
					2.584	0.401	10.21	4309	1332
					6.686	0.592	16.14	6759	1430
RLCBR-FC-98_SG3		99.1		7.56	**0.893**	**0.195**	**3.42**	**1705**	**889**
					2.591	0.360	6.37	2986	912
					4.922	0.572	12.19	5659	1095

**Initial penetration is the total plunger displacement recorded at the first loading to when loaded to the target plunger stress*
♣ Average recoverable deformation, u, of the last 5 cycles of the 100 load cycles
ψ Average plunger stress difference, σ_p, between the max. of loading and min. of unloading of the last 5 cycles of the 100 load cycles
♠ On the sixth specimen (RLCBR-G1-100_SG6) some errors in the strain gauge measurements were noted during testing, thus the results of this specimen are not included for further analysis

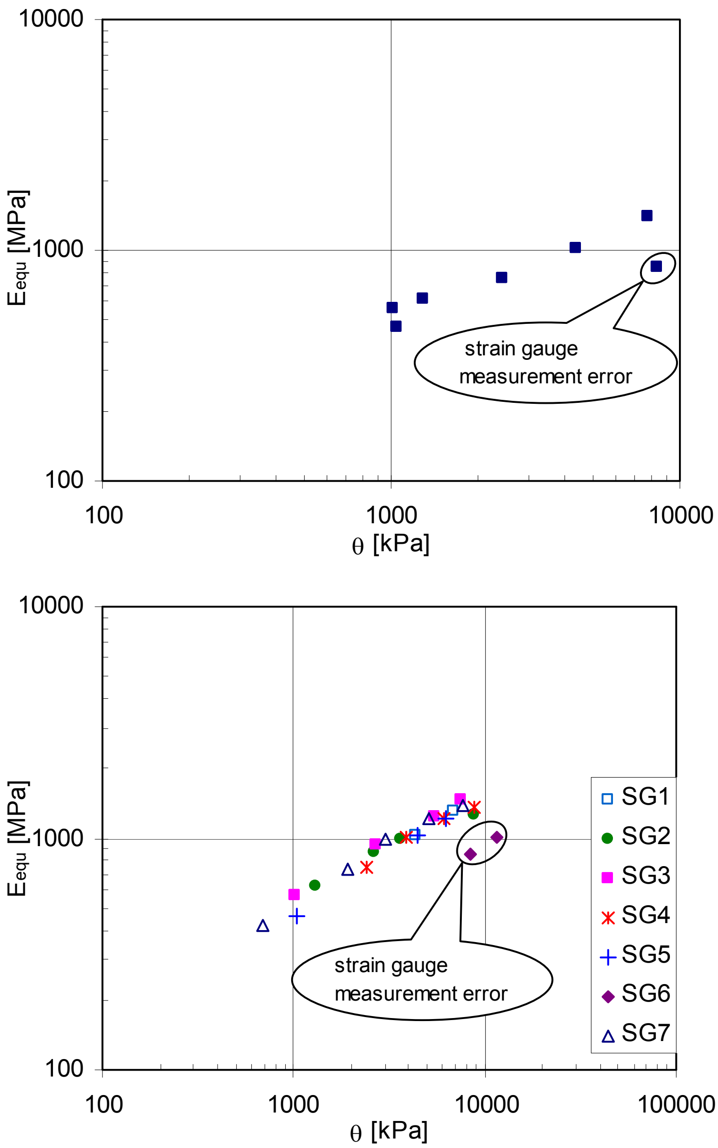

Figure 5.38 $E_{equ} - \theta$ plot for G1 tests on (a) virgin specimens (b) all loading

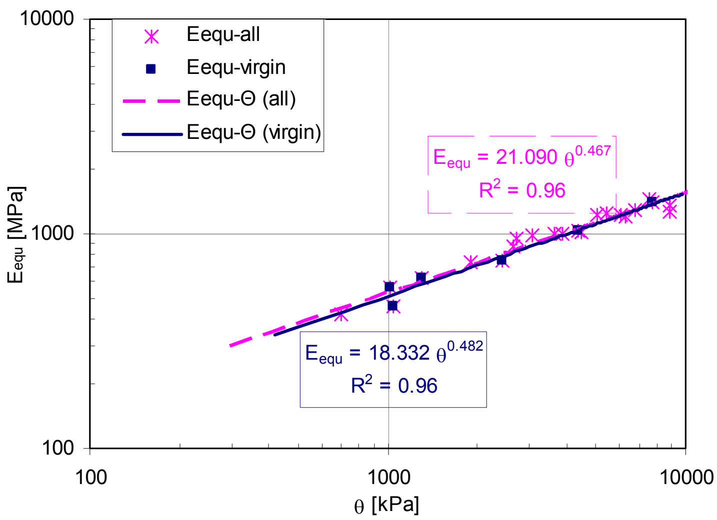

Figure 5.39 $E_{equ} - \theta$ model fit for G1 tests on virgin and multi-stage tests

Ferricrete - FC

For the ferricrete the RL-CBR test with strain gauges is performed only on three specimens. The E_{equ}-θ model fit is thus performed and plotted for all loadings in the multi-stage testing. The ferricrete test results show quite some scatter and the model fit in Figure 5.40 results in a smaller coefficient of determination $R^2 = 0.82$. Moreover, the E_{equ} result shows a rather low stress dependency. It should be noted however that the strain gauges output of specimen RLCBR-FC-98_SG2 was such that there were some reasons to believe there was a possible error in the strain gauge resulting in an overestimation of the E_{equ} to a certain extent. However since the test data for this material are limited and the error observed is not very large they are not excluded from the analysis.

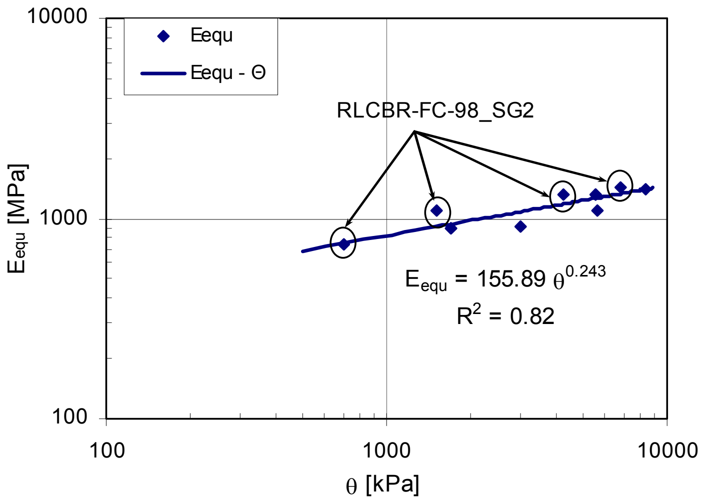

Figure 5.40 $E_{equ} - \theta$ model fit for FC tests on multi-stage tests

The equivalent modulus obtained from the RL-CBR tests with strain gauges for both the G1 and FC are compared to and verified by the resilient modulus of the triaxial tests determined in chapter 4. This verification is presented in chapter 6.

5.6.3 Comparison of without and with strain gauges characterization approach

Comparison of the two characterization approaches for testing RL-CBR without (WOSG) and with strain gauges (WSG) can be readily and more consistently done by using the measurements of the tests carried out for the RL-CBR tests with strain gauges. Using these measurements the equivalent modulus can also be computed based on only plunger stress and displacement excluding the stain gauge measurements.

Using the same measurement to compare the two different characterization techniques has an advantage. Comparing the two approaches based on the same specimens avoids any variation that may arise from different specimen condition and sample preparation variations. Therefore the results in table 5-5 are replicated in table 5-6 along with the equivalent modulus obtained through the equation 5-15 for both G1 and FC. In the table the equivalent modulus is computed for assumed Poisson's ratio of 0.25 and 0.45 in addition to the most adopted 0.35 in section 5.6.1. These results are also illustrated in graphical plots, in Figures 5.41 and 5.42, to compare the two techniques for the G1 and FC. The equivalent modulus can be plotted as a function of plunger stress or bulk stress estimated based on the tests with strain gauges.

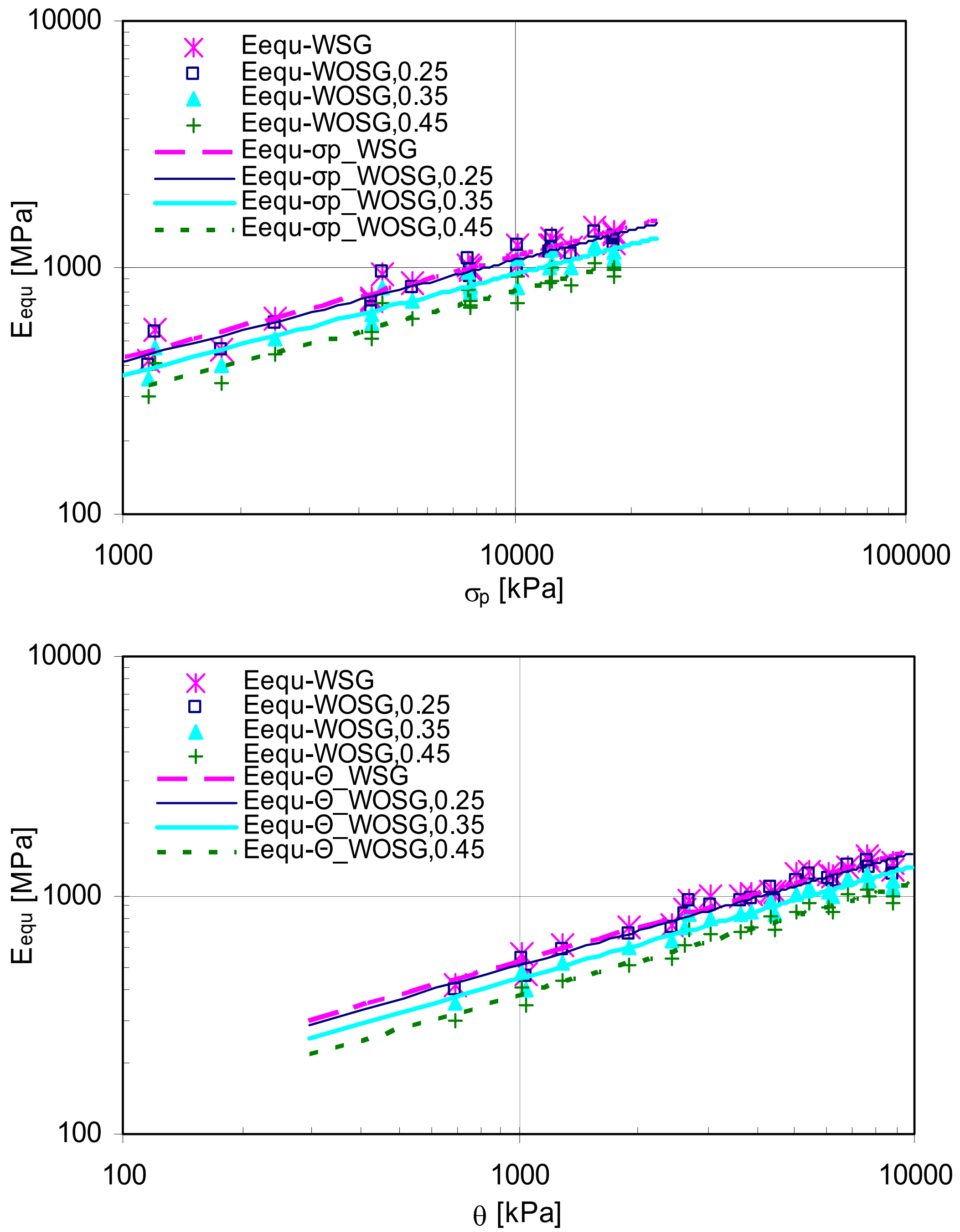

Figure 5.41 Comparison of equivalent modulus from the two approaches, with and without strain gauge measurements, for G1

Table 5-6 Equivalent modulus comparison for RL-CBR test with strain gauges (WSG) and without strain gauge measurements (WOSG)

Test code	Achi-eved DOC [%]	Achi-eved MC [%]	Elastic def. ♣ Δu [mm]	Plunger stress ψ $\Delta\sigma_p$ [MPa]	Bulk stress θ [kPa]	E_{equ} WSG* [MPa]	E_{equ} WOSG* [MPa] ν = *0.45*	ν = *0.35*	ν = *0.25*
RLCBR-G1-100_SG1	101.0	3.83	**0.343**	**7.63**	**4357**	**1028**	**814**	**953**	**1089**
			0.452	12.46	6787	1298	1005	1177	1344
RLCBR-G1-100_SG2	100.4	3.93	**0.205**	**2.46**	**1297**	**619**	**442**	**517**	**591**
			0.325	5.50	2631	871	620	726	829
			0.401	7.74	3642	994	705	826	943
			0.707	18.00	8853	1267	923	1082	1235
RLCBR-G1-100_SG3	100.5	3.83	**0.109**	**1.20**	**1018**	**564**	**408**	**478**	**546**
			0.237	4.58	2711	943	710	832	950
			0.405	10.21	5450	1241	921	1078	1231
			0.560	16.07	7583	1454	1044	1223	1396
RLCBR-G1-100_SG4	101.5	3.94	**0.289**	**4.31**	**2429**	**751**	**547**	**640**	**731**
			0.387	7.70	3880	1003	727	851	972
			0.512	12.40	6047	1218	882	1033	1179
			0.660	18.00	8854	1353	990	1160	1324
RLCBR-G1-100_SG5	100.7	3.78	**0.192**	**1.79**	**1043**	**463**	**343**	**402**	**459**
			0.520	10.20	4470	1025	714	836	955
			0.598	14.01	6261	1209	851	997	1139
RLCBR-G1-100_SG6♠	*100.4*	*3.87*	***0.630***	***12.53***	***8390***	***849***	***722***	***846***	***966***
			0.782	*17.92*	*11661*	*1007*	*830*	*972*	*1110*
RLCBR-G1-100_SG7	100.9	3.65	**0.661**	**17.92**	**7705**	**1397**	**984**	**1153**	**1316**
			0.525	12.35	5061	1223	856	1003	1145
			0.411	7.71	3044	989	685	802	916
			0.311	4.34	1907	739	511	599	684
			0.144	1.17	695	422	300	352	402
RLCBR-FC-98_SG1	99.3	6.67	**0.474**	**12.02**	**5528**	**1314**	**924**	**1083**	**1236**
			0.65	18.01	8445	1416	1006	1178	1346
RLCBR-FC-98_SG2	99.2	7.31	**0.081**	**1.19**	**668**	**761**	**547**	**641**	**731**
			0.165	3.32	1506	1099	743	870	993
			0.401	10.21	4309	1332	930	1089	1244
			0.592	16.14	6759	1430	991	1161	1325
RLCBR-FC-98_SG3	99.1	7.56	**0.195**	**3.42**	**1705**	**889**	**646**	**757**	**864**
			0.360	6.37	2986	912	647	758	865
			0.572	12.19	5659	1095	775	908	1036

♣ *Average recoverable deformation, u, of the last 5 cycles of the 100 load cycles*
ψ *Average plunger stress difference, σ_p, between the max. of loading and min. of unloading of the last 5 cycles of the 100 load cycles*
**WSG = with strain gauges and WOSG = without strain gauge*
♠ *On the sixth specimen (RLCBR-G1-100_SG6) some errors in the strain gauge measurements were noted during testing, thus the results of this specimen are not included for further analysis*

As can be observed in table 5-6 and Figures 5.41 and 5.42 the equivalent modulus, E_{equ}, from the RL-CBR testing with strain gauges, equations 5-16 to 5-19, is very close for both the G1 and FC to the E_{equ} estimated through equation 5-15 without strain gauge measurements when the Poisson's ratio value is assumed to be 0.25. The E_{equ}-values obtained from the estimation without strain gauge measurements for Poisson's ratios 0.35 and 0.45 are quite smaller, 12.5% and 25.3% respectively. The Poisson's ratio computed by the transfer function, equation 5-17, in section 5.6.2 for both the G1 and FC is presented in Figure 5-43. The figure shows that the Poisson's ratio estimated for G1 is in a range about 0.1 – 0.3 and for FC 0.1 – 0.15.

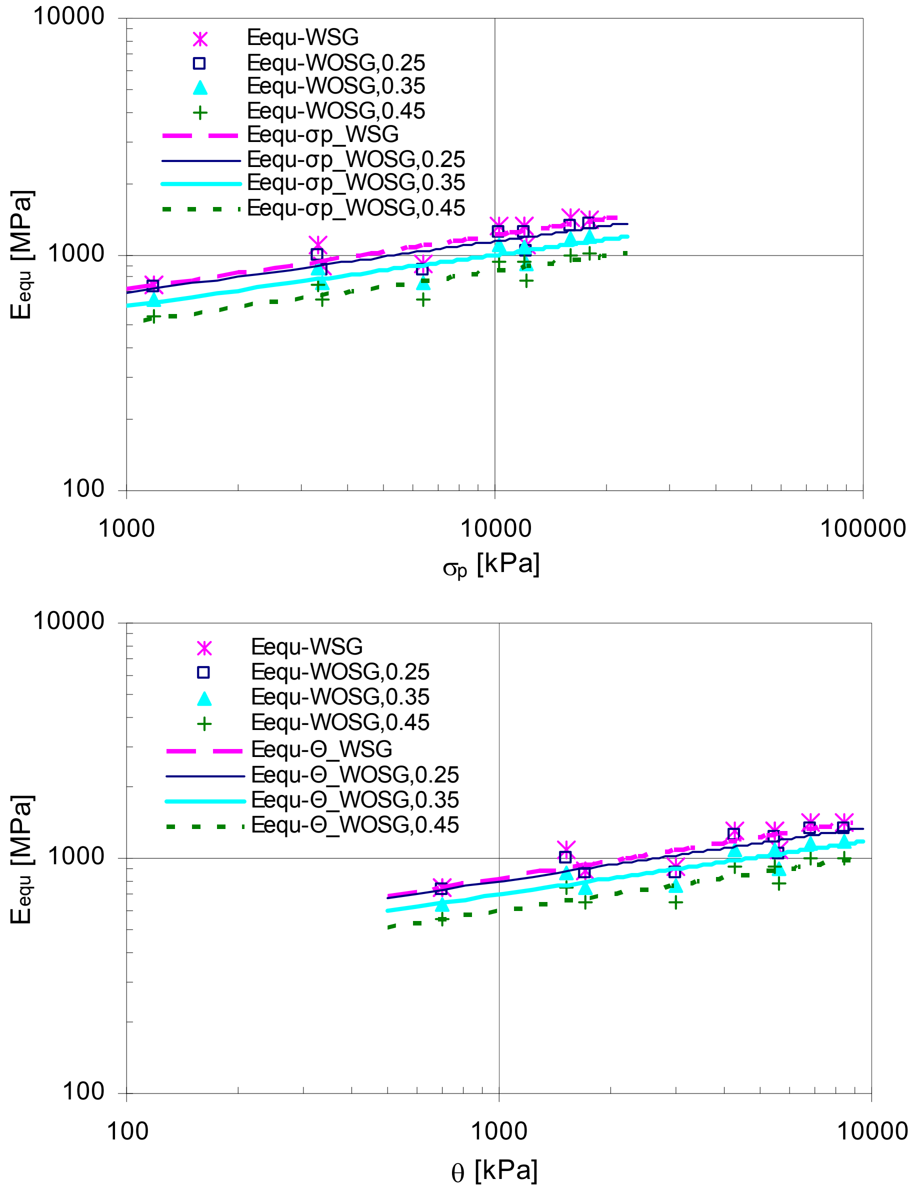

Figure 5.42 Comparison of equivalent modulus from the two approaches, with and without strain gauge measurements, for FC

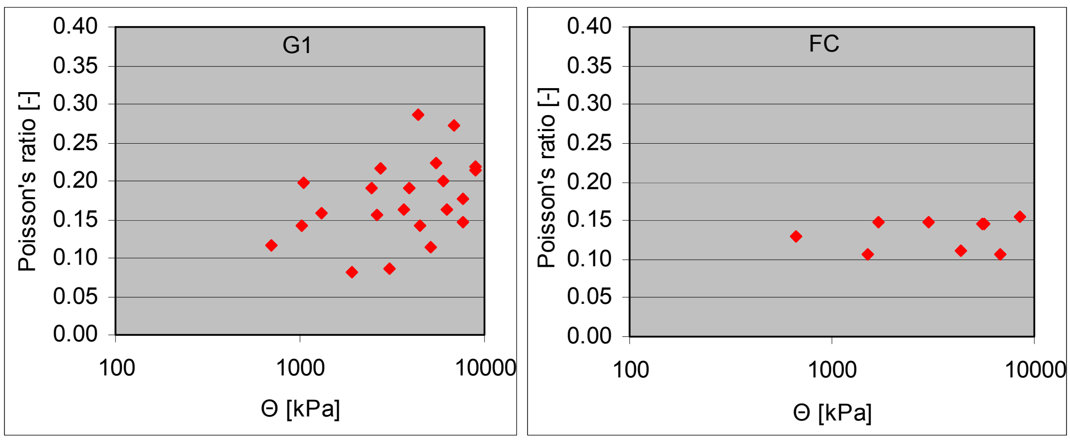

Figure 5.43 Poisson's ratio estimated by the transfer function for RL-CBR test with strain gauges for G1 and FC

Although the Poisson's ratio for such coarse granular materials is expected to be in the range 0.3 – 0.49, the high degree of compaction and high confinement from the stiff mould results in a specimen somewhat bounded. This bounded nature of the granular specimens in the CBR mould is also observed while de-molding. The granular specimens come out of the mould as bounded, see Figure 5-44.

Figure 5.44 RL-CBR specimens removed as bound from their mould

5.7 CONCLUSIONS

This chapter covers the characterization of the wide range of coarse granular materials, including the Netherlands mix-granulates, using the newly developed repeated load CBR test method. In addition to the laboratory characterization it has dealt with finite element modeling of the repeated load CBR test which is used to estimate the stiffness behavior of the UGMs. The following conclusions can be drawn with respect to the repeated load CBR testing and modeling.

- The RL-CBR testing procedure was used in the study to assess the resilient and permanent deformation characteristics of granular materials. The results show that the RL-CBR test can be used as a powerful tool to characterize the resilient and permanent behavior of granular materials when other more advanced test methods are unaffordable and not readily available.

- Plausible estimates of the equivalent modulus have been obtained by the use of repeated load CBR testing without strain gauge. Important information on resilient and permanent deformation behavior of the granular materials subjected to repeated loadings has also been obtained. This enhances the practical accessibility of characterizing mechanical behavior of unbound granular materials particularly for pavements in developing countries.

- The modified CBR values have shown clearly the effect of moisture content and DOC on the granular materials. The strength (resistance to penetration) of the materials increases as the moisture content decreases.

Increasing the DOC has also shown an increment in strength, as far as the compaction for the relatively weak natural gavels didn't result into an over compaction.

- The influence of the moisture content is observed in both the resilient and permanent deformation behavior, but its effect is more pronounced on the permanent deformation. For most of the granular materials an increase in moisture content results in a more permanent deformation. Similarly the effect of the degree of compaction is consistently reflected on the permanent deformation i.e. more compaction results in more resistance to permanent deformation.

- By measuring the mould deformation, and hence the degree of confinement developed in the CBR specimen, through strain gauges has provided an essential information in characterizing the elastic properties of the granular materials.

- The structural finite element model for the resilient analysis functions well. Despite of its limitation, i.e. the use of linear elastic theory for granular materials, the regression result from the FEM analysis represents the stress-dependent behavior of the applied granular materials. Yet the higher stress concentration at the contact edge of the plunger, due to representation of the discrete granular materials as a continuum structure, is setback of the modeling.

- The equivalent modulus of the granular materials can be predicted by relatively easy RL-CBR tests without strain gauge as accurate as to the prediction made by the RL-CBR with strain gauge if lower Poisson's ratio is assumed. This assumption of lower Poisson's ratio is valid for granular materials specimens which are highly compacted and highly confined with steel moulds.

REFERENCES

1. Wikipedia. *Materiomics*. [cited 2010 August 17]; Available from: http://en.wikipedia.org/wiki/Materiomics.
2. CEN, *Unbound and hydraulically bound mixtures - Part 47: Test method for the determination of California bearing ratio, immediate bearing index and linear swelling*, in *EN 13286-47*. 2004, European Committee for Standardization (CEN): Brussels.
3. Molenaar, A., *Characterization of Some Tropical Soils for Road Pavements.* Transportation Research Record: Journal of the Transportation Research Board, 2007. **1989**(-1): p. 186-193.
4. Molenaar, A.A.A., *Road Materials I: Cohesive and Non-cohesive Soils and Unbound Granular Materials for Bases and Sub-bases in Roads*, in *Lecture Note*. 2005, Faculty of Civil Engineering and Geosciences, Delft University of Technology: Delft.

5. Molenaar, A.A.A., *Repeated Load CBR Testing, A Simple but Effective Tool for the Characterization of Fine Soils and Unbound Materials*, in *Transportation Research Board TRB 2008 Annual Meeting* 2008: Washington DC.
6. Opiyo, T.O., *A Mechanistic Approach to Laterite-based Pavements*, in *Transport and Road Engineering (TRE)*. 1995, International Institute for Infrastructure, Hydraulic and Environment Engineering (IHE): Delft.
7. Van Niekerk, A.A., *Mechanical Behavior and Performance of Granular Bases and Subbases in Pavements*, in *Road and Railway Engineering, Faculty of Civil Engineering* 2002, Delft University of Technology: Delft.
8. Araya, A.A., A. Molenaar, and L.J.M. Houben. *Characterization of Unbound Granular Materials Using Repeated Load CBR and Triaxial Testing*. in *GeoShanghai 2010 International Conference*. 2010. Shanghai, China: ASCE.
9. TML. *Precise and flexible strain gauges*. [cited 2009 Nov.]; Available from: http://www.tml.jp/e/catalog/STRAIN_GAUGES.pdf.
10. Gonzalez, A., et al. *Nonlinear finite element modeling of unbound granular materials*. in *Advanced Characterisation of Pavement and Soil Engineering Materials*. 2007. Athens, Greece: Taylor & Francis.
11. Kim, M., E. Tutumluer, and J. Kwon, *Nonlinear Pavement Foundation Modeling for Three-Dimensional Finite-Element Analysis of Flexible Pavements.* International Journal of Geomechanics, 2009. **9**: p. 195.
12. Loizos, A. and A. Scarpas, *Verification of falling weight deflectometer backanalysis using a dynamic finite elements simulation.* International Journal of Pavement Engineering, 2005. **6**(2): p. 115-123.
13. HKS, *ABAQUS Theory and Users' Manual - Version 6.6*. 2006, Rhode Island USA: Hibbitt, Karlsson & Sorenson, Inc.
14. Chen, D.H., et al., *Assessment of computer programs for analysis of flexible pavement structure.* Transportation Research Record, 1995(1482): p. 123-133.
15. Zaghloul, S. and T.D. White, *Use of a three-dimensional, dynamic finite element program for analysis of flexible pavement.* Transportation Research Board, 1993(Transport Research Record 1388): p. 60-69.
16. Sukumaran, B., M. Willis, and N. Chamala. *Three Dimensional Finite Element Modeling of Flexible Pavements*. in *Advances in Pavement Engineering (GSP 130)*. 2005. Austin, Texas, USA: ASCE.

CHAPTER 6

VERIFICATION AND VALIDATION OF THE EQUIVALENT MODULUS

6.1 INTRODUCTION

In this research characterization of the mechanical behavior of unbound granular materials was performed on the six base and subbase materials using the cyclic load triaxial test and the repeated load CBR test (RL-CBR). The goal of this research is to develop a simple characterization technique for mechanical behavior of unbound granular materials.

An extensive characterization method based on the repeated load CBR test results obtained for the base and subbase granular materials is discussed in chapter 5. This characterization method provides an equivalent modulus of the materials as a basic mechanical parameter that can be used in pavement design. The equivalent modulus is explained by the finite element analysis and the theories are discussed in the same chapter. It is clear that in order to validate the theories that were developed and the determination of the equivalent modulus from the RL-CBR tests, predictions made by these theories should be verified on the basis of the cyclic load triaxial test resilient modulus.

It is remarked here that the stiffness behavior of unbound granular materials highly depends on the stress condition (i.e. the applied stress, the confining level and condition). Since these stress conditions are different in the two completely different test set-ups, the verification remains a relative one that compares trends. A pure one-to-one verification between the absolute values of the RL-CBR equivalent modulus and the triaxial resilient modulus measurements is not possible.

The verification and validation is performed as follows. For the equivalent modulus from the RL-CBR test without strain gauge the stress dependent equivalent modulus is compared with and calibrated by the resilient modulus through corrected or reduced plunger stress. This approach is further discussed in the section 6.2. From the RL-CBR tests with strain gauges the equivalent modulus as a function of bulk stress ($E_{equ} - \theta$ relation) is compared with and validated by the $M_r - \theta$ relation obtained from triaxial tests. These results are discussed in section 6.3.

6.2 VERIFICATION OF THE EQUIVALENT MODULUS FOR TESTS WITHOUT STRAIN GAUGE

The equivalent modulus obtained from the RL-CBR test can't be used directly for analysis and design of pavements as the test load level and the stresses in the specimen are very high compared to the triaxial test loadings and practical traffic loading. To use the output of the RL-CBR test for pavement analysis and design a calibration using the triaxial test results of the same material and test condition is necessary. Figures 6.1 to 6.6 show the trend how the modulus varies with their respective stress levels (bulk stress for the triaxial and plunger stress for the RL-CBR) for each material. In Figure 6.4 only the M_r-θ fitting line is shown for the triaxial test. The triaxial test for the MG is carried out earlier by Van Niekerk [1], the measured data are not indicated only the model parameters are used.

As mentioned above, in this approach the equivalent modulus is calibrated by computing a corrected or reduced plunger stress that provides a RL-CBR equivalent modulus comparable to the triaxial test resilient modulus. In this approach the model parameters k_1 and k_2 of the M_r-θ model have been used to correct the plunger stress as per equation 6-1.

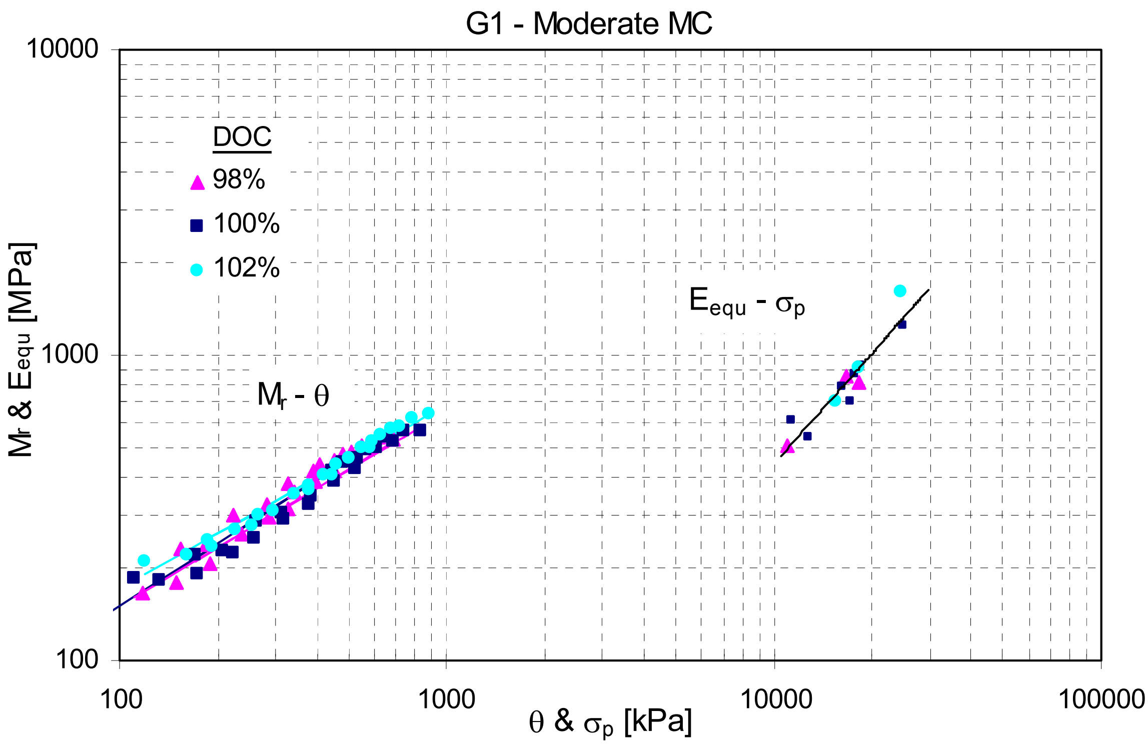

Figure 6.1 Comparison of resilient modulus vs. equivalent modulus for G1 at Moderate MC

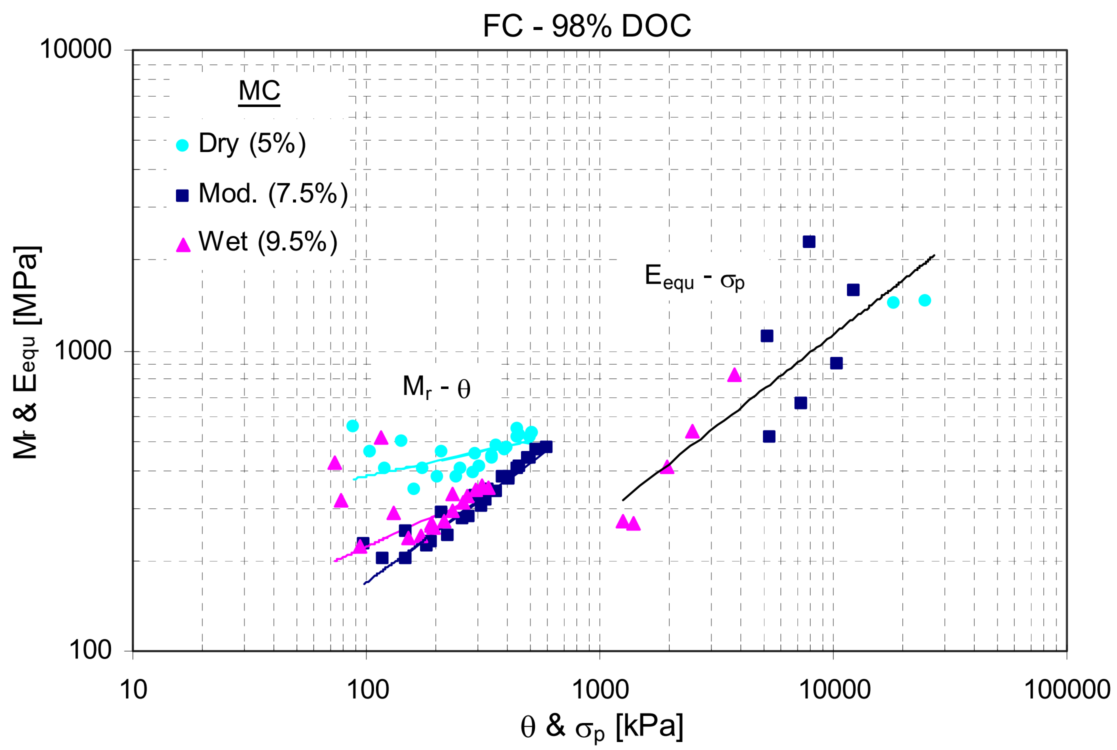

Figure 6.2 Comparison of resilient modulus vs. equivalent modulus for FC at 98% DOC

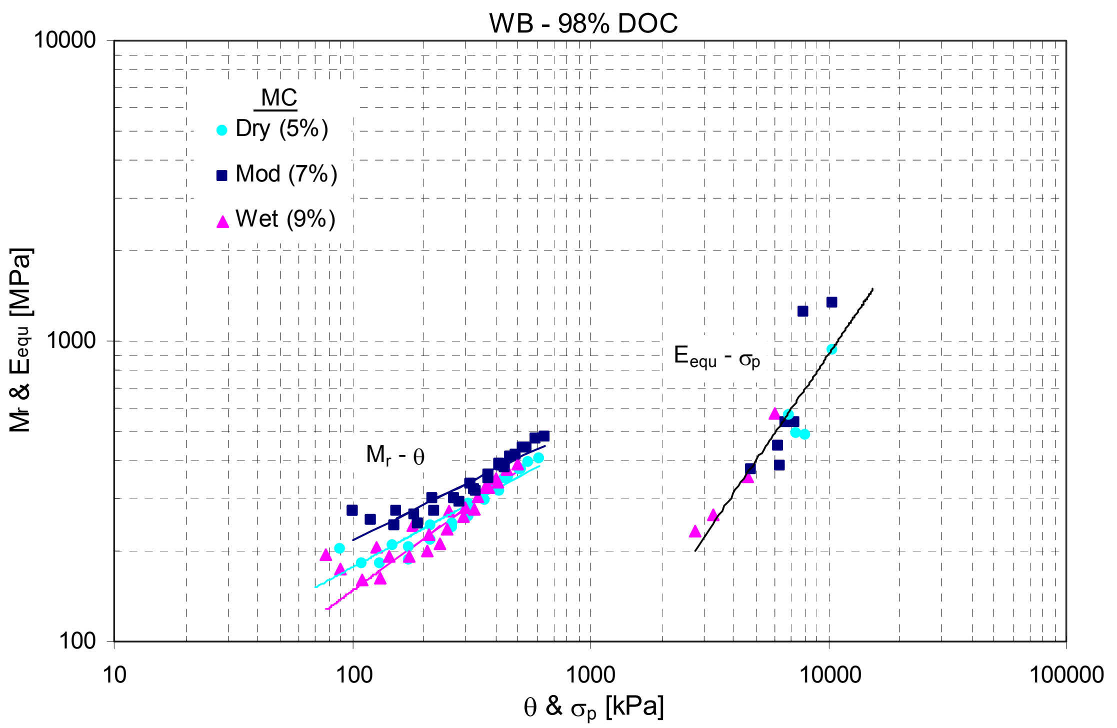

Figure 6.3 Comparison of resilient modulus vs. equivalent modulus for WB at 98% DOC

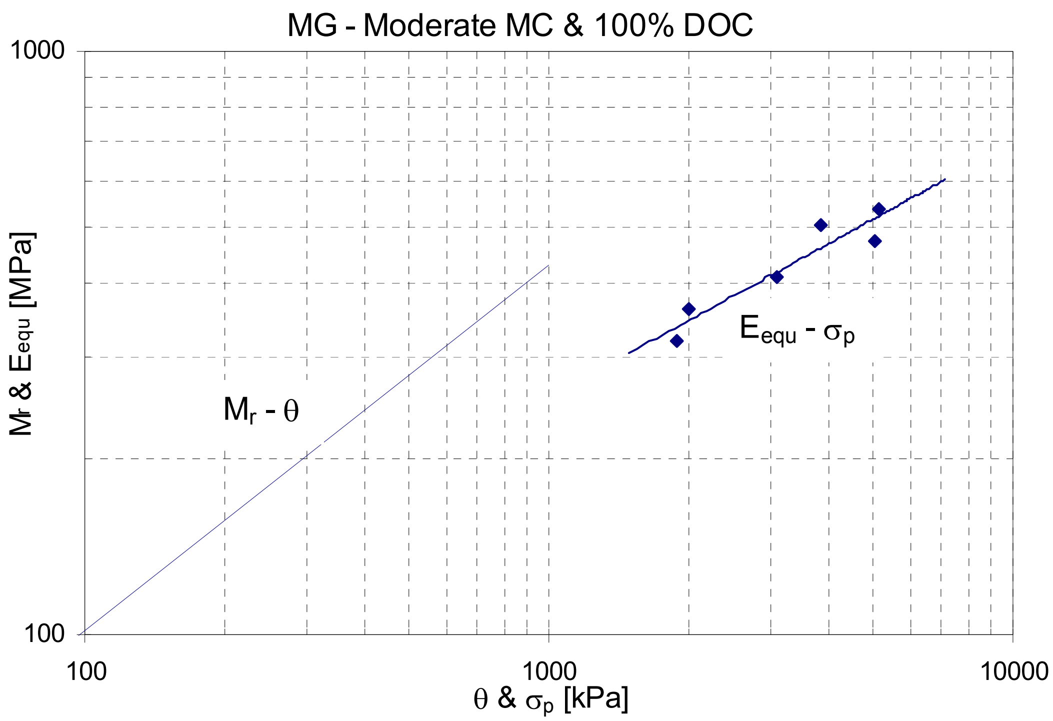

Figure 6.4 Comparison of resilient modulus vs. equivalent modulus for MG at Moderate MC and 100% DOC

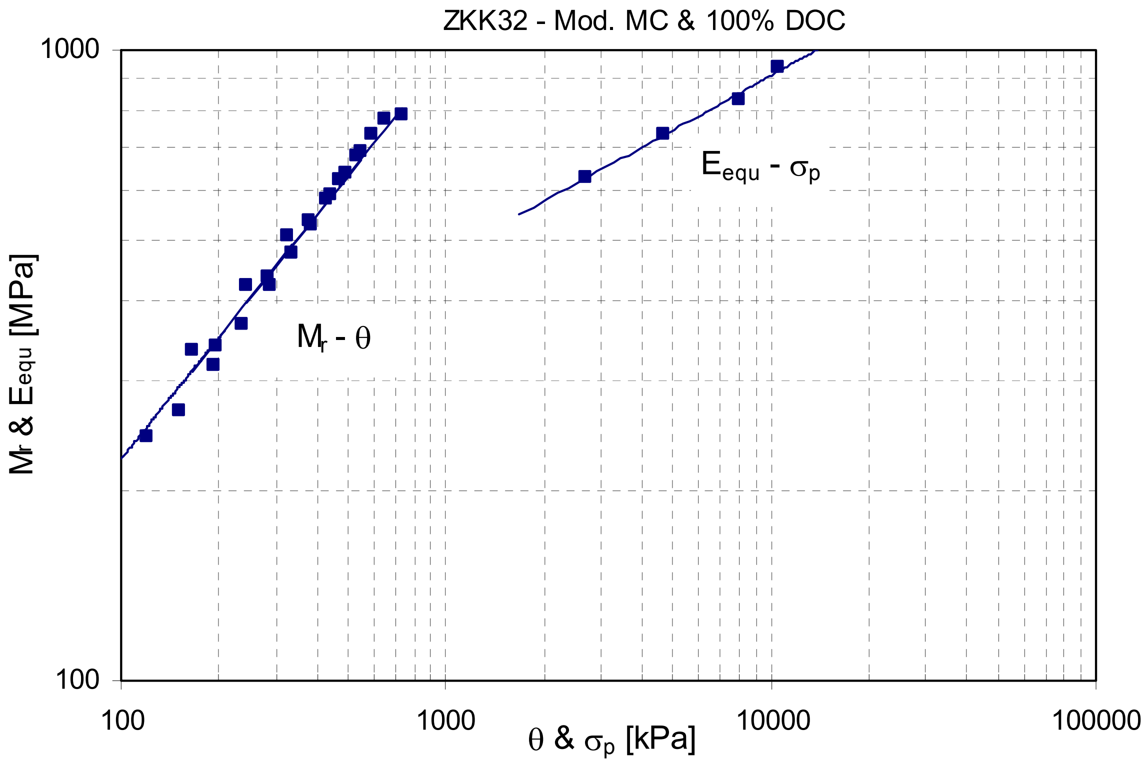

Figure 6.5 Comparison of resilient modulus vs. equivalent modulus for ZKK32 at Moderate MC and 100% DOC

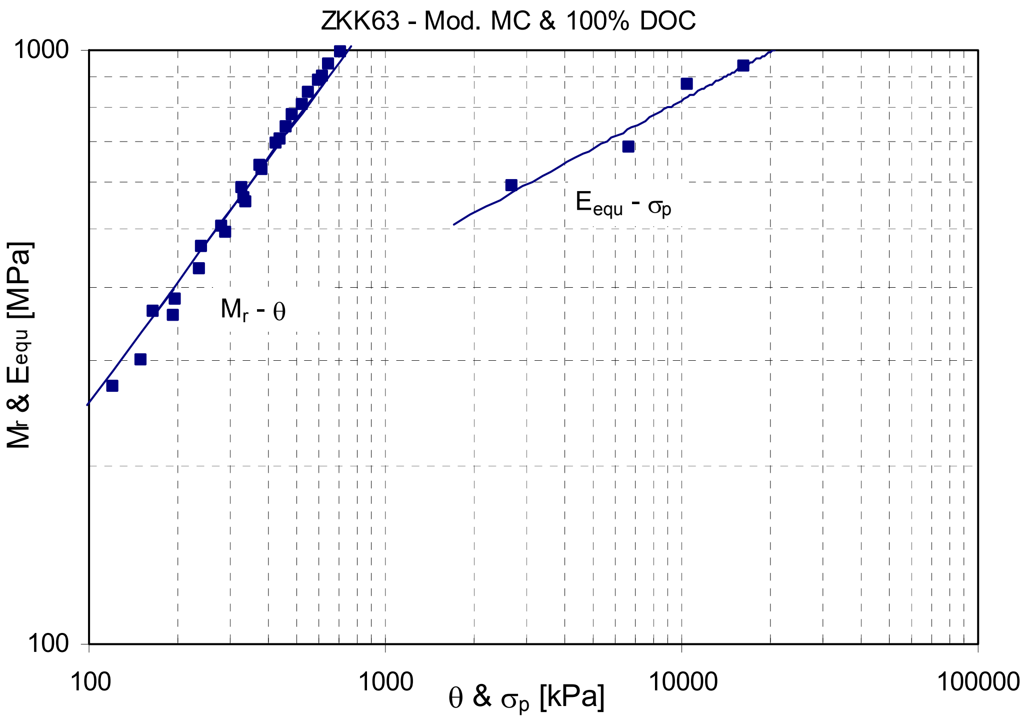

Figure 6.6 Comparison of resilient modulus vs. equivalent modulus for ZKK63 at Moderate MC and 100% DOC

Araya et al. [2] have made a correlation between the results of the two test techniques, the RL-CBR and triaxial, for three materials. Here a similar approach is used, for all the six materials considered in the research, by finding a reduced plunger stress to get an equivalent modulus that is comparable to the triaxial test result that can be used in pavement design and analysis.

For $E_{equ} \cong M_r$ from equations (5-4) and (4-10)

$$\frac{1.513(1-\nu^{1.104})\cdot\sigma_p\cdot r}{u^{1.012}} = k_1\left(\frac{\theta}{\sigma_0}\right)^{k_2}$$ for $\nu = 0.35$, $r = 40.75$ mm, $\sigma_0 = 1$ kPa

$$\sigma_p = \frac{u^{1.012}\cdot k_1\theta^{k_2}}{42.312} \qquad 6\text{-}1$$

The recoverable deformation, u, is measured from the repeated load CBR test, chapter 5. The parameters k_1 and k_2 are known from the triaxial test, chapter 4. The corrected plunger stresses are computed for a range of triaxial bulk stress levels, θ, 100 – 800 kPa and the effects of DOC and MC for each material condition are incorporated. Using a multidimensional least square regression technique, equation 6-2 is developed for estimation of the corrected plunger stress for the six materials. The regression analysis was done for each of the six materials individually and for all the materials as a whole. The results are shown in table 6-1 and Figures 6.7 and 6.8.

$$Log(\sigma_{cp}) = a_1 + a_2 MC + a_3 DOC + a_4 Log(\theta) \qquad 6\text{-}2$$

Where
σ_{cp} = corrected plunger stress [MPa]
MC = moisture content [%]
DOC = degree of compaction [%/100]
θ = bulk stress ($\sigma_1+\sigma_2+\sigma_3$) [kPa]
a_1 to a_4 = regression model parameters [-]

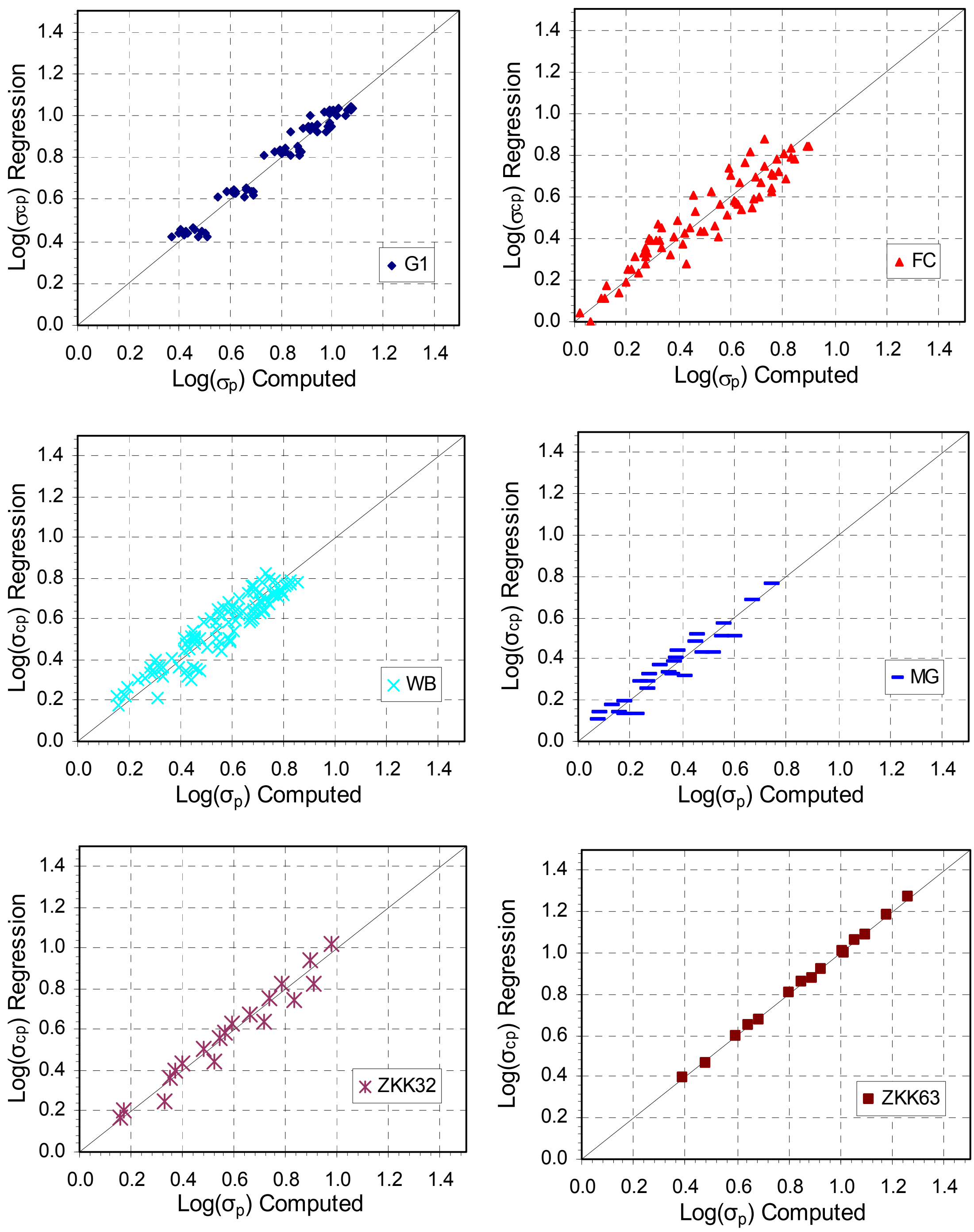

Figure 6.7 Comparison of the regression fit of equation 6-2 for each material with the computed values from equation 6-1

Table 6-1 Model parameters for equation 6-2

Material	a_1	a_2	a_3	a_4	R^2	No. data
G1	0.077	0.012	-0.957	0.641	0.962	65
FC	4.429	-0.149	-3.960	0.452	0.896	70
WB	-3.910	-0.006	3.399	0.474	0.865	100
ZKK32	-23.788	0.036	22.242	0.642	0.968	20
ZKK63	21.622	-1.021	-18.887	0.684	0.998	15
MG	-6.189	0.059	-4.345	0.626	0.960	55
All materials	0.314	-0.063	-0.726	0.543	0.686	305

In practice to get an equivalent modulus comparable to the triaxial resilient modulus one can conduct a RL-CBR test at different load levels and carrying out a pavement analysis for an assumed modulus to estimate the stress level in the different layers. The DOC and MC are estimated from the compaction level and moisture of the base layer in the road. The corrected equivalent modulus, comparable to the triaxial resilient modulus, can then be estimated in an iterative way from the RL-CBR test.

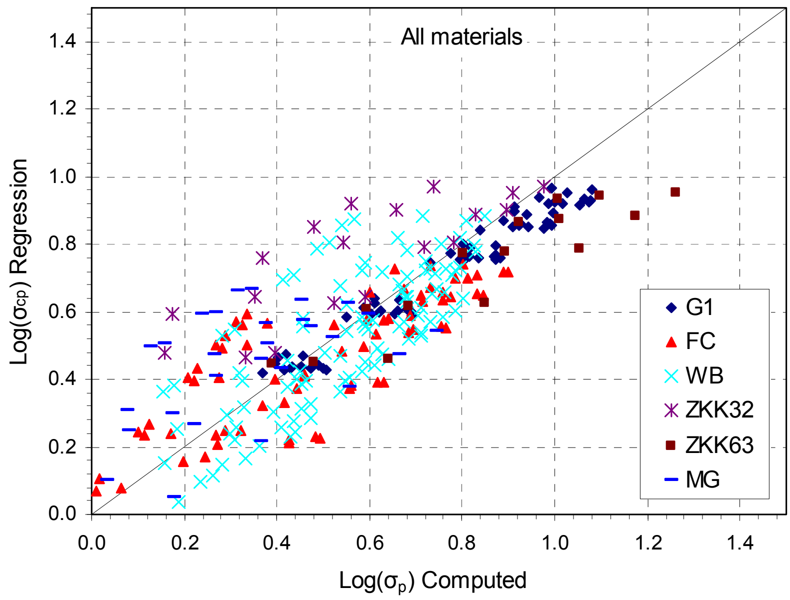

Figure 6.8 Comparison of the regression fit of equation 6-2 for all materials together with the computed values from equation 6-1

6.3 VALIDATION OF THE EQUIVALENT MODULUS FOR TESTS WITH STRAIN GAUGES

In section 5.6.2 the estimation of the equivalent modulus from RL-CBR tests with strain gauges is reported. The resilient modulus of these materials as measured by means of the cyclic load triaxial test is reported in chapter 4. The RL-CBR test with strain gauges characterization technique and the method of estimating the equivalent modulus are verified and validated by the resilient modulus measurements from the cyclic triaxial test.

In Figure 6.9 and 6.10 the E_{equ} reported in section 5.6.2 as a function of θ is presented for the G1 and FC along with their M_r-θ model of the triaxial test result from chapter 4. The stress state of a RL-CBR test specimen is complex and generally high stress levels are obtained due to the high confinement from the steel mould. This high stress level results in higher values of the equivalent modulus compared to the resilient modulus values measured at relatively low stress levels from the triaxial test. In addition the E_{equ} values are mostly smaller than one would expect from the M_r-θ line. This can be explained as follows.

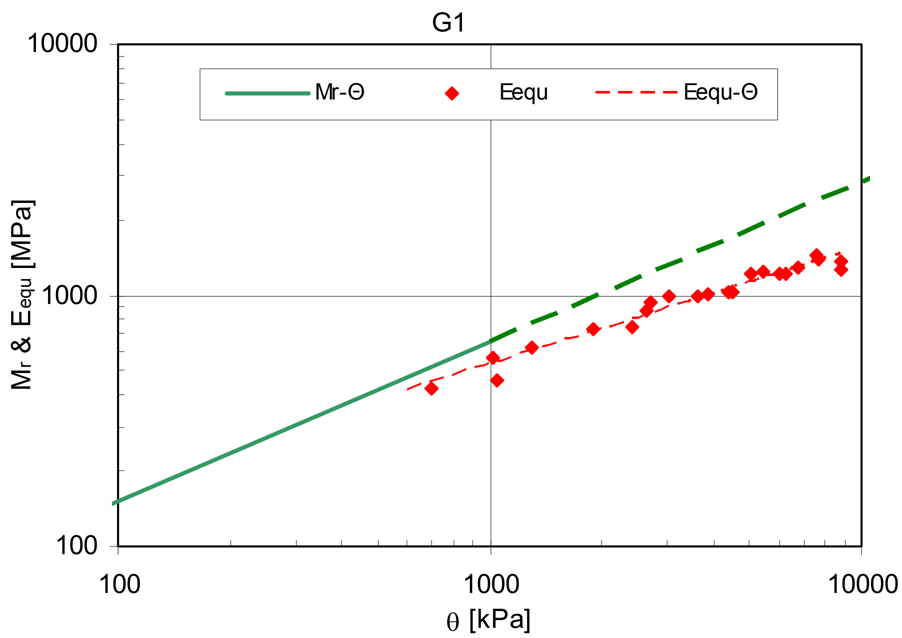

Figure 6.9 Triaxial M_r-θ model and RL-CBR E_{equ} as a function of θ for G1

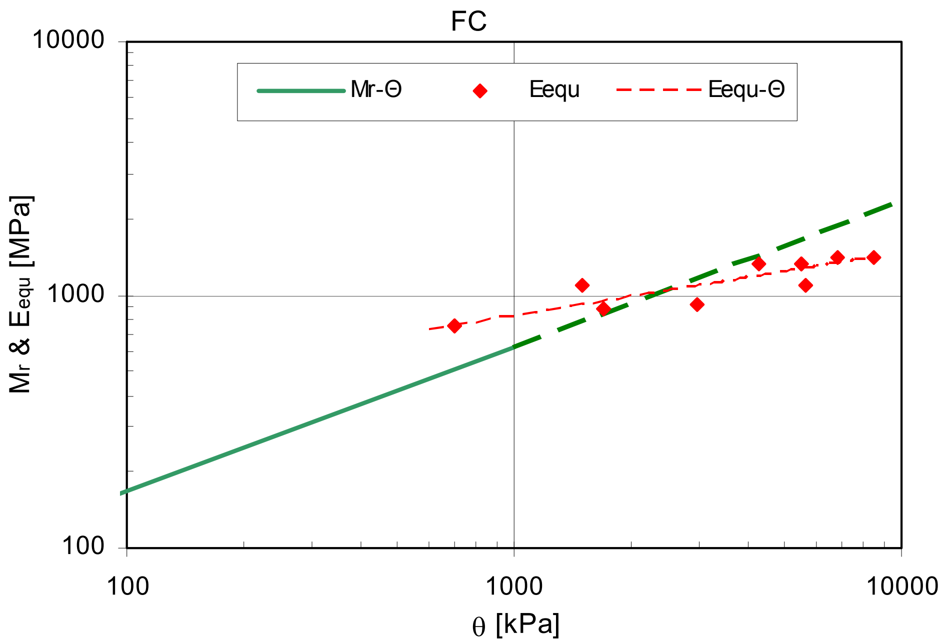

Figure 6.10 Triaxial M_r-θ model and RL-CBR E_{equ} as a function of θ for FC

One is the fact that the M_r-θ model is based on measurements at lower stress levels i.e. 100 – 800 bulk stress. However, in cyclic triaxial test measurements it has been observed that when granular materials are tested at much higher stress levels close to failure, the resilient modulus tends to decrease [3] as it theoretically should.

Second is the resilient modulus of the cyclic triaxial test as well as the equivalent modulus of the RL-CBR test are both a secant modulus based on maximum and minimum load and deformation differences. However, as shown in Figure 6.11(a) and (b) they have different stress paths. On the σ_1-σ_3 principal stress path, the σ_3 is an applied (imposed) confining stress for the triaxial test. For the CBR the confining stress σ_3 is a result of (developed from) material deformation and reorientation while restrained by the mould, thus increases along with the vertical stress σ_1 starting from some pre-confinement developed from compaction. This difference in overall test set-up including the loading rate and stress path might result in a different stress strain curve as shown in Figure 6-11(c).

The changing confinement in the RL-CBR test has also a significant effect on the bulk stress for a given applied load. For a RL-CBR test at high plunger load the confinement is proportionally very high, resulting in a high bulk stress, thus the E_{equ} will be to the right of the M_r-θ line say for a similar vertical stress σ_1. For a test at a low plunger load the confinement is proportionally very low, resulting in a low bulk stress. Thus E_{equ} will be to the left of the M_r-θ line for a similar low vertical stress σ_1, since the proportionally low σ_3 unlike the constant σ_3 in the triaxial, affects the bulk stress.

Figure 6.12 displays the measurements of the triaxial resilient modulus and the RL-CBR equivalent modulus. The figure exhibits that the RL-CBR equivalent modulus follows the trend of the triaxial resilient modulus measurements while stabilizing at higher stress level. Some permanent deformation has been observed with the 100 load cycles applied during the RL-CBR test with these high stress levels, indicating that the material is stressed beyond its elastic range. For both the G1 and FC the equivalent modulus of the RL-CBR test appears as a continuation of the resilient modulus of the triaxial data at high stress level. This indicates that the RL-CBR test is a more complex form of a triaxial test and that it can provide a good estimate of the stiffness modulus.

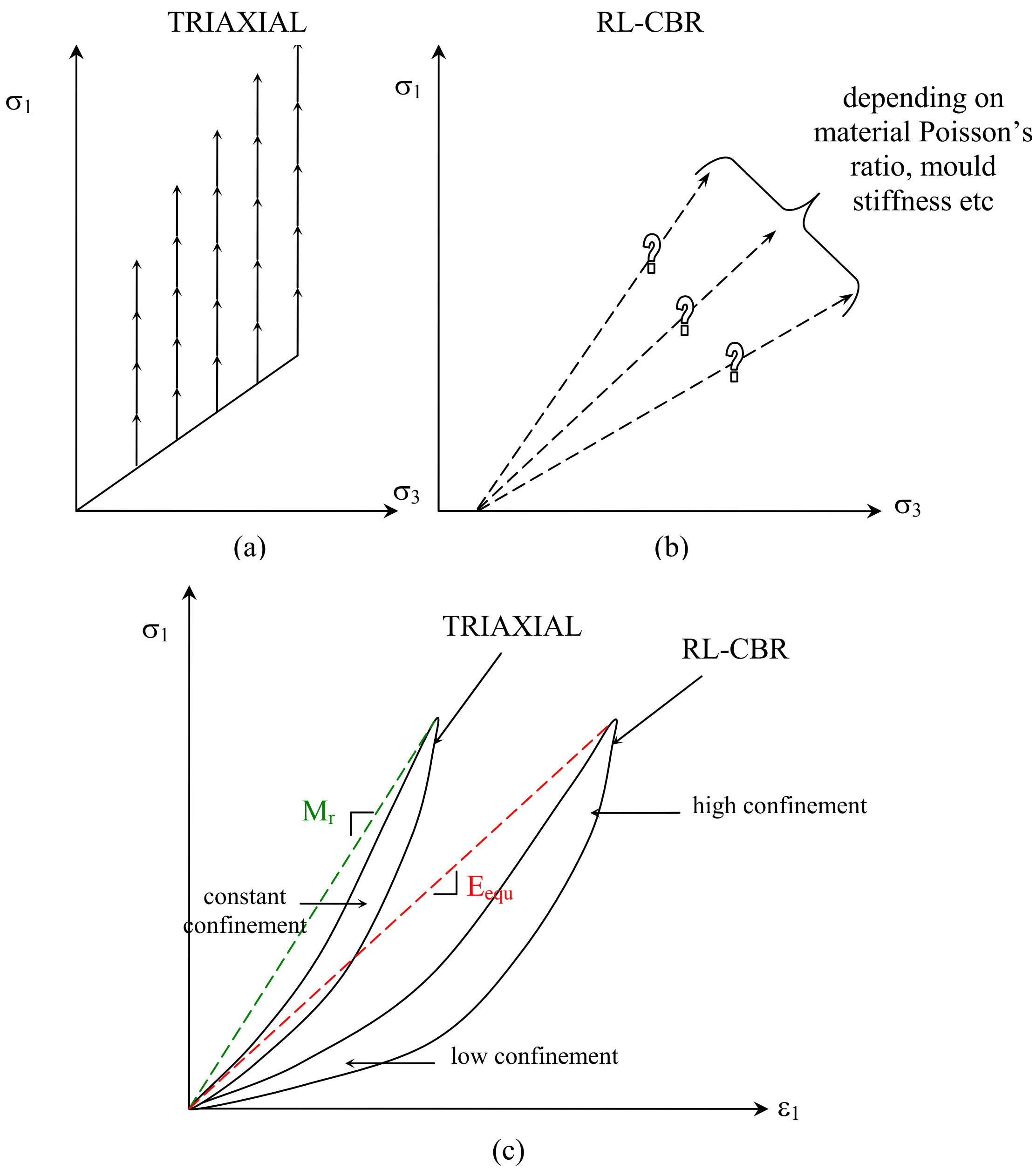

Figure 6.11 Stress paths in (a) cyclic triaxial test (b) RL-CBR test and (c) stress – strain relation for triaxial and RL-CBR tests

Observation of the M_r and E_{equ} data as a function of θ in Figure 6.12 reveals that a model can be developed that fits both the M_r and E_{equ} of the triaxial and RL-CBR test results. An S-type model equation 6-3, in log – log scale, has been fitted through the available data and the results are shown in Figure 6.13 for the G1 and Figure 6.14 for the FC material. In the model development a two parameter model (with k_1 and k_2) was used in the regression along with a minimum estimated modulus, M_{rMIN} [MPa], of 180 MPa at a minimum possible bulk stress, θ [kPa], of 100 kPa and a maximum modulus, $MAX(M_{rDATA})$ [MPa], which is the highest modulus obtained in the RL-CBR tests, as maximum limit for the S-curve.

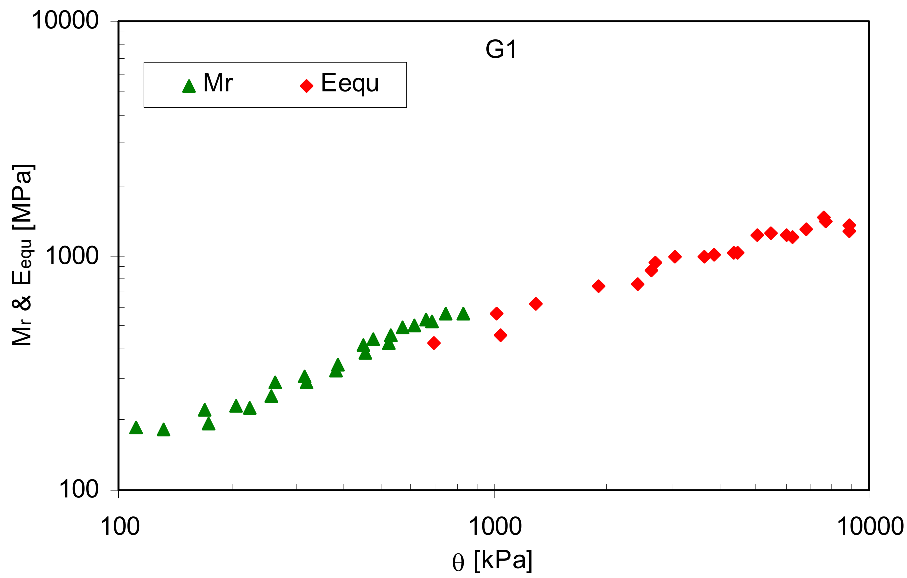

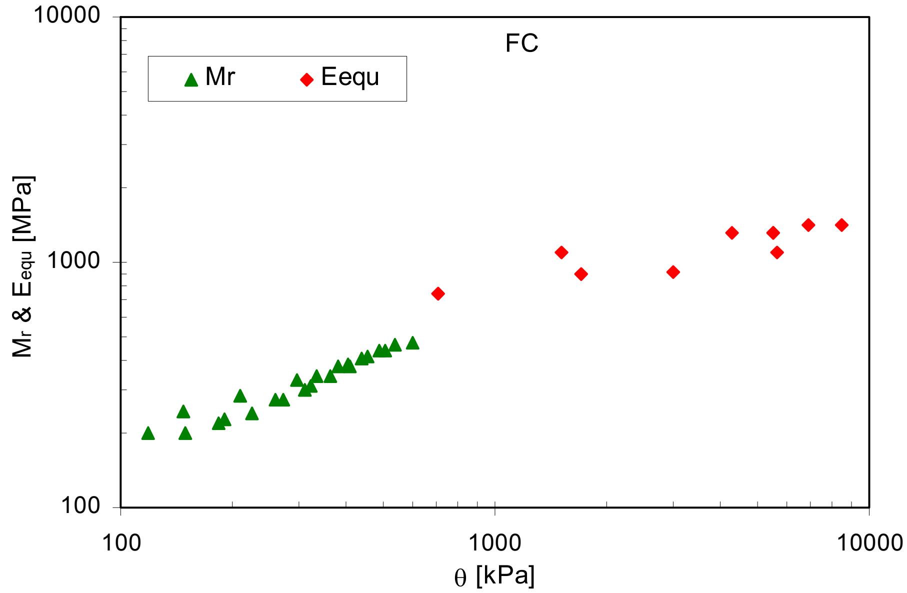

Figure 6.12 Cyclic triaxial test, M_r, and RL-CBR test, E_{equ}, as a function of bulk stress, θ, for G1 and FC

$$M_{r-equ} = M_{rMIN} + MAX\left(M_{rDATA}\right)\cdot\left(1-\exp\left(-\frac{Log\,(\theta-100)^{k_1}}{k_2}\cdot 10^{-3}\right)\right) \qquad 6\text{-}3$$

Where:

$M_{r\text{-}equ}$ = a predicted resilient modulus from RL-CBR test equivalent modulus comparable to triaxial resilient modulus [MPa]

M_{rMIN} = a minimum estimated modulus of the coarse granular materials tested 180 [MPa] at a minimum possible bulk stress of 100 kPa

MAX = Maximum value of RL-CBR equivalent modulus data [MPa]

M_{rDATA} = RL-CBR equivalent modulus data [MPa]
θ = bulk stress [kPa]
k_1 and k_2 = model parameters [-]

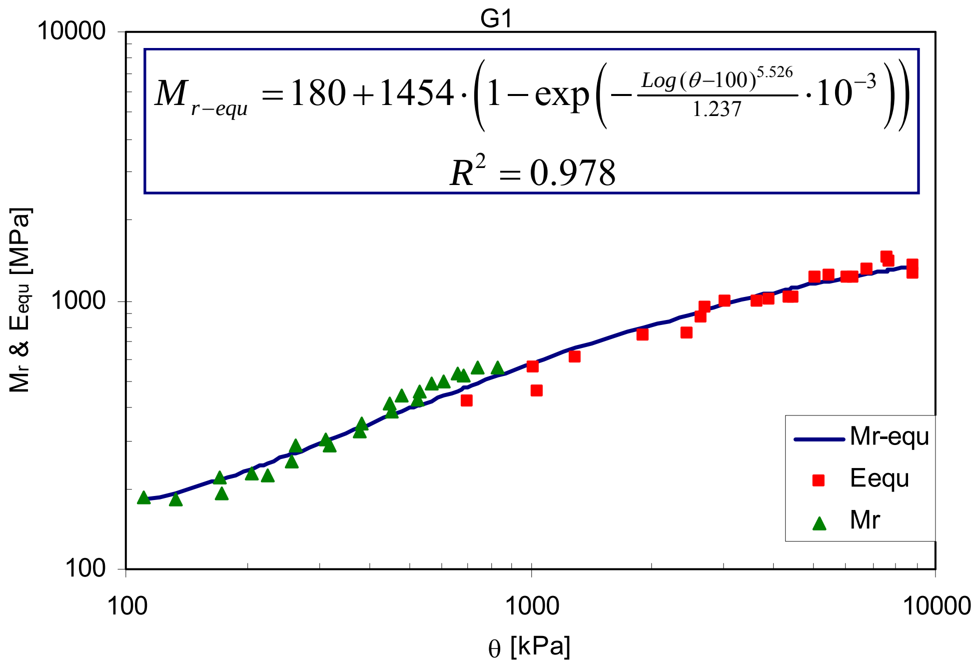

Figure 6.13 $M_{r\text{-}equ}$ fit for both triaxial M_r and RL-CBR E_{equ} for G1

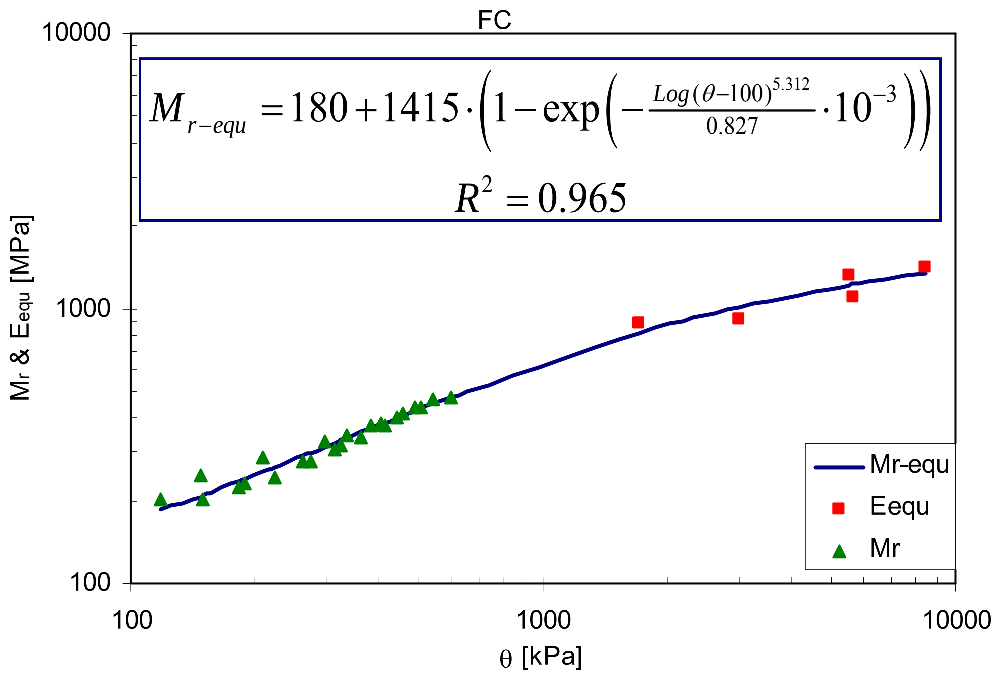

Figure 6.14 $M_{r\text{-}equ}$ fit for both triaxial M_r and RL-CBR E_{equ} for FC

From a practical point of view one has to be able to estimate a modulus equivalent to the triaxial resilient modulus from the RL-CBR test result without conducting a triaxial test. That means that one should be able to derive the same $M_{r\text{-}equ}$ using only the RL-CBR data. The models obtained in this way are shown in Figures 6.15 and 6.16 for the G1 and FC materials respectively.

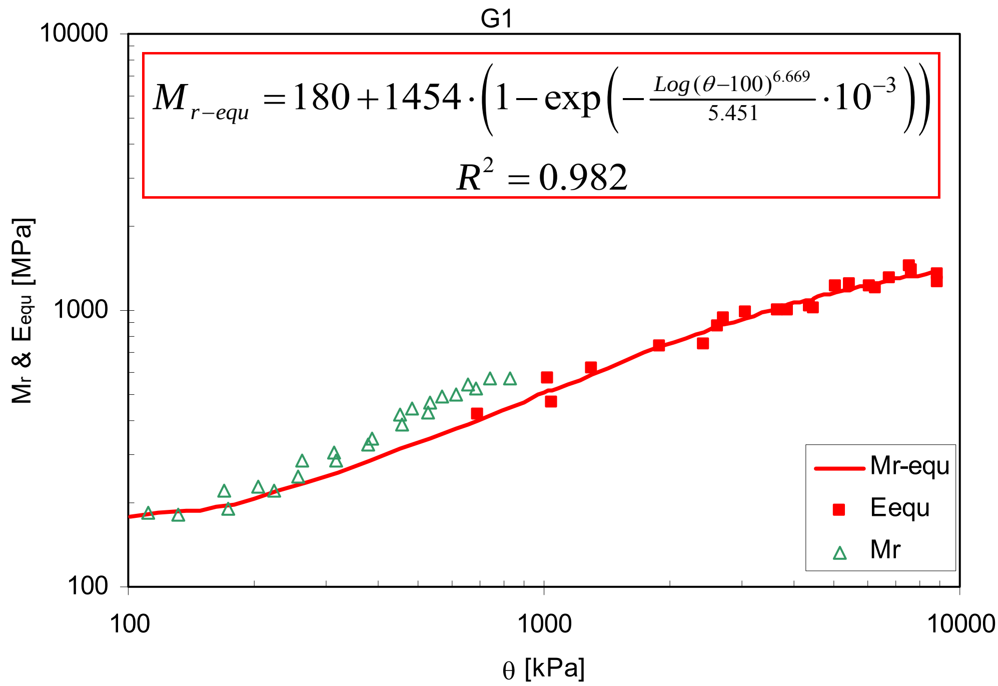

Figure 6.15 $M_{r\text{-equ}}$ model fit based on only RL-CBR E_{equ} for G1

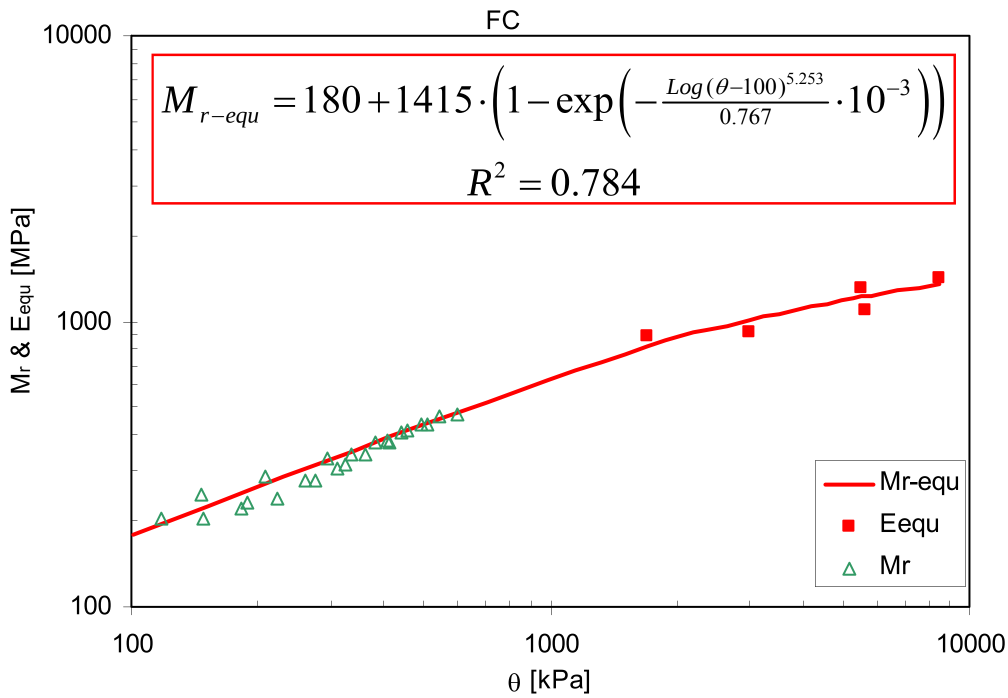

Figure 6.16 $M_{r\text{-equ}}$ model fit based on only RL-CBR E_{equ} for FC

The $M_{r\text{-equ}}$ prediction model based on only the RL-CBR test results under-estimates to a certain extent the resilient modulus M_r for the G1 at higher stress level of the triaxial test see Figures 6.15 and 6.17. Despite its limited data set, excluding the erroneous measurements by one of the specimens

(RLCBR-FC-98_SG2), Figures 6.16 and 6.17 exhibits a much better fit of the prediction curve with the triaxial resilient modulus measurements for FC based on the RL-CBR test result. The exclusion is made due to some error in the strain gauge measurements reported in section 5.6.2, Figure 5.40. Figure 6.17 compares the M_r values as predicted by the model based on the $M_{r\text{-}equ}$ RL-CBR model with the M_r values as obtained from Mr-θ model based on the triaxial test against the measured triaxial M_r values.

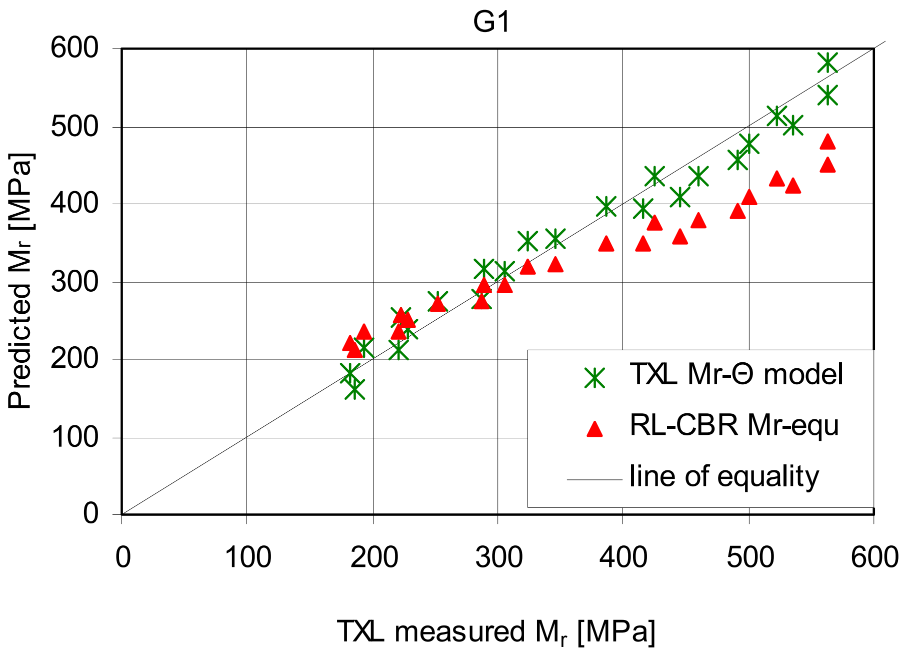

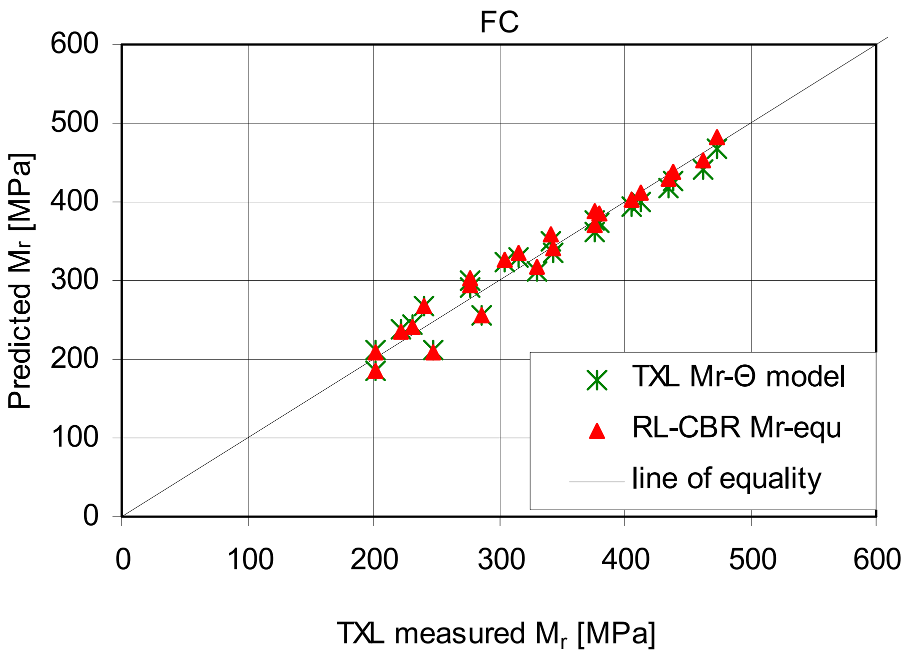

Figure 6.17 Comparing the estimated RL-CBR based $M_{r\text{-}equ}$ and triaxial based M_r-θ model to the measured triaxial M_r values

6.4 CONCLUSIONS

The verification and validation of the RL-CBR equivalent modulus is made using resilient modulus triaxial test results. For the two different characterization techniques, without and with strain gauges, a different method of validation is followed. The RL-CBR without strain gauge is calibrated against the triaxial resilient modulus through a relation that provides a reduced or corrected plunger stress. The corrected plunger stress can be used to iteratively estimate the modulus, equivalent to the triaxial resilient modulus, for a stress level occurring in the real pavement structure.

As summarized in table 6-1 and Figure 6.7 the reduced plunger stress method of calibration yields a good prediction for each individual material. But such estimation requires at least the knowledge of triaxial M_r–θ model parameters. A general relation for all the six materials was found but has less correlation. The relation for all the materials, table 6-1 and Figure 6-8, shows a good fit for the high quality G1 followed by ZKK63 but with high variation for the other materials.

The equivalent modulus, E_{equ}, from the RL-CBR test with strain gauges is verified against the triaxial resilient modulus, M_r, through a trend that both show as a function of the bulk stress. The two test set-ups are completely different, for instance in terms of stress distribution, confinement, loading rate etc, and this resulted in different modulus values. Moreover, the RL-CBR test is performed at a higher stress level and thus yields a higher modulus compared to the triaxial test. However, the equivalent modulus shows a good trend with the measured resilient modulus of the triaxial test. Equation 6-3 and Figures 6.13 to 6.16 exhibit that the equivalent modulus can be accurately estimated at any practical stress level within the (sub)base layer.

REFERENCES

1. Van Niekerk, A.A., *Mechanical Behavior and Performance of Granular Bases and Subbases in Pavements*, in *Road and Railway Engineering, Faculty of Civil Engineering* 2002, Delft University of Technology: Delft.
2. Araya, A.A., A.A.A. Molenaar, and L.J.M. Houben. *A Realistic Method of Characterizing Granular Materials for Low-Cost Road Pavements*. in *the 11th International Conference on Asphalt Pavements (ISAP 2010)*. 2010. Nagoya, Japan.
3. Huurman, M., *Permanent deformation in concrete block pavements*, in *Faculty of Civil Engineering and Geosciences*. 1997, Delft University of Technology: Delft.

CHAPTER 7

IMPORTANT ASPECTS TO CONSIDER

7.1 INTRODUCTION

In the previous chapters ample attention has been given to the cyclic load triaxial and CBR tests as they were used in this research. In these chapters the focus was merely on the test results and how these have to be interpreted. Little to no discussion was given about important features that become apparent when preparing test specimens and testing them. Since these features are considered to be important, special attention to some of them is given in this chapter. It is believed that this discussion is very helpful for researchers who will be doing similar type of work in the future.

7.2 MOISTURE AND COMPACTION

In chapter 4 and 5 the significant effect of moisture content on the material behavior has been clearly shown. This is particularly illustrated in sections 4.3.4, 4.6.1, 5.3.3 and 5.6.1. It is observed that of all the influence factors investigated the moisture content has a significant effect on the material properties, especially for natural granular materials. Very significant improvement in pavement performance can be realized by controlling the moisture content of granular layers during construction and through provision of an adequate and proper drainage system in the design and construction of the road pavement.

Another crucial influence factor investigated is the degree of compaction. In sections 4.3.4, 4.6.2, 5.3.4 and 5.6.1 it has been shown that very significant improvements in mechanical behavior, mainly strength and resistance to permanent deformation, can be realized by increasing the degree of compaction (DOC). The increase in degree of compaction, particularly for the very high quality crushed stone G1, results in great performance. This demonstrates that the very high compaction requirement for G1 materials in the South African specification [1], with a minimum of 88% apparent relative density (ARD) i.e. about 108% max. modified proctor dry density

(MMPD) is quite appreciable. However, for natural coarse gravels such as FC and WB precautions should be made to prevent an excessive degree of compaction that may bring over-compaction.

The negative effect of over-compaction for the natural aggregates FC and WB has been reflected in Figures 4.15, 4.35, 5.16 and 5.34. The performance of these materials at 100% DOC is less than at 98% DOC. The main reason for poor performance at high DOC is believed to be changing the gradation of the materials due to crushing the coarse particles. This is further investigated by cross checking the gradation through wet sieving after compaction at 100% DOC. The result, Figure 7.1, exhibits that the FC is greatly affected by over-compaction followed by the WB, while the effect is negligible for the high quality G1.

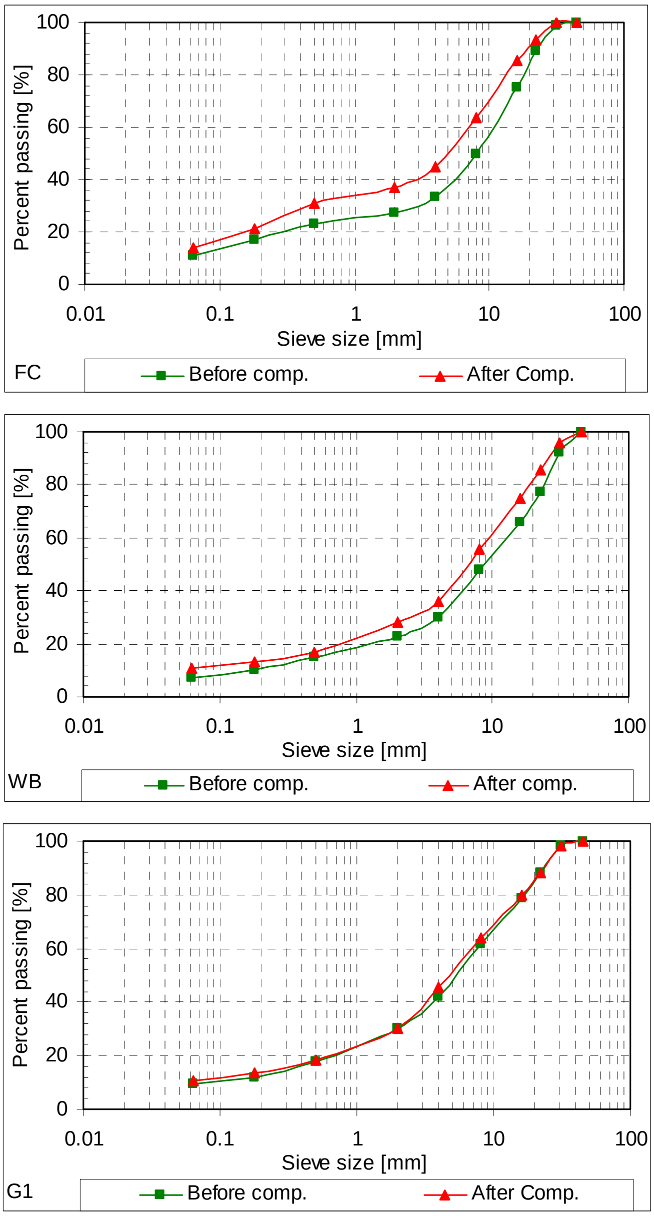

Figure 7.1 Gradation change through crushing due to compaction

It is also pertinent to note the significance and role of each mechanical behavior (strength, stiffness and resistance to permanent deformation) of the granular materials while considering application of a mechanistic pavement design procedure. Material type is one of the influence factors considered in the research. It is illustrated in sections 4.3.3 and 4.3.4 that the strength (resistance to shear failure) of G1 is significantly higher than the strength of FC and WB. Similarly the better performance of the G1 with respect to the resistance to permanent deformation is also clearly shown in section 5.3.

On the other hand, very high performance of the crushed rock G1 observed in the real field performance in South Africa is not reflected in the resilient modulus, chapter 4, and equivalent modulus, chapter 5, properties. Moreover, for the granular materials it was observed that the permanent deformation is relatively most affected by the investigated influence factors, while the resilient deformation behavior is least affected. The failure behavior is intermediately affected. Based on these findings, it can be stated that to use the resilient (elastic) properties alone as an input in a mechanistic design procedure is not sufficient for unbound granular pavement layers. It is extremely vital to incorporate rutting criteria and strength parameters in such a design procedure, in such a way the South African Mechanistic Design Method (SAMDM) [2] incorporates them.

7.3 SPECIMEN PREPARATION

Proper specimen preparation is one of the key tasks in laboratory experimentation. This is especially important for unbound granular sample preparation in which their result is highly affected by this process.

At the beginning of the experimentation compaction of the repeated load CBR specimen was first planned to be done with vibratory compression using the 150 kN capacity MTS actuator, Figure 7.2(a). A trial compaction was carried out with a number of compaction combination ranges i.e. 40 kN – 80 kN static compression forces and 20 – 60 kN dynamic compression forces, to produce a specimen for the repeated load CBR test. However, the maximum compaction that could be achieved through this method of compaction was about 93% MPDD (modified proctor dry density) for the FC and 77% ARD (apparent relative density) for the G1. This was far below the target in the test program with maximum of 100% MPDD for the FC and 88% ARD for the G1.

Later it was chosen to use the vibratory compaction apparatus, Figure 7.2(b), developed for the big triaxial test specimen of 300 mm diameter since the test materials will also be compared with triaxial test results with the same degree of compaction. As mentioned in chapter 3 this has the advantage that both the RL-CBR and triaxial specimens are compacted in an identical compaction method.

(a) (b)

Figure 7.2 (a) TU Delft MTS actuator used for trial compaction (b) TU Delft vibratory compaction apparatus actually used in the research

A limitation is observed, however, with the vibratory compaction too. As G1 is the strongest material first trial triaxial specimens were compacted for the G1 with a target of 84% and 88% ARD (i.e. 100% and 105% MMPD). Although 100% DOC (84% ARD) has been achieved without difficulties, it was not safe to achieve 105% DOC (88% ARD) as there was much noise and instability during compaction and some clamps of the mould were damaged due to high noise and instability. In addition the first Polyethylene (PE) membrane was completely damaged.

Another limitation observed with the specimen preparation by the vibratory compaction is related to the top surface of the compacted specimen, particularly for very wet and dry mixtures. In mixtures such as wet FC and dry G1, compacting with the vibratory compactor mainly at high DOC causes segregating the fines and water to the top surface like liquefaction. The compacted wet FC specimen contains wet mud at the top and the compacted dry G1 contains much dust at the top surface. For the RL-CBR where its test result highly depends on the top surface condition, a high DOC was avoided at these extreme wet and dry mixtures. Furthermore, the top surface is improved by applying an additional compression force since the laboratory vibration compaction without kneading in general results in loose compaction at the surface while providing good compaction at depth.

7.4 CONFINING PRESSURE DISTRIBTION

In chapter 4 it is reported that the confining pressure (σ_3) in the large cyclic triaxial apparatus is realized by a sub-atmospheric pressure (vacuum principle). Such a method of realization has the advantage of avoiding the necessity of a large size triaxial cell and allows direct access to the displacement transducers during testing. It however has also disadvantages. Some of the disadvantages are that the confining pressure is limited to a theoretically maximum of 100 kPa, the vacuum suction affects the moisture content and pore-water pressure between the grains by sucking water from the specimen. Moreover, a great concern is observed in the distribution of the confining vacuum pressure along the specimen height.

The inlets of the controlled confining pressure and the measuring vacuum gauges, as shown in Figure 4.6, are positioned at the top and bottom end of the 600 mm high triaxial specimen. During the experimentation it was noticed that the partial vacuum pressure is not equally distributed through the height of the sample, particularly for highly compacted high density G1 and wet mixtures of FC. Instead the vacuum gauges were measuring in short circuit from the respective inlets.

The pressure distribution setback was closely monitored by closing one of the inlets and realizing the pressure only from one side and reading the gauge at both ends. For some of the specimens, such the G1 (having a high fine content i.e. finer than 2 mm = 32.5%) compacted at high DOC and the FC (having cohesive fines) in wet mixture, the gauge readings at the two ends, with inlet only at one end, were significantly different. In some cases the gauge reading at the other end of the inlet was reduced by about 50% and in another instance hardly any confining pressure was read. This proves that the pressure distribution is not uniform over the height of the specimen even though the vacuum pressure was applied and controlled at both ends for all the experiments. In the absence of any provision to measure the confinement at the central height of the specimen, it was not possible to verify what the distribution looks like. Whether it is linear, parabolic or any type of other distribution over the middle part of the specimen height, where the displacement measurements are positioned, it is expected to be the part with the least confining pressure. The pressure distribution for less permeable specimens in general will be as shown in Figure 7.3.

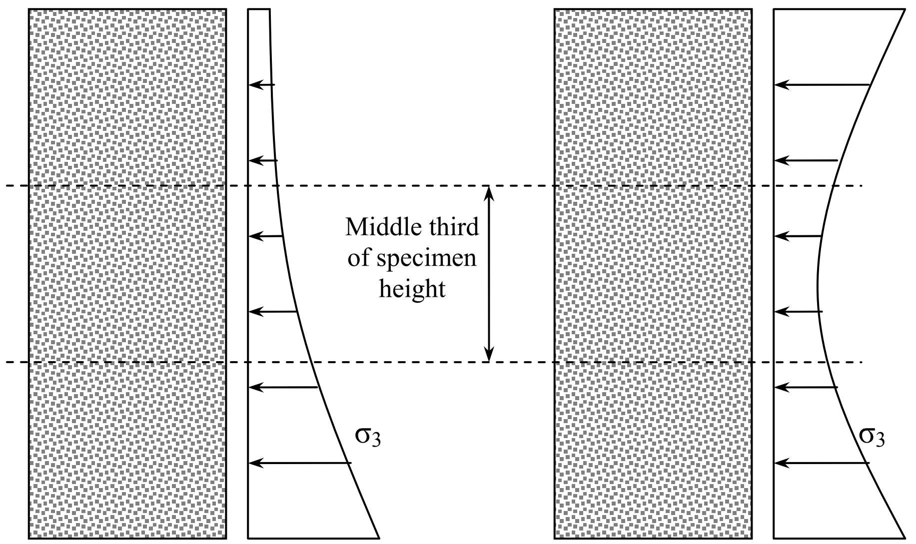

(a) Vacuum pressure application at bottom end (b) Vacuum pressure application at both ends

Figure 7.3 Confining pressure distribution along the height of a less permeable triaxial specimen

However, it has to be noted that this pressure distribution hurdle is not occurring for all specimens. It is mainly a problem for those impermeable specimens such as the G1 compacted at a very high DOC and the FC when mixed with high moisture content. The G1 when compacted at very high DOC looks like a concrete. Figure 7.4 shows how the highly compacted G1 looks like compared to the more permeable and coarse graded ZKK63. The highly (105% DOC) compacted G1 appears to be more intact and impermeable with dense and solid nature (more smooth outside surface), Figure 7.4(a), like concrete in comparison to the porous texture of the ZKK63 specimen, Figure 7.4(b).

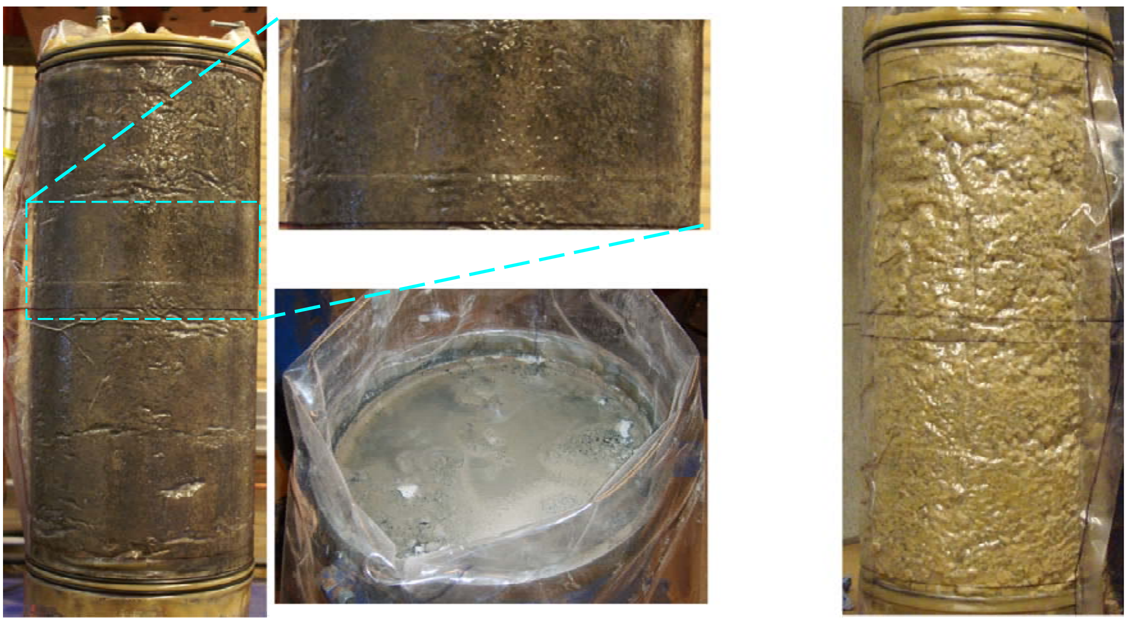

(a) specimen of G1 with very high DOC (b) specimen of ZKK63

Figure 7.4 Comparison of compacted G1 and ZKK63 triaxial specimen

7.5 ANISOTROPY AND DILATANCY

An attempt has been made to determine the anisotropic characteristics through a parameter, γ, in the modified Boyce model. This parameter is defined as the ratio of the horizontal modulus to the vertical modulus. As can be noted from table 4-7 the ratio is remarkably low for some of the materials and mixtures such as the ZKK, FC and G1. In parallel, the models such as M_r-θ, TU Delft and Universal model for homogenous isotropic materials analyzed with a single Poisson's ratio, furnish in general a higher (including values > 0.5) Poisson's ratio for those ZKK, FC and G1 materials, see tables 4-4 to 4-6.

The high Poisson's ratio (> 0.5) as a result of expanding in specimen volume as shown in Figure 4.29, commonly known as dilatancy, is related to the anisotropic nature of the UGM triaxial specimens. Based on thermodynamic principles Allaart [3] has proven, for homogenous isotropic, (non-)linear elastic materials in a secant description of E-modulus and Poisson's ratio, in reality Poisson's ratio values greater than 0.5 are possible. Further, Allaart has shown the relation between the vertical and horizontal E-modulus and Poisson's ratio's for anisotropic (non-)linear elastic materials as follows:

$$\frac{\nu_{hv}}{E_v} = \frac{\nu_{vh}}{E_h} \tag{7-1}$$

Where E_v = vertical elastic modulus
E_h = horizontal elastic modulus

The Poisson's ratios are defined in terms of the horizontal, ε_h, and vertical, ε_v, strains:

$$\nu_{hv} = \frac{\varepsilon_h}{\varepsilon_v} \tag{7-2}$$

ε_h, ε_v, are strains that arise from stress applied in vertical direction

$$\nu_{vh} = \frac{\varepsilon_v}{\varepsilon_h} \tag{7-3}$$

ε_v, ε_h, are strains that arise from stress applied in horizontal direction

From equation 7-1 it can be noticed that when the anisotropic parameter, $\gamma = E_h/E_v$, is small the ratio ν_{hv}/ν_{vh} will be large. The large ν_{hv}/ν_{vh} ratio means a bigger horizontal strain compared to the vertical strain. The total volume, with a factor of two from the horizontal strain (equation 2-14), is then increased, extended or dilated. The phenomenon "elastic dilation" can be explained by the alteration in the assembly of grains during loading and unloading, Figure 7-5.

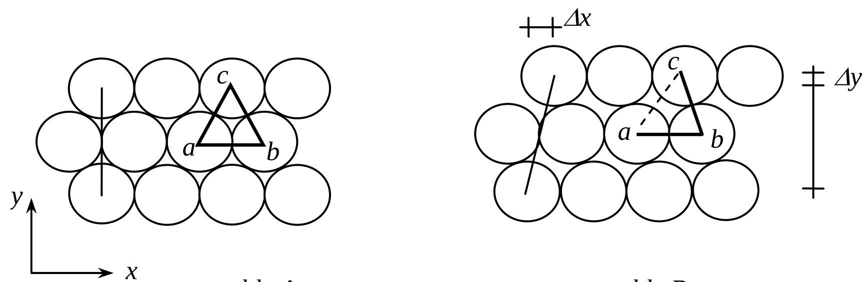

Figure 7.5 Alteration in the assembly of grains during loading and unloading [3]

If assembly A is subjected to a shear stress the grains are also pushed to the right (Δx in this drawing) and, since they were optimally packed, upwards as well (Δy, assembly B). The grains *a* and *c* no longer touch each other in assembly B.

If in assembly B the spherical pressure is raised, the grains will be pushed back towards assembly A. The grains *c* and *a* do not contact in assembly B. So it is obvious that grain *c* moves towards *a*. The shear strain decreases.

For laboratory compacted granular specimens the anisotropy is a result of the vertical compaction. In addition to the compaction effect the difference in stress magnitude between the vertical and horizontal direction could also result in a different elastic or resilient modulus. The resilient modulus of granular materials is stress dependent and the horizontal confining pressure in the triaxial testing is limited to 80 kPa while the stress in the vertical direction is much higher. Therefore this is also believed to be another reason for the anisotropy.

7.6 REPEATED LOAD CBR FOR THE ROAD INDUSTRY

Considering the wide application and availability of the standard CBR test throughout the world a repeated load CBR characterization technique for the mechanical behavior of UGMs is a very good option to implement in the road industry in general and in developing countries in particular.

The standard CBR test was originally developed mainly for soils and fine subgrade materials. The test set-up is established with a CBR mould size of 152.4 mm (6 inch) diameter. In such moulds aggregates coarser than 22.4 mm or 19 mm have to be excluded according to most standards such as EN and ASTM [4, 5] standards. For most base and subbase specifications with 0/31.5 mm, 0/45 mm or 0/63 mm coarse aggregates the removal of the coarse particles highly affects and deviates the grading from the gradation actually applied in the field. This may end up on characterizing a completely different mixture. For the purpose to include the full gradation of the coarse aggregates a larger CBR mould of 250 mm diameter and a larger plunger 81.5 mm diameter is adopted in this research.

It has to be recognized however that the use of the larger mould and plunger in the CBR test set-up attributes some difficulty in direct application for the road industry. Moreover it complicates the empiricism of the standard and more familiar CBR test terminologies and interpretation. The larger mould set-up is not likely to give the same CBR results as the standard one due to variation in the test set-up and, for coarse materials the change in gradation too as a result of downscaling on the standard moulds.

The RL-CBR test without strain gauge can be relatively easily implemented in standard road engineering laboratories where the standard CBR test equipment is available. The test can also be done without hydraulic actuator and data acquisition system. One can apply the load repetition by pressing the pushdown (load) and pushup (unload) button repetitively. The results of the test are shown in sections 5.3 and 5.6.1 and compared with the RL-CBR test with strain gauges in section 5.6.3 and with the cyclic triaxial test in section 6.2. The RL-CBR test without strain gauge reveals a great potential for application in the road industry. However, before direct application for practice it has to be further verified by conducting similar tests on other granular materials and different test set-ups, see section 8.3.

The RL-CBR test with strain gauges provides a relatively more sound approach compared to the RL-CBR test without strain gauge. The result reported in section 5.5 and 5.6.2 and its comparison with the triaxial test results in section 6.3 exhibits that the technique is quite useful and yields stiffness values comparable to those obtained through the advanced triaxial test. However, this test set-up is more complicated for practical application by demanding the use of strain gauges, amplifier and data acquisition systems. This is in addition to the already imposed larger mould and plunger. Thus, the RL-CBR test with strain gauges is especially suited for research purposes rather than for practical application. However, for practical application it is more useful to compare the more applicable RL-CBR test without strain gauge with the more accepted triaxial test. Nevertheless the RL-CBR test with strain gauges is still easier for the industry application than the much more complex cyclic triaxial test.

REFERENCES

1. CEAC, *Standard Specifications for Road and Bridge Works for State Road Authorities*. 1998, Civil Engineering Advisory Council (CEAC), Committee of Land Transport Officials (COLTO): South Africa.
2. Theyse, H.L., et al., *TRH4 Revision Phase I: Updating the transfer functions for the South African mechanistic design method*. 1995, Division for Roads and Transport Technology, CSIR, National Service Contract NSC24/1: Pretoria, South Africa.
3. Allaart, A.P., *Design principles for flexible pavements: a computational model for granular bases*. 1992, Delft University of Technology: Delft.

4. ASTM, *Standard test method for CBR (California Bearing Ratio) of laboratory-compacted soils*, in *ASTM D 1883-94*. 1978, American Society for Testing and Materials: Philadelphia.
5. CEN, *Unbound and hydraulically bound mixtures - Part 47: Test method for the determination of California bearing ratio, immediate bearing index and linear swelling*, in *EN 13286-47*. 2004, European Committee for Standardization (CEN): Brussels.

CHAPTER 8

CONCLUSIONS AND RECOMMENDATIONS

In this final chapter the main conclusions of this thesis are summarized and some recommendations are given. The main findings are presented as conclusions following the general introduction. The recommendations related to pavement design, construction and characterization of unbound granular materials are given with special emphasis on pavement engineering in developing countries.

8.1 INTRODUCTION

Over the past five decades, flexible pavement design has been gradually evolved from a purely empirical towards the analytical/mechanistic approach being used today. Despite major advancements in layered theory of pavements and development of sophisticated analytical tools, a gap still exists between theory and practice.

Pavement design procedures developed for use in developing countries are still all empirically based. The empirical design procedures used in these countries evidently deal with granular materials as their major structural layers, yet they are characterized in an empirical way. Index tests and empirically based strength tests such as the California Bearing Ratio test are used to characterize the materials and asses their structural contribution to flexible pavements.

These empirical approaches being based on vast experience and sound engineering judgment can be quite satisfactory provided they are used within the limits of the experience on which they are based. The problem however is that traffic has grown far beyond expectation both in volume and weight. This implies that roads are loaded beyond experience. This results in need for mechanistic-empirical (M-E) approach. Fundamentally sound laboratory testing techniques should be used to determine the structural characteristics of soils and granular materials for input to design calculations that form the basis of mechanistic pavement design systems.

Cyclic triaxial testing seems the best method, so far, to characterize the mechanical behavior of granular materials in the laboratory.

"Cyclic load triaxial test" is an easy thing to say but it is not so easily done. Cyclic load triaxial testing is still a research tool and certainly not an engineering tool which is used on a day to day basis, especially in case of coarse grained base and subbase materials for which large size triaxial samples are needed.

Granular material characterization is in general still done with the CBR test. In developing countries it is in fact the only available test.

The necessity of using M-E design methods and the lack of proper and affordable characterization technique "demand" for a test which is affordable, practical and that gives results which can be used as input in M-E deign procedures.

It is shown that the repeated load CBR test is such a test. Proof of this statement is given by the fact that correlation between the stiffness results of the two characterization techniques was found using the laboratory data.

These correlations were developed using data from an extensive experimental program, involving the (complex) cyclic load triaxial test and a newly developed repeated load CBR test. Coarse granular materials ranging from a solid crushed rock Greywacke Hornfels G1 to rather marginal ferricrete and weathered basalt gravels from the tropics as well as natural limestone for base course and frost protection layers and mix-granulates (crushed concrete and crushed masonry) from the temperate zone were investigated. The influence of the moisture content and degree of compaction on the shear strength and stiffness of the granular materials was investigated.

8.2 CONCLUSIONS

The experimental results obtained in the study and the analysis and modeling which were performed lead to a number of conclusions. The main conclusions of the research are presented below:

- Among all factors that affect the resilient behavior of granular materials (density, moisture content, aggregate type etc.) the most important factor is stress level.

- All the four models used (M_r-θ, the Universal, TU Delft and anisotropic K-G models) address the effect of stress state on the resilient response and fairly describe the stress dependency of the resilient modulus. The strong side of the anisotropic K-G model is the insight it provides regarding the anisotropic nature of the UGM specimens.

- In modeling the resilient behavior of the coarse granular materials a significant number of the material mixtures show anisotropic properties. In addition to the possible actual specimen volume increment (dilatancy) the effect of this anisotropy is also reflected in the large value (>0.5) of the constant Poisson's ratio.

- Relatively the effect of the moisture content on the resilient behavior of the granular materials is remarkable compared with the effect of the degree of compaction and material type considered in the investigation.

- The influence of the moisture content is more pronounced on the strength and permanent deformation behavior than on the resilient deformation behavior. For most of the granular materials an increase in moisture content results in more permanent deformation and smaller failure stress. Similarly the effect of the degree of compaction is more reflected on the permanent deformation i.e. more compaction results in more resistance to permanent deformation.

- The resilient modulus is not the best and not the only representative characteristics to evaluate the quality and structural capacity of coarse granular aggregates in pavements.

- Due to the non-uniform complex stress distribution in the RL-CBR compared to the triaxial test, fundamental material properties such as the stiffness modulus are less easy to determine. This holds true, however, on the scale and level where conventional soil mechanics and pavement engineering is dealing. The RL-CBR testing serves well its purpose as its primary goal is to get a good estimate from a simpler characterization technique at a more general scale.

- Measuring the mould deformation through strain gauges, and hence the degree of confinement developed in the CBR specimen, has provided essential information in characterizing the elastic property of the granular materials.

- The finite element model used for the resilient analysis functions well. Despite its limitation, i.e. the use of linear elastic theory for granular materials, the regression result from the FEM analysis represents the stress-dependent behavior of the applied granular materials.

- The equivalent modulus of the granular materials can be predicted by relatively easy to perform RL-CBR tests without strain gauge as accurate as the prediction made by the RL-CBR with strain gauges.

- A good general relationship is developed by the reduced plunger load for the equivalent stiffness modulus of RL-CBR tests without strain gauges.

This relation significantly improves if individual materials are considered.

- The equivalent modulus, E_{equ}, from RL-CBR tests with strain gauges allow to take the effect of the bulk stress in to account. This allowed verification of, E_{equ}, against the triaxial resilient modulus, M_r. The two test set-ups are completely different, for instance in terms of stress distribution, confinement, loading rate etc, and this results in different modulus values. Moreover the RL-CBR test is performed at a higher stress level, and thus yields a higher modulus, compared to the triaxial test. However, the RL-CBR equivalent modulus shows a good trend with (and provides a good prediction of) the measured resilient modulus of the triaxial test. This shows that a modulus equivalent to the triaxial resilient modulus can be estimated at a given practical stress level of the (sub)base layer from repeated load CBR tests.

- The RL-CBR test with strain gauges provides a relatively more sound approach compared to the RL-CBR test without strain gauge. Its comparison with the triaxial test results shows that the technique is quite useful, yielding equivalent modulus values comparable to the more accepted triaxial test resilient modulus values. However, demanding the use of strain gauges, amplifier and data acquisition systems makes this RL-CBR test method more complicated for practical application. This is in addition to the already imposed use of a larger mould and plunger. Therefore, it is more useful for research purposes than for practical application. Nevertheless it is still easier for application by industry than the much more complex cyclic triaxial test.

8.3 RECOMMENDATIONS

On the basis of the experimental research, the modeling and analyses discussed in this dissertation, coupled with the extensive literature study, the following recommendations are made:

- To use unbound granular materials to their full structural capacity in pavement structures, mechanistic pavement design procedures should incorporate strength and rutting resistance criteria for the unbound granular layers in addition to stiffness. The South African pavement design procedure has evolved farthest towards this.

- Unbound granular pavement layers that are likely to be exposed to uncontrolled moisture during the life of the pavement should be tested for their mechanical behavior at the worst possible, extreme dry or wet, in-situ moisture content. The optimum moisture content from the Proctor test appears to be reasonable as far as proper drainage is provided in the pavement construction.

- Over-compaction of weak and flaky natural coarse granular materials has a negative implication on the mechanical behavior of some of the granular materials. This is as a result of altering the gradation of the material due to crushing. Although the vibration compaction in the field pavement along with the kneading effect is expected to be in better position compared to the laboratory, the engineer in the field should prevent over-compacting of such materials. Over-compaction is believed to be more pronounced in the laboratory. This is because the laboratory compaction is carried out with very high vibratory frequency applied over a material confined inside ridged steel.

- The repeated load CBR test can be implemented in routine practice of pavement engineering as a relatively simple means of assessing the mechanical properties of granular materials. However, to accept this test as a fundamentally sound test further characterization research and validation is needed.

- For better understanding the effect of the magnitude of the mould confinement on the mechanical behavior of the granular materials further investigation shall be carried out with the repeated load CBR test with strain gauges. This can be conducted by using different mould thicknesses and/or different mould materials.

- The repeated load CBR testing with and without strain gauges shall be further investigated using the standard plunger and mould sizes parallel to the large mould and plunger adopted in this research. This may provide additional information to implement this characterization method in practice with the already existing CBR testing facilities.

- Unbound granular materials are likely to be better modeled with discrete element methods (DEM). If a finite element method is applied then user defined non-linear material behavior shall be used instead of linear elastic theories.

CURRICULUM VITAE

Name	Alemgena Alene Araya
Date of birth	28th March, 1974
Place of Birth	Mekelle, Ethiopia

Educational Background

2000-2002	Master of Science degree (MSc.) in Transport and Road Engineering at IHE/ Delft University of Technology, Delft, the Netherlands
1990-1995	Bachelor of Science (BSc.) in Civil Engineering at Faculty of Technology, Addis Ababa University, Ethiopia

Work Experience

2005-2011	PhD researcher	
	2005-2006	at Institute of Road Construction and Maintenance, Faculty of Civil Engineering, Vienna University of Technology
	2007-2011	at Road and Railway Engineering Section, Faculty of Civil Engineering and Geosciences, Delft University of Technology
2002-2005	Lecturer at Department of Civil Engineering, Mekelle University, Ethiopia	
	2002-2004	Head of Department of Civil Engineering
	2004-2005	Road and transport planner at Mekelle City Plan Preparation Project Office, Ethiopia
	2003-2005	Consultant, Promise Consulting Engineers, Ethiopia
1998-2000	Lecturer and Acting Head of Department of Civil Engineering, Mekelle University, Ethiopia	
1996-1998	Assistant Lecturer at Department of Civil Engineering, Mekelle University, Ethiopia	
1995-1996	Design Engineer at Commission for Sustainable Agriculture and Environmental Rehabilitation of Tigray (Co-SAERT), Ethiopia	